

การพัฒนาและจำลองกระบวนการผลิตเชื้อเพลิงเอทานอลและการประยุกต์ใช้ใน
ระบบเอสเทอร์ฟิเคชั่นของกรดซัคซินิกควบคู่กับการแยกไอผ่านเยื่อแผ่น



วิทยานิพนธ์นี้เป็นส่วนหนึ่งของการศึกษาตามหลักสูตรปริญญาวิทยาศาสตรดุษฎีบัณฑิต
สาขาวิชาเทคโนโลยีชีวภาพ
มหาวิทยาลัยเทคโนโลยีสุรนารี
ปีการศึกษา 2559

**PROCESS DEVELOPMENT AND SIMULATION OF
FUEL-ETHANOL PRODUCTION AND APPLICATION
TO VAPOR PERMEATION-ASSISTED
ESTERIFICATION OF SUCCINIC ACID**



Artit Kongkaew

A Thesis Submitted in Partial Fulfillment of the Requirements for the

Degree of Doctor of Philosophy in Biotechnology

Suranaree University of Technology

Academic Year 2016

**PROCESS DEVELOPMENT AND SIMULATION OF
FUEL-ETHANOL PRODUCTION AND APPLICATION TO VAPOR
PERMEATION-ASSISTED ESTERIFICATION OF SUCCINIC ACID**

Suranaree University of Technology has approved this thesis submitted in partial fulfillment of the requirements for the Degree of Philosophy.

Thesis Examining Committee

(Prof. Dr. Montarop Yamabhai)

Chairperson

(Assoc. Prof. Dr. Apichat Boontawan)

Member (Thesis Advisor)

(Prof. Dr. Jürgen Rarey)

Member (Thesis Co-Advisor)

(Prof. Dr. Adrian Flood)

Member

(Assoc. Prof. Dr. Sittipong Amnuaypanich)

Member

(Prof. Dr. Sukit Limpijumngong)

Vice Rector for Academic Affairs
and Innovation

(Prof. Dr. Neung Teaumroong)

Dean of Institute of Agricultural Technology

นายอาทิตย์ กองแก้ว : การพัฒนาและจำลองกระบวนการผลิตเชื้อเพลิงเอทานอลและการประยุกต์ใช้ในระบบเอสเทอร์ฟิเคชันของกรดซัคซินิกควบคู่กับการแยกไอน้ำผ่านเยื่อแผ่น (PROCESS DEVELOPMENT AND SIMULATION OF FUEL-ETHANOL PRODUCTION AND APPLICATION IN VAPOR PERMEATION-ASSIST ESTERIFICATION OF SUCCINIC ACID) อาจารย์ที่ปรึกษา : รองศาสตราจารย์ ดร.อภิชาติ บุญทาวัน, 219 หน้า.

วัตถุประสงค์ของการศึกษาในครั้งนี้คือการพัฒนาและจำลองระบบการผลิตเชื้อเพลิงเอทานอล ได้แก่ กระบวนการหมัก การกลั่น และการแยกน้ำ และนำไปประยุกต์ใช้ในระบบเอสเทอร์ฟิเคชันของกรดซัคซินิกควบคู่กับการแยกไอน้ำผ่านเยื่อแผ่น ในระบบการหมักควบคู่การกลั่นแบบกะ และหมักควบคู่การกลั่นแบบเติมเป็นระยะ พบว่า กระบวนการหมักควบคู่การกลั่นช่วยลดผลกระทบที่เกิดจากการยังยั้งโดยสารผลิตภัณฑ์ เนื่องจากเอทานอลซึ่งเป็นสารยับยั้งการเจริญของยีสต์ ถูกนำออกในช่วงเวลาของการหมัก โดยพบยีสต์ที่มีชีวิตมากถึงร้อยละ 60 ในน้ำหมักหลังกระบวนการหมัก และจากผลการทดลองของกระบวนการหมักควบคู่การกลั่นแบบทำซ้ำ พบว่า เอทานอลที่หมักได้จะถูกดึงออกอย่างต่อเนื่อง มีอัตราการกลั่นที่ 10.2 กรัมต่อชั่วโมง และมีความเข้มข้นของเอทานอลประมาณร้อยละ 80 โดยกระบวนการหมักดังกล่าวสามารถทำซ้ำได้ถึง 8 รอบ และได้เอทานอลมากถึง 1200 กรัม ระบบการหมักดังกล่าวได้นำไปทำการจำลองในระบบการหมักควบคู่การกลั่นแบบต่อเนื่องในถังหมักขนาด 200 ลิตร พบว่า ร้อยละ 82 ของเอทานอลถูกผลิตที่ 18.5 ลิตร ต่อวัน จากผลการคำนวณต้นทุนการผลิต พบว่า ต้นทุนการผลิตของเอทานอลด้วยวิธีดังกล่าวอยู่ที่ 27.50 บาทต่อลิตร ในการปรับปรุงระบบ พบว่า ต้นทุนการผลิตลดลงอยู่ที่ 19.25 บาทต่อลิตร ระบบการกลั่นประสิทธิภาพสูงขนาดเล็กซึ่งออกแบบและผลิตเองได้ถูกนำมาประยุกต์ใช้ โดยระบบดังกล่าวสามารถกลั่นเอทานอลที่มีความบริสุทธิ์มากถึงร้อยละ 93 จากสารตั้งต้นที่มีปริมาณเอทานอลแตกต่างกัน จากผลการจำลองพบว่า ระบบดังกล่าวสามารถผลิตเอทานอลที่มีความบริสุทธิ์ร้อยละ 90 และมีอัตราการกลั่นที่ 6.99 มิลลิลิตรต่อนาที และในส่วนของน้ำทิ้งมีปริมาณเอทานอลที่ร้อยละ 7 เมื่อทำการจำลองระบบโดยใช้โปรแกรมคอมพิวเตอร์

ในส่วน of ระบบการผลิตเอทานอลใรรน้ำ เมมเบรนชนิดซีโอไลต์ที่เอซึ่งเป็นเยื่อแผ่นที่ใช้ในกระบวนการทำบริสุทธิ์ของน้ำถูกผลิต โดยใช้ซีจีเอ็มกลายเป็นแหล่งซิลิกาเปรียบเทียบกับการใช้ซิลิกาจากสารเคมี ผลการทดลองพบว่า การล่อผลึกแบบจุ่มให้ปริมาณฟลักซ์ และสัมประสิทธิ์การแยกที่สูงที่สุด คือสามารถแยกน้ำออกได้ที่ร้อยละ 92 และมีค่าฟลักซ์และสัมประสิทธิ์การแยกที่ 0.6 กิโลกรัมต่อลิตรต่อชั่วโมงและ 218 ตามลำดับ เมมเบรนที่สังเคราะห์ได้ถูกนำมาศึกษาในทางจุลศาสตร์โดยใช้แบบจำลองทางคณิตศาสตร์เปรียบเทียบกับเมมเบรนสำหรับแยกน้ำที่ได้จากท้องตลาด พบว่าค่าสัมประสิทธิ์การแพร่ของเอทานอลและน้ำของเมมเบรนเซรามิกมีค่าเท่ากับ 2.5×10^{-9} และ 4.52×10^{-6} โมลต่อวินาทีต่อตารางเมตรตามลำดับ จากผลการคำนวณสรุปได้ว่าค่าพารามิเตอร์ของการแยกซึ่ง

ได้แก่ฟลักซ์และสัมประสิทธิ์การแยกของทั้งจากการคำนวณทางทฤษฎี และจากการทดลองมีค่าที่ค่อนข้างสอดคล้องกัน จากผลการนำค่าสัมประสิทธิ์การแพร่ไปประยุกต์ใช้กับการจำลองการกำจัดน้ำของเอทานอล พบว่า 23.45 กิโลกรัมของ เอทานอลที่ได้มีความบริสุทธิ์ที่ร้อยละ 97.99 ได้ถูกผลิตขึ้น และจากการคำนวณพบว่าต้องใช้แท่งเซรามิกเมมเบรน 16 แท่งเพื่อให้ได้เอทานอลใรน้ำที่ความเข้มข้นร้อยละ 99.5

ในส่วนของการบวนการเอสเทอร์ฟิเคชัน แบบจำลองของการผลิตเอทานอลใรน้ำได้ถูกนำมาประยุกต์ใช้ในกระบวนการเอสเทอร์ฟิเคชันของกรดซัคซินิกกับเอทานอล ค่าพารามิเตอร์ได้แก่ ค่าคงที่ปฏิกิริยา (k -value), ค่าสัมประสิทธิ์แอกทิวิตี (γ), ค่าพลังงานกระตุ้น (E_a) และค่าคงที่สมดุลของปฏิกิริยา (k_{EQ}) โดยใช้แบบจำลองของ NRTL จากผลการคำนวณ ที่เริ่มต้นของปฏิกิริยามีค่าอัตราการเกิดปฏิกิริยาจากกรดซัคซินิกไปเป็นโมโนเอซิลซัคซิเนต (r_1) และโมโนเอซิลซัคซิเนตเป็นไดเอซิลซัคซิเนต (r_2) ที่ 1.659×10^{-4} และ 0 โมลต่อวินาทีต่อลูกบาศก์เมตรตามลำดับ และจากการเปรียบเทียบผลของการเปลี่ยนแปลงความเข้มข้นระหว่างค่าจากการคำนวณและจากการทดลองพบว่าค่าทั้งสองนั้นสอดคล้องกัน และสามารถไปประยุกต์ใช้ในการจำลองระบบได้ จากผลการจำลองระบบเอสเทอร์ฟิเคชัน พบว่า อัตราการผลิตไดเอซิลซัคซิเนตมีค่าเท่ากับ 0.24 กิโลโมลต่อชั่วโมง และมีค่าการเปลี่ยนจากสารตั้งต้นเป็นสารผลิตภัณฑ์ที่ร้อยละ 93.23 จากการเปรียบเทียบเมมเบรนทั้งสามชนิดพบว่าเมมเบรนเซรามิกให้ประสิทธิภาพในการผลิตสูงสุด และเมมเบรนพอลิเมอร์กับเมมเบรนจากการทดลองมีค่าการเปลี่ยนจากสารตั้งต้นเป็นสารผลิตภัณฑ์ที่ร้อยละ 82.7 และ 79.3 ตามลำดับ

สาขาวิชาเทคโนโลยีชีวภาพ
ปีการศึกษา 2559

ลายมือชื่อนักศึกษา _____
ลายมือชื่ออาจารย์ที่ปรึกษา _____
ลายมือชื่ออาจารย์ที่ปรึกษาร่วม _____

ARTIT KONGKAEW : PROCESS DEVELOPMENT AND SIMULATION OF
FUEL-ETHANOL PRODUCTION AND APPLICATION TO VAPOR
PERMEATION-ASSISTED ESTERIFICATION OF SUCCINIC ACID. THESIS
ADVISOR : ASSOC. PROF. APICHAT BOONTAWAN, Ph.D., 219 PP.

ETHANOL/EXTRACTIVE FERMENTATION/PROCESS SIMULATION/
MATHEMATICAL MODEL/VAPOR PERMEATION/SUCCINIC ACID
ESTERIFICATION

The aim of this research was to optimize and simulate the fuel ethanol production including fermentation, distillation and dehydration, as well as applied in vapor permeation-assisted esterification of the succinic acid/ethanol system. The batch extractive and fed-batch extractive fermentation were investigated. The extractive fermentation decreased product inhibition by continuously removing the ethanol from the fermented broth. Approximately 60% relative viability was observed in fermented broth. The fermented ethanol was continuously fractionated from the system at 10.2 g/h with 80 wt% concentration and 8 fermentation cycles using 1 inoculation was performed in fed-batch extractive mode. Additionally, 1200 g of ethanol was extracted in the period of fermentation. A simulation of the 200 liter continuous extractive fermentation system using ASPEN PLUS was performed. The exiting vapor from the fractionation column was composed of 82 wt% ethanol with 18.5 liters per day productivity. The estimated production cost of extractive fermentation was 27.50 baht per liter. In addition, process modification for economic and systemic improvement was carried out and utilities cost of after process modification was 19.25 baht per liter. This distillation system illustrated the high efficiency in ethanol rectification, thus a maximum concentration of 93 wt% ethanol solution was extracted from various ethanol content in the fermentation broth. The 90 wt%

ethanol at 6.99 mL/min was purified from the fermented broth and contained 7 wt% ethanol in a stillage stream when simulated by ASPEN PLUS.

In the part of ethanol dehydration, the hydrophilic NaA zeolite membrane was fabricated using rice husk ash (RHA) as a silica source compared with the silica from chemical source. A dip-coated membrane fabrication led to the highest separation factor and flux. The extracted water was 92 wt% with flux and the separation factors at $0.6 \text{ kg m}^{-2} \text{ hr}^{-1}$ and 218, respectively. The calculated k -value of commercial ceramic membrane was calculated at 2.5×10^{-9} and $4.52 \times 10^{-6} \text{ mol.s}^{-1}.\text{m}^{-2}.\text{Pa}^{-1}$ of k_e and k_w value. The simulated data resulted in 23.45 kg was produced from a single membrane module with a 97.99 wt% ethanol concentration, while 16 membrane tubes were required for absolute ethanol production (99.5 wt%).

In the esterification part, the simulated ethanol dehydration process was applied and integrated with the succinic acid/ethanol esterification unit. The kinetic parameters such as reaction rate constant (k -value), activity coefficient (γ), activation energy (E_a) and equilibrium constant (k_{EQ}) were evaluated using the NRTL model. At the start of the reaction, the calculated net rate of SA to MES (r_1) and MES to DES (r_2) were 1.659×10^{-4} and $0 \text{ mol.s}^{-1}.\text{m}^{-3}$, respectively. There was good agreement between the calculated and experimental data and the two datasets could be fitted simultaneously. The simulated DES showed 0.24 kmol/hr productivity and 93.23% conversion yield. The commercial ceramic membrane showed the highest DES productivity. While the conversion yield from the self-made membrane and polymer membrane were 82.7 and 79.3%, respectively.

School of Biotechnology

Academic Year 2016

Student's Signature _____

Advisor's Signature _____

Co-advisor's Signature _____

ACKNOWLEDGEMENTS

I would like to thank Suranaree University of Technology for financial and laboratory facilities supports during my study. I would like to express my sincere gratitude to my advisor, Assoc. Prof. Apichat Boontawan for his continuous support during of my Ph.D study and related research, for his patience, motivation, and knowledge. His guidance helped me in all time of research.

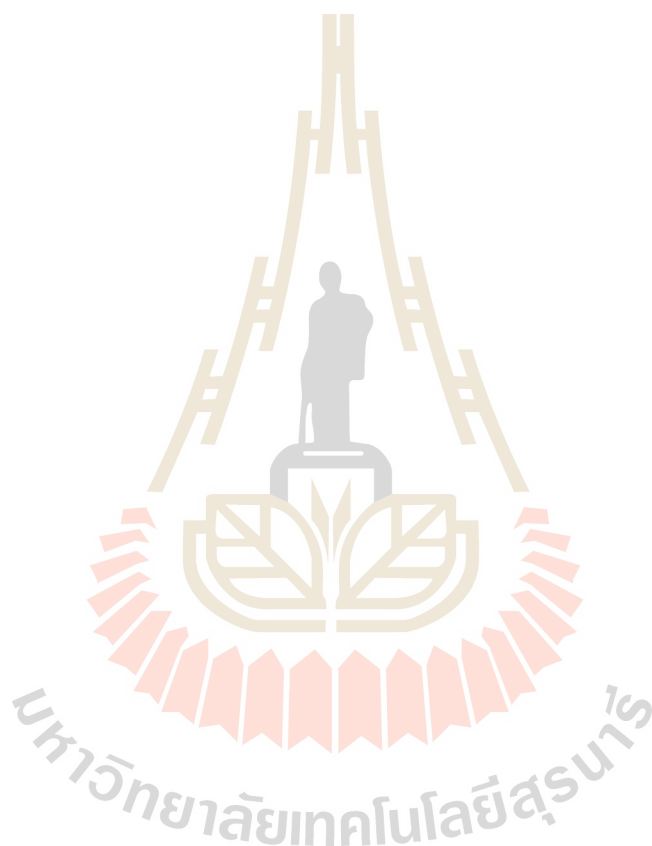
I deeply grateful to my co-advisor, Prof. Jürgen Reiner Rarey for his guidance, encouragement, support and provided a valuable experience during I had studied in Germany. I would love to express my special advisor, Dr. Chaiwat Kongmanklang for this support and appreciated suggestion.

Besides my advisor, I would like to express my gratitude to thesis committee: Prof. Adrian Flood, Prof. Montarop Yamabhai, and Assoc. Prof. Sittipong Amnuaypanich for their insightful comments and inspiration, and also provided the interesting question which incented me to widen my research from various perspectives.

The special thanks my fellow labmates (P' Earn, Kwan, Bow, Top, Far) and 3 Vietnamese girls (Nhan, Thuy, Ken) for the good environment, familiarity and for all the fun we have had together. I also thanks to my German partners (Jan and Michael) for their advised and giving points to fulfill of this report. Furthermore, I also extends appreciate to all CSTE staff from F10, School of Ceramic Engineering, SUT for their suggestion and official support.

Last but not the least, I would like to thank my parents and my sister for their courage, supports, faith and advice whenever needed. They have always been a great source of inspiration to take on any challenge in life.

Artit Kongkaew



CONTENTS

	Page
ABSTRACT IN THAI	I
ABSTRACT IN ENGLISH.....	III
ACKNOWLEDGEMENTS	V
CONTENTS	VII
LIST OF TABLES.....	XVI
LIST OF FIGURES	XX
LIST OF ABBREVIATIONS	XXVII
CHAPTER	
I INTRODUCTION	1
1.1 Significant of research	1
1.2 Research objectives	3
1.3 Research hypothesis.....	3
1.4 Scope and limitations of the study.....	4
1.5 Expected result	4
II LITERATURE REVIEWS	5
2.1 Succinic acid.....	5
2.2 Production of succinic acid	6
2.2.1 Production of succinic acid by chemical process.....	7
2.2.2 Production of succinic acid by fermentation process.....	8
2.3 Downstream processing of succinic acid.....	10

CONTENTS (Continued)

	Page
2.3.1 Precipitation and crystallization.....	10
2.3.2 Adsorption	13
2.3.3 Electrodialysis (ED) and electrodeionization (EDI)	13
2.3.4 Solvent extractions	14
2.3.5 Nanofiltration (NF).....	14
2.3.6 Esterification.....	16
2.3.6.1 Dual fermentation bio-refineries.....	19
2.3.6.2 Pervaporation-assisted esterification	23
2.3.6.3 Vapor permeation-assisted esterification	24
2.4 Preparation of hydrophilic membranes for dehydration	26
2.4.1 Zeolites A and its structure	27
2.4.2 Application of zeolite NaA for ethanol dehydration.....	28
2.5 Ethanol	29
2.5.1 The use of bio-ethanol as fuel and environmental effects	30
2.5.2 Ethanol fermentation	31
2.5.3 Extractive fermentation	32
2.6 Process simulation program	34
2.7 References	36
III BATCH EXTRACTIVE AND REPEATED-BATCH EXTRACTIVE FERMENTATION OF ETHANOL USING BLACKSTRAP MOLASSES AS A CARBON SOURCE	41

CONTENTS (Continued)

	Page
3.1 Abstract.....	41
3.2 Introduction	42
3.3 Methodology	44
3.3.1 Materials	44
3.3.2 Conventional and extractive fermentation of ethanol	44
3.3.3 Repeated-batch extractive fermentation	45
3.3.4 Analysis	46
3.3.4.1 Reducing sugar of fermented molasses.....	46
3.3.4.2 Ethanol, fusel oil and volatile compound concentrations.....	47
3.3.4.3 Organic acid concentrations.....	47
3.3.4.4 Viable cell count.....	47
3.4 Result and discussions	48
3.4.1 Substrate and product inhibition effect.....	48
3.4.2 Effect of initial molasses concentration on fermentation performance....	48
3.4.3 Conventional batch fermentation and batch extractive fermentation.....	52
3.4.4 Extractive fermentation of ethanol in repeated-batch mode.....	55
3.5 Conclusions	58
3.6 References	59
IV DEVELOPMENT AND OPTIMIZATION OF 200 LITERS	
CONTINUOUS EXTRACTIVE FERMENTATION SYSTEM	
USING ASPEN PLUS: PRACTICAL AND ECONOMICAL ASPECT.....	63

CONTENTS (Continued)

	Page
4.1 Abstract.....	63
4.2 Introduction	64
4.3 Methodology: process simulation using ASPEN PLUS.....	67
4.4 Results and discussions.....	68
4.4.1 Thermodynamic properties of the related material.....	68
4.4.2 Simulation of 200 liters extractive fermentation system.....	70
4.4.2.1 Simulation of bio-reactor and component specification.....	71
4.4.2.2 Model development of the fractionation column.....	73
4.4.2.3 Simulation of the Venturi system.....	78
4.4.3 Economical consideration of continuous extractive fermentation system.....	83
4.4.4 Modification options to improve efficiency	85
4.4.4.1 Recover the ethanol loss through Venturi system.....	85
4.4.4.2 Ethanol recovery from the waste stream	87
4.4.4.3 Changing the boundary conditions.....	88
4.5 Conclusions	92
4.6 References.....	92
V DEVELOPMENT AND SIMULATION OF HIGH PERFORMANCE LABORATORY-SCALE ETHANOL DISTILLATION SYSTEM	98
5.1 Abstract.....	98
5.2 Introduction	99

CONTENTS (Continued)

	Page
5.3 Instrumental design and experimental set-up.....	104
5.4 Results and discussions.....	106
5.4.1 Effect of feed concentration and cooling jacket temperature on distillation performance.....	106
5.4.2 Simulation of continuous distillation system using ASPEN PLUS.....	108
5.4.3 Sensitivity analysis.....	110
5.4.3.1 Sensitivity of flash and reboiler unit.....	110
5.4.3.2 Sensitivity analysis and advantages of heat exchanger.....	113
5.5 Conclusions.....	115
5.6 References.....	115
VI FABRICATION OF SODIUM A ZEOLITE MEMBRANE FOR WATER- ETHANOL SEPARATION IN VAPOR PERMEATION SYSTEM USING RICE HUSK ASH AS A SILICA SOURCE.....	117
6.1 Abstract.....	117
6.2 Introduction.....	118
6.3 Methodology.....	120
6.3.1 Chemicals and materials.....	120
6.3.2 Extraction of silica source from rice husk.....	120
6.3.3 The α -Al ₂ O ₃ support preparation.....	121
6.3.4 Preparation of the NaA seeds.....	121
6.3.5 The sodium zeolite A formulation and synthesis.....	122

CONTENTS (Continued)

	Page
6.3.6 Seeding procedures.....	123
6.3.6.1 Dip-coating method.....	123
6.3.6.2 Sonicate seeding method	123
6.3.6.3 Vacuum seeding method.....	123
6.3.7 Membrane characterization.....	123
6.3.7.1 Separation factor and flux.....	123
6.3.7.2 Crystallinity of NaA seeds using XRD	125
6.3.7.3 Morphology of NaA seeds using SEM.....	125
6.4 Results and discussions.....	126
6.4.1 Structural characterization of membrane support	126
6.4.2 Synthesis of NaA seeds powder.....	126
6.4.3 Effect of seeding technique on the NaA membrane properties using chemical as a silica source.....	127
6.4.4 Synthesis of NaA membrane using RHA as a silica source: effect of various seeding techniques and hydrothermal condition.....	133
6.5 Conclusions	143
6.6 References.....	143
VII A MATHAMETICAL MODEL OF BINARY MIXTURE ETHANOL/ WATER SEPARATION AND SIMULATION OF ETHANOL DEHYDRATION PROCESS: A COMPARISON BETWEEN SELF-MADE AND COMMERCIAL MEMBRANES.....	148

CONTENTS (Continued)

	Page
7.1 Abstract.....	148
7.2 Introduction	149
7.3 Methodology	154
7.3.1 Commercial ceramic and polymer membrane	154
7.3.2 Mathematical analysis and process simulation	154
7.3.3 Simulation of ethanol dehydration process using ASPEN PLUS.....	155
7.4 Results and discussions.....	156
7.4.1 Influence of feed concentration and operating pressure on separation performance: comparison with commercial water separation membranes.....	156
7.4.2 Consideration of the mathematical model equations	161
7.4.3 Calculation of diffusion coefficient (<i>k</i> -value).....	164
7.4.4 Simulation of ethanol dehydration process using calculated <i>k</i> -value and real parameters	173
7.4.5 Sensitivity analysis of simulated ethanol dehydration process.....	177
7.4.6 Simulation of ethanol dehydration process using ASPEN PLUS: economical evaluation	180
7.5 Conclusions	182
7.6 References	183

CONTENTS (Continued)

	Page
VIII KINETIC ANALYSIS OF DIETHYL SUCCINATE PRODUCTION VIA VAPOR PERMEATION-ASSIST ESTERIFICATION TECHNIQUE: MATHEMATICAL AND PROCESS SIMULATION	184
8.1 Abstract.....	184
8.2 Introduction	185
8.3 Methodology	188
8.3.1 Chemicals.....	188
8.3.2 Esterification of succinic acid.....	189
8.3.3 Analysis	189
8.3.3.1 Succinic acid concentration	189
8.3.3.2 Volatile compounds and ethanol concentration	189
8.3.3.3 Water content analysis.....	190
8.3.4 Kinetic model consideration	190
8.3.5 Simulation of DES production using VP-assisted esterification technique via ASPEN PLUS.....	192
8.4 Results and discussions.....	193
8.4.1 Esterification of succinic acid.....	193
8.4.2 Reaction kinetics of succinic acid/ethanol esterification: comparison between predicted and experimental data.....	194
8.4.3 Process simulation of DES production using VP-assisted esterification.....	202

CONTENTS (Continued)

	Page
8.5 Conclusions	204
8.6 References	205
XI OVERALL CONCLUSIONS	207
APPENDICES	210
APPENDIX A Composition of kaolin.....	211
APPENDIX B Zeolite A formula calculation.....	212
APPENDIX C Geometrically design of self-made membrane housing.....	214
APPENDIX D Calculation of diffusion coefficient	215
BIOGRAPHY	219

LIST OF TABLES

Table	Page
2.1 Physico-chemical properties of succinic acid.....	6
2.2 Characteristic of interested zeolite.....	28
2.3 Physico-chemical properties of ethanol	30
2.4 The literature related the application of fuel-ethanol in the environmental effects....	33
3.1 Effect of jacket temperature on distillate rate, %ethanol, ethanol flow rate and concentration of fusal oil.....	54
4.1 The units operation, models and operating condition in the extractive fermentation system applied in ASPEN PLUS.....	68
4.2 Calculated mole fraction for glucose conversion in simulated program.....	73
4.3 Composition, mass and volume flow as well as mass fraction of bio-reactor.....	74
4.4 Composition, mass and volume flow as well as mass fraction of fractionation unit operation.....	78
4.5 Composition, mass and volume flow as well as mass fraction of after Venturi system	80
4.6 Utilities usage and utilities cost of the 200 liters extractive fermentation qualities ...	84
4.7 Net cost flow of feed, power and cost of ethanol production.....	84
4.8 Results of the gas scrubbing the exhaust gas flow Venturi	87
4.9 Component mass flow and fraction of waste stream recovery	88
4.10 Utilities usage and utilities cost of the laboratory-scale distillation system for ethanol recovering in waste stream.....	88

LIST OF TABLES (Continued)

Table	Page
4.11	Component flow and fraction of product and stillage after the ambient-temperature in selective region was used..... 90
4.12	Utilities usage and utilities cost of the extractive fermentation system using ambient-temperature in selective region and coupled with laboratory-scale distillation system..... 91
5.1	Pure components parameters: Van der Waals properties of r_i and q_i , and Antoine's equation constant A_i , B_i and C_i 101
5.2	The effect of various feed concentrations and jacket temperature on distilled and bottom ethanol concentration and flow rate..... 107
5.3	Composition, mass and volume flow as well as mass fraction of small-scale distillation system (actual condition) 110
5.4	Utilities usage and utilities cost of the small-scale distillation system 110
5.5	Component mass flow and fraction of modified distillation system..... 113
5.6	Utilities usage and utilities cost of the small-scale distillation system 113
6.1	Effect of permeate ethanol concentration, flux and separation factor at various surface properties and seeding technique 130
6.2	Effect of permeate water concentration, flux and separation factor at various seeding technique on synthesized membrane using RHA as a silica source..... 136
6.3	Effect of permeate ethanol concentration, flux and separation factor at various hydrothermal incubate condition on synthesized membrane using RHA as a silica source. 139

LIST OF TABLES (Continued)

Table	Page
7.1	The units operation, models and operating condition in ethanol dehydration system applied in ASPEN PLUS 156
7.2	Mass fraction of permeated ethanol and water, separation factor and flux in difference feed concentration and pressure using commercial polymer (Sulzer) as a water separation membrane 158
7.3	Mass fraction of permeated ethanol and water, separation factor and flux in difference feed concentration and pressure using commercial ceramic (Mitsui Engineering) as a water separation membrane 159
7.4	Mass fraction of permeated ethanol and water, separation factor and flux in difference feed concentration and pressure using self-made synthesized membrane (sample 045) 160
7.5	Calculated flux and mole fraction of water and ethanol at various operating pressure and feed concentration 169
7.6	Comparison of calculated k -value, OF value and k_w/k_e ratio in three types water separation membranes 173
7.7	Comparison of various membrane types on total flow and mass fraction of permeate and retentate side as well as number of tubular membrane to obtained 99.5 wt% ethanol 177
7.8	Product flow rate, ethanol in permeate side and number of tubes to obtain 99.5 wt% ethanol in various feed concentration 180
7.9	Composition mass flow and mass fraction of the dehydration process 181

LIST OF TABLES (Continued)

Table		Page
7.10	Utilities usage and utilities cost of dehydration process	182
8.1	Binary parameters of the related components for NRTL model.....	193
8.2	Kinetic parameters for pseudo-homogeneous model	195
8.3	The calculated G_{ij} and τ_{ij} value of each component related with the succinic acid/ethanol esterification	198
8.4	Components mole flow, total mole and volume flow of simulated VP assisted esterification.....	203
8.5	Simulated data of product stream mole flow and volume flow of various types of membrane in VP assisted esterification	204

LIST OF FIGURES

Figure	Page
2.1 The chemical structure of succinic acid.	5
2.2 Various chemicals and products that can be synthesized from succinic acid.....	7
2.3 Chemical route of the production of succinic acid from maleic anhydride.....	8
2.4 Catabolic pathway of succinic acid production of wild-type <i>A.Succinogens</i>	10
2.5 Steps in purification of succinic acid from fermentation broth by precipitation technique	12
2.6 Steps in purification of succinic acid from fermentation broth by precipitation technique	16
2.7 Schematic diagram for esterification of succinic acid with ethanol.....	17
2.8 Bioconversion of glucose to ethanol and organic acid process and relationship to purified organic acid.....	20
2.9 Working principle of the fractionating column based on partial condensation technique.....	21
2.10 Working principle and mass transfer consideration of the VP technique	23
2.11 Schematic diagram of a pervaporation-assisted esterification system	25
2.12 Experimental set-up for vapor permeation-assisted esterification (top), and schematic diagram of vapor permeation technique	25
2.13 Schematic diagram of composite ceramic membrane with outer coating	27
2.14 Pathways for dissimilation of glucose to ethanol in yeast via glycolysis and the hexose monophosphate shunt	32

LIST OF FIGURES (Continued)

Figure	Page
2.15	Experimental setup for extractive fermentation of ethanol using vacuum fractionation technique 35
3.1	The actual picture (A) and diagram (B) of laboratory-scale extractive fermentation 46
3.2	Variation of the specific productivity as a function of the substrate (A), and initial ethanol concentration (B) 49
3.3	Time-course of viable cell count (◆), reducing sugar (■), and ethanol (▲) during fermentation using blackstrap molasses as a carbon source at various initial concentration A) 25 wt%, B) 30 wt%, C) 35 wt%, D) 45 wt% and E) 60wt%. 51
3.4	Productivity of ethanol fermentation at various initial molasses concentration. 52
3.5	Time-course of viable cell count (◆), reducing sugar (■), ethanol (▲) and distilled ethanol (o) during fermentation using blackstrap molasses as a carbon source via A) conventional fermentation and B) extractive fermentation 53
3.6	Time-course of viable cell count (◆), reducing sugar (■), ethanol (▲) and accumulated ethanol (o) during repeated-batch extractive fermentation 56
3.7	Percentage viability (gray bar) and productivity (white bar) for each fermentation cycle 58
4.1	Fundamental fluid flow on the Venturi effect and pressure gradient 66
4.2	Selected activity coefficients at infinite dilution 69

LIST OF FIGURES (Continued)

Figure	Page
4.3	VLE ethanol / water (at 60 mbar) calculated using DDBST database..... 70
4.4	The 200 liters extractive fermentation system..... 71
4.5	The bio-reactor diagram designed in ASPEN PLUS 72
4.6	Sensitivity analysis for the pressure dependence of ethanol flow (●) and fraction (■) using ASPEN PLUS..... 75
4.7	Ethanol/water VLE behavior in column. (1) water refluxed on the column wall, (2) formation of water droplet in the stream and (3) vapor-liquid equilibrium between droplets and vapor. 76
4.8	Fractionation column diagram designed in ASPEN PLUS, consist of 4 reflux streams..... 77
4.9	The actual systemic diagram (left) and ASPEN PLUS designed diagram (right) of venturi system 79
4.10	Sensitivity analysis of non-condensed ethanol fraction (above) and flow (below) in venturi tank at various cooling temperature..... 81
4.11	Assembled unit operation of extractive fermentation system..... 82
4.12	Additional of gas scrubber in Venturi system in order to non-condensed ethanol recover 86
5.1	The typical distillation system 101
5.2	The distillation tray diagram..... 102
5.3	The McCabe and Thiele diagram of vapor/liquid equilibrium stages analysis in ethanol/water system..... 103

LIST OF FIGURES (Continued)

Figure	Page
5.4	The process diagram (above) and actual image (below) of the laboratory-scale distillation system..... 105
5.5	Typical vapor liquid equilibrium (VLE) of ethanol/water system..... 108
5.6	The small scale distillation system designed in ASPEN PLUS..... 109
5.7	Sensitivity analysis of flash power on ethanol product and stillage flow (above) Sensitivity analysis of reboiling power on ethanol product and stillage flow (below)..... 112
5.8	Sensitivity analysis of various heat exchanger area on flash utilities cost (above) and heating cost in various feed rate: with heat exchanger (■) and without heat exchanger (o) (below)..... 114
6.1	Zeolite NaA structure and illustration of α -cage (super cage) and β -cage sodalite cage..... 119
6.2	The diagram of self-made membrane testing module..... 124
6.3	XRD chromatogram of the kaolin support 127
6.4	SEM images of the support from pure kaolin (A) and kaolin mixed with 3 wt% CaCO ₃ (B) 128
6.5	SEM images of the NaA seeds powder using chemical as a silica source (A) and RHA as a silica source (B)..... 129
6.6	XRD chromatograms of the NaA seeds powder using chemical as a silica source (A) and RHA as a silica source (B) (red peak was a NaA chromatograms from database)..... 130

LIST OF FIGURES (Continued)

Figure	Page
6.7 XRD chromatograms of the synthesized NaA zeolite membranes in various support properties including pure kaolin [048] (A), kaolin mixed with 3 wt% CaCO ₃ [044] (B), various seeding techniques including dip coating 1 time [045] (C) and dip coating 2 times [043] (D)	134
6.8 SEM images of NaA zeolite synthesized on the substrate in various support properties including pure kaolin [048] (A), kaolin mixed with 3 wt% CaCO ₃ [044] (B), various seeding techniques including dip coating 1 time [045] (C), dip coating 2 times [043] (D) and cross-section of the sample [045] (E).....	135
6.9 SEM images of NaA zeolite synthesized on the substrate using RHA as a silica source in various seeding techniques including vacuum seeding [079] (A), sonicate seeding [075] (B), dip-coating [065] (C) and 2 times dip-coating [068] (D).....	138
6.10 XRD chromatograms of NaA zeolite synthesized on the substrate using RHA as a silica source using dip-coating [065] (above) and 2 times dip-coating [068] (below) technique.	139
6.11 SEM images of NaA zeolite synthesized on the substrate using RHA as a silica source in various hydrothermal synthesis condition including 60°C 17 hrs [056] (A), 80°C 4 hrs [062] (B), 80°C 7 hrs [079], (C), 100°C 3 hrs [069] (D) and 100°C 5 hrs [070] (E).....	141

LIST OF FIGURES (Continued)

Figure	Page
6.12 XRD chromatograms of NaA zeolite synthesized on the substrate using RHA as a silica source in various hydrothermal synthesis condition including 60°C 17 hrs [056] (A), 80°C 7 hrs [079], (B) and 100°C 3 hrs [069] (C).....	142
7.1 Total flux at various operating pressure using commercial polymer membrane (Sulzer) in various feed ethanol concentration: ● 85 wt%, ■ 90 wt%, ▲ 95 wt% and ◆ 99 wt%	158
7.2 Total flux at various operating pressure using commercial ceramic membrane (Mitsui Engineering) in various feed ethanol concentration: ● 90 wt%, ■ 97.5 wt%, ▲ 95 wt% and ◆ 99 wt%.....	159
7.3 Total flux at various operating pressure using self-made synthesized membrane (sample 045) in various feed ethanol concentration: ● 85 wt%, ■ 90 wt%, ▲ 95 wt% and ◆ 99 wt%	160
7.4 The comparison between experimental data (○) and calculated data (after k -value adjustment) (-) of molar flux (above) and mole fraction (below)	171
7.5 Theoretical molar flux in various operating pressure (above) and ethanol feed concentration (below)	172
7.6 The calculated minimum value of k_v ratio.....	173
7.7 Amount of tubular membranes in order to obtain absolute ethanol (retentate side) in various feed rate including 10 kg/hr (■), 20 kg/hr (▲), 50 kg/hr (○) and 100 kg/hr (◆) using 95 wt% feed.	178

LIST OF FIGURES (Continued)

Figure	Page
7.8	Ethanol product mass fraction in various feed rate when 10 membrane tubes with 95 wt% feed rate were used 178
7.9	Ethanol product mass fraction (◆) and mass flux (○) in various feed concentration when 10 membrane tubes with 25 kg/hr feed rate were used. 179
7.10	Dehydration process designed in ASPEN PLUS 181
8.1	Schematic diagram for esterification of succinic acid with ethanol..... 186
8.2	Schematic diagrams for the experimental setup of NF (A), and VP-assisted esterification reaction between SA and ethanol (B)..... 188
8.3	Concentration profile of succinic acid (–△–), diethyl succinate (–□–), monoethyl succinate (–×–), water (–◇–) and ethanol (–○–) during esterification reaction of SA and ethanol 194
8.4	Comparison between experimental mole fraction profile of succinic acid (△), diethyl succinate (□), monoethyl succinate (×), water (◇) and ethanol (○) and predicted mole fraction profile of succinic acid (– -), diethyl succinate (—), monoethyl succinate (— -), water (.....) and ethanol (—) 201
8.5	The VP-assisted esterification of succinic acid/ethanol designed model..... 202

LIST OF ABBYREVIATIONS

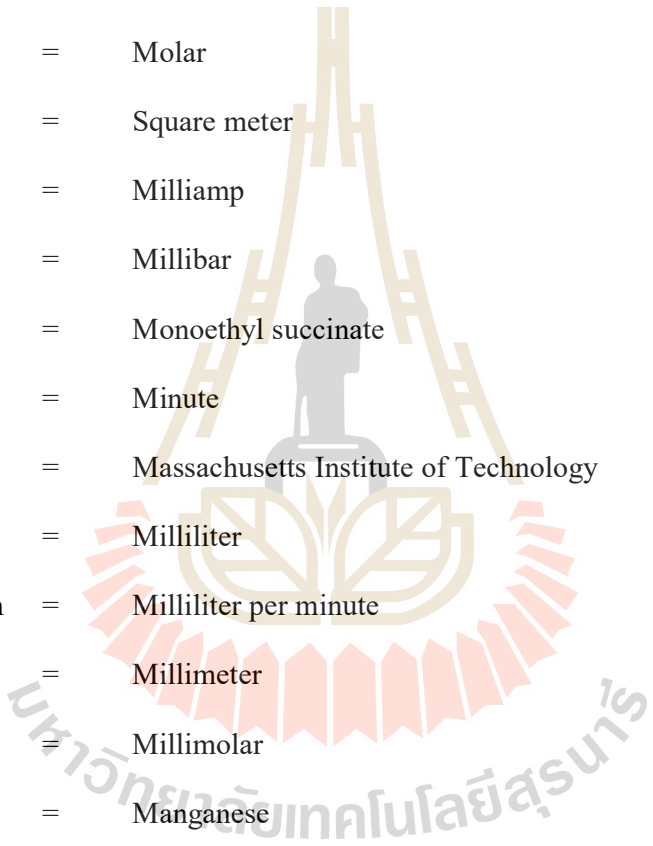
$\bar{\phi}_i^V$	=	Vapor fugacity coefficient
$\alpha\text{-Al}_2\text{O}_3$	=	Alpha-aluminum oxide
$^\circ\text{Brix}$	=	Degree brix
$^\circ\text{C}$	=	Degree Celsius
ΔE	=	Variation of activation energy
μg	=	Microgram
ΔH	=	Enthalpy of formation
μm	=	Micrometer
ρ	=	Mass density
α	=	Separation factor
θ	=	Theta
\AA	=	Angstrom
A	=	Area
Al	=	Arsenic
As	=	Copper
ASPEN	=	Advanced system for process engineering
CaCO_3	=	Calcium carbonate
CaO	=	Calcium oxide
CBUs	=	Composite building units
cm	=	Centimeter
cm^2	=	Square centimeter

LIST OF ABBREVIATIONS (Continued)

CO ₂	=	Carbon dioxide
DAP	=	Di-ammonium phosphate
DDBST	=	Dortmund data bank
DES	=	Diethyl succinate
DI	=	Deionized
DNS	=	Dinitrosalicylic acid
d_p	=	Pore diameter
E_a	=	Activation energy
Eq.	=	Equation
EtOH	=	Ethanol
\bar{f}_i^V	=	Fugacity of a component i in the vapor phase
Fe	=	Ferrous iron
FID	=	Flame ionization
g	=	Gram
g	=	Gravitational constant
g/L hr	=	Gram per liter hour
g/L	=	Gram per liter
GC	=	Gas chromatography
H ₂ O	=	Water
H ₂ SO ₄	=	Sulfuric acid
HCl	=	Hydrochloric acid
HPLC	=	High performance liquid chromatography
hr	=	Hour

LIST OF ABBREVIATIONS (Continued)

IAA	=	Iiso-amyl acetate
J_{calc_e}	=	Calculation ethanol flux
J_{calc_total}	=	Sum of calculation flux
J_{calc_w}	=	Calculation water flux
J_e	=	Mass ethanol flux
J_{emol}	=	Molar ethanol flux
$J_{realpar}$	=	Mass flux using real parameters
J_w	=	Mass water flux
J_{wmol}	=	Molar water flux
K	=	Henry's constant
K'_i	=	Substrate inhibition constant
K'_s	=	Saturation constant
k_e	=	Diffusion coefficient of ethanol
k_w	=	Diffusion coefficient of water
K_{EQ}	=	Equilibrium constant
$\text{kg m}^{-2} \text{hr}^{-1}$	=	Kilogram per square meter per hour
kg	=	Kilogram
kg/hr	=	Kilogram per hour
kmol	=	Kilo mole
$\text{KNaC}_4\text{H}_4\text{O}_6$	=	Potassium sodium tartrate
kPa	=	Kilo pascal
kV	=	Kilo volt
kW	=	Kilo watt

LIST OF ABBREVIATIONS (Continued)

<i>L</i>	=	Thickness of the membrane
L	=	Liter
LTA	=	Linde Type A
M	=	Molar
m ²	=	Square meter
mA	=	Milliamp
mbar	=	Millibar
MES	=	Monoethyl succinate
min	=	Minute
MIT	=	Massachusetts Institute of Technology
mL	=	Milliliter
mL/min	=	Milliliter per minute
mm	=	Millimeter
mM	=	Millimolar
Mn	=	Manganese
MW	=	Molecular weight
<i>MW</i> _{avg}	=	Average molecular weight
Na ²⁺	=	Sodium ion
Na ₂ HPO ₄	=	Sodium hydrogen phosphate
NAA	=	Normal-amyl acetate
NaA	=	Sodium A
NaOH	=	Sodium hydroxide
NF	=	Nanofiltration

LIST OF ABBREVIATIONS (Continued)

NFS	=	Non-fermentable substances
nm	=	nanometer
NRTL	=	Non-random two-liquid
OAE	=	Office of Agricultural Economics
OF	=	Objective function
P	=	Product concentration
P'_m	=	Maximum product concentration
P_i^{sat}	=	Saturate vapor pressure
PBS	=	Poly-butylenesuccinate
P_F	=	Pressure in feed side
pH	=	Hydrogen ion power
PLA	=	Poly lactide
P_P	=	Pressure in permeate side
ppm	=	Part per million
PVC	=	Polyvinyl chloride
r	=	Reaction rate
ret_{total}	=	Mass of retentate
R_{gas}	=	Gas constant
RHA	=	Rice hull ash
RO	=	Reverse osmosis
rpm	=	Round per minute
S	=	Substrate concentration
SEM	=	Scanning electron microscope

LIST OF ABBREVIATIONS (Continued)

SiO_2	=	Silica oxide
t_{end}	=	Reaction time
U.S.A.	=	United States of America
UNIF-DMD	=	UNIFAC Dortmund modified
UV	=	Ultraviolet
VLE	=	Vapor-liquid equilibrium
v_{max}	=	Maximum specific production rate
VP	=	Vapor permeation
w_{CAT}	=	Weight of catalyst
W_{Feed_EtOH}	=	Mass fraction of ethanol in feed side
W_{Feed_H2O}	=	Mass fraction of water in feed side
W_{Perm_EtOH}	=	Mass fraction of ethanol in permeate side
W_{Perm_H2O}	=	Mass fraction of water in permeate side
wt%	=	Weight percent
x_{calc}	=	The dataset of x from calculation
x_e	=	Mole fraction of ethanol in feed side
x_E	=	Mole fraction of ethanol
x_{exp}	=	The dataset of x from experiment
XRD	=	X-ray diffraction
x_w	=	Mole fraction of water in feed side
x_w	=	Mole fraction of water
y_{calc_e}	=	The dataset of ethanol of y from calculation
y_{calc_w}	=	The dataset of water of y from calculation

LIST OF ABBREVIATIONS (Continued)

y_e	=	Mole fraction of ethanol in permeate side
y_{exp}	=	The dataset of y from experiment
y_w	=	Mole fraction of water in permeate side
Zn	=	Zinc
γ_i	=	Activity coefficient of component i
ε	=	Porosity of the membrane
$\theta_{i,m}$	=	Ratio of stoichiometric coefficients of component i

CHAPTER I

INTRODUCTION

1.1 Significant of research

Succinic acid is an important chemical that can be used in food, pharmaceutical, cosmetic, and chemical industries. Recently, there is increasing interest in the production of “green” chemicals and biodegradable polymers, such as diethyl succinate (DES), and polybutylenesuccinate (PBS). Development of purification processes for succinic acid from fermentation broth plays a major role in the reduction of total production cost in order to compete with the petroleum-based production. Esterification is a downstream process that can remove contaminating organic acids in case of differing boiling points of their respective ester compounds. The esterification of succinic acid involves the chemical reaction with alcohols in this case ethanol to produce the diethyl succinate. The subsequent step is distillation followed by hydrolysis of the purified diethyl succinate with water to yield alcohol and succinic acid. Esterification reactions are characterized by thermodynamic limitations of the conversion. Higher ester yields can be obtained by shifting the equilibrium towards products using hybrid processes such as reactive distillation and membrane-assisted reactors instead of using a large excess of alcohol. Membrane separation processes have gained increasing attention in many esterification processes as an effective energy-saving separation technique. In this regard, the integration of hydrophilic membranes into conventional esterification processes is very attractive as the separation is based on the transport of the reacting components through the membrane. In combination with a reactor,

a membrane can be used to continuously remove water to shift the reaction equilibrium in order to improve yield and volumetric productivity.

ASPEN PLUS, as the sophisticated process simulation software, can be used to performed process optimization, technology reliability, economic benefit, and analysis of environmental assessment. It has been proved by many performances that ASPEN PLUS can be successfully applied to simulate the steady state process including sensitivity analysis, design optimization, and case study in fuel-ethanol and other chemical compounds.

Until now, most ceramic membranes for dehydration of ethanol solutions are produced abroad (e.g. Germany, Japan and China). They are composite membranes where the zeolites top layers are thinly coated on the outer porous surface of an α - Al_2O_3 tube. Thailand long since has a highly denoted industry for ceramic products. Therefore, it has a high potential for the development of ceramic membranes in order to substitute the imported membranes.

In this work, both fermentation and purification of succinic acid was carried out. The extractive fermentation of ethanol was done using blackstrap molasses as a starch source. The industrial scale extractive fermentation was performed using simulation program. For the esterification step, the zeolite tubular membranes were developed for dehydration of esterification of fermentation-derived succinic acid and ethanol. The surface properties of tubular membranes were investigated using X-ray diffraction (XRD) and scanning electron microscope (SEM). The effects of different preparation parameters on mass fluxes and separation factors was determined including the effect of temperature, feed pressure, and feed water concentration, respectively. The experimental data was used for mathematical modelling using the MathCad program. The resulting fabricated membrane was compared with the commercial membrane in term of selectivity and flux as well as applied in the assisted-esterification system for DES production.

1.2 Research objectives

1. To study the extractive fermentation technique of ethanol using blackstrap molasses as a carbon source.
2. To simulate the 200 liters extractive fermentation reactor using simulation program with respect to both methodology and economic.
3. To establish the high-performance continuous distillation column for purification of ethanol and simulate on industrial scale.
4. To develop reproducible NaA zeolite membranes for water removal using rice husk ash as a silica source compare with chemical souces.
5. To study the mathematical model and investigate the effect of operating conditions on dehydration performance using vapor permeation technique, and compare the results with commercially available ceramic membranes.
6. To apply the resulting membranes to the esterification reaction of succinic acid as well as study and simulate the succinic acid/ethanol esterification kinetics using simulation program and compare the self-made to available commercial membranes.

1.3 Research hypothesis

Succinic acid is an important chemical that can be used in biodegradable polymers, such as poly-butylenesuccinate (PBS). The esterification including the chemical reaction with ethanol is the most effective technique for purification. Extractive fermentation represents an energy and time efficient technique in energy and time for ethanol production due to the combination of fermentation and distillation system. The construction of water removal ceramic membranes using local materials will be performed. The synthesized water separation membrane will be employed in the esterification of succinic acid. The anhydrous

ethanol and succinic acid purification on laboratory scale will be mathematically studied for scale-up to industrial scale.

1.4 Scope and limitations of the study

In this research, production of anhydrous ethanol was performed using extractive fermentation of ethanol. Blackstrap molasses was used as a carbon source due to its abundance and low price. The experimental data from extractive fermentation were reproduced by a simulation program (ASPEN PLUS). The flat plate NaA zeolite membrane was developed for dehydration of esterification of fermentation-derived succinic acid and anhydrous ethanol production. The membrane surface properties were investigated using XRD and SEM. The effects of different operating parameters on mass flux and separation factor were determined including the effect of temperature, feed pressure, and feed water concentration, respectively. The experimental data was used for mathematical modelling using the MathCad program. The resulting membranes were compared to the commercial membrane in term of selectivity and flux as well as applied in the assisted-esterification system for DES production.

1.5 Expected result

The expected result is optimized process parameters for succinic acid and ethanol purification using the appropriate ceramic membrane which were applied in esterification-assisted vapor permeation step. Study of the chemical reaction in the mathematically terms of each process is useful for scaling-up to industrial production. Also, these methods can be applied in various processes such as others organic acid purification, production fuel grade bio-ethanol and bio-diesel.

CHAPTER II

LITERATURE REVIEW

2.1 Succinic acid

Succinic acid or butanedioic acid (IUPAC systematic name) is an organic acid having the molecular formula $C_4H_6O_4$. It is a dicarboxylic acid with four carbon atoms. It occurs naturally in plant and animal tissues. It is very important for the body because it is used in the Krebs cycle (citric acid cycle) and involved in intermediary metabolic processes. There is growing interest in the production of succinic acid from renewable resources by microbial fermentation because succinic acid can be used in numerous applications. Succinic acid is widely applied in many industries such as food industry, pharmaceuticals industry, agriculture industry, cosmetic, photography and textile. Chemical structure and physico-chemical properties of succinic acid are shown in Figure 2.1 and Table 2.1, respectively.



Figure. 2.1 The chemical structure of succinic acid.

The current worldwide use of succinic acid is around 20,000 to 30,000 tons per year and this increases by approximately 10 percents per year. Succinic acid could become a future commercial fractional replacement petrochemicals in many applications as illustrated in Figure. 2.2. Succinic acid can be used as a precursor of many industrial chemicals such as adipic acid, 1,4-butanediol, tetrahydrofuran, *N*-methyl pyrrolidinone, 2-pyrrolidinone,

succinate salts and gamma-butyrolactonesuccinic acid. More importantly, it is used to the synthesis of biodegradable polymers such as poly butylenesuccinate (PBS) and polyamide to produce bioplastics. Bioplastics are a form of plastics derived from renewable biomass sources. Nowadays, the most important of bioplastic is polylactic acid or polylactide (PLA) and the estimated potential market for PBS is expected at 270,000 tons per year (McKinlay *et al.*, 2007).

Table 2.1 Physico-chemical properties of succinic acid.

Physical state	Odorless and colorless white crystals
Molar mass	118.09 g/mole
Density	1.56 g/mL
Melting point	184 °C
Boiling point	235 °C
Solubility in water	58 g/L (20 °C)
Acidity (pK _a)	pK _{a1} = 4.2, pK _{a2} = 5.6

2.2 Production of succinic acid

Succinic acid can be produced in different ways including the petrochemical-based synthesis and the fermentation route. The first requires high construction and operation costs. More than 15,000 tons of industrial succinic acid is produced from butane via the intermediate maleic anhydride. It is sold at a spot price of about U.S. \$ 5.90 - 8.80 per kg depending on its purity (Zeikus *et al.*, 1999). The latter route is fermentation method. There are many succinic acid producers including *Actinobacillus succinogenes*, *Anaerobiospirillum succiniciproducens*, *Mannheimia. succiniciproducens* and recombinant *Escherichai coli*. At present only natural succinic acid sold in the food market is produced by fermentation.

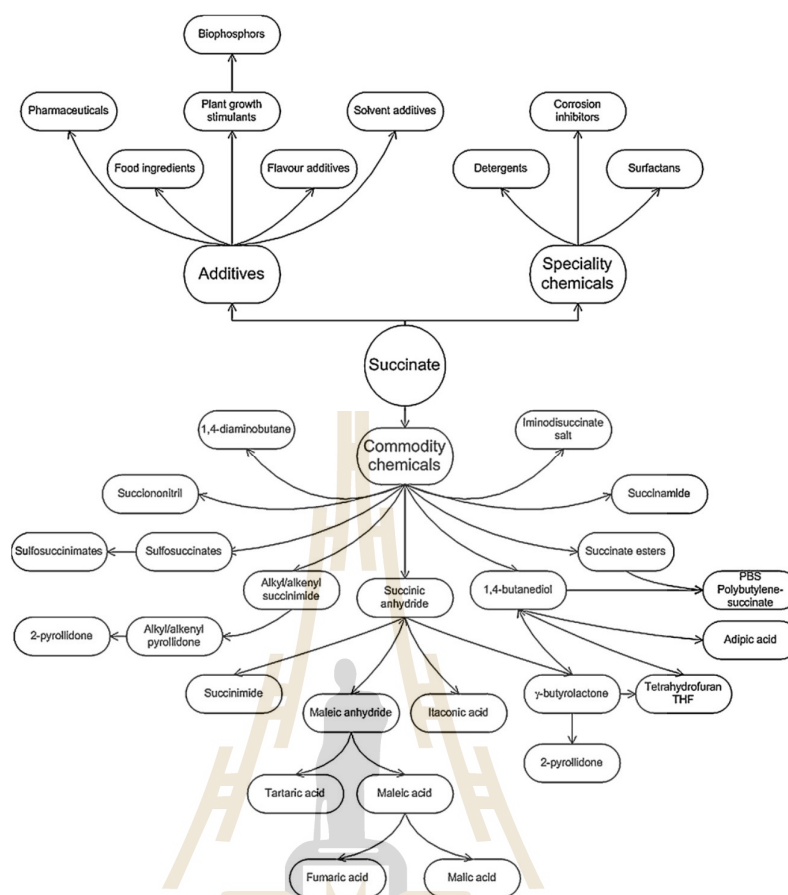


Figure 2.2 Various chemicals and products that can be synthesized from succinic acid (Beauprez *et al.*, 2010).

2.2.1 Production of succinic acid by chemical process

Succinic acid produced from petrochemical resources is derived from maleic anhydride, which is produced from n-butane through oxidation over vanadium-phosphorous oxide catalysts. The simplified reaction pathway of n-butane to maleic anhydride is shown in Figure 2.3 (Zhang *et al.*, 2009). The reaction from maleic anhydride to succinic acid begins by hydrolysis, breaking one of the single bonds between carbon and oxygen, forming maleic acid. The addition of hydrogen breaks the carbon-carbon double bond and completes the reaction, forming succinic acid. However, succinic acid produced from fossil fuels is not a natural product.

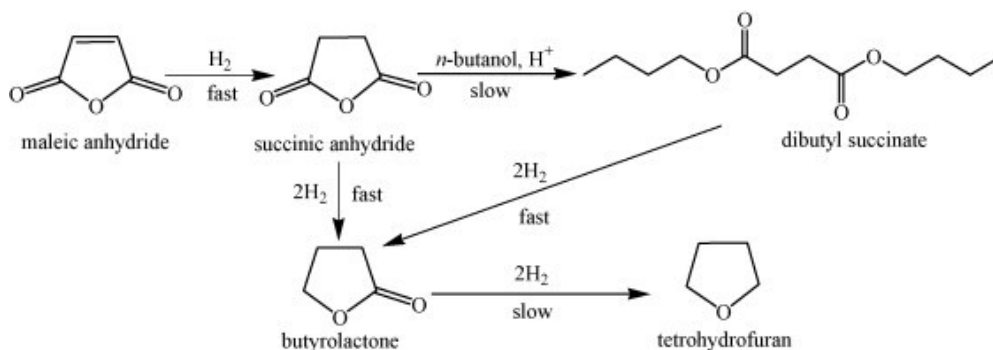


Figure 2.3 Chemical route of the production of succinic acid from maleic anhydride.

2.2.2 Production of succinic acid by fermentation process

Succinic acid can be produced from the most abundant sugars in plants biomass including glucose, fructose, arabinose, and xylose, respectively. Some anaerobic bacteria, such as *E. coli*, *A. succiniciproducens*, *M. succiniciproducens*, *C. glutamicum* and *A. succinogenes*, are capable to produce succinic acid as a major fermentation product of their metabolism. However, the later species is the most promising due to its high volumetric productivity, high succinic acid titer, and less by-products formation. The strain was originally isolated from bovine ruminal contents. This bacterium is a facultative anaerobic and Gram-negative rod or occasionally filamentous bacterium. *Actinobacillus succinogenes* grows at optimum growth temperature and pH of 37 °C and 6.8, respectively. At the optimum condition, glucose can be metabolized to produce succinate, formate, acetate, and ethanol as the major products. The micro-organism can produce succinic acid from various carbon sources such as arabinose, cellobiose, fructose, galactose, glucose, lactose, maltose, mannitol, mannose, sorbitol, sucrose, xylose or salicin under anaerobic condition (Zeikus *et al.*, 1999).

A. succinogenes tolerates a high glucose concentration of 150 g/L (Lin *et al.*, 2008). A simplified map of a wild type *A. succinogenes* succinate-producing metabolism is given in Figure 2.4. *A. succinogenes*'s metabolism was originally investigated using *in vitro*

enzyme assays, and by examining fermentation profiles under different growth conditions. Five key enzymes are responsible for succinic acid production including phosphoenolpyruvate carboxykinase (*PEPCK*), malate dehydrogenase (*MDH*), malic enzyme (*ME_{enz}*), fumarase (*Fm*) and fumarate reductase (*Frd*) (Song and Lee, 2006). PEP carboxylation is the crucial step for succinic acid production in rumen bacteria. It is the major CO₂-fixing enzyme which produces Oxaloacetic acid (OAA) before being converted to succinate by the reductive TCA branch, also called C₄ pathway. The pathway is defined as Phosphoenolpyruvate (PEP) → OAA → Malic acid (Mal) → Fumaric acid (Fum) → Succinic acid (Suc). The activity of the enzyme is strongly regulated by pH and CO₂ concentration in the fermentation broth. In theory, 1 mole of CO₂ is required to form 1 mole of succinic acid. The higher CO₂ level resulted in an increased succinic acid production at the expense of ethanol and formic acid. The pathway that produces formate, acetate, lactate and ethanol is called the C₃ pathway defined as PEP → Pyruvic acid (Pyr) → Acetyl CoA (AcCoA) → Acetic (Ace) + Ethanol (EtOH), and also includes Pyr → Lactic acid (Lac). *A. succinogenes* is able to produce relatively more succinic acid than other microorganisms (Samuelov *et al.*, 1991) and concomitant production of metabolic by-products such as acetic, formic, and lactic acids are problematic because it reduces the succinic acid yield and makes the purification process difficult and costly. As a result, the yield of succinic acid can be increased by disrupting the carbon fluxes to lactate, formate, and acetate by inactivating lactate dehydrogenase (LDH), pyruvate formate-lyase (PFL), phosphotransacetylase (PTS), and acetate kinase (AK), respectively.

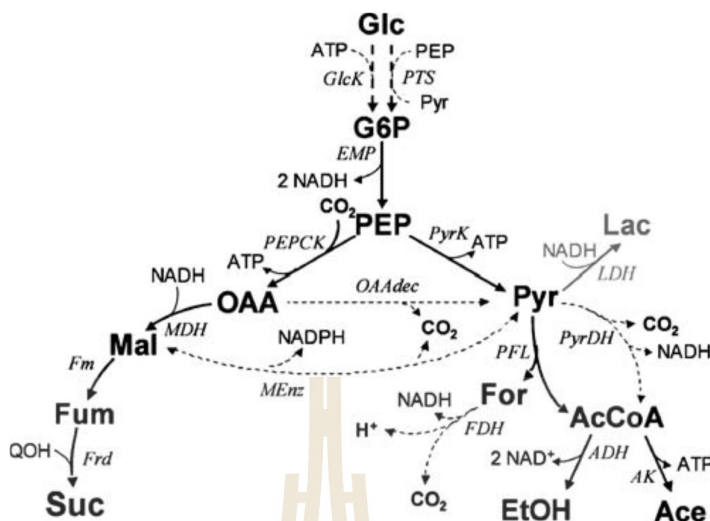


Figure 2.4 Catabolic pathway of succinic acid production of wild-type *A. Succinogens* (McKinlay *et al.*, 2007).

2.3 Downstream processing of succinic acid

The downstream processing step is defined as the step to recover and purify the product after fermentation, including the recycling of salvageable components and the proper treatment and disposal of waste. Considering that the downstream purification cost in the fermentation based process normally accounts for more than 50% of the total production cost (Cheng *et al.*, 2012). As a result, it is crucial to develop an economical purification process of succinic acid from fermentation broth. In the case of succinic acid purification, separation of byproducts including acetic, formic, lactic and pyruvic acids is the most crucial. Several methods for the purification of succinic acid including precipitation/crystallization, adsorption, membrane separation processes, solvent extraction, and esterification were reported. Detailed explanation of each technique can be given below.

2.3.1 Precipitation and crystallization

The optimal pH to generate succinic acid was adjusted and reducing cell toxicity by added calcium carbonate as shown in Figure 2.5. The major role of adding a calcium ion source is for neutralizing the fermentation broth, and to precipitate the succinate as calcium

succinate because of its low solubility in water. Isolation of calcium succinate can be achieved by using a filtration method before treating it with sulfuric acid to form calcium sulfate (gypsum) and succinic acid. Further treatment of the succinic acid can be done with a strong acidic ion ex-changer follow by a weak basic ion exchanger in order to remove impurities, and obtain a highly purified succinic acid product. In the preferred procedure, the calcium succinate is isolated from the fermentation broth by filtration; the filtrate is heated to precipitate additional calcium succinate and the spent filtrate which contains nutrients is recycled to the bioreactor. In addition in fermentation process may have been produced by-products such as calcium lactate. However, all impurities have to be removed in order to yield a high purity succinic acid to be used for the plastics industry.

Crystallization as a separation and purification technique may be defined as a phase change in which a crystalline product is obtained from a solution. A solution is a mixture of two or more species that form a homogeneous single phase. Solutions are normally thought of in terms of liquids or solid suspension. The solution to be ready for crystallization must be supersaturated. The solution in which the solute concentration exceeds the equilibrium (saturated) solute concentration at a given temperature is known as a supersaturated solution. There are four main methods to generate supersaturated including temperature change (mainly cooling), evaporation of solvent, chemical reaction, and changing the solvent composition.

Song *et al.* (2007) studied the recovery of succinic acid from metabolically engineered *M. succiniciproducens* strain by using the combination technique including reactive extraction, vacuum distillation and crystallization, respectively. After performing the reactive distillation, broth was vacuum distilled at 0.7 atm and 75°C for 2 hrs to facilitate crystallization and eliminate residual volatile carboxylic acid. Crystallization of succinic acid was carried out at 4°C and pH 2.0 by adding HCl. Experimental results showed that, the

purity of succinic acid after vacuum distillation is 55.70% with 99.17% yield. While the purity of succinic acid after crystallization is 98.17% with 66.44% yields.

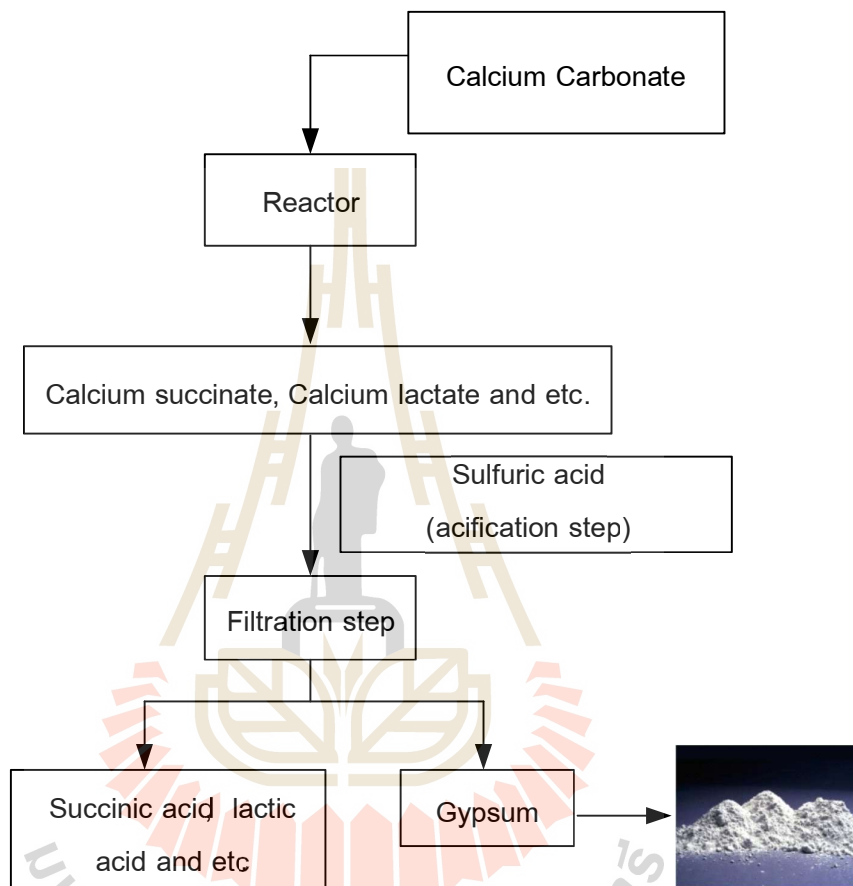


Figure 2.5 Steps in purification of succinic acid from fermentation broth by precipitation technique.

Li *et al.* (2010) compared the different crystallization techniques including direct crystallization and modified calcium precipitation. In direct crystallization, the pH of aqueous broth was adjusted to 2.0 by HCl. The clear filtrated broth was cooled to 2 - 4°C in the crystallizer for 5 hrs and crystal product was removed. In the modified calcium precipitation method, $\text{Ca}(\text{OH})_2$ slurry was added to the fermentation broth. Calcium succinate was eliminated and pH adjusted to 2.0 and the precipitate of calcium sulfate was removed. It was found that, the crystallization method obtained succinic acid yield at 70%

and 90% purity, while calcium precipitation gave 52% and 92% of yield and purity respectively.

2.3.2 Adsorption

Adsorption has shown a good potential and some data have been gathered for the distribution properties of other carboxylic acids, including acetic, lactic, and citric acids. Adsorption with weak alkaline anion exchange adsorbents is a good method to separate succinic acid from the fermentation broth. The adsorbent NERCB 09 was effective to separate succinic acid from the model solution and fermentation broth because of its high capacity, selectivity, and adsorption rate (Song and Lee, 2006). Adsorption is a promising separation method for recovery of the succinic acid because adsorbents have the advantages of low price, quick recovery, and low regeneration cost. Ion exchange adsorption has also been widely used in many organic acids separations (Li *et al.*, 2009). However, adsorption is the technique that has been characterized by low separation degrees because other organic acids can also be absorbed by the adsorbent. Therefore, this step is considered only as a primary recovery of succinic from fermentation broth. Further purification steps are required in order to obtain a high purity succinic acid.

2.3.3 Electrodialysis (ED) and electrodeionization (EDI)

Electrodialysis (ED) is a well-known separation process where ionized or weakly ionized compounds in aqueous solution based on transport through ion exchange membranes in an electric field. The succinate salt-containing whole broth, including cells, is transported from bioreactor and subjected to electro-dialysis to recover and concentrate the succinate salt in an aqueous stream. The succinate salt-containing aqueous stream is subjected to water-splitting electro-dialysis to form an aqueous succinic acid solution and a based on which can be recycled to the bioreactor. The aqueous succinic acid solution is then subjected an ion exchange polish purification with first a cationic exchanger and then an anion exchange to remove positively charged impurities and to yield a highly purified form

of succinic acid. The final product preferably will contain about 70 to about 95% succinic acid, up to 30%, usually between approximately 5% to 20% of acetic acid, less than 1% nitrogenous impurities and less than 10 ppm of sulfate ions or other contaminating ions. Electrodialysis is easily used to separate succinate from nonionized compounds with proper ion exchange membrane, although membranes are usually expensive and easily polluted. The succinic acid purification process composed of conventional electrodialysis followed by water-splitting electrodialysis membrane stacks, which removes most of the salt cation and produces highly pure acid stream. Although this process increased the concentration of succinic acid from 51.5% to 79.6% (w/w) and completely removed proteins and salts, the concentration of acetic acid increased from 13.2% to 19.9% (Song and Lee, 2006).

2.3.4 Solvent extractions

Solvent extractions are used for the purification, enrichment, separation and analysis of various components in mixtures. The system is based on the principle that a solute can distribute itself in a certain ratio between two immiscible solvents. The traditional product recovery method is based on precipitation of the insoluble calcium salt of carboxylic acids with $\text{Ca}(\text{OH})_2$ or CaCO_3 followed by re-acidification with H_2SO_4 . The disadvantage of this process is handling large amounts of solid and slurry, and the production of equal amounts of calcium sulfate waste. Extraction with conventional solvents, such as ether, is impractical for the recovery of most carboxylic acids because the low activity coefficient of the acid in the aqueous phase does not allow for a substantial transfer of the acid into the solvent. This recovery technique is therefore still in experimental level.

2.3.5 Nanofiltration (NF)

Nanofiltration is a membrane filtration based method that uses nanometer pores sized that pass through the membrane. The NF membranes have pore sizes from 1 - 10 angstrom, smaller than those used in micro-filtration and ultra-filtration, but just larger than that in reverse osmosis. It was reported by many research groups that many NF

membranes show the rejection to monovalent anions such as formate, acetate, lactate and divalent anions such as succinate (Petersen, 1993; Hilal *et al.*, 2004). However, a main disadvantage associated with nanotechnology, as with all membrane filter technology, is the cost and maintenance of the membranes used. The NF membranes are an expensive part of the process. Repairs and replacement of membranes is dependent on total dissolved solids, operating pressure, flow rate and components of the feed.

Choi *et al.* (2008) studied and applied the NF membrane for the purification of succinic acid from waste water. Two commercial NF membranes were used including ES10 (an aromatic polyamide membrane with 100 Da molecular weight cut-off) and NF270 (a polyamide membrane with 200-300 Da molecular weight cut-off). The simulated waste water was made by varying feed concentration and pH. The influence of operating pressure on the rejection of succinic acid was calculated. It was found that, the both ES10 and NF270 membrane contribute the rejection of succinic acid more than 95% at pH 6 – 8. The degree of succinic acid rejection of ES10 membrane did not significantly change with feed concentration (50 – 500 mg/L) and operating pressure. Whereas, the succinic acid rejection increased gradually up to 90% when increasing the pressure in the NF270 membrane. Hence, the ES10 and NF270 showed a relatively good rejection performance of succinic acid and advantage in the purification of succinic acid in the waste water.

Recently, Lubsungneon and their colleague (2014) studied and integrated process that consist of nanofiltration (NF) and vapor permeation (VP) as a series of purification steps for fermentation-derived succinic acid using *A. succinogenes* ATTC 55618. The microfiltration (MF) for exclusion of bacterial cells in fermentation broth was also applied to this process. The NF showed its usefulness for protein and color removal rather than separation among organic acids (Figure 2.6). Separation of organic acids was achieved based on esterification and vacuum fractionation. Removal of water in the esterification system was performed using a commercial zeolite NaA membrane the results

for NF and VP-assisted esterification revealed as enhances yield and high-purity of di-ethyl succinate.

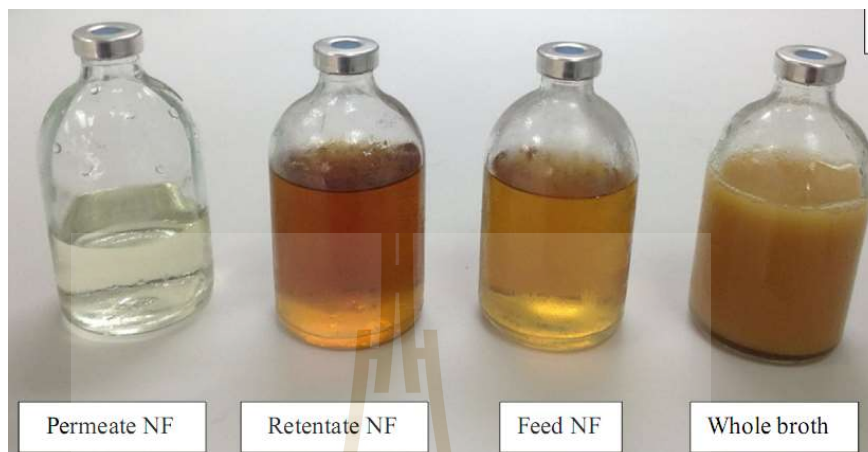


Figure 2.6 Steps in purification of succinic acid from fermentation broth by precipitation technique (Lubsungneon *et al.*, 2014).

2.3.6 Esterification

High purity succinic acid can also be produced by esterification of crude succinic acid with alcohols to yield succinate ester. The process is followed by distillation, hydrolysis of the distilled lactate ester to yield the alcohol and succinic acid. Esterification is the only downstream process, which separates other organic acids from succinic acid. Esterification gives esters of succinic acid, and further hydrolysis of esters is necessary to get the product as pure succinic acid. Fermentation broth containing succinic acid needs to be pretreated to remove some other impurities before esterification reaction. Ethanol is a preferred reactant because it is cheap and easy to produce. For succinic acid, it is a di-basic acid having two carboxylic acid functional groups. Succinic acid can be esterified with ethanol through a series of reactions to yield DES and 2 moles of water are produced as by-product. A schematic reaction scheme for esterification of succinic acid with ethanol is shown in Figure. 2.7.

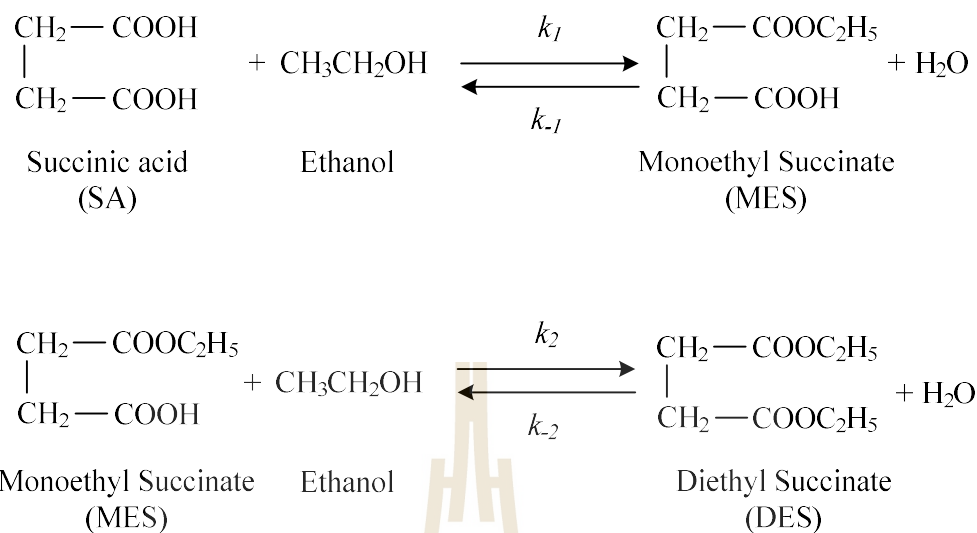


Figure 2.7 Esterification reaction of succinic acid with ethanol.

A conventional process to synthesize DES typically would use a stream of succinic acid and ethanol which are esterified in a batch or CSTR using sulfuric acid as a homogeneous catalyst. Many of the difficulties associated with use of homogeneous catalysts can be eliminated through use of heterogeneous catalysts like ion exchange resins or supported clays. The heterogeneous catalyst allows easy mechanical separation of the catalyst from reaction media by decantation or filtration, reduces or eliminates corrosion problems, and facilitates continuous process operation. Succinate esters are of low toxicity and low vapor pressure and have exceptional solvent properties, making them attractive candidates as replacements for petroleum based solvents.

Esterification reactions are characterized by thermodynamic limitations on the conversion yield. Higher ester yields can be obtained by shifting the equilibrium towards products formation using hybrid processes such as reactive distillation and membrane-assisted reactors instead of using a large excess of alcohol. Membrane separation processes have gained increasing attention in many esterification processes as an effective energy-saving separation technique (Benedict *et al.*, 2006). In this regard, the integration of

hydrophilic membranes into conventional esterification processes is very attractive as the separation is based on the transport of the reacting components through the membrane. Mass transfer is determined by the solubility and diffusivity of the components to be separated, and it is not limited by the relative volatility of the components as in distillation processes. In combination with a reactor, a membrane can be used to continuously remove one of the reaction products to shift the reaction equilibrium in order to improve yield, and in most cases the removed product is water.

The kinetics of esterification reactions between succinic acid and ethanol have been extensively investigated by many researchers (Benedict *et al.*, 2006, Delhomme *et al.*, 2012). Since the esterification reaction of succinic acid and ethanol is a second order reversible reaction, the reaction rate of diethyl succinate (r_{DES}) can be written as:

$$r_{DES} = \frac{1}{m_{cat}} \frac{1}{v_i} \frac{dn_{DES}}{dt} = 1.357 \times 10^6 \exp\left(\frac{-55.04}{RT}\right) \left(a_{SA} a_{EtOH} - \left(\frac{a_{DES} a_{H_2O}}{K} \right) \right) \quad (2.1)$$

Where; m_{cat} is the mass of the catalyst and v_i is the stoichiometric coefficient. R is the gas constant, T is the temperature. The equilibrium constant K_{eq} was experimentally determined as a function of the mole fraction and the activity coefficients of the products and reactants. This expression was obtained by correlating the kinetic data using Amberlyst 15 as a catalyst, and calculating the activity coefficients with the UNIQUAC parameters obtained in the study of the phase equilibrium of the same esterification reaction. In addition, the relationship between the reaction rates of the four components can be expressed depending on their stoichiometric factors:

$$r_{DES} = r_{H_2O} = -r_{SA} = -r_{EtOH} \quad (2.2)$$

Where, the subscripts H₂O, SA and EtOH denote water, succinic acid, and ethanol, respectively. Since the esterification reactions are investigated in batch mode, the yield of diethyl succinate can be calculated by the following equation:

$$\text{Yield of diethyl succinate (\%)} = m_{\text{DES}}/m_{\text{DES,cal}} \times 100 \quad (2.3)$$

Where, m_{DES} is the mass of diethyl succinate obtained from the experiment, and $m_{\text{DES,cal}}$ is the mass of diethyl succinate calculated from the total conversion of succinic acid.

2.3.6.1 Dual fermentation bio-refineries

In recent years, there has been an increasing effort to combine separation with reaction to improve process performance. Membrane separation technologies offer advantages over existing mass transfer processes. Such advantages can comprise; high selectivity, low energy consumption and moderate cost to performance ratio. In this regard, membrane technology has emerged as one of the viable separation processes. Since membranes allow selective permeation of one component from a multi-component mixture, these can help to enhance the conversion of reactants for thermodynamically or kinetically limited reactions via selective removal of one or more product species from the reaction mixture. When multiple reactions are involved, the yield or selectivity of a desired product, usually an intermediate, can be enhanced by controlled addition of one or more reactants and removal of one or more intermediates (Lipnizki *et al.* 1999). The combination of ethanol production and organic acid purification was illustrated in Figure 2.8.

Production of anhydrous ethanol is the necessary preliminary process in the organic acid purification. It consists of several steps including fermentation, distillation and dehydration. Fermentation of ethanol will be described in the next part. Distillation is defined as a process in which liquid or vapor mixture of two or more substances is separated into its component fractions of desired purity, by the application and removal of heat. Distillation is based on the fact that the vapor of a boiling mixture will be richer in one of the components that have lower boiling points, therefore when this vapor is cooled and condensed, the condensate will contain more volatile components. At the same time, the original mixture will contain more of the less volatile material.

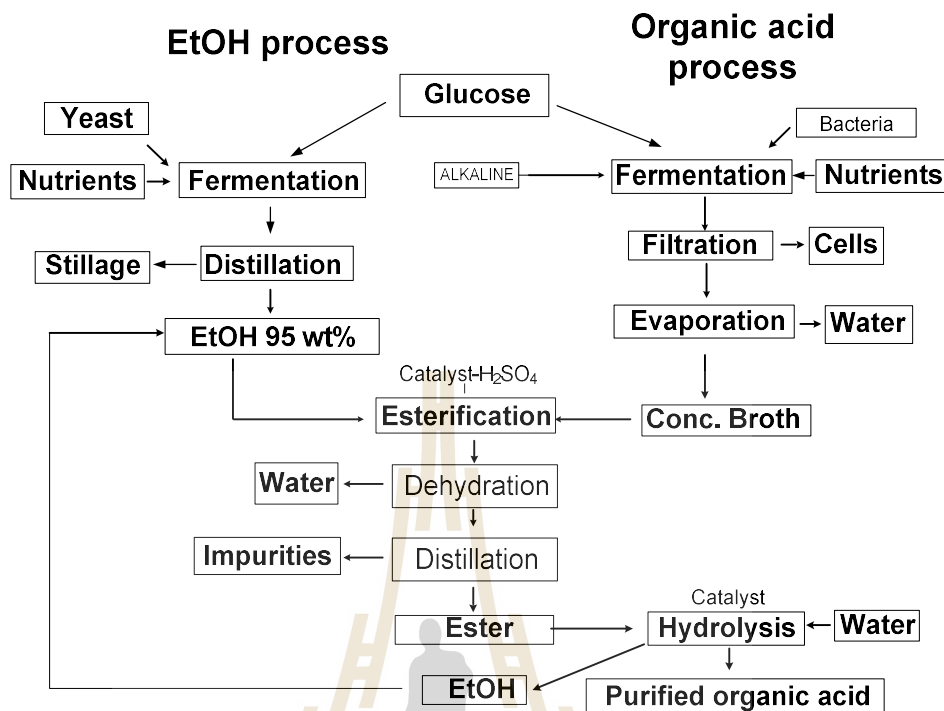


Figure 2.8 Bioconversion of glucose to ethanol and organic acid process and relationship to purified organic acid.

Recently, a high efficient lab scale distillation system using forced-mixing concept was successfully developed in SUT. The design is very unique in terms of the column internal, and distillation performance. The schematic diagram of the distillation unit based on forced-mixing concept is illustrated in Figure 2.9. In general, the column is constructed from stainless steel. A hotplate stirrer is employed as the main heating element. The length of both rectifying and stripping sections is equally 40 cm whereas the size of the reboiler is 2.5 L. A set of internal impellers is fixed on a central shaft driven by a 100 Watts variable speed motor. The middle impeller located at the feeding point serves as a dispenser whereas the lower set of impellers has a function of stripping ethanol from fermentation broth in the upward direction. The upper set of impellers forces the rising vapor to the inner wall of the column where partial condensation occurs. The high agitation rate generates close contact between the rising vapor, and descending liquid resulting in an extremely high

number of condensation-vaporization cycles. In addition, a water jacket is installed below the exit point of the column where distillate temperature (T_1) can be precisely controlled by re-circulation of a cooling liquid. As a result, high efficiency separation can be obtained within a short distance of rectifying column, and reflux is not necessary.

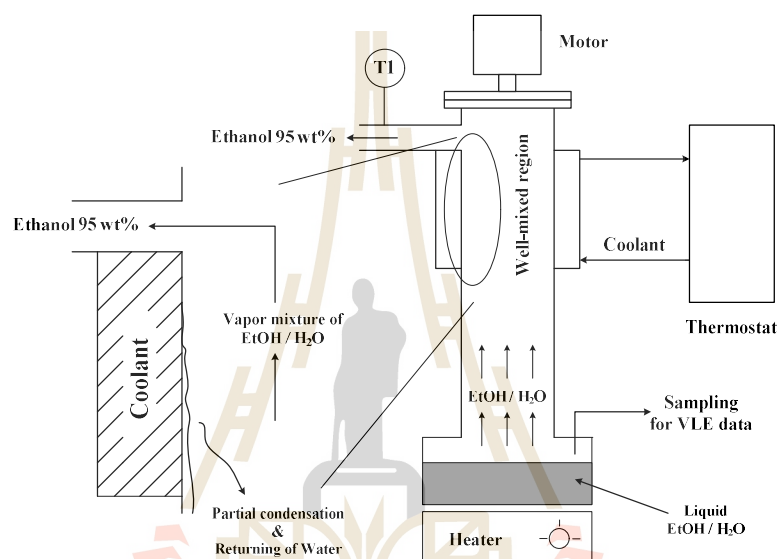


Figure 2.9 Working principle of the fractionating column based on partial condensation technique (Pimkaew and Boontawan, 2010).

The use of ceramic membranes for dehydration of ethanol solutions has already been investigated by many researchers. Modeling of the mass transfer in membrane processes is one of the fundamental aspects to understand the system performance. The adsorbent process makes use of difference in size between water and ethanol molecules. Water molecules have size of 0.28 nm while ethanol molecules have bigger size of 0.43 nm. This allows zeolite with adsorbing space of 0.3-0.4 nm to selectively adsorb water molecules while vapors pass through the bed. The distillate ethanol was dehydrated before returning to the reactor with the help of a peristaltic pump. This operation increases the life of the membrane because zeolite membranes are highly unstable in acidic

environments especially in direct contact with the acidic reactants. The esterification reaction terminated when water concentration in the reactor was lower than 0.02 wt%.

The mass balance of water over the system can be further considered according to the amount formed and the mass transfer caused by dehydration by the membrane processes as followed:

$$\frac{dn_{H_2O}}{dt} = m_{cat}r_{H_2O} - AQ_{H_2O} \quad (2.4)$$

Where, n_{H_2O} is the number of moles of water on the feed side, t is the time, m_{cat} is the mass of catalyst, r_{H_2O} is the esterification rate of water in the reactor, A is the membrane area, and Q_i is the molar flux of component I (mole.m⁻².h⁻¹), respectively.

The separation performance can be described in terms of the total permeation flux through the membrane per unit area per time, and the separation factor (α) of the membrane was defined as:

$$\alpha = \frac{w_{i,p} w_{j,f}}{w_{i,f} w_{j,p}} \quad (2.5)$$

Where $w_{i,p}$ and $w_{j,f}$ are the weight fractions of components i and j on the permeate side, and $w_{i,f}$ and $w_{j,p}$ the weight fractions of components i and j on the feed side, respectively. On the basis of the solution/diffusion model, the flux of component I across the membrane is proportional to its partial vapor pressure difference on both sides of the membrane as shown in Figure 2.10. (Pettersen and Lien, 1995):

$$J_i = \frac{dq}{dA} = Q(x_i P_F - y_i P_P) \quad (2.10)$$

Where J_i is the molar flux of the component i (mole.s⁻¹.m⁻²), q is the molar transfer rate (mole.s⁻¹), Q_i is the permeance of the component i (mole.s⁻¹.m⁻².Pa⁻¹), A is the membrane area (m²), x_i is the mole fraction in the feed side, P_F is the feed pressure (Pa), y_i is the mole fraction in the permeate, and P_P is the permeate pressure (Pa), respectively.

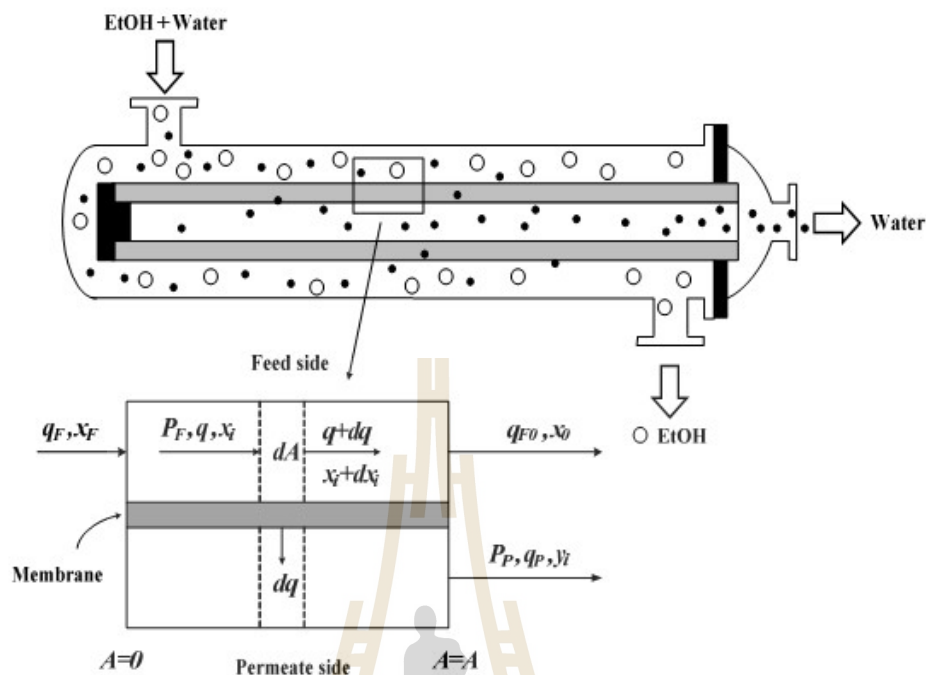


Figure 2.10 Working principle and mass transfer consideration of the VP technique (Pimkaew and Boontawan, 2010).

2.3.6.2 Pervaporation-assisted esterification

Pervaporation is a membrane separation process where one side of the membrane is in contact with the liquid feeding solution, and permeation of the migrating species through the membrane matrix is induced by the application of a vacuum pump or an inert carrier gas on the other side of the membrane (Lipnizki *et al.* 1999). The transport mechanism for the pervaporation system can be explained using the solution-diffusion model which involves two major steps. The first step involves absorption of chemical molecules onto the membrane surface. The second step is the diffusion across the membrane matrix due to partial pressure difference. The chemical compound then vaporize somewhere in the membrane, and can be obtained as a vapor under vacuum before being collected in a cold trap or condenser. Separation of the fluid mixture can be successfully achieved with a selection of membranes exhibiting both high permeation rate and good selectivity. In

combination with a reactor, pervaporation process can be used to continuously remove water formed during the esterification process with the main objective to shift the equilibrium of the reaction resulting in higher yield and volumetric productivity (Delgado *et al.*, 2008).

Benedict *et al.* (2006) studied solid-catalyzed, pervaporation-assisted esterification of lactic acid and succinic acid with ethanol. Conversions in excess of the equilibrium conversion attainable in a reactor without product separation were attained by selective removal of water from the reaction mixture by pervaporation. Stripping of water pushed the equilibrium conversion very close to unity, demonstrating the efficiency of pervaporation-aided esterification. High water flux through the pervaporation membrane was obtained by maintaining high recirculation rate of the liquid and low permeate pressure. Pervaporation performance was promoted with increasing temperature. Conventional multistage distillation was adequate to separate and recover ethyl lactate and diethyl succinate from pervaporation retentate, since the alcohol-ester mixtures under consideration are not prone to azeotrope formation. Existence of mixtures of ethanol and lactic and succinic acids in single phase at above room temperature coupled with significant difference in boiling points of the two esters contributes well to simultaneous esterification of the two acids.

2.3.6.3 Vapor permeation-assisted esterification

In contrary to pervaporation, the feed side needs to be vaporized prior to enter the vapor permeation module. In addition, the vapor feed can be pressurized and superheated resulting in higher dehydration rate as already shown in Figure 2.12.

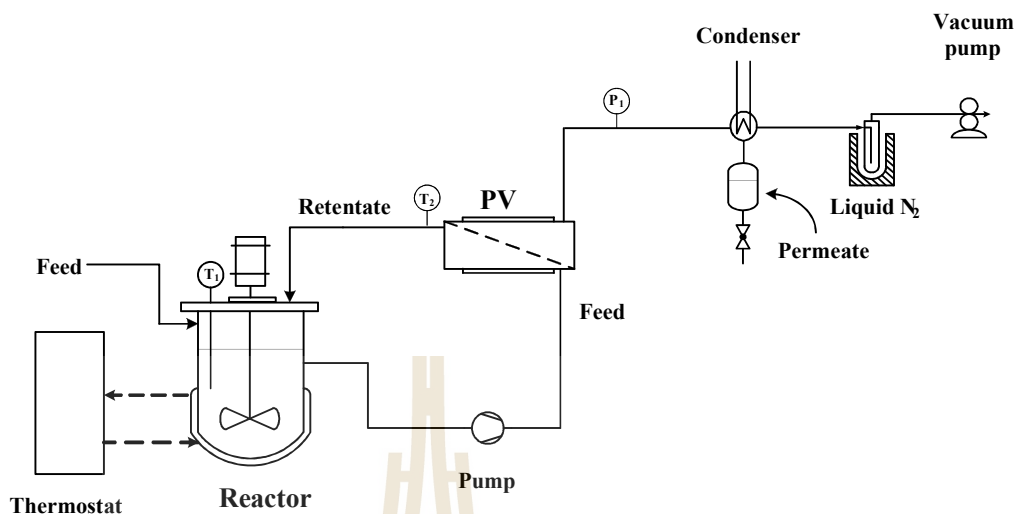


Figure 2.11 Schematic diagram of a pervaporation-assisted esterification system.

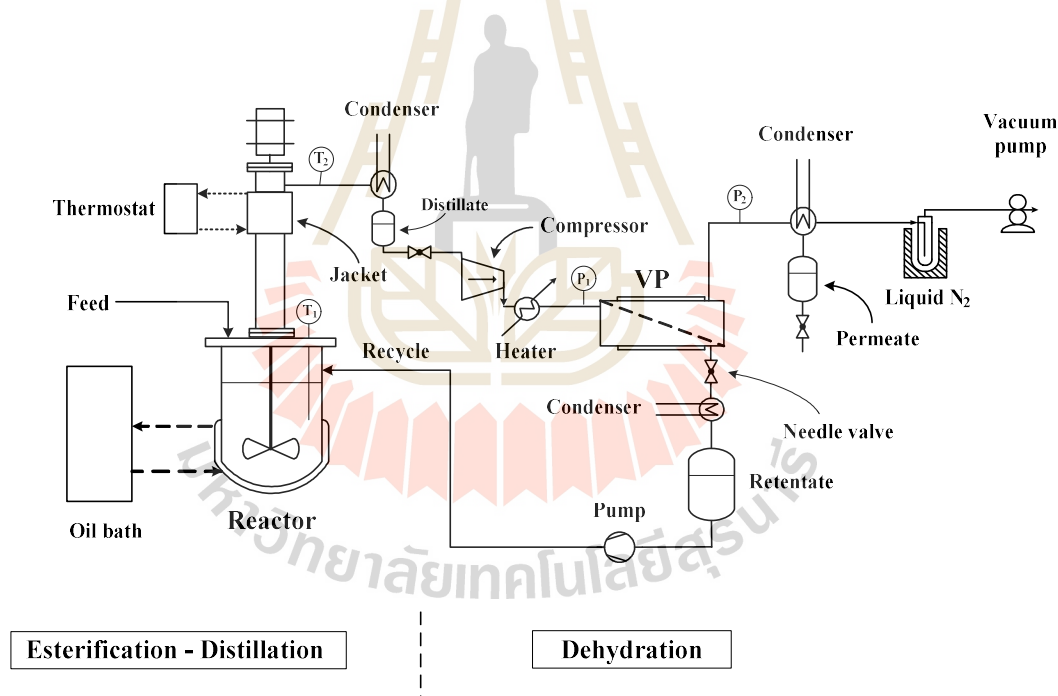


Figure 2.12 Experimental set-up for vapor permeation-assisted esterification (top), and schematic diagram of vapor permeation technique.

Khunnonkwao *et al.* (2012) studied vapor permeation-assisted esterification of lactic acid with ethanol. After fermentation, the pre-treated fermentation broth was esterified with ethanol using sulfuric acid as the catalyst. The mixture was allowed

to reach equilibrium for 2 h before increasing the temperature of the liquid mixture to its boiling point. Fractionation was carried out by control the exit temperature of the vapor. With a suitable control condition, the distillate ethanol comprised of water concentration at 5% without ethyl lactate. The temperature of the reaction solution was kept constant by using a heating circulator. The schematic diagram of the experimental setup for vapor permeation-assisted esterification was shown in Figure 2.12. The NaA zeolite membrane (Mitsui Engineering and Shipbuilding, Japan) was installed in jacket stainless steel housing. A high pressure piston pump head mounted on a 1/10 hp pump drive was employed to increase the liquid feed pressure with the help of a needle valve. Prior to entering the membrane module, the pressurized liquid feed was heated to the desired inlet temperature through a shell and tube heat exchanger by using an oil bath. On the downstream side, the permeate vapor is condensed by using two parallel glass cold traps filled with liquid nitrogen to ensure that permeate was completely collected. The downstream pressure will be maintained at approximately 3 mbar by using a vacuum pump.

2.4 Preparation of hydrophilic membranes for dehydration

The application of ceramic membranes for dehydration of ethanol/water mixtures have been investigated by many researchers using both vapor permeation and pervaporation techniques. The membranes have been prepared from various materials such as palladium alloys, microporous silica, molecular sieve carbon, zeolites, and solid oxides. As the thermal and chemical stabilities of these membranes are higher than those of polymeric membranes, they can be applied to membrane reactors for simultaneously remove water from the esterification reactions. In general, the preparation of composite ceramic membranes begins with the production of micro-porous supportive tubular membrane with the porosity of approximately 40%. Subsequently, a coating technique is used to finely coat the supportive

layer with zeolite solutions. Figure 2.13 shows a schematic diagram of the composite ceramic membrane with outer coating.

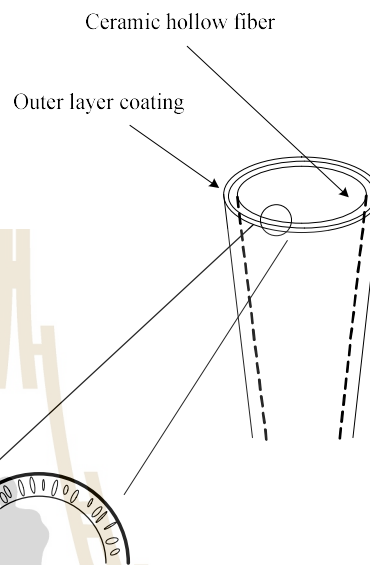
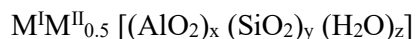


Figure 2.13 Schematic diagram of composite ceramic membrane with outer coating.

2.4.1 Zeolites A and its structure

Zeolites are water containing crystalline aluminosilicates of natural or synthetic origin with highly ordered structures. They consist of SiO_2 and AlO_4 tetrahedral, which are linked through common oxygen atoms to give a three-dimensional network through which long channels run. In the interior of these channels, which are characteristic of zeolites, water molecules and mobile alkali metal ions are located, which can be exchanged with other cations. These compensate for content. The interior of the pore system, with its atomic scale dimensions, is the catalytically active surface of the zeolite. The inner pore structure depends on the composition, zeolite type, and the cations. The general formula of zeolite is:



Where M^I and M^{II} are alkali and alkali earth metals. The indices x and y denote the oxide variables, and z is the number of molecules of water of hydration. The composition is characterized by the Si/Al atomic ratio and the pore size of zeolite

Table 2.2 Characteristic of interested zeolite (Hagen, 1999).

Type	Pore diameter (nm)	Pore aperture
Zeolite Y	0.74	12-ring
Pentasil zeolite	0.54×0.56	10-ring (ellipsoid)
Zeolite A	0.41	8-ring
Sodalite	0.26	4-ring

Zeolite A is the zeolite that shows the LTA (Linde Type A) structure. It is one of the most important industrial zeolites. Hundreds of thousands of tons of this zeolite are produced every year for application as diverse as water softening in detergents, additive in polyvinyl chloride (PVC) thermoplastic, industrial gas drying as well as production of dehydrated ethanol. The CBUs (composite building units) of LTA are the double 4 rings consist of β cage (sodalite cage) and the α cage (super cage). Zeolite A has a three-dimensional pore system and molecular can be diffuse in all three directions in space by moving across the 8-rings windows that have a free diameter (*cavity*) of approximately 4 Å. The composition of zeolite A as usually obtained from industrial manufacturers is close to $[\text{Na}_{96}(\text{H}_2\text{O})_{216}[\text{Al}_{96}\text{Si}_{96}\text{O}_{384}]]\text{-LTA}$ (Auerbach, et al., 2003)

2.4.2 Application of NaA zeolite for ethanol dehydration

Sato, *et al.* (2008) studied dehydration of ethanol solutions using hybrid distillation and vapor permeation. The NaA zeolite membrane was synthesized using a dip-coating technique on α alumina tubes with the average pore size of 0.8 microns. Effects of

operating parameters were investigated including time and temperature for seeding conditions. The synthesized membrane was tested for morphology by using scanning electron microscope and x-ray diffraction. Experimental results showed that the crystal was uniformly coated over the supportive layer with the thickness of approximately 1 μm . A high separation factor was obtained at more than 10,000 whilst the maximum water flux was observed at 31 $\text{kg}\cdot\text{m}^{-2}\cdot\text{h}^{-1}$.

Zhang and Liu (2011) fabricated the water-selective NaA zeolite membrane, which supported on a porous metal sheet at 50 μm thickness. The porous metal support was a metallic NiO sheet that contained approximately 1 μm pore size and 50% porosity. The NaA zeolite coating was carried out using 0.3 μm of zeolite for seeding and incubated at 99°C for 4 hours for hydrothermally crystal growth. High quality of NaA zeolite membrane of lower than 2 μm thickness was obtained and illustrated a water/ethanol separation factor of up to 10,000 and water permeation flux about 4 $\text{kg}\cdot\text{m}^{-2}\cdot\text{h}^{-1}$. The durability of membrane was performed in 66 hours continuously testing in vapor permeation system.

2.5 Ethanol

Ethanol, also called ethyl alcohol, is a volatile, flammable, colorless liquid, the best known as the type of alcohol found in alcoholic beverages. Ethanol is a 2-carbon alcohol with the molecular formula $\text{CH}_3\text{CH}_2\text{OH}$. Its empirical formula is $\text{C}_2\text{H}_6\text{O}$. Ethanol is often abbreviated as EtOH, using the common organic chemistry notation of representing the ethyl group (C_2H_5). Physical properties of alcohol fuels are shown in Table 2.3.

Ethanol can be produced by either biological or chemical synthesis. Bio-ethanol has a higher octane number, broader flammability limits, higher flame speeds and higher heats of vaporization than gasoline. These properties allow for a higher compression ratio, shorter burn time and leaner burn engine, which lead to theoretical efficiency advantages over

gasoline in an internal combustion engine (Balat *et al.*, 2005). However, disadvantages of bio-ethanol include its lower energy density than gasoline (bio-ethanol has 66% of the energy that gasoline has), its corrosiveness, low flame luminosity, miscibility with water, and toxicity to ecosystems (MacLean and Lave, 2003).

Table 2.3 Physico-chemical properties of ethanol (Najafpour and Lim, 2002).

Properties	Value
Empirical formula	CH ₃ CH ₂ OH
Molecular weight	46
Normal boiling point, °C	78.32
Critical temperature, °C	243.1
Density, d ₄ ²⁰ , g/ml	0.7893
Heat of combustion at 25°C, J/g	29676.69
Auto ignition temperature, °C	793.0

2.5.1 The use of bio-ethanol as fuel and environmental effects

The environmental effects of bio-ethanol used as an alternative fuel have been dealt with in numerous publications. It appears that, the main reasons of the success of bio-ethanol are the following (Baeyens *et al.*, 2015);

- Used as renewable energy to partially substitute oil and increase security of supply
- Used as octane enhancer in unleaded gasoline to replace methyl-tert-butyl-ether (MTBE)
- Used as oxygenated compound for clean combustion of the gasoline, thus reducing the tailpipe emissions and improving the ambient air quality

- Used as renewable fuel to reduce CO₂ emissions and its contribution to a reduces effect on climate change

The specific recent literature related the environmental effects has been listed in Table 2.4. The environmental advantages of using ethanol as a fuel are recognized since it reduces harmful tailpipe emission of carbon monoxide, particulate matter and nitrogen oxide. Argonne National Laboratory (ANL) has completely analyzed the greenhouse gas emissions of different engine and fuel combustions. Comparing ethanol blends with pure gasoline, they demonstrated reductions of 8% with the bio-diesel known as B20, 17% with the conventional E85 ethanol blend, and a reduction of emissions by 64% when using cellulosic ethanol. Regardless of these positive effects, literature also draws our attention to the fact that ethanol combustion in an internal combustion engine can increase the emission of products of incomplete combustion, leading to a significantly larger photo-chemical reactivity that generates much more ground level ozone.

2.5.2 Ethanol fermentation

Ethanol fermentation is a biological process in which sugar such as glucose, fructose or sucrose are converted to ethanol. The conversion of glucose to 2 pyruvates within 10 intermediate stages is known as Glycolysis pathway. (Figure 2.14), involves the production of 2 moles each of ethanol, CO₂, and ATP per mole of glucose fermented. Therefore, on a weight basis, each gram of glucose can theoretically give 51 % alcohol. The yield attained in practical fermentations, however, does not exceed 90-95% of the theoretical value. This is due to the requirement for some nutrients to be utilized in the synthesis of new biomass and other cell maintenance-related reactions. Side reactions also occur in the fermentation (usually to glycerol) which many consume up to 4-5% of the total substrate. If these reactions could be eliminated, an additional 2.7% yield of ethanol from substrate would result (Roehr, 2001).

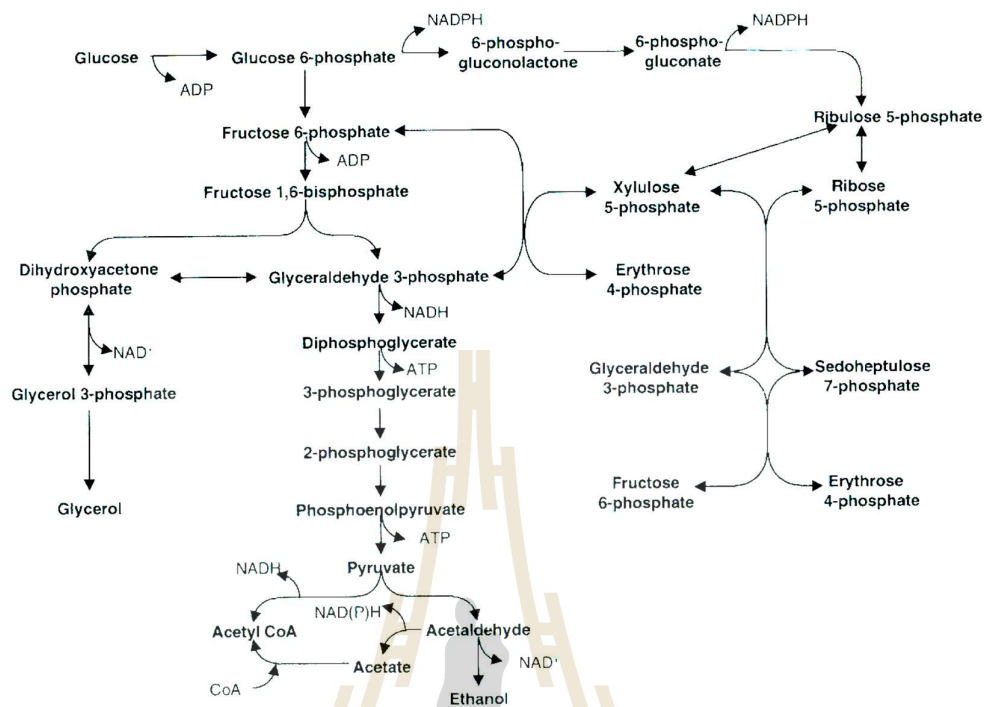


Figure 2.14 Pathways for dissimilation of glucose to ethanol in yeast via glycolysis and the hexose monophosphate shunt.

Source: Boulton and Quain (2001)

2.5.3 Extractive fermentation

There are many minor problem associated with ethanol fermentation processes to be solved when optimal operation is the target. One of them is the lack of the processes reliability in the presence of fluctuation in operational conditions, which lead to changes in the kinetic behavior, with impact on yield, productivity and conversion. The typical ethanol fermentation processes yield approximately 10 – 14% in the fermentation broth due to low concentration of substrate used in this process. In addition, these conditions are necessary since conventional alcoholic fermentation is a typical inhibitory process, with cells growth rate affected by cellular, substrate and product concentration (Rivera *et al.*, 2006).

Table 2.4 The literature related the application of fuel-ethanol in the environmental effects.

Authors	Objectives	Main results
Turner <i>et al.</i> , 2011.	Combustion performance of bio-ethanol at various blend ratios in gasoline direct injection engine	<ul style="list-style-type: none"> - Faster combustion, higher in-cylinder pressure; - Similar or reduced NO_x emission; - Reduced CO emission; - Increased engine efficiency.
Yoon and Lee, 2012	Bio-ethanol affects combustion and emission reduction in an SI engine	<ul style="list-style-type: none"> - CO and volatile HC decrease; - NO_x tends to increase as ambient air temperature increases.
Bhupendra <i>et al.</i> , 2011	Adding ethanol in a small capacity Diesel engine	<ul style="list-style-type: none"> - Optimum 15% of ethanol; - Unburned hydrocarbon emissions decrease; - Load smoke opacity is lowest at 14% ethanol.
Lopez-Aparicio and Hak, 2013	Use of bio-ethanol fueled buses by air pollution screening and on-road measurements	<ul style="list-style-type: none"> - Higher emissions of acetaldehyde and acetic acid during driving conditions
Saxena <i>et al.</i> , 2012	Wet ethanol in HCCI engines with exhaust heat recovery	<ul style="list-style-type: none"> - HCCI engines can use ethanol fuel with up to 20% H₂O; - Low NO_x, CO emissions at high intake pressures, high equivalence ratios, and delayed combustion timings.
Masahiro <i>et al.</i> , 2010	NO _x -PM trade-off in a single cylinder diesel engine by means of bio-ethanol and exhaust gas recirculation (EGR)	<ul style="list-style-type: none"> - Very low levels of NO_x and PM (meeting 2009 Japanese Standards); - 50% ethanol blended diesel fuel and high EGR ratios are preferred.
Hansdah <i>et al.</i> , 2013	DI diesel engine fueled with bio-ethanol diesel emulsions	<ul style="list-style-type: none"> - 5, 10 and 15% ethanol addition tested; - NO reduced by 4%; - Smoke emission cut by 20%; - 5% blend has best performance.
Grisel and Edgar, 2008	Emission abatement by bio-ethanol and diesel/bio-ethanol blends	<ul style="list-style-type: none"> - Addition of bio-ethanol to diesel decreases particulate matter (PM) generation and increase the diesel PM oxidation.
Mohammad <i>et al.</i> , 2008	Integrated bio-ethanol fermentation and CHP	<ul style="list-style-type: none"> - All heat required in the plant can be generated from biogas produced by digesting the stillage.
Wukovits <i>et al.</i> , 2007	CHP using various blends of gasoline in an IC engine	<ul style="list-style-type: none"> - Cylinder pressure and fermentation increase at higher bio-ethanol blends; - CO emissions are reduced by up to 50%

In recent times, our lab has been successfully developing extractive fermentation of ethanol using vacuum fractionation technique with high efficiency column and used glucose as a carbon source. The experimental set-up diagram was illustrated in Figure 2.15. After 1 hr of inoculation, the pressure of system was decreased to 45 mBar by using vacuum pump. The fermentation broth began to boil and vapor of ethanol/water was fractionated and the temperature of the exiting vapor was maintained at 19.4°C. The volumetric production of this technique was more than twofold that of conventional fermentation (12.5 g.L⁻¹.hr⁻¹). The concentration of the distillate ethanol was typically 94 wt% while the relative viability of cells was 95%. Due to the extremely high relative viability of cell at end of fermentation, glucose powder was added to fermentation broth for the repeat-batch fermentation. It was found that, the addition of glucose was repeated for another 8 times, and system was very stable for 230 hrs. Almost 2000 g of distillate ethanol was continuously collected at 94wt%. After that, the fermentation performance was reduced due to the accumulation of lactic acid in the medium.

2.6 Process simulation program

Process simulation is used for the design, development, analysis, and optimization of technical processes and is mainly applied to chemical plants and chemical processes, but also to power stations, and similar technical facilities. Process simulation is a model-based representation of chemicals, physical, biological and other processes and unit operation in software. Basic prerequisites are a thorough knowledge of chemical and physical properties of pure components and mixtures, of reactions, and of mathematical models which, in combination, allow the calculation of a process in computers. Process simulation software describes processes in flow diagrams where unit operations are positioned and connected by product streams. The software has to solve the mass and energy balance to find a stable operating point. The goal of a process simulation is to find optimal conditions for an

examined process. This is essentially an optimization problem which has to be solved in an iterative fashion. Process simulation always uses models which introduce approximations and assumptions but allow the description of a property over a wide range of temperatures and pressures which might not be covered by real data. Models also allow interpolation and extrapolation - within certain limits - and enable the search for conditions outside the range of known properties.

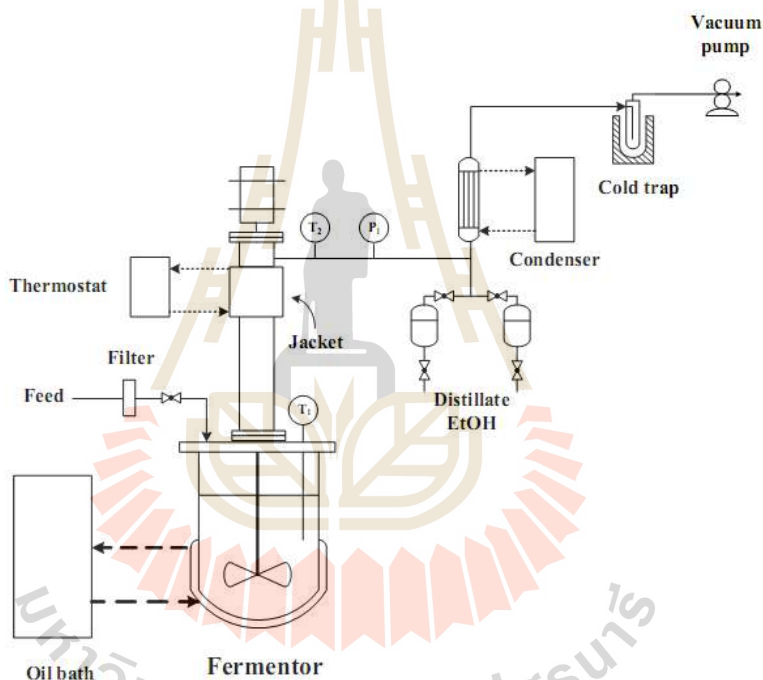


Figure 2.15 Experimental setup for extractive fermentation of ethanol using vacuum fractionation technique.

The purpose of analysis/simulation is to model and predict the performance of a process. It involves the decomposition of the process into its constituent elements (e.g. units) for individual study of performance. The process characteristics e.g. flow-rates, compositions, temperatures, pressures, properties, equipment sizes, etc. are predicted using analysis techniques. These techniques include mathematical models, empirical correlations and computer-aided process simulation tools (e.g. ASPEN PLUS). In addition, process

analysis may involve the use of experimental means to predict and validate performance. Therefore, in process simulation, we are given the process inputs and flow-sheet and are required to predict process outputs. The lab will focus on ASPEN Plus. It is a computer-aided software which uses the underlying physical relationships (e.g., material and energy balances, thermodynamic equilibrium, rate equations) to predict process performance (e.g., stream properties, operating conditions, and equipment sizes (Eden and Abdelhady, 2007). There are several advantages of computer aided simulation:

- Allows the designer to quickly test the performance of synthesized process flowsheets and provide feedback to the process synthesis activities.
- Can be coordinated with process synthesis to develop optimum integrated designs.
- Minimizes experimental and scale-up efforts.
- Explores process flexibility and sensitivity by answering "what-if" questions.
- Quantitatively models the process and sheds insights on process performance.

2.7 References

- Baeyens, J., Kang, Q., Appels, L., Dewil, R., Lv, Y. and Tan, T. (2015). Challenges and opportunities in improving the production of bio-ethanol. **Prog. Energ. Combust.** 47: 60-88.
- Balat, M. (2005). Global bio-fuel processing and production trends, **Energ. Explor. Exploit.** 25:195–218.
- Beauprez, J. J., De Mey, M. and Soetaert, W. K. (2010). Microbial succinic acid production: Natural versus metabolic engineered producers. **Process Biochem.** 45(7): 1103 – 1114.

- Benedict, D. J., Parulekar, S. J. and Tsai, S. P. (2006). Pervaporation-assisted esterification of lactic and succinic acids with downstream ester recovery. **J. Membr. Sci.** 281 (2006) 435-445.
- Bhupendra, S.C., Naveen, K., Shyam, S.P. and Yong, D.J. (2011). Experimental studies on fumigation of ethanol in a small capacity diesel engine. **Energy.** 36: 1030 - 1038.
- Boulton, C. and Quain, D. (2001). **Brewing yeast and fermentation.** Blackwell Science Ltd, Blackwell Publishing Company.
- Cheng, K. K., Zhao, X. B., Zeng, J., Wu, R. C., Xu, Y. Z., Liu, D. H. and Zhang, J. A. (2012) Downstream processing of biotechnological produced succinic acid, **Appl. Microbiol. Biotechnol.** 95: 841-850.
- Choi, J. H., Fukushi, K. and Yamamoto, K. (2008). A study on the removal of organic acid from waste water using nanofiltration membrane. **Sep. Purif. Technol.** 59: 17 - 25.
- Delgado, P., Sanz, M. T. and Beltrán, S. (2008). Pervaporation study for different binary mixtures in the esterification system of lactic acid with ethanol. **Sep. Purif. Tech.** 64: 78–87.
- Delhomme, C., Goh, S. L. M., Kühn, F. E. and Weuster-Botz, D. (2012). Esterification of bio-based succinic acid in biphasic systems: Comparison of chemical and biological catalysts. **J. Mol. Catal. B-Enzym.** 80: 39–47.
- Eden, M.R. and Abdelhady A., (2007), Introduction to Aspen Plus Simulation, Physical Properties and Selection of Thermodynamic Models, Chemical Engineering Department Auburn University CHEN 4460.
- Grisel, C. and Edgar, A. (2008). Bioethanol and diesel/bioethanol blends emissions abatement. **Fuel.** 87: 3537 - 3542.
- Hansdah, D., Murugan, S. and Das, L.M. (2013). Experimental studies on a DI diesel engine fueled with bioethanol-diesel emulsions. **Alex. Eng. J.** 52: 267 - 276.

- Hilal, N., Al-Zoubi, H., Darwish, N. A., Mohammad, A. W. and Abu Arabi, M. (2004). A comprehensive review of nanofiltration membranes: treatment, pretreatment, modeling, and atomic force microscopy. **Desalination**. 170: 281–308.
- Khunnonkwao, P., Boontawan, P., Haltrich, D., Maischberger, T. and Boontawan, A. (2012). Purification of L-(+)-lactic acid from pre-treated fermentation broth using vapor permeation-assisted esterification. **Process Biochem**. 47: 1948-1956.
- Li, Q., Wang, D., Wu, Y., Li, W. L., Zhang, Y., Xing, J. and Su, Z. (2010). One step recovery of succinic acid from fermentation broths by crystallization. **Sep. Purif. Technol**. 72: 294-300.
- Lin, S. K. C., Du, C., Koutinas, A., Wang, R. and Webb, C. (2008). Substrate and product inhibition kinetics in succinic acid production by *Actinobacillus succinogenes*. **Biochem. Eng. J**. 41(2): 128–135.
- Lipnizki, F., Field, R. W. and Ten, P. K. (1999). Pervaporation-based hybrid process: a review of process design, applications and economics. **J. Membr. Sci**. 153: 183 – 210.
- Lopez-Aparicio, S. and Hak, C. (2013). Evaluation of the use of bioethanol fuelled buses based on ambient air pollution screening and on-road measurements. **Sci. Total Environ**. 452 -453:40 - 49.
- Lubsungneon, J., Srisuno, S., Rodtong, S. and Boontawan, A. (2014). Nanofiltration coupled with vapor permeation-assisted esterification as an effective purification step for fermentation-derived succinic acid. **J. Membr. Sci**. 459: 132-142.
- Masahiro, I., Shohei, Y., Hironobu, U. and Daisaku, S. (2010). Remarkable improvement of NO_xePM trade-off in a diesel engine by means of bioethanol and EGR. **Energy**. 35: 4572 - 4581.
- McKinlay, J. B., Vieille, C., Zeikus, J. G. (2007). Prospect for a bio-based succinate industry. **Appl. Microbiol. Biotechnol**. 76: 727-740.

- Mohammad, A., Barat, G. and Iman, B. (2008). Technical comparison of a CHP using various blends of gasohol in an IC engine. **Renew. Energy**. 33: 1469 - 1474.
- Najafpour, G.D. and Lim, J. (2002). Evaluation and isolation of ethanol producer strain SMP-6. **Regional Symposium on Chemical Engineering**. 229–236.
- Petersen, R. J. (1993). Composite reverse osmosis and nanofiltration membranes. **J. Membr. Sci.** 83: 81–150.
- Pettersen, T. and Lien, K.M. (1995). Design of hybrid distillation and vapor permeation processes. **J. Membr. Sci.** 99: 21-30.
- Pimkaew, S. and Boontawan, A., (2010). Process optimization for motor fuel grade ethanol production using hybrid vapor permeation and pressure swing adsorption technique. **Eur. J. Sci. Res.**, 644-646.
- Rivera, E. C., Costa, A. C. (2006). Evaluation of optimization techniques for parameter estimation: Application to ethanol fermentation considering the effect of temperature. **Process Biochem.** 41: 1682 – 1687.
- Roehr, M. (2001). *The Biotechnology of Ethanol: Classical and future applications*. Chichester: Wiley-VCH. 232 pp.
- Samuelov, N. S., Lamed, R., Lowe, S. and Zeikus, J. G. (1991). Influence of CO₂-HCO₃ levels and pH on growth, succinate production, and enzyme activities of *Anaerobiospirillum succiniciproducens*. **Appl. Environ. Microbiol.** 57(10): 3013 – 3019.
- Sato, K., Sugimoto, K. and Nakane, T. (2008). Preparation of higher flux NaA zeolite membrane on asymmetric porous support and permeation behavior at higher temperatures up to 145 °C in vapor permeation. **J. Membr. Sci.** 307: 181–95.
- Saxena, S., Schneider, S., Aceves, S. and Dibble, R. (2012). Wet ethanol in HCCI engines with exhaust heat recovery to improve the energy balance of ethanol fuels. **Appl. Energy**. 98: 448 - 457.

- Song, H. and Lee, S. Y. (2006). Production of succinic acid by bacterial fermentation. **Enzyme Microb. Technol.** 39: 352-361.
- Song, H., Huh, Y. S., Lee, S. Y., Hong, W. H. and Hong, Y. K. (2007). Recovery of succinic acid produced by fermentation of a metabolically engineered *Mannheimia succiniciproducens* strain. **J. Biotechnol.** 132: 445-452.
- Turner, D, Xu, H.M., Cracknell, R.F., Natarajan, V. and Chen, X.D. (2011). Combustion performance of bio-ethanol at various blend ratios in a gasoline direct injection engine. **Fuel.** 90: 1999-2006.
- Wukovits, W., Pfeffer, M., Liebmann, B. and Friedl, A. Integration of the bio-ethanol process in a network of facilities for heat and power production from renewable sources using process simulation. In: 17th European symposium on computer aided process engineering; 2007.
- Yoon, S.H. and Lee, C.S. (2012). Effect of undiluted bioethanol on combustion and emissions reduction in a SI engine at various charge air conditions. **Fuel.** 97: 887 - 890.
- Zeikus, J. G., Jain, M. K. and Elankovan, P. (1999). Biotechnology of succinic acid production and markets for derived industrial products. **Appl Microbiol Biotechnol.** 51(5): 545 – 552.
- Zhang, J. and Liu, W. (2011). Thin porous metal sheet-supported NaA zeolite membrane for water/ethanol separation. **J. Membr. Sci.** 371: 197 – 210.
- Zhang, X., Jantama, K., Shanmugam, K. T. and Ingram, L. O. (2009). Reengineering *escherichia coli* for succinate production in mineral salts medium. **Appl. Environ. Microbiol.** 75(24): 7807 – 7813.

CHAPTER III

BATCH EXTRACTIVE AND FED-BATCH EXTRACTIVE FERMENTATION OF ETHANOL USING BLACKSTRAP MOLASSES AS A CARBON SOURCE

3.1 Abstract

The batch extractive and fed-batch extractive method of ethanol production using blackstrap molasses as a carbon sources was investigated. The effect of initial substrate and product inhibition was analyzed. The maximum product concentration (P'_m) on specific ethanol production was approximately 100 g, while the productivity decreased gradually when ethanol concentration in the fermented broth increased. The appropriate initial molasses concentration was selected at 25 °Brix or 1:4 molasses/water dilution which results in 4.87 g.L⁻¹.hr⁻¹ ethanol productivity and 80% relative viability after 24 hours of fermentation. The extractive fermentation illustrated the reduction of product inhibition effect by continuous removal the ethanol from the fermented broth. A 60% relative viability was observed in fermented broth with a higher productivity value. For the reason of living cells present in the medium, fed-batch extractive fermentation was performed by adding the concentrated molasses in to the fermented medium after the fermentation had finish. The ethanol was continuously fractionated from the system at the average rate of 10.2 g/h with the concentration of approximately 80 wt% with the 8 cycles of fermentation. Nevertheless,

calculated ethanol productivity and relative viability for each fermentation cycle decrease gradually due to the accumulation of toxic substances in the fermented broth.

Keywords: Extractive fermentation, Blackstrap molasses, Product inhibition

3.2 Introduction

Sugarcane molasses is a by-product of sugar production from sugarcane juice, which contains valuable nutrients such as minerals, proteins and high-quality fermentable sugar. Thus, sugarcane molasses was typically used as a cattle feed, specialized yeast propagation or as a flavoring agent in food (Gopal and Kammen, 2009). Office of Agricultural Economics (OAE) of Thailand reported that approximately 104 million tons of sugarcane is cultivated in 2015 while approximately 4.3 million tons of molasses was produced. Sugarcane processing was divided into ethanol production (2.9 million tons, 68%), another industrial (1 million ton, 22%) and export to another country (0.41 million ton, 10%) (Office of Agricultural Economics of Thailand, 2016). Thus, Thailand is a world-class sugarcane cultivator and molasses producer.

Fuel ethanol represent high purity ethanol with less than 0.02% water. It is one of the most promising alternative future fuels due to its high energy content, uncomplicated production process and because it can be produced from agricultural residual as a carbon source. However, a major challenge in the production of ethanol is the separation and purification (approximately 70% of the overall ethanol production cost). For a typical process, the end-product inhibition during the fermentation occurs at approximately 10-14 wt% ethanol in the fermentation broths. It is generally recognized that ethanol fermentation suffers from both substrate and product inhibition. The Monod equation involved product and substrate inhibition model can be described as follows (Lin *et al*, 2008);

$$v = v_{\max} \left(\frac{S}{K'_S + S + (S^2 / K'_i)} \right) \left[\prod \left(1 - \frac{P}{P'_m} \right) \right]^{a_i} \quad (3.1)$$

Where; v is the specific production rate, v_{\max} is the maximum specific production rate, S is the substrate concentration, K'_S is the saturation constant, K'_i is the substrate inhibition constant, P is the product concentration, and P'_m is the maximum product concentration, respectively. In addition, the superscript a_i represents the exponential constant of the inhibitory product, respectively.

Ethanol fermentation combination with *in situ* product separation has attracted considerable interests over the past few decades. It combines biochemical reaction with selective mass transport of ethanol from the reaction site. Since, the ethanol concentration is kept low in the bioreactor, the reaction equilibrium shifts forward resulting in an increase of the product yield (Lye and Woodley, 1999). In order to maximize fermentation performance, different methods have been introduced to simultaneously separate the toxic ethanol product from fermentation broths including pervaporative membrane bioreactor (Thongsugmak and Sirkar, 2009; Chen *et al*, 2012; O'Brien *et al*, 2004), membrane distillation bioreactor (Gryta *et al*, 2000; Lewandowicz *et al*, 2011), gas stripping (Tayler *et al*, 2010), solvent extraction (Cordana and Sánchez, 2007), and vacuum fermentation (Nguyen *et al*, 2011). Nevertheless, the distillate or permeate ethanol products obtained from these techniques contain a large amount of water typically in the range between 20-40 wt%. As a result, an additional distillation step is required in order to obtain 95wt% ethanol prior to dehydration step.

Recently, our lab has been successfully developed extractive fermentation of ethanol using a vacuum fractionation technique with a high efficiency column and used glucose as a carbon source. The pressure of the system was decreased to 45 mbar by using a vacuum pump for the evaporation of ethanol/water and fractionated at the temperature of the exiting vapor was maintained at 19.4°C. The volumetric productivity of this technique was double

than the conventional fermentation at 12.5 g/L hr., while obtaining distilled ethanol at 94 wt%. In addition, this process has been successfully done for the repeat-batch fermentation. It was found that, the addition of glucose was repeated for another 8 times, and system was very stable for 230 hrs. Distillate ethanol was continuously collected for almost 2000 g.

In this research part, the extractive fermentation of ethanol was economically and systemically developed. Blackstrap molasses was used as a carbon source instead of sugar because of its abundance and lower price. The data from conventional and fed-batch extractive fermentation was used for the scaling-up to the industrial plant size. The extractive fermentation process from blackstrap molasses was optimized using ASPEN PLUS.

3.3 Methodology

3.3.1 Materials

- Blackstrap molasses used as a carbon source for fermentation and extractive fermentation process was purchased from Mitr Phol sugar cooperation, Chaityaphum.
- Yeast for fermentation was a dried-baker yeast purchased from a local bakery's shop in NakhonRatchasima.
- All chemicals for the experiment were purchased from Sigma-Aldrich (imported by Italmar (Thailand) Co. Ltd.).

3.3.2 Conventional and extractive fermentation of ethanol

Extractive ethanol fermentation was performed in a 2 liters reactor connected to a high efficiency fractionating column. The flow diagram and real experimental set-up is shown in Figure 3.1. The concentration of blackstrap molasses medium was varied for the fermentative optimization. The 1.8 litre working volume of blackstrap molasses medium was introduced to the bioreactor by a peristaltic pump, di-ammonium phosphate and citric acid were supplemented as nitrogen sources. The 25 g/L of dried-baker yeast was added to the reactor. During the fermentation, system pressure was reduced to approximately 40 mbar by using a suction water pump system (EYELA A1000S, Japan). The temperature was controlled at 37°C and the fermentation broth was stirred continuously at 100 rpm, while antifoam was interval supplemented during the fermentation. The ethanol/water vapor mixture was continuously boiled from the bioreactor, and enters the distillation column. The temperature of column cooling region was varied for the appropriate product concentration and flow rate. Samples of the fermentation broth were collected every 6 hrs. Viable cell count, reducing sugar and ethanol content from both medium and distillate were collected and analyzed. The various organic acids were analyzed using high performance liquid chromatography (HPLC), fusel oil including butanol and propanol as well as volatile compounds including acetaldehyde, isoamyl alcohol, n-amyl alcohol were determined using gas chromatography (GC).

3.3.3 Fed-batch extractive fermentation

The condition of fed-batch extractive fermentation was carried out according with batch extractive fermentation. After 24 hours of fermentation, raw blackstrap molasses was added into the reactor to start the next fermentation cycle. The concentrated molasses was supplemented every 24 hours of the fermentation period as long as possible. The yield

and productivity of ethanol fermentation for each cycles were calculated. The fermentation was stopped when the productivity and viable cell count approached zero.

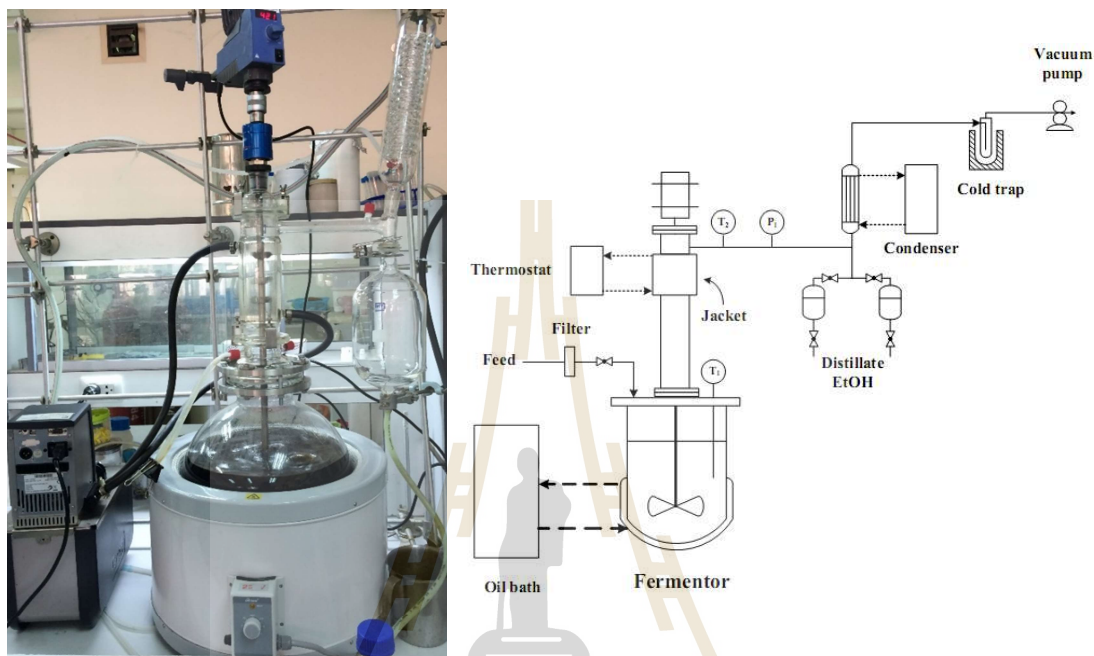


Figure 3.1 The actual picture (A) and diagram (B) of the laboratory-scale extractive fermentation.

3.3.4 Analysis

3.3.4.1 Reducing sugar of fermented molasses

The amount of reducing sugar from fermented molasses was analyzed according to Miller (1951). One mL of diluted wort was mixed with 1 mL of DNS solution (10 g of 3, 5-dinitrosalicylic acid, 300 g of Potassium sodium tartrate ($\text{KNaC}_4\text{H}_4\text{O}_6$) in 200 mL of 2 N Sodium hydroxide (NaOH) and adjusted to 1 litre with RO water). The mixtures were mix thoroughly and development of color was conducted by boiling the reaction tube for 5 min. The concentration of reducing sugar was calculated against standard solutions with known glucose concentration (0.2, 0.4, 0.6, 0.8, and 1.0 g/L).

3.3.4.2 Ethanol, fusel oil and volatile compound concentrations

Ethanol, fusel oil including propanol, butanol and volatile compound concentrations was analyzed using a gas chromatograph (GC) equipped with a flame ionization (FID) detector (SRI Instrument, USA). Helium, 99.99% pure, was used as carrier gas. The GC column (Carbowax®, Restek, USA) is a 30 m × 0.32 mm bonded phase fused silica capillary column. The injector and detectors were set at 250 and 300 °C. The injection volume was 1 µL. The oven was operated at programmed increasing temperature, from 50 to 250 °C at the rate of 15 °C/min.

3.3.4.3 Organic acid concentrations

Organic acids concentration were analyzed by HPLC (Agilent 1200, Agilent Technology Inc., U.S.A.), and quantification by UV detection was made at the wavelength of 210 nm. Samples was analyzed using a mobile phase of 1% acetonitrile + 99% 20 mM Na₂HPO₄ (pH 2.0) at a flow rate of 1 mL/min. The HPLC column is ZORBAX SB-Aq (4.6 mm × 150 mm). The column oven was maintained at 35 °C.

3.3.4.4 Viable cell count

Viable cell count of yeast cells in the fermentation medium was performed regularly during fermentation using a haematocytometer. The fermentation medium was diluted with DI water to an appropriate cell concentration and then mixed with methylene blue solution (0.1 g methylene blue in 100 mL water) before observation under microscope. The concentration of cell was calculated according to Rigother *et al.* (1994).

3.4 Results and discussions

3.4.1 Substrate and product inhibition effect

Substrates and product inhibition kinetics were individually studied in order to understand the effect of each compound on fermentation performance. In this experiment, glucose was used to study the substrate inhibition effect. For the substrate inhibition kinetics, the effect of initial glucose concentration ranging from 0-400 g/L on the specific ethanol productivity are presented in Figure 3.2A. The result showed that the glucose inhibition effect on specific ethanol productivity, the highest value of 4.08 g ethanol.g⁻¹.h⁻¹ was observed at a glucose concentration of 100 g/l. The value slowly decreases with increasing glucose concentration. The calculated saturation constant (K_s) and the substrate inhibition constant (K_i) were 8.92 and 620.71 g/L, respectively. The maximum specific ethanol production rate was found between 200-300 g/L of glucose.

In case of substrate inhibition, ethanol concentration is the most important factor on the fermentation performance. The specific ethanol productivity as a function of initial ethanol concentration was shown in Figure 3.2B. The calculated maximum product concentration (P'_m) on specific ethanol production was approximately 100 g. That means, the fermentative yeast activity was about zero when ethanol in medium was presented a concentration was 100 g/L. The specific production rate (ν) was zero when the product concentration (P) is equal to P'_m in accordance with Eq. (3.1). Experimental data confirmed that ethanol concentration is an important factor on fermentation performance.

3.4.2 Effect of initial molasses concentration on fermentation performance

Previous experiments showed that, initial glucose concentration affects the yeast activity and ethanol productivity. Sugarcane molasses was diluted to 25, 30, 35, 45, 60 °Brix to further investigate the suitable starting sugar concentration for extractive

fermentation. Figure 3.3 show the time-dependence of sugar and ethanol concentration and percentage viability of yeast. Satisfactory results of yeast survival occurred at 25 – 45 °Brix (70 – 80 wt%) after the end of fermentation. The highest value of 78 g/L ethanol concentration was obtained at 25 and 30 °Brix. It was concluded that, higher concentration of sugar affected on activity of yeast according to the results of the previous experiment.

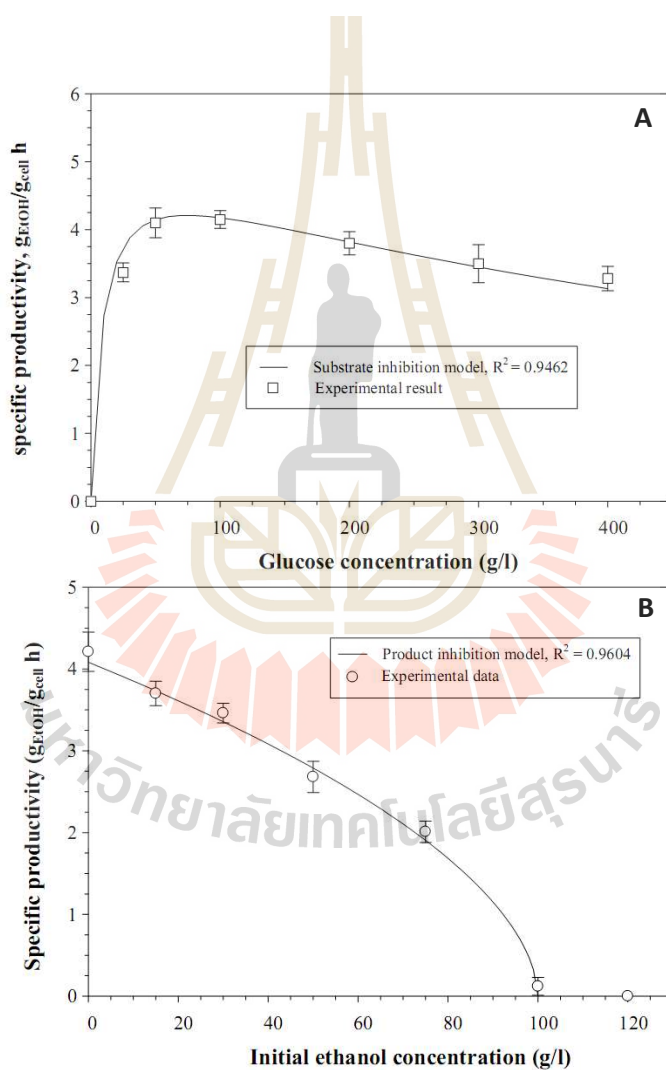


Figure 3.2 Variation of the specific productivity as a function of the substrate (A), and initial ethanol concentration (B).

Therefore, the maximum of ethanol productivity was 7.18 g/L.hr at the initial sugar concentration of 35% (Table 3.1). In addition, decrease in productivity was observed at more than 50 °Brix. Some authors have reported that higher concentration of substrates inhibits growth and fermentation of yeast as a result of high osmotic pressure (Nishino *et al.*, 1985; Takeshige and Ouchi, 1995). On the other hand, higher dilution increases equipment and process cost (e.g., reactor size, distillation boil-up duty). Siqueira *et al.* (2008) reported that the most suitable initial concentration was 30 °Brix of soybean molasses as a carbon source. Stehlik-Tomas *et al.* (1997) studied initial sugarcane molasses concentration in batch, fed-batch and continuous process. They optimized 24 °Brix as optimal for ethanol production. Other authors also reported that yeast growth on beet molasses medium was significantly retarded when the initial sugar concentration was greater than 120 g/L (Wolniewiez *et al.*, 1990). In this work, 25 °Brix or 1:4 molasses/water dilution was selected for study in the laboratory, pilot as well as industrial scale out of economical reasons.

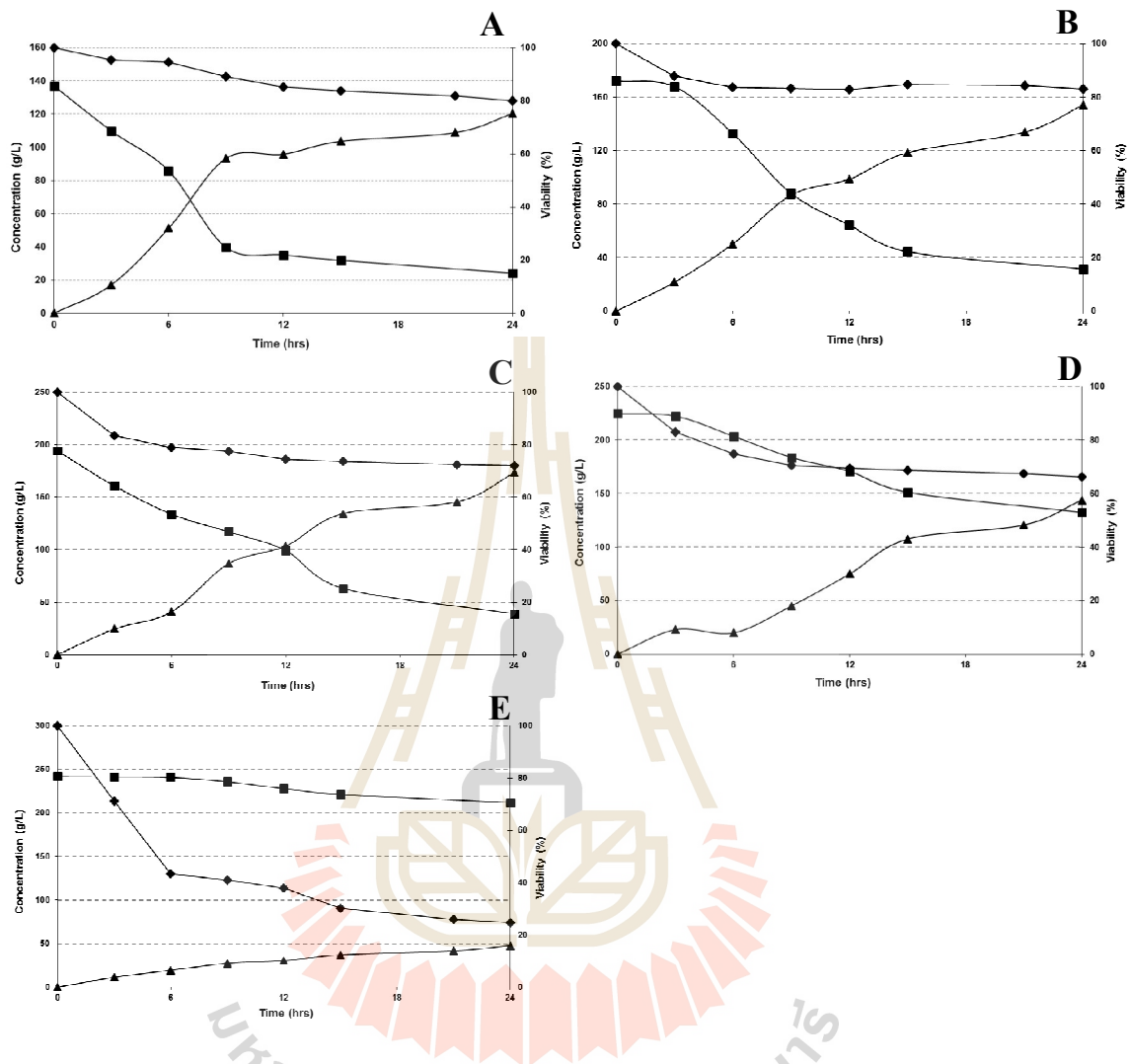


Figure 3.3 Time-course of viable cell count (◆), reducing sugar (■), and ethanol (▲) during fermentation using blackstrap molasses as a carbon source at various initial concentration A) 25 wt%, B) 30 wt%, C) 35 wt%, D) 45 wt% and E) 60wt%.

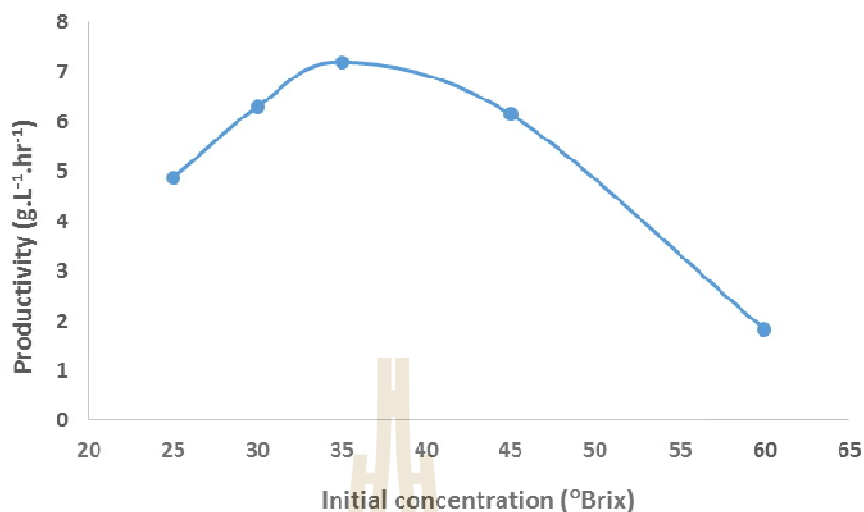


Figure 3.4 Productivity of ethanol fermentation at various initial molasses concentrations.

3.4.3 Conventional batch fermentation and batch extractive fermentation

From the experimental data of the previous section, it becomes clear that ethanol is a toxic substance for cells. The maintenance of ethanol concentration at low level in the medium should improve volumetric productivity and glucose consumption rate due to the minimal product inhibition effect. The conventional batch fermentation was performed at the 25 °Brix concentration. Figure 3.5A illustrated the conventional fermentation profile including glucose consumption, ethanol formation, and relative viability of the yeast cells as function of time. The concentration of sugar was rapidly decreased during the first 12 hours of fermentation. Then, the consumption rate reduced, while ethanol concentration continuously increased. The sharp decrease of cell viability was evidence for product inhibition cells during fermentation. Therefore, this is the key motivation for the extractive fermentation approach. The cells viability approached zero after 36 hours of fermentation period at the 80 g/L ethanol concentration as observed by the methylene blue test.

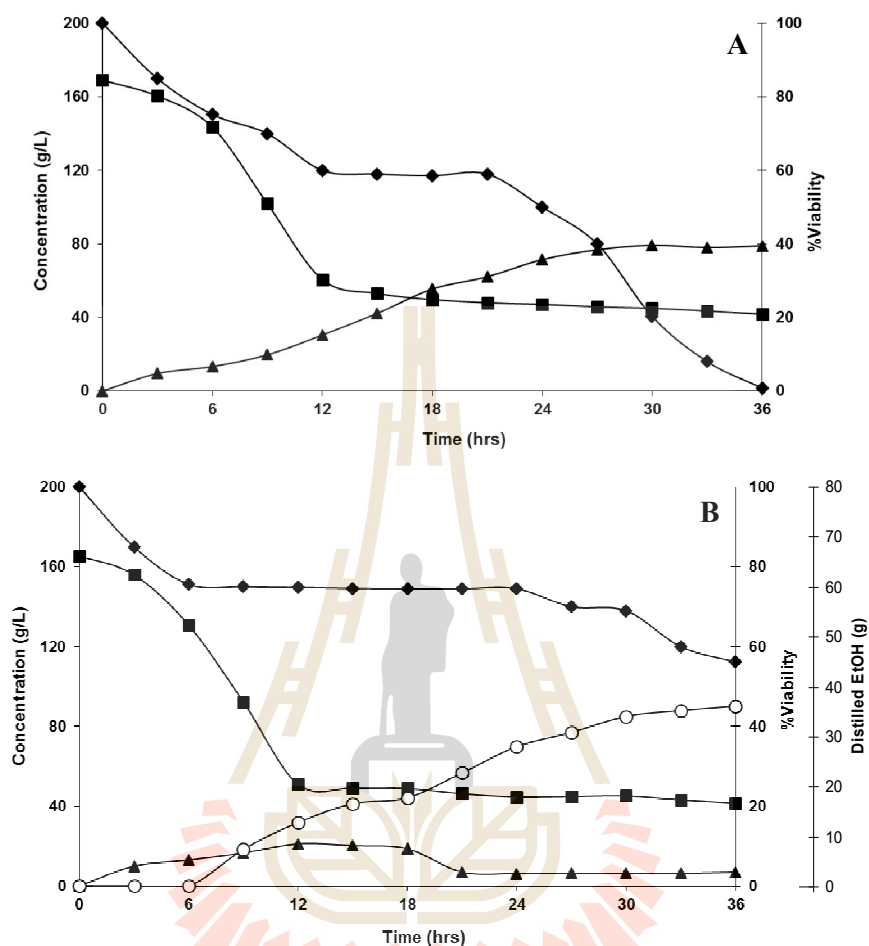


Figure 3.5 Time-dependence of viable cell count (◆), reducing sugar (■), ethanol (▲) and distilled ethanol (○) during fermentation using blackstrap molasses as a carbon source via A) conventional fermentation and B) extractive fermentation.

The extractive fermentation using vacuum fractionation was applied by reducing the system pressure to 45 mbar. At this low pressure, a mixed ethanol/water vapor boiled to the top of column. The cooling region has the purpose to partially condense the vapor and thus decrease the concentration of the less volatile component of water. This phenomenon was called “partial condensation” in the technical term. The purity of the distilled ethanol

could be controlled by the temperature of the cooling region. The results at various cooling temperature (exiting ethanol concentration, distillate rate and quantity of volatile compound as well as fusel oil) are shown in Table 3.1.

Table 3.1 Effect of jacket temperature on distillate rate, %ethanol, ethanol flow rate and concentration of fusel oil.

Jacket temperature (°C)	Distillate rate (g/hr)	%Distillated ethanol	Ethanol flow rate (g/hr)	By-product concentration (mg/L)			
				Propanol	Butanol	IAA	NAA
0	8.1	90.3	7.28	85.8	14.2	334.5	28.2
2.5	10.6	88.2	9.35	77	12.6	321.3	26.7
5	13.3	79.6	10.56	93	14.6	380.6	27.9
7.5	15.6	71.5	11.13	98.4	14.7	380	26.8
10	16.7	67.7	11.28	106.9	12.3	378.5	27.6
15	19.2	62.0	9.99	76.8	10.7	314.1	21.4
25	22.5	55.3	12.44	73.5	10.0	305.6	19.5
35	25.8	43.6	11.25	66.3	9.7	270.1	17.7

IAA = iso-amyl acetate NAA = normal-amyl acetate

The experimental jacket temperature data suggest that higher jacket temperature affected the distillated rate. Higher temperature improved the distillate rate, however the ethanol concentration reduced due to the higher water content of the exiting vapor. At a jacket temperature of 0°C 90 wt% of distillated ethanol at 8.1 g/hr distillate rate were obtained, whereas 55.5 and 43.6 wt% of ethanol resulted from using tap-water and non-additional cooling (ambient temperature) at 22.5 and 25.8 g/hr distillate rate, respectively. Higher alcohols and further volatile compounds as by-product were produced by cells during fermentation. The amount of fusel alcohol including propanol and butanol were in range of 66 – 100 and 10 – 14 ppm, respectively, which is exceedingly larger than reported by others (Arshad *et al.*, 2008). It was conclude that, jacket temperature not affected with the

extraction rate of fusel oil and volatile compounds. The dissimilar concentration came from the diluted water in the distilled solution. Hence, 5 °C was selected as a jacket temperature in the extractive fermentation system.

In order to improve the ethanol fermentation process, extractive fermentation was carried out by placing the high-performance fractionation column on the top of reactor for removing ethanol during the fermentation. Figure 3.4B represent the fermentation profile of the extractive process. The vacuum was applied after 6 hours of inoculation, consequently ethanol was continuously extracted from the reactor. Concentration of the distilled ethanol was typically 80 wt%, whereas the ethanol concentration in the fermentation broth was constantly low and never reached 20 g/L due to the “log phase” of the cells that cause growth the high productivity at the starting point until 18 hours of fermentation time. The result was in accordance with the sugar concentration profile. Following the log phase, ethanol concentration in the broth was lower than 10 g/L due to the lower productivity. Loung (1985) reported that, the ethanol accumulated in the medium inhibits the metabolic activity of yeast, presenting a significant effect on the rate of cell growth at concentration above 15 g/L. The total ethanol produced in this experiment was 70 g which the value was in the same magnitude of batch fermentation. Nevertheless, this system has advantages over conventional batch fermentation particularly the high relative viability of the yeast cells as evidenced by methylene blue test. Extractive fermentation improved the consumption rate and productivity due to the reduction of product inhibition effect. More than 50% of the relative viability was observed throughout 36 hours of operation, this result indicated that more molasses can be added to produce more ethanol.

3.4.4 Extractive fermentation of ethanol in fed-batch mode

The overall benefit from this extractive bioreactor was represented from the previous part in that it was a one stage integrated process. More than 50% relative viability

at the end of batch extractive fermentation suggesting that more substrate can be added into the system. For fed-batch extractive fermentation, 50 g of concentrated blackstrap molasses was added into the reactor to initiate each new fermentation cycle. The time dependence of sugar and ethanol concentration, mass of distillate ethanol and relative cell viability during fed-batch extractive fermentation is shown in Figure 3.6. Ethanol was continuously fractionated from the fermenter at the average rate of 10.2 g/h with a concentration of approximately 80 wt%. Experimental results also revealed a constant ethanol concentration in the fermentation broth in the range of 20 g/L.

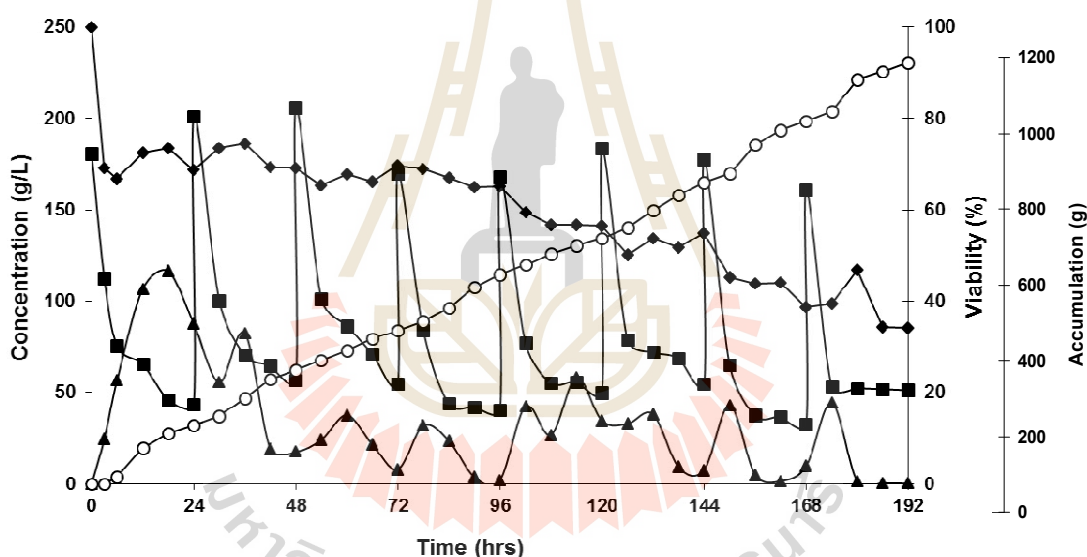


Figure 3.6 Time-course of viable cell count (◆), reducing sugar (■), ethanol (▲) and accumulated ethanol (○) during fed-batch extractive fermentation.

The subsequent addition of concentrated molasses was carried out when the sugar concentration was constant. The addition of molasses was repeated for another 7 times, and the system was very stable for almost 200 hours. Almost 1200 g of ethanol were continuously collected at 80 wt% concentration even after the 8th cycle. Nevertheless, calculated ethanol productivity and relative cell viability decrease gradually for each fermentation cycle as shown in Figure 3.7. It was found that the productivity gradually

reduced in accordance with the relative cell viability of yeast. Only 35% of cells survived throughout the 8th fermentation cycles. The reduction of viability and fermentation performance during the fed – batch fermentation originate both from accumulated by-products as well as non-fermentable toxic substance in the concentrated molasses.

Several explanations can be found in literature to describe the cause of inhibition effect during the fed – batch fermentation. Ashad *et al.* (2008) and Chovau *et al.* (2011) reported that, the organic acids such as lactic acid and acetic acid were among the by-products generated during ethanol fermentation cause of the decrease of pH in the fermentation broth. In addition, the pH of the fermentation broth was not controlled and organic acids are less volatile and accumulate in the fermentation broth and finally cause inhibition. Olbrich (2006), studied and described the harmful factors in molasses and defined the toxic substances into three groups. Firstly, sulfurous acid that resulting from the use of SO₂ in the sugar manufacturing process. However, the sulfurous acid can be removed by using the strong oxidizing agents and thoroughly stirring and heating to 80 – 95°C. Secondly, nitrates and nitrites that have been found in molasses at a concentration of approximately 0.34%. Finally, volatile organic acid such as formic acid, acetic acid, and propionic acid in range of 0.3 – 0.6% according with the by-products formation of the cells. Furthermore, the heavy metals as the toxicity in living cells including aluminum (Al), Arsenic (As), copper (Cu), iron (Fe), manganese (Mn) and zinc (Zn) have been found in concentrated molasses at 0.54, 0.24, 8.7, 0.35, 11.1 and 19.7 µg/ g molasses, respectively (Teclu *et al.*, 2009)

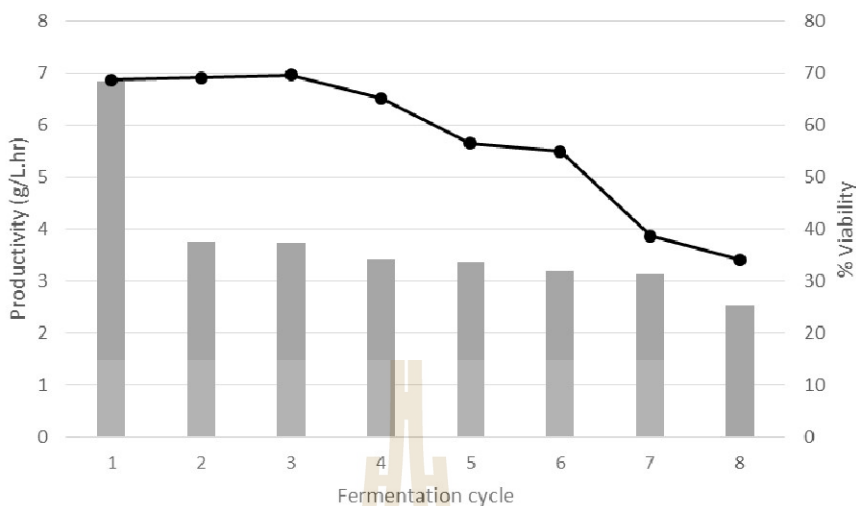


Figure 3.7 Percentage viability (line) and productivity (grey bar) for each fermentation cycle.

In conclusion, fed-batch extractive fermentation showed that a long continuation of is possible as long as the concentration of inhibitory products is kept low. More than 10 times of high purity ethanol was constantly extracted when compare with the conventional batch fermentation. Due to the simple design of the equipment, the system should easily scale up to small-to-medium industrial plants. However, the final inhibition effect occurred because of the formation of by-products and the toxicity from the molasses. In order to avoid these problems, continuous extractive fermentation could be a possible suitable approach. There are no inhibitory substances that accumulate in the reactor due to the fresh diluted molasses and because fermented medium will continually circulated. This process was developed and simulated in the next section.

3.5 Conclusion

The product and substrate inhibition effect is a major problem in ethanol production. The ethanol productivity decreased sharply in the presence of ethanol at concentration higher than 100 g/L. The extractive fermentation system was established for reducing the product and substrate inhibition effect during fermentation. All thing considered, the 60% of survived yeast occurred in the extractive fermentation system, moreover 80 wt% of ethanol was continuously removed from fermentation broth. The activated cells in the fermentation broth could be used in the fed-batch mode. There were 8 cycles of fermentation using only 1 time inoculation. Hence, production cost and time could be lower compared to conventional fermentation due to simple design of the system, long life of the biocatalyst, and low water consumption for medium preparation. The results provide an opportunity for technical and economical feasibility of ethanol production on a medium scale. The 200 liters continuous extractive fermentation was simulated in ASPEN PLUS.

3.6 References

- Arshad, M., Khan, Z.M., Rehman, K., Shah, F.A. and Rajoka, M.I. (2008). Optimization of process variables for minimization of byproduct formation during fermentation of blackstrap molasses to ethanol at industrial scale. **Lett. Appl. Microbiol.** 47: 410 - 414.
- Chen, C., Tang, X., Xiao, Z., Zhou, Y., Jiang, Y. and Fu, S. (2012). Ethanol fermentation kinetics in a continuous and closed-circulating system with a pervaporation membrane bioreactor. **Bioresource Technol.** 114: 707-710.

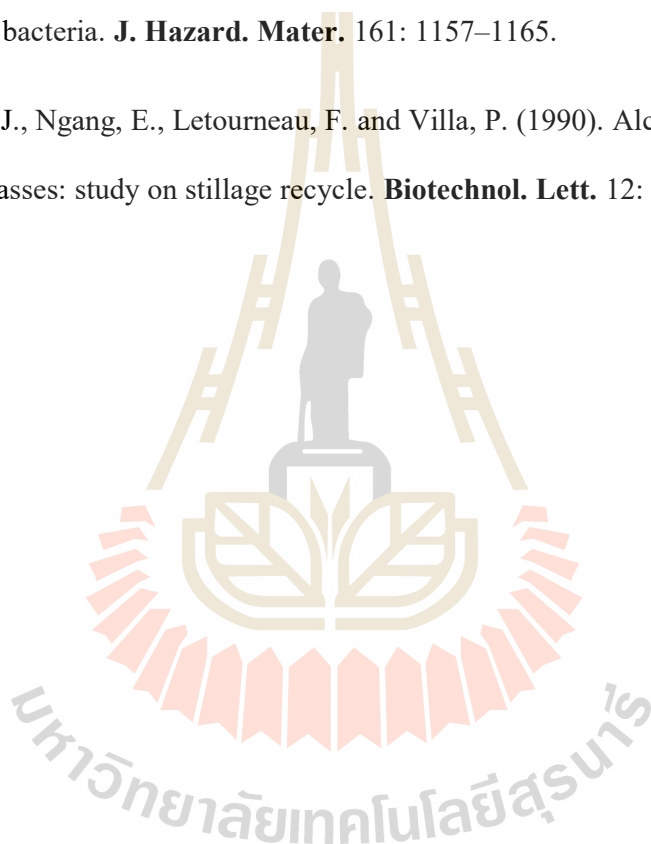
- Chovau, S., Gaykawad, G., Straathof, A.J.J., Van der Bruggen, B., (2011). Influence of fermentation by-products on the purification of ethanol from water using pervaporation, **Bioresource Technol.** 102, 1669-1674.
- Cordana, C.A. and Sánchez, Ò, J. (2007). Fuel ethanol production: Process design trends and integration opportunities. **Bioresource Technol.** 98: 2415-2457.
- Gopal, A.R. and Kammen D.K. (2009). Molasses for ethanol: the economic and environmental impacts of a new pathway for the life cycle greenhouse gas analysis of sugarcane ethanol. **Environ. Res. Lett.** 4: 1-5.
- Gryta, M., Morawski, A. W. and Tomaszewska, M. (2000). Ethanol production in membrane distillation bioreactor. **Catal. Today.** 56: 159-165.
- Lewandowicz, G., Bialas, W., Marczewski, B. and Szymanowska, D. (2011). Application of membrane distillation for ethanol recovery during fuel ethanol production. **J. Membr. Sci.** 375: 212-219.
- Lin, S. K. C., Du, C., Koutinas, A., Wang, R. and Webb, C. (2008). Substrate and product inhibition kinetics in succinic acid production by *Actinobacillus succinogenes*. **Biochem. Eng. J.** 41(2): 128-135.
- Loung, J.H.T. (1985). Kinetic of ethanol inhibition in alcohol fermentation. **Biotechnol. Bioeng.** 27(3): 280 – 285.
- Lye, G. J. and Woodley, J. M. (1999). Application of *in situ* product removal techniques to biocatalytic processes. **Trend Biotechnol.** 17: 395-402.
- Miller, L. G. (1951). Use of dinitrosalicylic acid reagent for determination of reducing sugar. **Anal. Chem.** 31(3): 426-428.

- Nguyen, V. D., Auresenia, J., Kosuge, H., Tan, R. R. and Brondial, Y. (2011). Vacuum fermentation integrated with separation process for ethanol production. **Biochem. Eng. J.** 55: 208-214.
- Nishino, H., Miyazaki, S. and Tohjo, K. (1985). Effect of osmotic pressure on growth rate and fermentation activity of wine yeast. **Am. J. Enol. Vitic.** 36(2): 170 – 174.
- O'Brien, D.J., Senske, G., Kurantz, M.J. and Craig Jr., J.C. (2004). Ethanol recovery from corn fiber hydrolysate fermentations by pervaporation. **Bioresource Technol.** 92: 15-19.
- Olbrich, H. **The molasses** (2006). Biotechnologie-Kempe GmbH. 131 pp.
- Rigothier, M.C., Maccario, J. and Gayral, P. (1994). Inhibitory activity of *Saccharomyces* yeast on the adhesion of *Entamoeba histolytica* trophozoites to human erythrocytes in vitro. **Parasitol. Res.** 80: 10-15.
- Siqueira, P.F, Karp, S.G., Carvalho, J.C., Sturm, W., Rodríguez-León, J.A., Tholozan, J.L., Singhania, R.R. Pandey, A. and Soccol, C. R. (2008). Production of bio-ethanol from soybean molasses by *Saccharomyces cerevisiae* at laboratory, pilot and industrial scales. **Biores. Tech.** 99: 8156–8163.
- Stehlik-Tomas, V., Grba, S. and Runjiperic, V. (1997). Zinc uptake of *Saccharomyces cerevisiae* and its impact on alcohol fermentation. **Chem. Biochem. Eng.** 11: 147 – 151.
- Takeshige, K. and Ouchi, K. (1995). Effect of yeast invertase on ethanol production in molasses. **J. Ferment. Bioeng.** 79(5): 513 – 515.
- Tayler, F., Marquez, M. A., Johnston, D. B., Goldberg, N. M. and Hicks, K. B. (2010). Continuous high-solids corn liquefaction and fermentation with stripping of ethanol. **Bioresource Technol.** 101: 4403-4408.

Thongsukmak, A. and Sirkar, K. K. (2009). Extractive pervaporation to separate ethanol from its dilute aqueous solutions characteristic of ethanol-producing fermentation processes. **J. Membr. Sci.** 329: 119-129.

Teclu, D., Tivchev, G., Laing, M. and Wallis, M. (2009). Determination of the elemental composition of molasses and its suitability as carbon source for growth of sulphate-reducing bacteria. **J. Hazard. Mater.** 161: 1157–1165.

Wolniewicz, J.J., Ngang, E., Letourneau, F. and Villa, P. (1990). Alcoholic fermentation of beer molasses: study on stillage recycle. **Biotechnol. Lett.** 12: 73 – 78.



CHAPTER IV

DEVELOPMENT AND OPTIMIZATION OF A 200 LITER CONTINUOUS EXTRACTIVE FERMENTATION SYSTEM USING ASPEN PLUS: PRACTICAL AND ECONOMIC ASPECTS

4.1 Abstract

The simulation of a 200 liter continuous extractive fermentation system using ASPEN PLUS was performed using blackstrap molasses as a carbon source. The process can be divided into 3 groups; bio-reactor, fractionation column and Venturi system. The 17.28 kg or 8.4 wt% ethanol was produced in the bio-reactor as well as by-products such as fusel alcohol, organic acids and volatile compounds. The RadFrac column was applied for the fractionating column that contains 4 reflux streams defined as partial condensation streams. The exiting vapor from the fractionation column was composed of 82 wt% ethanol with 1.3 kg/hr flow rate in accordance with the actual experimental value. The Venturi system recover and condenses the ethanol vapor. It was summarized that, 18.5 liter of product that contains 82 wt% ethanol solution with insignificant amounts of by-products was produced from 200 liters extractive fermentation system per day. For the economic analysis, production cost including raw material and utilities cost was approximately 500 Baht per day or 27.50 Baht per liter. The process was obtained with respect to economic and systemic performance. This includes recovery of ethanol loss using a gas scrubber connected to the vapor exiting the

Venturi tank. The 0.3 liter of ethanol was recovered from the exhaust Venturi stream per day. Ethanol from the stillage stream containing 4 wt% of ethanol was purified using a laboratory-scale distillation system. Almost 80wt% of ethanol was purified at the throughput of 8.69 liters per day at the calculated utilities costs of 24 Baht per liter. For the utilities assessment, the main power consumption was the cooling liquid in the column. When ambient-liquid temperature was applied here, 42 liters of 55 wt% ethanol was extracted from fermented broth. The low concentrated ethanol was purified once more, to yield of 29.4 liters at 83 wt% of ethanol after fractionation. The calculated utility costs after process modification were 19.25 Baht per liter of ethanol. Approximately 30% of production cost was reduced.

Keyword: Process simulation and development, Continuous extractive fermentation, Venturi system, Economical and sensitivity analysis

4.2 Introduction

Process simulation is a computational representation of real world systems or process that can be used for the design, development, analysis and optimization of the technical process. It is mainly applied to chemical plants and chemical process as well as power plants requirement and similar technical facilities. In addition, simulation software can describe processes in flow diagrams where unit operation are positioned and connected by both product and feed stream. The objective of a process simulation is to find the optimal operating parameter for the examined system in term of productivity, cost of production and environmental and safety constraints as well as prediction of the process performance. The process characteristics e.g. flow rates, compositions, temperatures, pressures, properties, equipment sizes, etc. are predicted using analysis techniques including mathematical models, empirical correlations and computer-aided process simulation tools. For this purpose,

ASPEN (advanced system for process engineering) was developed and starting in 1981 at Massachusetts Institute of Technology (MIT) under a United States Department of Energy project to simulate coal conversion processes after the project by Aspen Technology Inc. was found to further develop and commercialize the simulation. It has now become a powerful tool for engineers to model chemical, power generation and other processes. Further simulators on the market are Pro/II, Hysys, UNISIM, CHEMCAD, Prosim etc.

The simulated ethanol fermentation and downstream processing using ASPEN have been reported by several authors (Galbe and Zacchi, 1992; McAloon *et al.*, 2000; Bolun *et al.*, 2006; Verhoef *et al.*, 2008; Quintero and Cardona, 2011; Tasic and Veljkovic, 2011). In this section, simulation of ethanol production via a 200 liter continuous extractive fermentation is described. The most reliant unit operation for the performance this process is the Venturi system. The Venturi tube and Venturi effect have been established and described as the reduction of the fluid pressure that results when a fluid flows through a constricted section of a pipe. Many process schemes have been studied and apply the venturi such as a venturi nozzle (Lim *et al.*, 2011; Lavante *et al.*, 2015; Tomov *et al.*, 2016), venturi scrubber (Rahimi *et al.*, 2011; Zhou *et al.*, 2016), gas flow measurement (Jitschin, 2004) or Herschel venturi tube (Brinkhorst *et al.*, 2015) Figure 4.1 demonstrates the venturi effect and differential pressure inside the venturi tube.

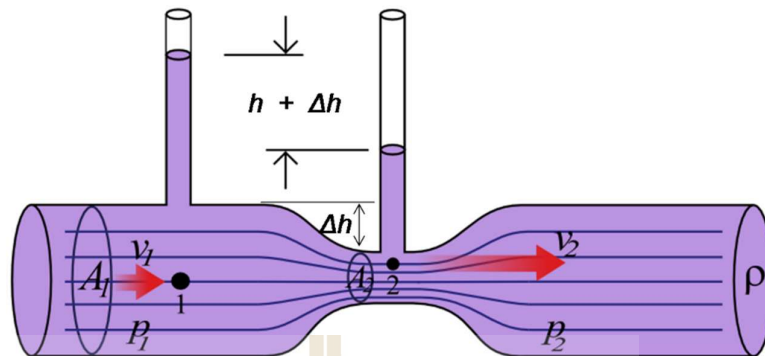


Figure 4.1 Fundamental fluid flow for the Venturi effect and pressure gradient (wikipedia.org).

The Venturi effect was published in 1797 by Giovanni Venturi. The Bernoulli's principle was applied to a fluid that flows through a tube with a constriction such as in Figure 4.1. He derived his principle from the conservation of energy and the energy density for a flowing fluid as:

$$\text{Energy density} = \frac{\text{energy}}{\text{volume}} = P + \frac{1}{2}\rho v^2 + \rho g h \quad (4.1)$$

Where P is the pressure at the location of interest, ρ is the mass density, g is the gravitational constant and h is the altitude. The second term $\frac{1}{2}\rho v^2$ represent the kinetic energy of the fluid due to its average flow and the third term $\rho g h$ represent it potential energy in the gravity field. According to the conservation of energy, the energy density is constant, so it holds for two different regions in the flow as shown:

$$P_1 + \frac{1}{2}\rho v_1^2 + \rho g h_1 = P_2 + \frac{1}{2}\rho v_2^2 + \rho g h_2 \quad (4.2)$$

For two regions at the same height ($h_1 = h_2$), an increase in flow velocity in one region must necessarily correspond to a decrease in pressure in order to fulfill the equation. The kinetic energy is increased at the expense of pressure energy, while the total energy remains

constant. The Venturi effect was applied as a vacuum pump for the extractive fermentation system. Furthermore, the cooling water that circulated in the system also absorbed the exiting vapor. This dual-function unit operation may be expected to be a cost effective technique. In this section, ethanol production via a 200 L continuous extractive fermentation technique was developed using ASPEN PLUS program. The unit operations for each process including bio-reactor, fractionation column and venture system were simulated. Also, possibility, productivity, environmental consideration and process economics were assessed.

4.3 Methodology: process simulation using ASPEN PLUS

Simulation of extractive fermentation was carried out on the industrial scale using ASPEN PLUS version 8.6 (Aspen Technology Inc., Cambridge, Massachusetts, USA.). The procedures for process simulation mainly involved: defining chemical components, selecting the thermodynamic model, choosing proper operating units and setting up input conditions (flow rate, temperature, pressure, etc.). The average mass fractions for concentrated blackstrap molasses including water (0.2), sugar (0.62), inorganic (0.08) and non-fermentable substances (0.1) were obtained from the literature (Olbrich, 2006). The ASPEN PLUS library contained information for the following components used in the simulation: water, sugar, CO₂, ethanol, inorganic substances, propanol, butanol, ethyl acetate, methanol, acetic acid and acetaldehyde. The UNIFAC- modified DMD (UNIFAC Dortmund) is a modified UNIFAC method to predict vapor-liquid and liquid-liquid equilibriums as well as activity coefficients for strongly non-ideal liquid solutions of chemical components. It was used as the base method (Gmehing *et al.*, 2012). The major units operation in the extractive fermentation system were summarized by ASPEN PLUS model as represented in Table 4.1.

Table 4.1 The units operation, models and operating condition in the extractive fermentation system applied in ASPEN PLUS.

Part	Unit operation	Aspen plus model	Operating detail
Bio-reactor	Reactor	RStoic	35°C, 1 bar
	Pre-heating	Heater	35°C, 1 bar
	Flash	Flash2	35°C, 0.06 bar
	Mixer	Mixer	-
Fractionation column	Column	RadFrac	Calculation type: Equilibrium Stages: 5 Condenser: Partial-vapor Reboiler: None Distillate rate: 1.3 kg/hr Pressure: 0.06 bar Subcooled temperature: 5°C
Venturi	Venturi tube	Flash2	5°C, 1 bar
	Cooling	Heater	5°C, 1 bar
	Pump	Pump	Discharge pressure: 6 bar
	Splitter	FSplit	-
Manipulators	Venturi stream splitter	Calculator	Product = Input-Vapout
	Recycle stream splitter	Calculator	Waste = Feed

4.4 Results and discussions

4.4.1 Thermodynamic properties of the related materials

To simplify the system, the yeast, and all by-products were assumed not to affect the VLE behavior in the reactor. The focus of this research was analyzed based on the phase equilibrium of ethanol-water-glucose and by-product mixture. In addition, the effect of CO₂ on the phase equilibria in the reactor and in the rectification column was examined.

Figure 4.2 shown the activity coefficients at infinite dilution of ethanol and water. The area that marked in square represented the data pairs in the temperature range of reactor. Likewise, a data point for the activity coefficients of ethanol was found in a glucose

/ water solution in Dortmund's database. We can see that, the activity coefficient of this ternary mixture appeared in the upper area of scattered activity coefficients. It can be assumed that, a further increase in the glucose concentration enhanced the volatility of ethanol.

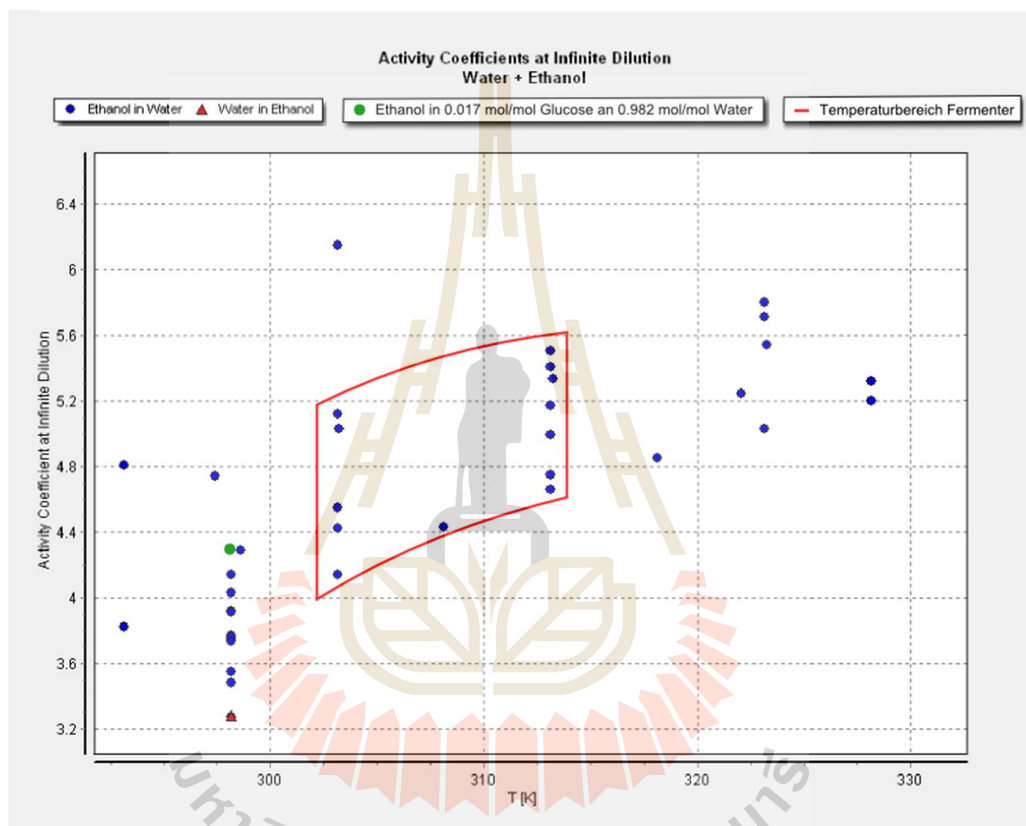


Figure 4.2 Selected activity coefficients at infinite dilution (DDBST database).

Considering a binary mixture of ethanol and water, Vapor-liquid equilibrium (VLE) data at 60 mbar was analyzed using DDBST database. It has to be considered that the ethanol / water mixture shows an azeotrope at about 94% wt. of ethanol (Figure 4.3). On an industrial scale a further dehydration of ethanol can be carried out. This requires an ethanol concentration of at least 85% wt. to be economic in a subsequent dehydration membrane process.

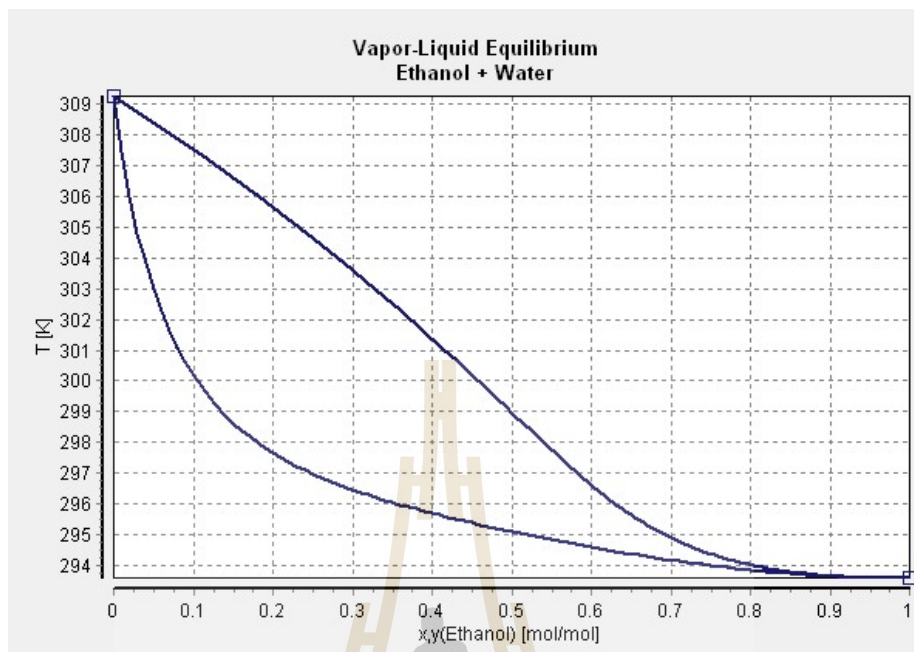


Figure 4.3 Predicted VLE ethanol / water (at 60 mbar) diagram using DDBST database.

4.4.2 Simulation of a 200 liter extractive fermentation system

The purpose of analysis/simulation is to model and predict the performance of a process. It involves the decomposition of the process into its constituent elements (e.g. units) for individual study of performance. The process characteristics (e.g. flow rates, compositions, temperatures, pressures, properties, equipment sizes, etc.) are predicted using analysis techniques. These techniques include mathematical models, empirical correlations and computer-aided process simulation tools. In order to assess the practically and economically potential of 200 L extractive fermentation, the actual vacuum extractive fermentation system represented in Figure 4.4. The computational simulation program was used with the purpose for obtained the beneficial and optimal data in the realistic approach. To simplify the overall system, the units operation were individually simulated and divided into 3 parts including bio-reactor (1), high-performance fractionation column (2) and Venturi system (3).

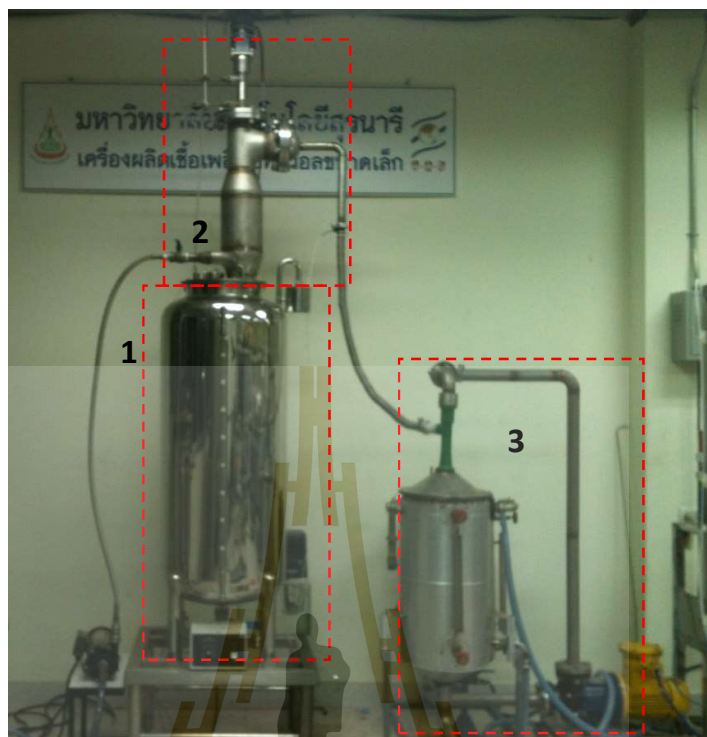


Figure 4.4 The 200 liters extractive fermentation system.

4.4.2.1 Simulation of bio-reactor and component specification

Before running the simulation program, identification of each feed stream composition is important ensure. The simulated bio-reactor system from blackstrap molasses was designed according to Figure 4.5. The concentrated molasses (MOLAS) was mixed with water in the proportional of 1:4 and then, blended with the optional ingredients including yeast, anti-biotic and di-ammonium phosphate (non-associated fermentative

system). The simulated medium was pre-heated to 35°C before fed to the reactor (FEED). The fermented broth was presented at the stream PROD.

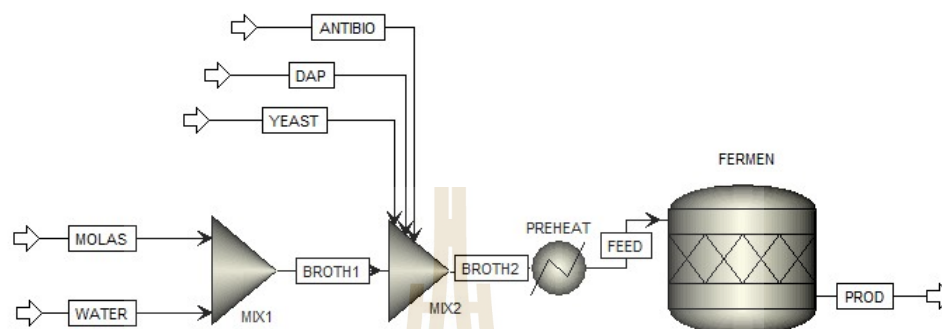


Figure 4.5 The bio-reactor diagram designed in ASPEN PLUS.

In this experiment, the fermentative reaction was performed based on stoichiometric conversion. The data obtained from the actual conventional fermentation including ethanol and by-products such as fusel oil, volatile compounds and organic acid were calculated and applied to the most accurately and correctly simulation output. In terms of CO₂ content, the analysis of total CO₂ concentration during the fermentation is impractical. The actual weight of CO₂ was calculated from the ethanol production. The calculated mole fraction of ethanol and CO₂ are roughly 1.712 although theoretical mole fraction of ethanol and CO₂ from glucose are 2.0. The NFS denote that the non-fermentable substances such as starch and oligo-saccharide that existed in the medium as well as ignored miscellaneous substances or minor by-product. Moreover, the fractional conversion was specified at 0.95 of the reactant. The calculated mole fraction of ethanol and by-product are shown in Table 4.2.

Table 4.2 Calculated mole fraction for glucose conversion from the simulation program.

Composition	Mass concentration (g/L)	Calculated mole fraction
Ethanol	78.90	1.71
Carbon dioxide	75.37	1.71
Methanol	0.033	0.001
Propanol	0.0013	2.16×10^{-5}
Butanol	0.0010	1.35×10^{-5}
Acetaldehyde	0.044	0.001
Ethyl acetate	0.107	0.0012
Acetic acid	0.046	0.00077
NFS	-	0.14

Table 4.3 represents the results of the simulated bio-reactor including total mole and mass flow, mass fraction and states fraction of the broth before and after fermentation. It was found that, 17.28 kg of 8.4 wt% ethanol was produced in the 200 L reactor whereas 2 kg glucose still remained in the reactor. Approximately 8 and 23 g of total fusel oil content and volatile compounds were created during the fermentation. Nevertheless, lower pressure for the ethanol boiling-up among the ambient temperature was applied to the extractive fermentation system. The sensitivity analysis of the optimum pressure was performed in ASPEN PLUS simulator. In this case, both the mass flow and the mass fraction of ethanol were determined in the vapor stream. Figure 4.6 shows the sensitivity analysis for the pressure dependence of the flow and mass fraction of ethanol. It concludes that pressures between 60 to 75 mbar provide a good compromise.

4.4.2.2 Model development of the fractionation column

In case of the extractive fermentation system, the fractionation column is the most significant unit for the ethanol purification. High concentration ethanol could be extracted from the fermentation broth and some water will reflux into the bottom due to the

partial condensation. Conversely, there are the specific column that not have the possibility to simulate using the existing facility a model. The behavior of the ethanol/water vapor was extrapolated according to following aspects.

Table 4.3 Composition, mass and volume flow as well as mass fraction of simulated bio-reactor.

Composition	Mass Flow (kg/day)		Mass Fraction	
	FEED	PROD	FEED	PROD
Water	148.44	148.44	0.73	0.73
Glucose	41.54	2.08	0.20	0.010
CO ₂	-	16.51	-	0.081
EtOH	-	17.28	-	0.085
NFS	6.70	12.32	0.033	0.060
Propanol	-	0.00030	-	1.39×10 ⁻⁶
Butanol	-	0.00022	-	1.07×10 ⁻⁶
Ethyl acetate	-	0.023	-	0.00012
MeOH	-	0.0073	-	3.59×10 ⁻⁵
Acetic acid	-	0.010	-	4.94×10 ⁻⁵
Acetaldehyde	-	0.0096	-	4.72×10 ⁻⁵
Mole Flow (kmol/day)	8.63	9.22		
Mass Flow (kg/day)	204.04	204.04		
Temperature (°C)	35	35		
Pressure (bar)	1.01	1.01		
Vapor Fraction	0	0.031		
Liquid Fraction	0.99	0.95		
Solid Fraction	0.01	0.014		

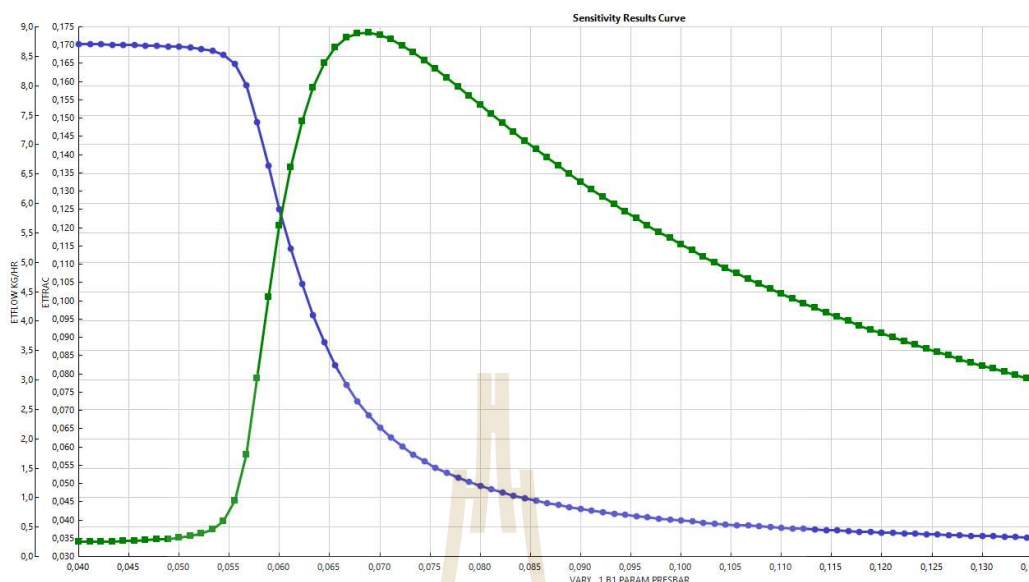


Figure 4.6 Sensitivity analysis for the pressure dependence of ethanol flow (●) and fraction (■) using ASPEN PLUS.

Figure 4.7 shows the VLE behavior of ethanol/water in the column. The condensation of water occurring on the wall as well as in the gas stream. Initially, the water droplet on the column wall was created by the vapor stream along the cooling wall as a result of the working of the propeller. Secondly, directly condensation and formation of droplet in the vapor stream. In addition, vapor-liquid equilibrium between droplets and vapor was established in this system.

As mentioned before, this is a specific column that is not available in ASPEN PLUS model library. The suitable approach to simulate this column is a “trial and error” technique based on the real experimental data. The number of stages, distillate and bottom rate, and split rate were customized randomly until the equivalent of both actual and the simulated value were obtained.

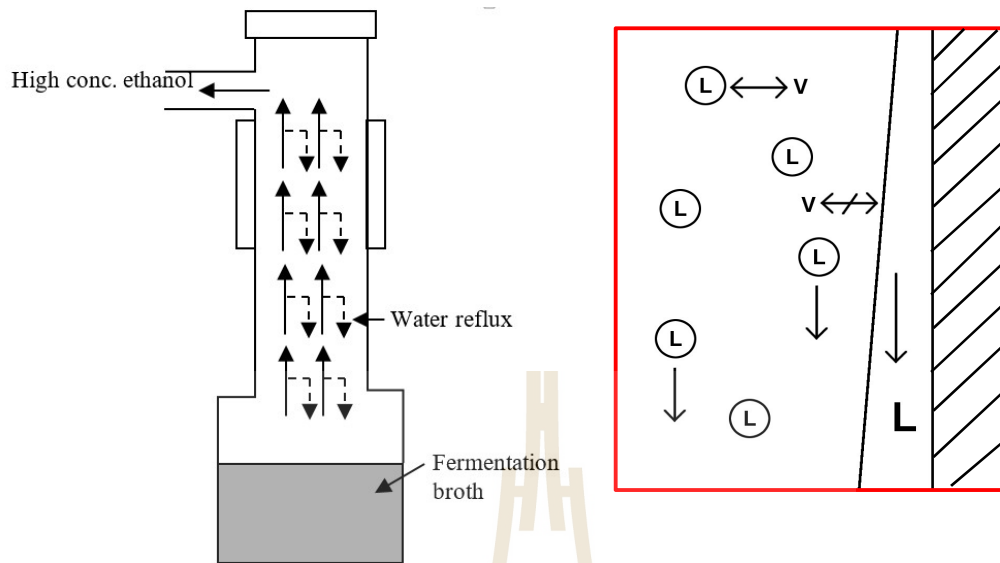


Figure 4.7 Direction of ethanol vapor (solid line) and water (dot line) in fractionation column (left) and Ethanol/water VLE behavior in column (right). (1) water refluxed on the column wall, (2) formation of water droplet in the stream and (3) vapor-liquid equilibrium between droplets and vapor.

In order to replicate this behavior in ASPEN PLUS, a RadFrac column with 5 stages was used without reboiler (Figure 4.8). The fermented broth was partially vaporized in a flash and introduced to the column. The split rate of side streams referred to the partial condensation was set at the 4th, 3rd, and 2nd stage for 2, 2 and 1 kg/hr of the stream at the column bottom, respectively (TOT REFLUX). The condenser cools the reflux stream at 5 °C, whereas the distillate rate was 1.3 kg/hr. By this setting, a sufficiently large volume flow of the ethanol could be achieved at the top of the column with depending on the feed composition comprises approximately 82% wt (VAPOUT).

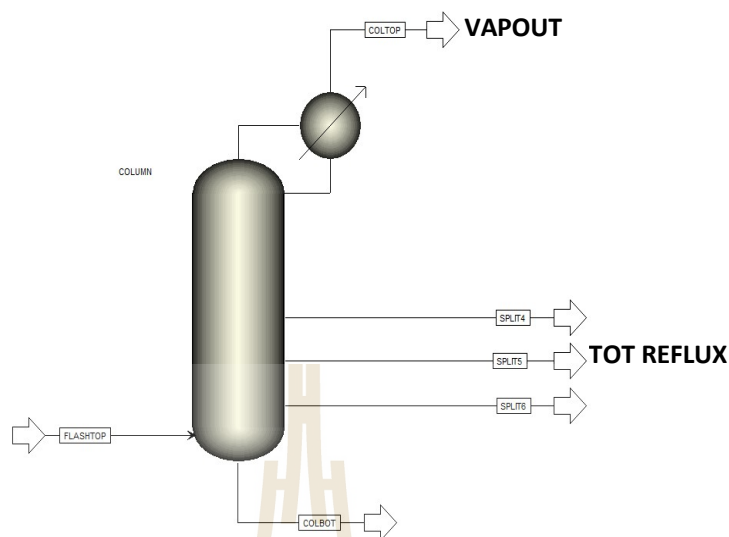


Figure 4.8 Fractionation column diagram designed in ASPEN PLUS, consist of 4 reflux streams.

Table 4.4 shows the total mole flow, mass flow, state fraction, temperature and mass fraction of each component of vapor out and drop down stream. The total mass flow of vapor stream through the top of column is roughly 1.3 kg/hr with an ethanol and water fraction of 0.824 and 0.172, correspondingly.

In this case, CO_2 in the stream was neglected because it could be removed afterward. The total fusel alcohols were extracted (approximately 0.2 g per 1 kg of the solution). Additionally, this column demonstrated the high fractionating performance as a consequence of the total reflux content which contain 95wt% water and only 4.9wt% of ethanol. All things considered, the designed fractionating column was successfully simulated using ASPEN PLUS and the results are comparable with the realistic column and system. The precisely value of the total reflux amount and vapor out are not confirmed. In particular,

determination of distillate rate in vapor phase or the reflux rate inside the reactor was not practical.

Table 4.4 Composition, mass and volume flow as well as mass fraction of fractionation unit operation.

Composition	Mass Flow (kg/day)		Mass Fraction	
	VAPOUT	TOTREF	VAPOUT	TOTREF
Water	0.10	4.84	0.077	0.95
CO ₂	0.72	0.00054	0.55	0.00011
EtOH	0.48	0.25	0.37	0.049
Propanol	3.85×10^{-6}	8.25×10^{-6}	2.96×10^{-6}	1.62×10^{-6}
Butanol	4.76×10^{-7}	8.41×10^{-6}	3.66×10^{-6}	1.65×10^{-6}
Ethyl acetate	0.0010	6.06×10^{-6}	0.00078	1.19×10^{-6}
MeOH	0.00021	0.0001	0.00016	1.97×10^{-5}
Acetic acid	7.79×10^{-7}	0.00031	5.99×10^{-7}	6.12×10^{-5}
Acetaldehyde	0.00041	4.89×10^{-6}	0.00032	9.61×10^{-7}
Mole Flow (kmol/hr)	0.032	0.27		
Mass Flow (kg/hr)	1.3	7.20		
Volume Flow (L/min)	212.46	0.95		
Temperature(°C)	11.30	32.39		
Pressure (bar)	0.06	0.06		
Vapor Fraction	1	0.0005		
Liquid Fraction	0	0.9995		

4.4.2.3 Simulation of the Venturi system

In the earlier series of experiments using the laboratory reactor, ethanol was removed from the product stream by a condenser at -25 °C. The remaining product were continued to protect the vacuum pump through a cold trap with liquid nitrogen. This process is a very costly and particularly not suitable for industry. A Venturi pump with 5°C ethanol flow was used in all current experimental setup. The ethanol of the product

stream is condensed by the cold absorbent (ethanol solution), while simultaneously the necessary vacuum for extraction is occurred by the Venturi effect.

The flow diagram and ASPEN PLUS model of the Venturi system is shown in Figure 4.9. In the assumption that the Venturi tube is unavailable in the ASPEN PLUS unit database. The Venturi system has been modeled using an absorber, whereas the product stream from the top of column is contacted and condensed with the circulating liquid absorbent stream. The rate of product removal was defined by the variation of vapor stream input and product stream output.

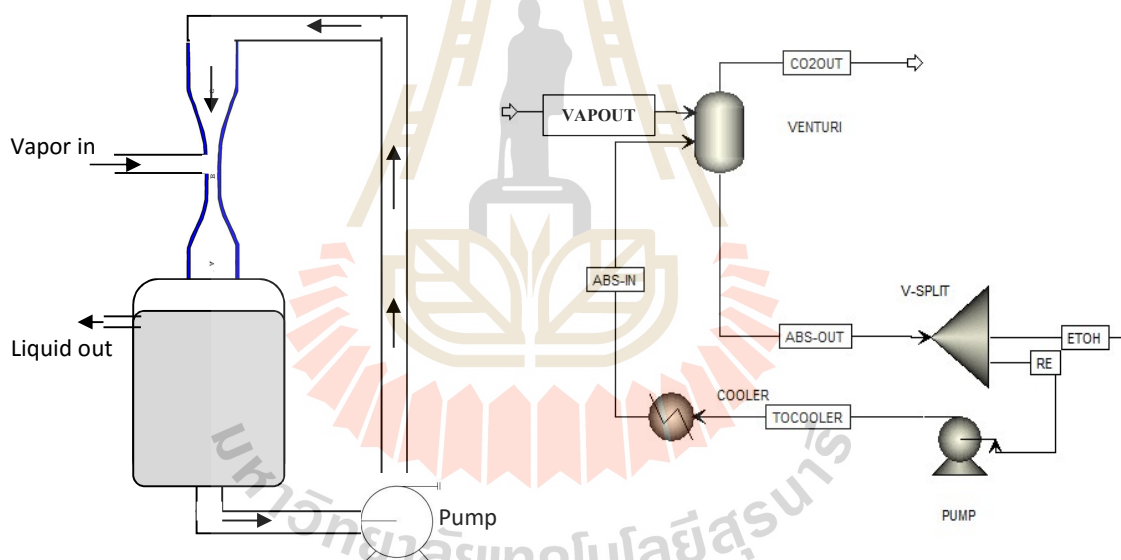


Figure 4.9 The actual systemic diagram (left) and ASPEN PLUS designed diagram (right) of venturi system.

The results for the simulated Venturi system including total mole and mass flow, mass fraction and composition mass flow of the input vapor stream are given in Fig. 4.8 (VAPOUR) and the product stream for liquid product (PROD) and vapor phase (CO2OUT) in Table 4.5. It was obvious that, 1.27 mL of ethanol solution was extracted from the Venturi tank per 1 minute. As calculated that, 18.5 liter of product solution was recovered

from 200 liters fermented broth or 9.25% yield. The product stream contains 82 wt% ethanol and insignificantly volume of fusel alcohols and volatile compounds, whereas the CO₂ content in the product liquid stream was negligible.

Table 4.5 Composition, mass and volume flow Venturi system.

Composition	Mass flow (kg/day)		
	VAPOUT	PROD	CO2OUT
Water	0.10	0.040	0.00074
CO ₂	0.72	0.019	0.65
EtOH	0.48	0.58	0.013
Propanol	3.85×10^{-6}	2.20×10^{-7}	-
Butanol	4.76×10^{-6}	2.73×10^{-8}	-
Ethyl acetate	0.0010	5.77×10^{-5}	1.11×10^{-5}
MeOH	0.00021	1.19×10^{-5}	5.42×10^{-7}
Acetic acid	7.79×10^{-7}	4.46×10^{-8}	-
Acetaldehyde	0.00041	2.36×10^{-5}	1.73×10^{-6}
Mass flow (kg/hr)	1.3	0.635895	0.664105
Volume flow (L/min)	212.4617	0.012658	5.820356
Temperature (°C)	11.30305	5	5
Pressure (bar)	0.06	1	1
Vapor Fraction	1	0	1
Liquid Fraction	0	1	0

Conversely, the ethanol vapor could not be completely recovered by the Venturi system at 5°C circulating liquid, approximately 2wt% of non-condensed ethanol vapor was observed at the CO₂OUT stream. As a consequence of circulating liquid temperature and flow rate affect the ethanol absorption and degree of ethanol condensation. Sensitivity analysis of circulating liquid temperature on non-condensed ethanol fraction and product flow rate were performed as showed in Figure 4.10. It can be seen that, the total of ethanol was recovered at -25°C of circulating liquid, otherwise 12wt% of ethanol was vaporized from the Venturi tank when circulating liquid was set at room temperature (35°C). Meanwhile, the product flow rate increase from 0.42 to 0.52 and 0.55 kg.hr⁻¹ when circulating

liquid temperature was decreased to 5 and -25 °C, respectively. In other word, 23.8 and 31% of product flow rate improved at the present of circulating liquid temperature at 5 and -25 °C, respectively.

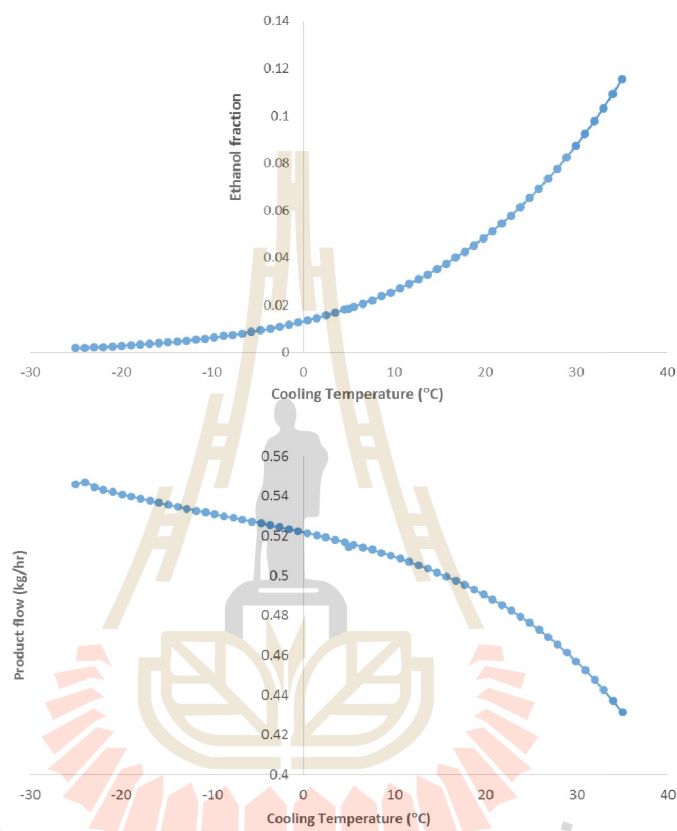
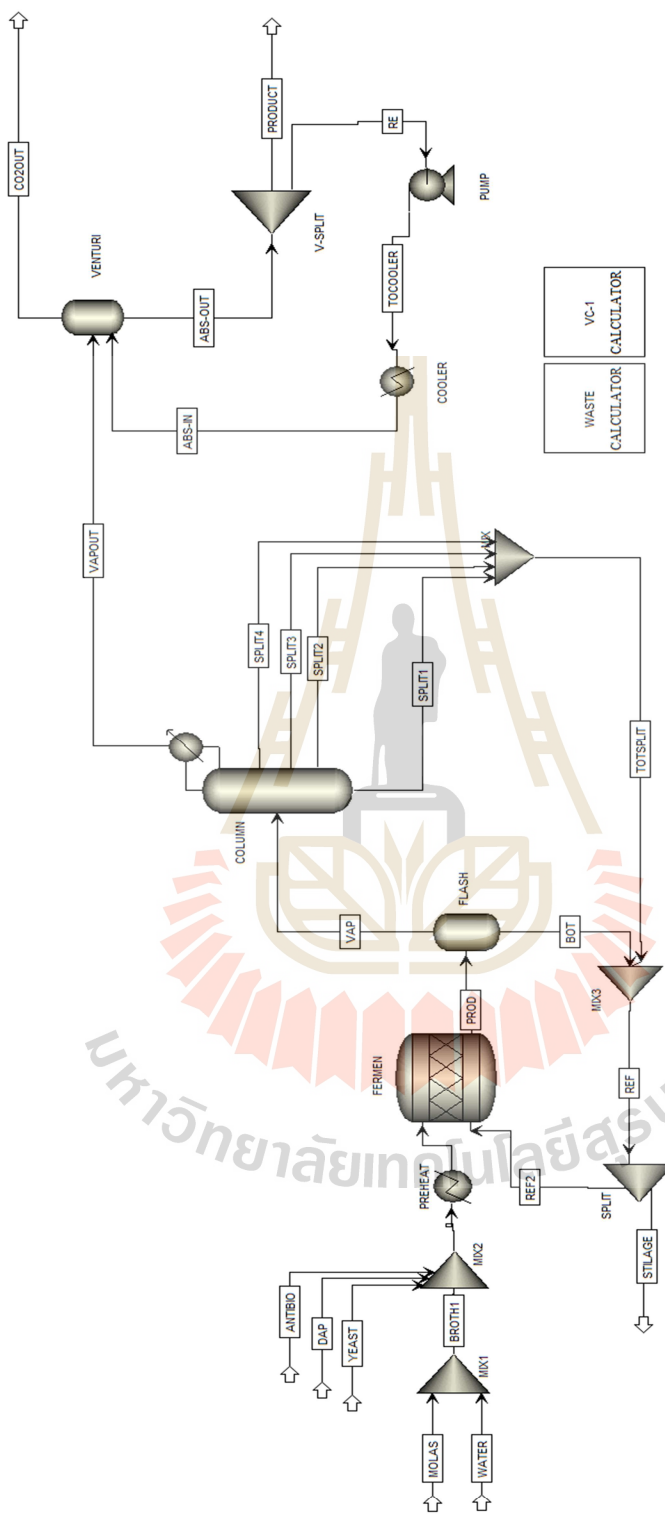


Figure 4.10 Sensitivity analysis of non-condensed ethanol fraction (above) and flow (below) in Venturi tank in various cooling temperature.

From that data above, cooler liquid circulation improved the condensation rate and yield of ethanol. In contrast, the electricity power for cooling water is the significant contribution to for the production cost. The appropriate condition of power usage and product output for the most economically benefit is the important challenge for building-up to the industrial scale.



4.4.3 Economical analysis of continuous extractive fermentation

Previously the 200 liters continuous ethanol-extractive fermentation from molasses was successfully simulated. The three parts of the process were assembled as illustrated in Figure 4.11. Overall and components mass and energy balances as well as productivity were analyzed. The simulation shows that the fermenter with room-temperature fractionating column might be mainly responsible for the energy consumption. For the calculation of the energy cost were assumed as follow:

- The fermenter was heated by natural gas, the column and condenser of the Venturi were cooled with electrical energy.
- The prices of raw materials for example raw blackstrap molasses as well as optional ingredients such as baker's yeast, DAP or citric acid were approximately 6 Baht per kg. Therefore, the 1:4 dilution of fermentation broth was around 1.5 Baht per liter
- Electrical price was 1.76 Baht per kilowatt (eppo.co.th), water supply price was 15.48 Baht per m³ (pwa.co.th), both are the middle-scale rate.
- The utilities for the agitator unit for both reactor and fractionation column were negligible.

The power usage and production cost of each unit operation were calculated from ASPEN PLUS as shown in Table 4.6.

The resulting energy consumption was roughly 5 kW per day. The cooling system was the main power consumer especially for partial condensing column. The power consumption of column cooling was 3.3 kW or two-third of the whole utilities of the process. For this reason, vapor stream that contained CO₂ requires the most distilling power (Gadalla *et al.*, 2005). Therefore alternative procedures for CO₂ distillation were reported (Goddin,

1984). Higher distillation temperature would lead to the reduction of ethanol concentration in the product stream (Table 3.2 in chapter III) that make possible to decrease the distillation utilities and production cost. The calculated cost for 82wt% ethanol production was 209 Baht at a productivity of 18.5 liters per day. The net cost of production was 27.50 Baht per liter when the feed price was included. The overall cost including feed and power and cost of production is summarized in Table 4.7.

Table 4.6 Utility usage and utility costs for the 200 liters extractive fermentation.

Unit operation	Reactor	Column	Venturi		Total
Operating type	Heating	Cooling	Cooling	Pump	
Utilities type	GAS	ELEC	ELEC	ELEC	
Usage (W)	227.07	3343.80	1328.86	132.59	5032.32
Cost (Baht/day)	9.42	138.65	55.10	5.50	208.67

Table 4.7 Net cost flow of feed, power and cost of ethanol production.

Net cost flow of feed (Baht/day)	300.00
Net cost flow of power (Baht/day)	208.67
Overall net cost flow (Baht/day)	508.67
Net productivity (L/day)	18.50
Cost of production (Baht/L)	27.50

For the economic assessment, the excessively high production cost originated from electrical cooling of the column. Furthermore, the non-recovered product including vaporized ethanol in the Venturi stream and residual ethanol in waste stream were presented. Assuming that this simulation represented the overestimated production cost. Production cost of bio-ethanol yield from different energy crops have been successfully summarized (Wang, 2002; Balat and Balat, 2009). They reported that, production cost of bio-ethanol using

sugarcane as carbon source was 11.2 Baht per liter, the conversion rate to ethanol 70 liters per ton of raw material. Whereas, production cost from cassava, corn and wheat were 24.5, 14.7 and 16.8 Baht per liter respectively, at the 150, 410 and 390 liter per ton conversion rate. The extractive fermentation is a less profitable process when compare with different literature sources. The economic improvement of this process was performed in the next topic.

4.4.4 Modification options to improve efficiency

From the economical assessment, the price of ethanol production from this process is still too costly. This is a consequence of the non-recovered product in the waste stream as well as excessive utilities in the fractionation column. There are several ways that should lead to an increase in efficiency of the simulated system. Some of them were directly introduced into the simulation, another one would cause a strong changes in the boundary conditions that cannot be assumed that the simulation is supplying proper results.

4.4.4.1 Recovering the ethanol loss through Venturi system

According to Table 4.5 and Figure 4.10, approximately 13.25 g of ethanol was vaporized per hour from the Venturi system. A lower temperature of circulating liquid could reduce the ethanol vapor loss, despite considerably increase the utilities power. The chosen method to returning the product was a gas scrubbing technique that connected with exiting vapor stream from the Venturi system. Several gas scrubber chemicals and ethanol recovery process have been reported (Ramachandran, 1996; Melnichuk and Kelly, 2005; Phillips, 2007). The gas stream was washed using the sprayed circulating liquid, the recovered stream was dropped down and recycled to the Venturi tank. The diagrams of added-on gas scrubber is shown in Figure 4.12

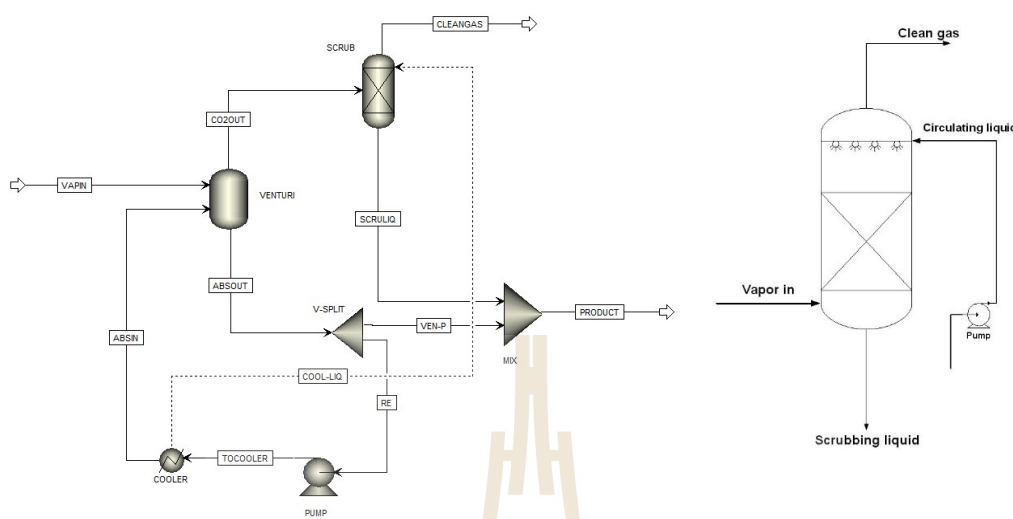


Figure 4.12 Additional of gas scrubber in Venturi system in order to recover non-condensed ethanol.

Assuming that ethanol vapor was completely recovered via the gas scrubber, 0.3 liter of ethanol can be extracted from exhaust Venturi stream per day (SCRULIQ). Results of the gas scrubbing the exhaust Venturi are given in Table 4.8. The total amount product was increased to 18.75 L.day⁻¹ (PRODUCT). The recovery was only 1.6% in 200 liters reactor that non-significant in cost effectiveness, but this has meant the exhaust stream is almost free from organic compounds and less demanding in terms of further work. Nevertheless, the performance of the gas scrubber is affected when apply in the industrial scale. As an illustration, the gas scrubber could harvested the lost ethanol at the rate of 171.84 kg per day in 100,000 liters reactor while simulated using ASPEN PLUS (data not shown). Accordingly, gas scrubber is an interested unit operation for improving the operating cost of extractive fermentation with Venturi system.

Table 4.8 Results of the gas scrubbing the exhaust gas flow Venturi

Mass Flow (kg/hr)	VEN-P	SCRU-LIQ	PRODUCT
Water	0.093	0.00012	0.093
CO ₂	0.024	0	0.024
EtOH	0.54	0.0099	0.55
Total Flow kg/hr	0.66	0.010	0.67
Total Flow L/day	18.45	0.30	18.75

4.4.4.2 Ethanol recovery from the waste stream

In the fermentation, 170 liters of stillage stream were produced at the concentration of 4% w/w ethanol. In other word, approximately 6.68 kg of ethanol was discarded per day. Therefore, ethanol purification from stillage stream was a necessary step for cost effectiveness improving. The laboratory-scale continuous distillation system which successfully developed and established in our lab was applied. The system specifications, experimental and simulation results will be discussed in the next chapter. The result of ethanol extraction from stillage are shown in Table 4.9.

Table 4.9 Component mass flow and fraction of waste stream recovery.

	Stillage	Product	Waste
Component mass flow (kg/hr)			
Water	6.66	0.061	6.60
EtOH	0.28	0.24	0.038
Component mass fraction			
Water	0.96	0.20	0.99
EtOH	0.04	0.80	0.0057
Volume flow (L/day)	168.99	8.69	167.64
Temperature (°C)	25	25	68.19

It was found that, the distillation system represented an adequate performance for ethanol extraction, especially from the low concentration of substrate. Almost 80wt% of ethanol was purified from 4wt% stillage at the throughput of 8.69 liters per day. Meanwhile, the non-recovered ethanol residual was only 0.5wt%. The utility costs for laboratory-scale continuous distillation system are summarized in Table 4.10.

The major use originated from both heating section (flash and reboiler) that approximately 98% of the overall utilities cost. The total utility cost was 211 Baht per day with the 24 Baht per liter production cost. Otherwise, power of the heating unit had an influence on both productivity and quality of the final product. As a result of simulation, the 70wt% of ethanol with 14.2 liters per day productivity were produced at the present of 2 kW and 1 kW usage power of flash and reboiler unit, respectively (data not shown).

Table 4.10 Utility usage and utility costs of the laboratory-scale distillation system for ethanol recovering in waste stream.

Unit operation	Pump	Flash	Reboiler	Condenser
Utilities type	ELEC	ELEC	ELEC	Water (L/day)
Usage (W)	1.98	3000	2000	226
Cost (Baht/day)	0.082	124.47	82.98	3.94

4.4.4.3 Changing the boundary conditions

The main reason of the high energy and production cost is the very expensive electrical cooling of the column at 5 °C. In general, this problem could be solved by further heating the reactor leading to increasing column temperature. In the case of

fermentation, the maximum temperature is determined by heat-sensitivity of the yeast culture. The temperature could be raised from the current 35 °C to 40 - 45°C by using the high-temperature resistant yeast strains. Among the known yeast species used in fermentation process, *K. marxianus* is thought to have the best performance in term of growth and fermentation at high temperature. It has been experimentally reported that the strains *K. marxianus* grow well at temperature as high as 45°C to 52°C and can efficiently produce ethanol at temperature of between 38°C to 45°C (Anderson *et al.*, 1986; Fleming *et al.*, 1993; Barron *et al.*, 1995; Boyle *et al.*, 1997; Lark *et al.*, 1997; Ballesteros *et al.*, 1991, 2002, 2004; Negro *et al.*, 2003; Hong *et al.*, 2007; Limtong *et al.*, 2007; Nonklang *et al.*, 2008; Suryawati *et al.*, 2008). Additionally, the application of thermo-tolerant yeasts in ethanol fermentation using blackstrap molasses has been studied and reported by several authors (Gough *et al.*, 1996; Banat *et al.*, 1996; Singh *et al.*, 1998; Rajoka *et al.*, 2005; Abdel-Banat *et al.*, 2010). Hence, it should be possible in cooperation to reduce the cooling of the column, and increase the pressure which might be confirmed by measurements.

However, the application of thermo-tolerant yeast would results in relatively small reduction of energy consumption and energy costs. In contrast, a very strong cost reduction would be possible if the cooling temperatures increased. As a results of Table 3.2 in Chapter III, the use of water at ambient temperature (25-27°C) would save cost. Approximately 55 wt% ethanol was extracted from the top of column at 22.5 g per hour productivity. From that viewpoint, the final product concentration would decrease, otherwise the cooling utility was uninvolved. Due to the high boil-up ratio, this column was relatively energy-saving and the high temperature at the top of the cooling is possible with water so that the operating costs of the column are relatively low. In addition, the ethanol stream cloud be withdrawn in gaseous form and further rectified using small-scale distillation system. The

bottom stream of the azeotrope column could be recycled to the reactor, at that time that without ethanol is lost. The modified process was simulated and summarized in Table 4.11.

Table 4.11 Component flow and fraction of product and stillage after the ambient-temperature in selective region was used.

	PRODUCT	STILAGE
Component mass flow (kg/hr)		
Water	0.68	5.38
Glucose	0	0.017
CO ₂	0.086	0.00054
EtOH	0.82	0.077
Component mass fraction		
Water	0.43	0.85
Glucose	0	0.0027
CO ₂	0.054	8.62×10 ⁻⁵
EtOH	0.51	0.012
Mass Flow (kg/hr)	1.58	6.30
Volume Flow (L/day)	41.73	145.0
Temperature (°C)	5	34.40
Pressure (bar)	1	1

According to Table 4.9, roughly 55 wt% ethanol was removed from the fermentation broth at 41.73 liters per day productivity, simultaneously 145 liters of waste stream was eliminated at the 1.2 wt% concentration. The ethanol from product output streams were further purified using distillation system. The utility power requirement of flash and reboiler was 2 and 1 kW respectively, also water was used as a cooling in column and condenser. The simulated data was analyzed and concluded that 29.4 liters of 83 wt% of from ethanol product.

Table 4.12 Utilities usage and utilities cost of the extractive fermentation system using ambient-temperature in selective region and coupled with laboratory-scale distillation system.

Operating type	Reactor			Rectification			
	Heating	Cooling	Pump	Pump	Flash	Reboiler	Condenser
Utilities type	GAS	ELEC	ELEC	ELEC	ELEC	ELEC	Water (L/day)
Usage (W)	227.07	1328.86	132.59	0.48	2000	1000	1451.38
Cost (Baht/day)	9.42	55.1	5.5	0.03	130.2	65.1	2.80

The calculated overall production cost was approximately 268 Baht per day (excluded cost from raw material). The production cost of extractive fermentation (without cooling region) coupled with ethanol rectification as summarized in Table 4.12. It was concluded that, the utilities cost of 83 wt% ethanol production was 9.1 Baht per liter, otherwise 19.25 Baht per liter when raw material was included.

In conclusion, cost efficiency improving of 200 liters extractive fermentation system was successfully developed. Approximately 30% production cost reduced after process modified, likewise 19.25 Baht per liter of ethanol was calculated. The cost of production would be decreased when applied to the industrial scale, suitable for sugar industry due to the abundance of raw material. However, this demonstration is a optional concept for process economical improving, the actual operation has not completely done yet. Hence, the capital cost and worthiness of optional process installation would considered further.

4.5 Conclusion

This chapter, the 200 liters of extractive fermentation system was successfully simulated and developed using ASPEN PLUS. The fermentation characteristic, fractionating performance and Venturi system were simulated based on the actual data in chapter III in order to obtain the most precisely value of scaling-up. By way of example, the fermentation ethanol and by-product must be calculated the actual observe yield for interpreting in ASPEN PLUS reaction data. Additionally, the fractionating distillate rate and exiting vapor components must be standardized along with the actual value. In fact, 18.5 liter which contains 82 wt% ethanol solution was produced from 200 liters extractive fermentation per day. The 27.50 Baht per liter of product was calculated via the extractive fermentation system. The systematic development was carried out using simulation program such as recovered the waste stream or changing the boundary condition. For instance, the installation of gas scrubber in order to harvested the non-condensed vapor stream in Venturi tank. Re-distillation of waste stream using laboratory scale distillation system as well as reducing of cooling power requirement in the selective region. That mention above, the production cost decreased about 30% after process improvement. This demonstration is an optional concept for process economical improving, the actual operation has not completely done yet. The capital cost and worthiness of optional process installation would considered further.

4.6 References

Abdel-Banat, B.M.A., Hoshida, H., Ano, A., Nonklang, S. and Akada, R. (2010). High-temperature fermentation: how can processes for ethanol production at high

- temperatures become superior to the traditional process using mesophilic yeast? **Appl. Microbiol. Biotechnol.** 85: 861–867.
- Anderson, P.J., McNeil, K. and Watson, K. (1986) High-efficiency carbohydrate fermentation to ethanol at temperatures above 40°C by *Kluyveromyces marxianus* var. *marxianus* isolated from sugar mills. **Appl. Environ. Microbiol.** 51:1314–1320.
- Balat, M. and Balat, H. (2009). Recent trends in global production and utilization of bio-ethanol fuel. **Appl. Energ.** 86: 2273–2282.
- Ballesteros, I., Ballesteros, M., Cabañas, A., Carrasco, J., Martín, C., Negro, M.J., Saez, F. and Saez, R. (1991) Selection of thermotolerant yeasts for simultaneous saccharification and fermentation (SSF) of cellulose to ethanol. **Appl. Biochem. Biotechnol.** 28–29: 307–315.
- Ballesteros, M., Oliva, J.M., Manzanares, P., Negro, M.J. and Ballesteros, I. (2002) Ethanol production from paper material using a simultaneous saccharification and fermentation system in a fed-batch basis. **World J. Microbiol. Biotechnol.** 18: 559–561.
- Ballesteros, M., Oliva, J.M., Negro, M.J., Manzanares, P. and Ballesteros, I. (2004) Ethanol from lignocellulosic materials by a simultaneous saccharification and fermentation process (SFS) with *Kluyveromyces marxianus* CECT 10875. **Process Biochem.** 39: 1843–1848.
- Banat, I.M., Singh, D. and Marchant, R. (1996). The use of a thermotolerant fermentative *Kluyveromyces marxianus* IMB3 yeast strain for ethanol production. **Acta Biotechnol.** 16: 215 – 223.
- Barron, N., Marchant, R., McHale, L. and McHale, A.P. (1995). Studies on the use of a thermotolerant strain of *Kluyveromyces marxianus* in simultaneous saccharification and ethanol formation from cellulose. **Appl. Microbiol. Biotechnol.** 43: 518–520.

- Bolun, Y., Jiang, W., Guosheng, Z., Huajun, W. and Shiqing, L. (2006). Multiplicity analysis in reactive distillation column using Aspen Plus. **Chinese J. Chem. Eng.** 14(3): 301-308.
- Boyle, M., Barron, N. and McHale, A.P. (1997). Simultaneous saccharification and fermentation of straw to ethanol using the thermotolerant yeast strain *Kluyveromyces marxianus* imb3. **Biotechnol. Lett.** 19: 49–51.
- Brinkhorst, S., von Lavante, E. and Wendt, G. (2015). Numerical investigation of cavitating Herschel Venturi-Tubes applied to liquid flow metering. **Flow Meas. Instrum.** 43: 23-33.
- Fleming, M., Barron, N., Marehant, R., McHale, L. and McHale, A.P. (1993). Studies on the growth of a thermotolerant yeast strain, *Kluyveromyces marxianus* IMB3, on sucrose containing media. **Biotechnol. Lett.** 15: 1195–1198.
- Gadalla, M.A., Olujic, Z., Jansens, P.J., Jobson, M. and Smith, R. (2005). Reducing CO₂ emissions and energy consumption of heat-integrated distillation systems. **Environ. Sci. Technol.** 39(17): 6860–6870.
- Galbe, M. and Zacchi, G. (1994). Simulation of ethanol production process based on enzymatic hydrolysis of woody biomass. **Comput. Chem. Eng.** 18: 687 – 691.
- Gmehling, J., Kolbe, B., Kleiber, M. and Rarey, J. (2012). **Chemical Thermodynamics for Process Simulation**. 1st ed. Wiley-VCH Verlag GmbH & Co. KGaA.
- Goddin, C.S., inventors; Standard Oil Company, assignee. Cryogenic distillative removal of CO₂ from high CO₂ content hydrocarbon containing streams
US patent 4459142 A. 1984 July 10.

- Gough, S., Flynn, O., Hack, C.J. and Marchant, R. (1996). Fermentation of molasses using a thermotolerant yeast, *Kluyveromyces marxianus* IMB3: simplex optimization of media supplements. **Appl. Microbiol. Biot.** 46(2): 187 – 190.
- Hong, J., Wang, Y., Kumagai, H. and Tamaki, H. (2007). Construction of thermotolerant yeast expressing thermostable cellulase genes. **J. Biotechnol.** 130: 114–123.
- Jitschin, W. (2004). Gas flow measurement by thin orifice and classical Venturi tube. **Vacuum.** 76: 89-100.
- Lark, N., Xia, Y.K., Qin, C.G., Gong, C.S. and Tsao, G.T. (1997). Production of ethanol from recycled paper sludge using cellulase and yeast *Kluyveromyces marxianus*. **Biomass. Bioenerg.** 12: 135–143.
- Lavante, E., Kaya, H., Winzösch, F., Brinkhorst, S. and Mickan, B. (2015). Flow structure in critical flow Venturi nozzle and its effect on the flow rate. **Flow Meas. Instrum.** 44: 97–106.
- Lim, J.M., Yoon, B.H., Oh, Y.K. and Park, K.A. (2011). The humidity effect on air flow rates in a critical flow venturi nozzle. **Flow Meas. Instrum.** 22: 402–405.
- Limtong, S., Srisuk, N., Yongmanitchai, W., Yurimoto, H., Nakase, T. and Kato, N. (2005). *Pichia thermomethanolica* sp. nov., a novel thermotolerant, methylotrophic yeast isolated in Thailand. **Int. J. Syst. Evol. Microbiol.** 55: 2225–2229.
- McAloon, A., Taylor, F., Yee, W., Ibsen, K. and Wooley, R. (2000). Determining the cost of producing ethanol from corn starch and lignocellulosic feed stocks. Technical report. NREL/TP-580-28893.

- Melnichuk, L.J. and Kelly, K.V., inventor; Woodland Chemical System Inc., assignee. Process for producing saleable liquids from organic material. US patent 6919488 B2. 2005 July 19.
- Negro, M.J., Manzanares, P., Ballesteros, I., Oliva, J.M., Cabanas, A. and Ballesteros, M. (2003). Hydrothermal pretreatment conditions to enhance ethanol production from poplar biomass. **Appl. Biochem. Biotechnol.** 105: 87–100.
- Nonklang, S., Abdel-Banat, B.M.A., Cha-aim, K., Moonjai, N., Hoshida, H., Limtong, S., Yamada, M. and Akada, R. (2008). High-temperature ethanol fermentation and transformation with linear DNA in the thermotolerant yeast *Kluyveromyces marxianus* DMKU3–1042. **Appl. Environ. Microbiol.** 74: 7514–7521.
- Olbrich, H. **The molasses** (2006). Biotechnologie-Kempe GmbH. 131 pp.
- Phillips, S.D. (2007). Technoeconomic analysis of a lignocellulosic biomass indirect gasification process to make ethanol via mixed alcohols synthesis. **Ind. Eng. Chem. Res.** 46: 8887 – 8897.
- Quintero, J.A. and Cardona, C.A. (2011). Process simulation of fuel ethanol production from lignocellulosics using Aspen Plus. **Ind. Eng. Chem. Res.** 50(10): 6205 – 6212.
- Rahimi, A., Niksiar, A. and Mobasheri, M. (2011). Considering roles of heat and mass transfer for increasing the ability of pressure drop models in venturi scrubbers. **Chem. Eng. Process.** 50: 104–112.
- Rajoka, M.I., Ferhan, M. and Khalid, A.M. (2005). Kinetics and thermodynamics of ethanol production by a thermotolerant mutant of *Saccharomyces cerevisiae* in a microprocessor-controlled bioreactor. **Lett. Appl. Microbiol.** 40(5): 316 – 321.
- Ramachandran, R. inventor; The Boc Group, Inc., Process for the production of ethanol and isopropanol. US patent 5488185 A. 1996 January 30.

- Singh, D., Banat, I.M., Nigam, P. and Marchant, R. (1998). Industrial scale ethanol production using the thermotolerant yeast *Kluyveromyces marxianus* IMB3 in an Indian distillery **Biot. Lett.** 20(8): 753–755.
- Suryawati, L., Wilkins, M.R., Bellmer, D.D., Huhnke, R.L., Maness, N.O. and Banat, I.M. (2008). Simultaneous saccharification and fermentation of kanlow switchgrass pretreated by hydrothermolysis using *Kluyveromyces marxianus* IMB4. **Biotechnol. Bioeng.** 101: 894–902.
- Tasic, M. and Veljkovic, V. B. (2011). Simulation of fuel ethanol production from potato tubers. **Comput. Chem. Eng.** 35: 2284–2293.
- Tomov, P., Khelladi, S., Ravelet, F., Sarraf, C., Bakir, F and Vertenoeuil, P. (2016). Experimental study of aerated cavitation in a horizontal venturi nozzle. **Exp. Therm. Fluid Sci.** 70: 85–95.
- Verhoef, A., Degreve, J., Huybrechs, B., Veen, H. V., Pex, P. and Van der Bruggen, B. (2008). Simulation of a hybrid pervaporation–distillation process. **Comput. Chem. Eng.** 32: 1135–1146.
- Wang W. (2002). Cassava production for industrial utilization in China – present and future perspective. In: Cassava research and development in Asia: exploring new opportunities for an ancient crop, 7th Regional Cassava Workshop, pp. 33–38, Bangkok, Thailand, October 28–November 1.
- Zhou, Y., Sun, Z., Gu, H. and Miao, Z. (2016). Performance of iodide vapor absorption in the venturi scrubber working in self-priming mode. **Ann. Nucl. Energy.** 87: 426–443.

CHAPTER V

DEVELOPMENT AND SIMULATION OF HIGH PERFORMANCE LABORATORY-SCALE ETHANOL DISTILLATION SYSTEM

5.1 Abstract

A laboratory high-performance distillation system was designed and established in our lab. The performance and efficiency of the system was determined using different ethanol concentration feeds. This distillation system represented a highly efficient in ethanol rectification. The 93 wt% ethanol solution was extracted from any ethanol content in fermentation broth with the exiting controlled vapor temperature at about 77.0 – 77.5 °C. Nevertheless, the deficiency of stripping performance was represented in this system, especially 72 wt% ethanol concentration presented in bottom stream from the 80 wt% ethanol feed. The simulated data from ASPEN PLUS are highly accurate when compared with the experimental data. The 6.99 mL/min of 90 wt% ethanol was purified from the fermented broth and contained 7 wt% ethanol in stillage stream which is consistent with the experimental data. The sensitivity analysis was performed. The flash operation at 1 kW was an optimal power requirement for feed heating beside the reboiler unit with 2 kW due to the energy conservation aspect. The adjusted heating leading to the reduction of utilities cost by approximately 43.8%. Moreover, the presence of a heat exchanger unit also decreased the heating energy and utilities cost, the 0.1 m² heat exchanger area was an appropriate size.

Keyword: Laboratory-scale distillation system, Heating unit, Heat exchanger

5.2 Introduction

Distillation is a process of separating the component substances from a liquid mixture by evaporation and the condensation. It is the oldest and the most universal process of chemical technology and other branches of industry incorporating separation of mixtures. It is particularly well suited for high purity separations since any degree of separation can be obtained with a fixed energy consumption by increasing the number of equilibrium stages.

To describe the degree of separation between ethanol and water in a column or in a column section, ethanol is expressed as a light component while water expressed as heavy component, the separation factor equation as follow:

$$\alpha = \frac{(X_E/X_W)_T}{(X_E/X_W)_B} \quad (5.1)$$

Where X denotes mole fraction of a component, subscript E denotes ethanol (light component), W denotes water (heavy component), T denotes the top of the section, and B the bottom.

For ethanol/water system, the classical thermodynamic models commonly used in the literature to treat these mixtures at low pressure require a great amount of binary parameters to be determined from experimental data (Gmehling and Onken, 1982). The fundamental equation of Vapor–Liquid Equilibrium can be expressed as the equality of fugacities of each component in the mixture of both phases;

$$\bar{f}_i^L = \bar{f}_i^V \quad (5.2)$$

The fugacity of a component i in the real vapor phase (\bar{f}_i^V) is usually expressed through the vapor fugacity coefficient (ϕ_i^V)

$$\bar{f}_i^V = y_i \phi_i^V P \quad (5.3)$$

At low pressure (less than 2 bars), it is supposed that the vapor phase is ideal gas which means $\phi_i^V = 1$, Therefore,

$$\bar{f}_i^V = y_i P \quad (5.4)$$

In addition, the fugacity of a component in the liquid phase is expressed through either the liquid fugacity coefficient (ϕ_i^L), or the activity coefficient (γ_i). The standard state fugacity (\bar{f}_i^0) can be replaced by the saturated vapor pressure (P_i^{sat}) at the temperature of the system. As a result,

$$\bar{f}_i^L = x_i \gamma_i P_i^{sat} \quad (5.5)$$

Therefore,

$$y_i P = x_i \gamma_i P_i^{sat} \quad (5.6)$$

In equation 5.6, P is the pressure, x_i is the liquid phase mole fraction of component i , γ_i is the activity coefficient calculated by using the UNIQUAC model, and P_i^{sat} is the saturation vapor pressure of component i which can be expressed through Antoine's equation, respectively. The values of pure components parameters of Van der Waals properties, and Antoine's equation constants which a class of semi-empirical correlations that describing the relation between vapor pressure and temperature of pure components follow:

$$\log_{10} p = A - \frac{B}{C + T} \quad (5.7)$$

The Antoine's constant of water and ethanol are given in Table 5.1.

Table 5.1 Pure components parameters: Van der Waals properties of r_i and q_i , and Antoine's equation constant A_i , B_i and C_i (Ghemling and Onken, 1982).

Compounds	r_i	q_i	Antoine's equation		
			A_i	B_i	C_i
Ethanol	2.1055	1.9720	7.1688	1552.60	222.42
Water	0.9200	1.4000	7.0436	1636.91	224.92

The fundamentals of ethanol distillation are described by Madson (2003) and Petlyuk (2004). The schematic diagram of a distillation column with a condenser and reboiler is illustrate in Figure 5.1.

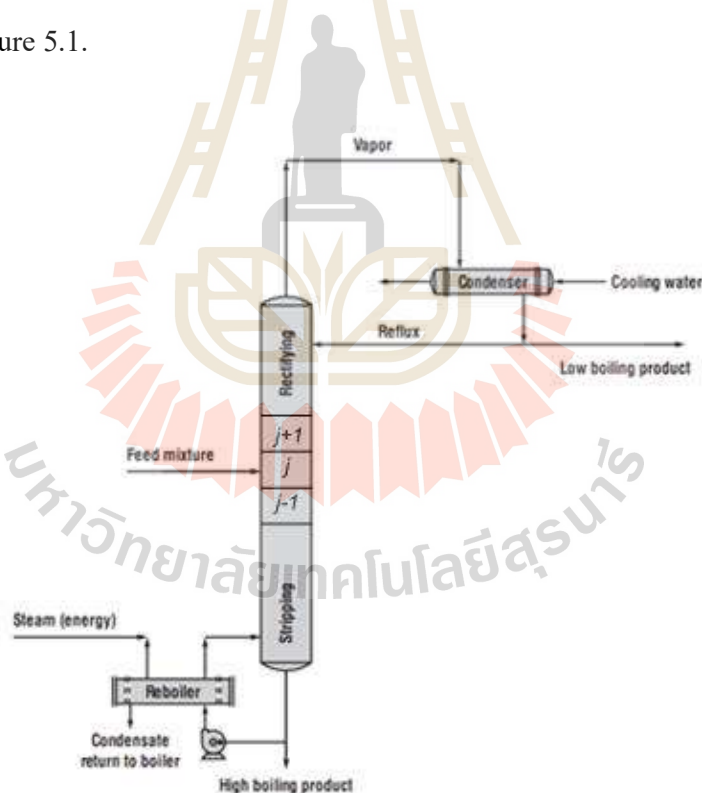


Figure 5.1 The typical distillation system Source: Madson (2003).

In general, the reboiler generates a vapor flow which flows upwards along the column length. The condenser provides a liquid flow, which flows down from tray to tray from top to bottom. Hence, the column contains a number of similar, internal components that are

referred to as “tray” (may also be called stage or plate). The purpose of the trays is to allow intimate contact between rising vapors and descending liquids correlated separation of vapor and liquid. Assuming that the feed was entered in the middle of the tower (j), the liquid flow from tray $j+1$ then meet the vapor flow from tray $j-1$. These flows are not equilibrium and, therefore a mass exchange take place on the tray. A part of the lightest components converts from liquid into vapor phase, and a part of the heaviest of components (or higher boiling temperatures) converts from vapor into the liquid phase. The mechanism and fluid flow in tray as shown in Figure 5.2.

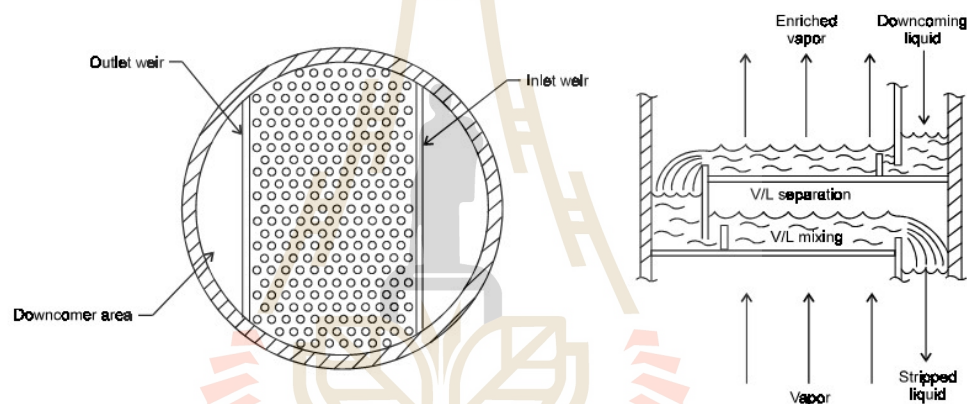


Figure 5.2 The distillation tray diagram (Madson, 2003)

The theoretically ideal stages for ethanol purification have been studied and reported for ages by Robinson and Gilliland (1950). Supposing that the feed contains 10wt% of ethanol and final product is 95wt%, whereas stillage has 0.02 wt% ethanol. Figure 5.3 referred to as a McCabe-Thiele diagram that comprise of two operating lines: one for the rectification section and one for the stripping section. The slope of the operating line is called the internal reflux ratio. As well, the dashed lines represent the graphical solution to the design calculations for the number of theoretical stages required to accomplish a desired degree of separation of the feed component. It was concluded that, there are 22 stages divided

to 14 rectifying stages and 8 stripping stages or at least 13 meters height of the distillation tower for the satisfy ethanol azeotropic concentration.

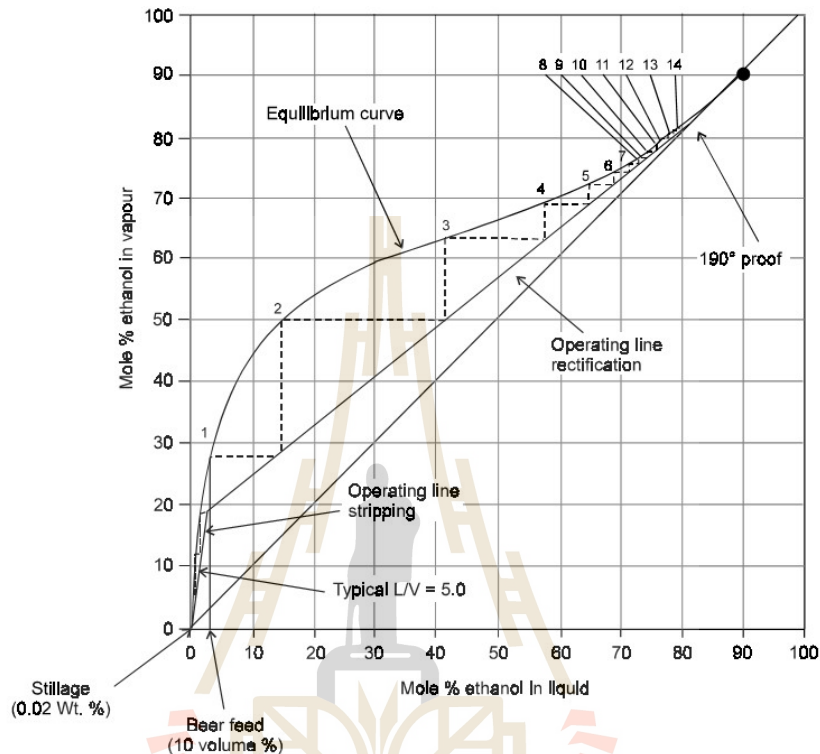


Figure 5.3 The McCabe and Thiele diagram of vapor/liquid equilibrium stages analysis in ethanol/water system (McCabe and Thiele, 1925).

The various design and application of the ethanol distillation techniques have been reported in the past decades. As an illustration, azotropic distillation (Gomis *et al.*, 2015), extractive distillation (Gil *et al.*, 2012), membrane distillation (Tomaszewska and Bialonczyk, 2016) and solar distillation (Jareanjit *et al.*, 2014). This chapter, a laboratory high-performance distillation system was designed and established from our lab. These systemic designs such as fractionating column and rectifying mechanism are moderately different from the conventional distillation or any system that was mentioned above. The designed model is a small scale system which is appropriate for a small fuel-ethanol factory or local distillation business due to the capital cost is significantly lower than the exported

distillation system. This section, efficiency of the designed distillation system was investigated as well as the pilot and industrial plant were assessed and scaled-up using simulation program.

5.3 Instrumental design and experimental set-up

For the designed fractionation system, the unique of this system was the designed distillation tower with the heating jacket that is constructed from stainless steel. The length of both rectifying and stripping sections is 1.2 meters. The 3 kW of flash heating was installed for vapor generation prior entered to column. The excess of feed entered was rinsed down to the bottom then exchanged the heat capacity with the feed-in through the heat exchanger. In the core of column, a set of impellers is fixed on a central shaft driven serves as a dispenser whereas the lower set of impellers has a function of stripping ethanol from fermentation broth in the upward direction. During the operation, the high agitation rate (1000 rpm) generates close contact between the rising vapor, and descending liquid. At the bottom of column, the heating unit at 2 kW was installed as a reboiler in order to re-heat the bottom stream. In addition, a cooling water jacket was installed below the exit point of the column where distillate temperature (T3) that can be precisely controlled by re-circulation of a cooling liquid as a partial condensation. The process diagram and actual image of the laboratory-scale distillation system represented in Figure 5.4.

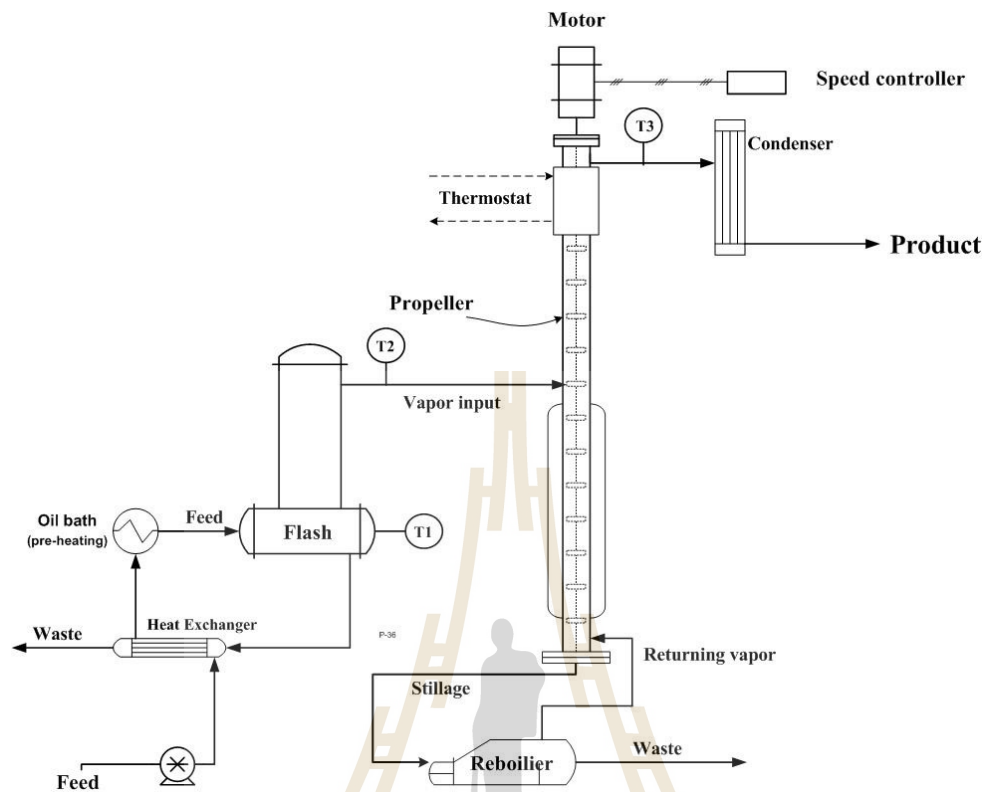


Figure 5.4 The process diagram (above) and actual image (below) of the laboratory-scale distillation system.

In the experimental designed, the synthesized feed was divided into 3 groups including: 4wt% ethanol as stillage feed, 12 wt% ethanol as conventional fermented feed and 80wt% ethanol as the after Venturi feed. The distilled and bottom samples were collected and ethanol concentration was analyzed by Densitometer (L-Dens 313, Anton Parr, Germany). The bottom stream was the summation of released Flash and Reboiler stream.

5.4 Results and discussions

5.4.1 Effect of feed concentration and cooling jacket temperature on distillation performance

In order to specify the performance of designed distillation system, the synthesized feed was divided into 3 groups including 4wt% ethanol as stillage feed, 12 wt% ethanol as conventional fermented feed and 80wt% ethanol as the after venturi feed. The experimental data could use as a database prior to simulate in ASPEN PLUS. The effect of various feed concentrations and cooling jacket temperature at 70 – 80 °C on distillation performance including distilled and bottom ethanol concentration and flow rate as summarized in Table 5.2.

The effectiveness of small-scale ethanol purification was performed in the fixed feed rate at 100 mL/min. It was obvious that, the exiting vapor temperature considerably affected the quality of distilled product. The most concentrated ethanol was observed at 93 wt% with the exiting vapor temperature (T3) at about 77.0 – 77.5 °C whereas the higher vapor temperature results on the lower concentration of ethanol. This phenomena could be clearly describe by the vapor-liquid equilibrium (VLE) diagram (Figure 5.5), water is sensitively vaporized when the temperature was slightly increased (square dot). Although,

the theoretical temperature equilibrium was a little difference with the experiment due to the lack in precision and accuracy of measuring instrument.

Table 5.2 The effect of various feed concentrations and jacket temperature on distilled and bottom ethanol concentration and flow rate.

Feed conc. (wt%)	Jacket temperature (°C)	Vapor temperature T3 (°C)	Ethanol conc. (wt%)		Rate (mL/min)	
			Bottom	Distillate	Bottom	Distillate
4	70.0	79.54	2.50	86.50	99.48	0.43
	72.5	80.07	2.45	85.30	99.20	0.85
	75.0	80.23	2.60	84.80	98.57	1.24
	77.5	81.45	2.55	82.30	97.80	2.03
	80.0	81.97	2.30	80.40	97.54	2.50
12	70.0	77.43	7.20	93.00	97.06	2.10
	72.5	77.63	6.30	92.20	95.79	4.21
	75.0	77.92	5.10	90.50	94.29	5.71
	77.5	78.72	4.50	88.20	92.66	7.34
	80.0	79.43	4.00	86.50	92.20	8.18
80	70.0	77.10	73.40	93.30	85.63	14.38
	72.5	77.50	72.80	92.40	84.50	15.50
	75.0	78.09	72.30	90.50	79.38	20.63
	77.5	78.22	71.50	90.30	74.75	25.25
	80.0	78.80	70.60	87.00	71.50	28.50

At the 12 wt% and 80 wt% feed concentration, the most concentrated ethanol was observed at 93 wt%. It was proved that, the initial concentration was unaffected by the distilled concentration, in contrast affected by the distilled and bottom rate. Higher distilled ethanol concentration resulting in the lower distillate rate while the bottom rate increased. The average distilled/ bottom splitting ratio was found at 0.06 and 0.30 at the 12 wt% and 80 wt% feed concentration, respectively. Likewise, the deficiency of stripping performance was represented in this system. It can be seen that, approximately 5-6 wt% ethanol presented in the bottom stream at the 12 wt% feed with 95 mL/min, especially 72 wt% concentration at the 80 wt% feed with 85 mL/min. For this reason, this unit is designed

using counter current operation (not for the trays or stages). The downward ethanol stream could directly be declined down into the bottom of the column, even though the existing of reboiler would recover ethanol in the bottom side. However, this could be avoided by the recycle of bottom into the feed stream or increase the Flash and Reboiling power in order to enhance the vaporization rate and improve productivity. Therefore, 12 wt% ethanol feed was selected as a testing condition. This distillation condition was simulated using ASPEN PLUS and would be used in the pilot-scale process.

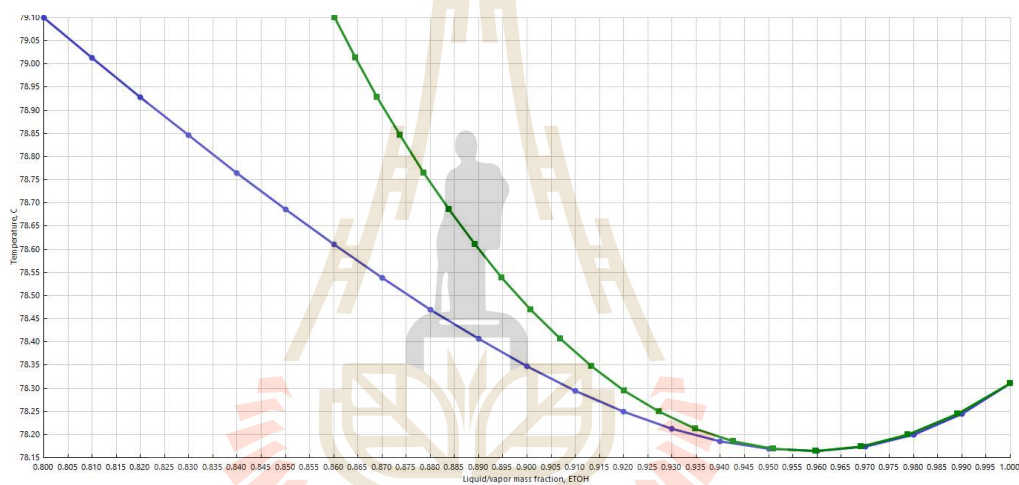


Figure 5.5 Typical vapor liquid equilibrium (VLE) of ethanol/water system.

5.4.2 Simulation of the continuous distillation system using ASPEN PLUS

In this topic, a small scale ethanol distillation system was simulated based on the experimental data as shown in Figure 5.6.

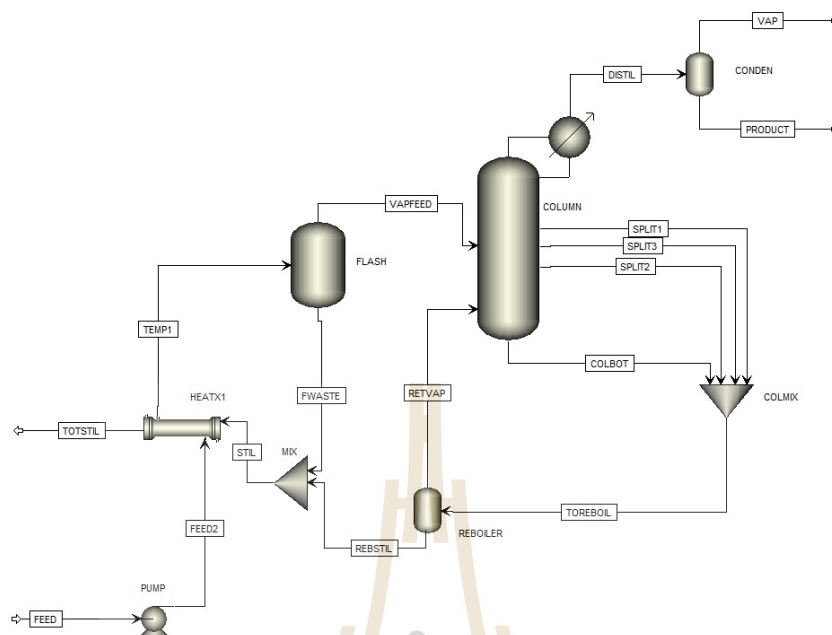


Figure 5.6 The small scale distillation system designed in ASPEN PLUS.

The operational parameters for this system were chosen according to the laboratory-scale process. For example 3 kW flash, 2 kW reboiler, ethanol harvest using condenser, 75°C since the selective region and 150 cm² of heat exchanger (counter current). In case of fractionating column, the distillate rate was fixed according with the experimental data at 0.007 L/min as well as the split fractions at the 2nd, 3rd and 4th stage were set to 0.008, 0.01, 0.012 L/min, respectively. It was found that, there was 14 stages column that require to obtain the desirable ethanol product at 90 wt% (data not shown). The concentration of ethanol in product and stillage stream as well as stream flow rate are summarized in Table 5.3.

The utility costs of the distillation system were analyzed and summarized in Table 5.4. The major utility cost was found in Flash and column heating at 197.31 and 241.63 Baht per day, respectively. A reduction in utility costs and process optimization is reminded in order to obtain the economic feasibility. Simultaneously, the sensitivity analysis of this process by ASPEN PLUS was performed and presented in the next topic.

Table 5.3 Composition, mass and volume flow as well as mass fraction of small-scale distillation system (actual condition).

	Feed	Product	TotStil
Component mass flow (kg/hr)			
Water	5.11	0.03	5.08
EtOH	0.70	0.30	0.39
Component mass fraction			
Water	0.88	0.10	0.93
EtOH	0.12	0.90	0.07
Mass Flow (kg/hr)	5.81	0.34	5.47
Volume Flow (mL/min)	100.10	6.99	96.57
Temperature (°C)	25.00	30.00	58.88

Table 5.4 Utilities usage and utilities cost of the small-scale distillation system.

Unit operation	Pump	Flash	Reboiler	Column	Condenser
Utilities type	ELEC	ELEC	ELEC	ELEC	Water (L/day)
Usage (kW)	0.002	3.00	2.00	3.67	445.96
Cost (Baht/day)	0.11	197.31	131.54	241.63	0.87

5.4.3 Sensitivity analysis

The purpose of the sensitivity analysis is to determine the most appropriate and worthiness condition of the process. In this topic, sensitivity analysis was divided into 2 parts: sensitivity of heating unit and sensitivity of heat exchanger.

5.4.3.1 Sensitivity of flash and reboiler unit

Flash was used in order to generate a vapor stream into the fractionating column. The flash power utility was varied from zero (non-flash installation) to 6 kW, the ethanol flow in product and stillage stream is given in Figure 5.7. The Flash duty has significant affect on the ethanol extraction rate. The ethanol product flow increased

progressively up to a duty of 1 kW, after that slightly decreased. The mass balance have occurred in the stillage flow, ethanol stillage flow decreased progressively up to a duty of 1 kW, after that slightly increased. The decreasing of ethanol in product stream at high flash power is a consequence of the exceeding generation of both ethanol and water vapor stream. The additional water vapor might be extracted from the fractionating column. It seems to be that, an excess of flash duties resulting on the excessive utilized on the selective region in the column also. Too high vapor enthalpy requires a high power for condensation as well. The result of ethanol flow from various flash duties is similar with the result from various reboiling duties (Figure 5.7). The ethanol flow increased considerably from zero (non-reboiling unit) until 2 kW, then non-significantly increased up to 10 kW. In addition, the reboiling power had little effect on the ethanol in the stillage stream that was relatively constant when the power increased.

In conclusion, excessive heating power could be disadvantageous on both economical and productive factors. The appropriate flash and reboiler power were 1 and 2 kW, in that order whereas the heat exchanger increased to 0.1 m². Conversely, higher heating power leads to the higher operating cost while not affecting productivity. The modified process was simulated in ASPEN PLUS and the utilities cost was analyzed as demonstrated in Table 5.6.

According to Table 5.5, the reduction of flash power had benefits to ethanol product quality. There was 92.2 wt% ethanol with approximately 7 mL/min productivity. The stillage stream decreased to 93.55 mL/min. Furthermore, a reduction of utility cost was observed after process optimization. The operating cost of flash decreased to 65.77 Baht/day as well as operating cost of column reduced to 122.69 Baht/day. To put it briefly, the process optimization was successful in improving the product quality at insignificant productivity. Also, operating cost was minimized and reduced by approximately 43.8%.

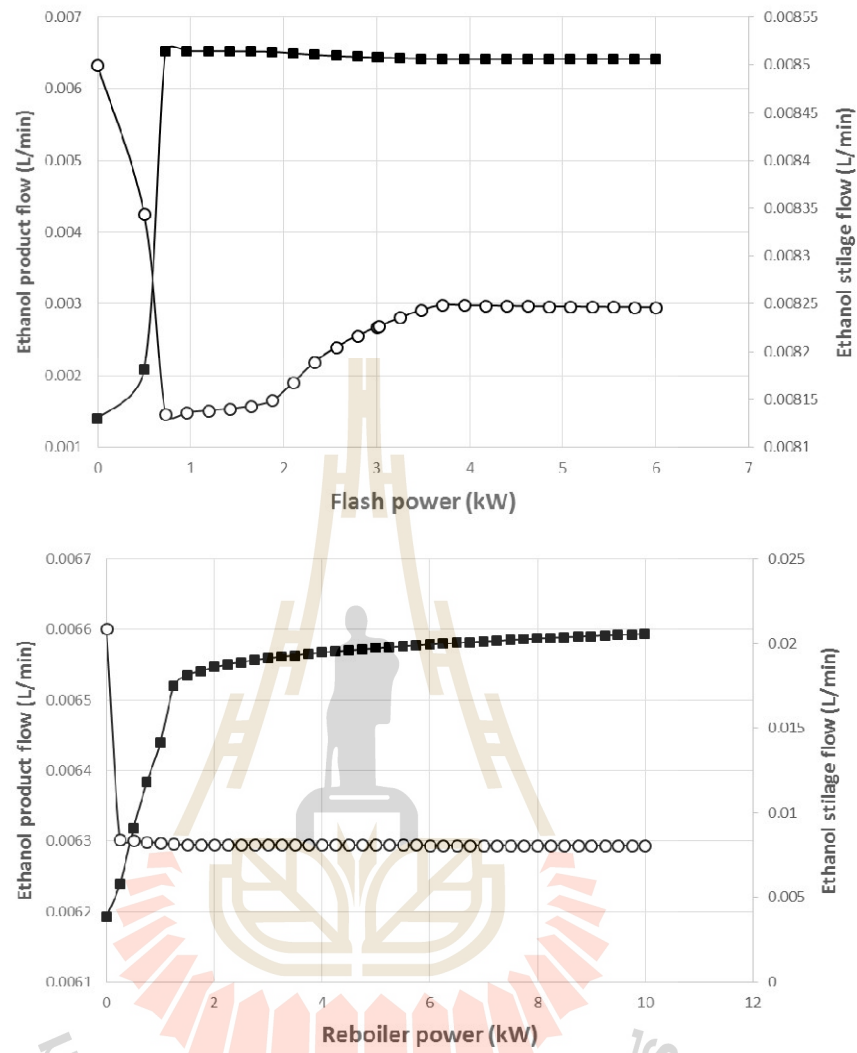


Figure 5.7 Sensitivity analysis of flash power (above) and reboiling power (below) on ethanol product (■) and stillage (○) flow.

Table 5.5 Component mass flow and fraction of modified distillation system.

	Product	TotStil
Component mass flow (kg/hr)		
Water	0.026	5.08
EtOH	0.31	0.39
Component mass fraction		
Water	0.077	0.93
EtOH	0.92	0.07
Mass flow (kg/hr)	0.34	5.47
Volume flow (mL/min)	6.99	93.55
Temperature (°C)	30	28.66

Table 5.6 Utilities usage and utilities cost of the small-scale distillation system.

Unit operation	Pump	Flash	Reboiler	Column	Condenser
Utilities type	ELEC	ELEC	ELEC	ELEC	Water (L/day)
Usage (kW)	0.002	1.00	2.00	1.86	445.96
Cost (Baht/day)	0.11	65.77	131.54	122.69	0.87

5.4.3.2 Sensitivity analysis and advantages of heat exchanger

A heat exchanger is a device that is used to transfer heat between any substances to another. The heat exchanger could be contacted to a barrier of fluid on the other side without bringing the fluids into direct contact. The purpose of heat exchanger installed in this system is energy conservation. The feed stream (cold) was indirectly contacted with the stillage stream (hot) and the heat was transferred to the feed stream. The flash heating cost at different heat exchanger area and comparison with and without heat exchanger were investigated and illustrated in Figure 5.8.

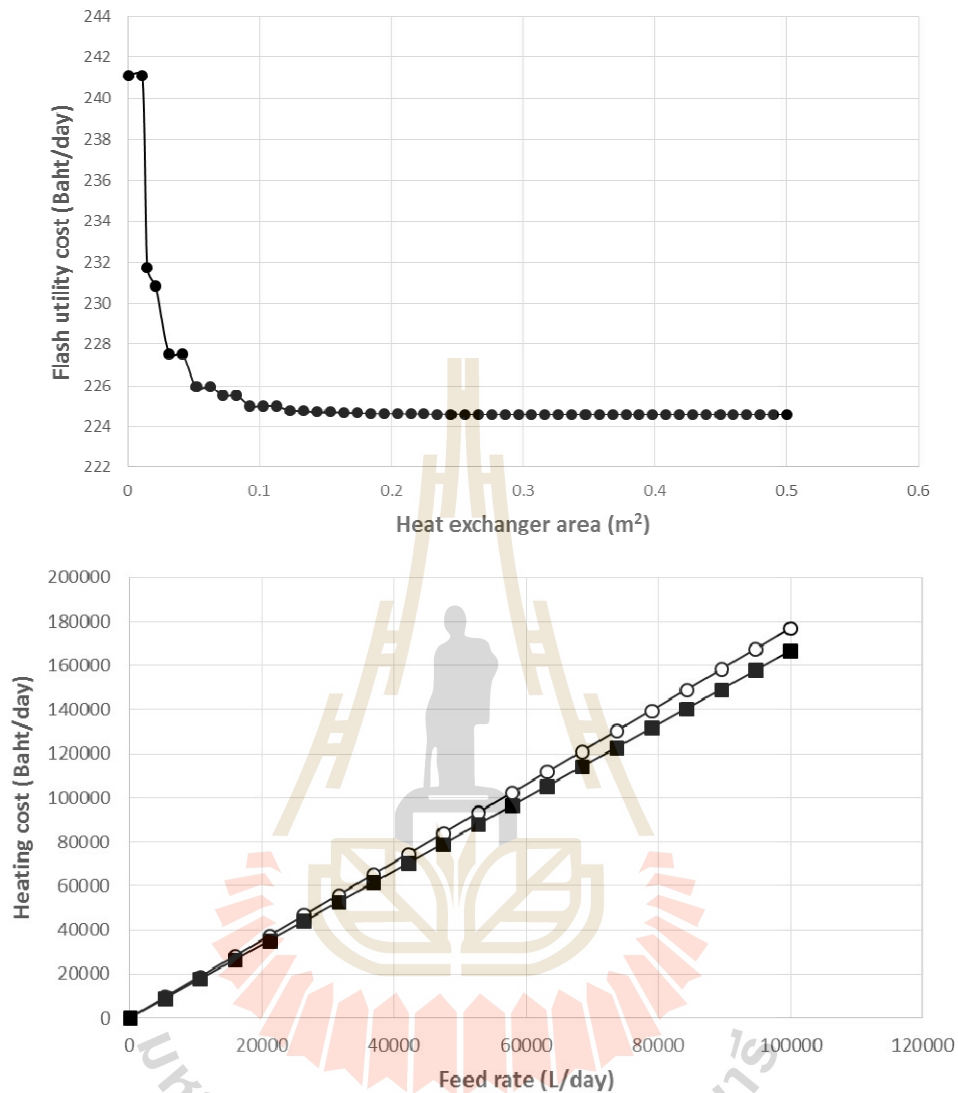


Figure 5.8 Sensitivity analysis of various heat exchanger area on flash utilities cost (above) and heating cost in various feed rate: with heat exchanger (■) and without heat exchanger (○) (below).

The resented of heat exchanger illustrated the energy saving. It was obvious that, heating utilities were reduced as a function of heating area, the flash utility cost reduced continuously then constant after 0.1 m² heat exchanger area. The most effective heat exchanger area was observed at 0.1 m² and reduced the utility cost by around 6.67% per day at 100 mL per min or 144 liters per day. The application of the heat exchanger is the most

apparently demonstrated in the industrial scale. Figure 5.10 shows the heating cost at different feed rates, it was concluded that the different between use and not use the exchanger was larger when the feed rate increased. For example, feed rate at 100,000 L per day could save heating costs of roughly 20,000 Baht per day.

5.5 Conclusion

A small scale distillation system was successfully designed and established in our lab. The designed model appropriate for a small fuel-ethanol factory or local distillation business due to the capital cost is significantly lower than the exported distillation system as well as power requirement. The performance optimization of this equipment was performed and found that more than 90 wt% ethanol was purified from any feed concentration. The optimization of heating power including flash and reboiler is a necessary step in order to specify the feasibility of production cost and installation. Likewise, heat exchanger and its surface area were optimized.

5.6 References

- Ghemling, J., and U. Onken. (1982). Vapor-liquid equilibrium data collection, DECHEMA, Frankfurt.
- Gil, I.D., Gómez, J.M. and Rodríguez, G. (2012). Control of an extractive distillation process to dehydrate ethanol using glycerol as entrainer. **Comput. Chem. Eng.** 39: 129 – 142.

- Gomis, V., Pedraza, R., Saquete, M.D., Font, A. and García-Cano, J. (2015). Ethanol dehydration via azeotropic distillation with gasoline fraction mixtures as entrainers: A pilot-scale study with industrially produced bioethanol and naphtha. **Fuel. Process. Technol.** 140: 198–204.
- Jareanjit, J., Siangsukone, P., Wongwailikhit, K. and Tiansuwan, J. (2014). Development of a mathematical model and simulation of mass transfer of solar ethanol distillation in modified brewery tank. **Appl. Therm. Eng.** 73: 723-731.
- Madson, P.W. (2003). In Jacques, K.A., Lyons, T.P. and Kelsall, D.R. (eds.). **The alcohol textbook**. 4th ed. Nottingham University Press, UK.
- McCabe, W.L. and Thiele, E.W. (1925). Graphical design of fractionating column. **Ind. Eng. Chem.** 17: 606 – 611.
- Petlyuk, F.B. (2004). **Distillation theory and its application to optimal design of separation unit**. Cambridge University Press, UK.
- Robinson and Gilliland. (1950). *Elements of fractional distillation*, McGraw Hill Book Co., Inc.
- Tomaszewsk, M. and Białonczyk, L. (2016). Ethanol production from whey in a bioreactor coupled with direct contact membrane distillation. **Catal. Today.** 268: 156–163.

CHAPTER VI

FABRICATION OF SODIUM A ZEOLITE MEMBRANE FOR WATER- ETHANOL SEPARATION IN VAPOR PERMEATION SYSTEM USING RICE HUSK ASH AS A SILICA SOURCE

6.1 Abstract

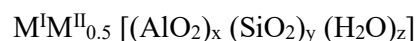
Rice husk is a major by-product of the rice-processing industries. The burned rice husk provided a high content of SiO₂ in the range of 85 – 98%. The hydrophilic NaA zeolite membrane was fabricated using rice husk ash (RHA) as a cheap alternative silica source compared with the silica from chemical sources. The various seeding technique including dip-coating, sonication seeding and vacuum seeding were applied and compared. The synthesized NaA seed for seeding was done at an average particle size of approximately 6 μm that was confirmed by XRD chromatogram and SEM image. Dip-coated membranes achieved higher separation factors and flux than the non-treated substrate. The extracted water was 92 wt% with flux and separation factor at 0.6 kg m⁻² hr⁻¹ and 218, respectively. Conversely, 2 times dip-coated technique showed a disadvantage with respect to separation efficiency. The optimum hydrothermal incubation temperature and time were investigated. The most suitable incubation temperature and time was in the range of 80 – 100 °C and 3 -5 hours, respectively. Nevertheless, the separation performance of the synthesized membranes was unfavorable when compared with previous authors and commercial hydrophilic

membranes. The probable reason is the very large NaA seed in the seeding technique. The approximately 6 μm that was used in the experimental possibly resulted in lower separation factor and flux. The resulted in the formation of an incontinuous and uneven zeolite membrane leading to the inefficient separation factor. The high thickness of the seed layer (50 μm when observed by SEM image) which probably the main reason of the very low flux.

Keywords: RHA, NaA Zeolite, Vapor permeation, Seeding technique

6.2 Introduction

Sodium A (NaA) zeolite or zeolite A is an alumino-silicate framework that is synthesized from silica (silicon compound) and alumina (aluminum compound) under heating condition. NaA zeolite membrane can be made by coating the NaA zeolite on the surface of a support such as alumina and silica support and has been used as a membrane for water dehydration due to the pore size of the NaA zeolite close to the kinetic size of water molecules (approximately 0.32 nm) while the kinetic size of ethanol is around 0.45 nm. The Na^{2+} molecule provide the hydrophilic property of membrane which can stimulated the water transportation. The general formula of zeolite is:



Where M^{I} and M^{II} are alkali and alkali earth metals. The indices x and y denote the oxide variables, and z is the number of molecules of water of hydration. The composition is characterized by the Si/Al atomic ratio and the pore size of the zeolite.

Zeolite A is the zeolite that exhibits the LTA (Linde Type A) structure. It is one of the most important industrial zeolites. Hundreds of thousands of tons of this zeolite are produced every year for application as diverse as water softening in detergents, additive in polyvinyl chloride (PVC) thermoplastic, industrial gas drying as well as production of dehydration

ethanol. The CBUs (composite building units) of LTA are the double 4 rings consist of β cage (sodalite cage) and the α cage (super cage) (Figure 6.1). Zeolite A has a three-dimensional pore system and molecular can be diffuse in all three directions in space by moving across the 8-rings windows that have a free diameter (*cavity*) of approximately 4 Å. The composition of zeolite A as usually obtained from industrial manufacturers is close to $[\text{Na}_{96}(\text{H}_2\text{O})_{216}[\text{Al}_{96}\text{Si}_{96}\text{O}_{384}]]\text{-LTA}$ (Auerbach *et al.*, 2003)

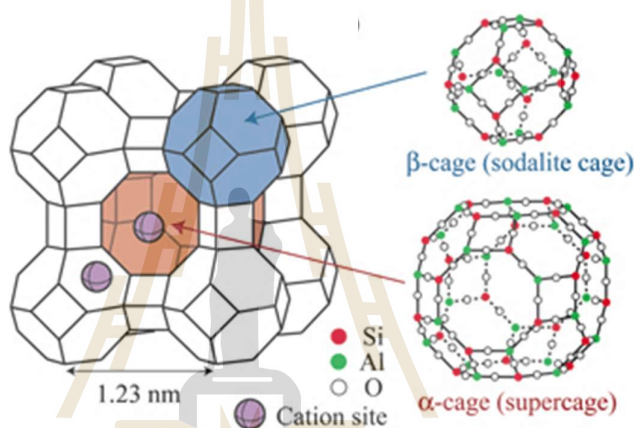


Figure 6.1 NaA Zeolite structure and illustration of α -cage (super cage) and β -cage sodalite cage.

Source: <http://highschoolnanoscience.cnsi.ucla.edu>

Thailand is a world class rice producing and the largest rice exporting country and rice husks are an unwanted by-product of the rice milling (Wang *et al.*, 1998; Kordatos *et al.*, 2008). Rice husk ash (RHA) can be produced by burning of rice husks in a low oxygen atmosphere content at 500 - 700°C and contains approximately 95% of amorphous silica (Artkla *et al.*, 2008). The application of RHA as a silica source for zeolite synthesis has been reported by several authors, for instance ZSM-5 (Rawtani *et al.*, 1989; Chareonpanich *et al.*, 2004; Mohamed *et al.*, 2008; Kordatos *et al.*, 2008; Panpa and Jinawath, 2009 and Ali *et al.*, 2011), ZSM-48 (Wang *et al.*, 1998), ZSM-11 (Dey *et al.*, 2012), zeolite Y (Yusof *et al.*, 2010 and Tan, *et al.*, 2011), zeolite NaX (Dalai *et al.*, 1985) and zeolite NaA (Yusof *et al.*, 2009;

Azizi and Yousefpour, 2010). In this chapter, the sodium A zeolite was synthesized and crystallized in the α -Al₂O₃ ceramic support. The rice husk ash was used as a silica sources for hydrophilic water separation membrane fabrication compared with silica source from chemical. Influences of seeding techniques, hydrothermal temperature and time on separation performance were determined.

6.3 Methodology

6.3.1 Chemicals and materials

- Chemicals for NaA zeolite synthesis including sodium tri-silicate, sodium hydroxide and sodium aluminate were purchased from Sigma-Aldrich (imported by Italmar (Thailand) Co. Ltd.)
- Rice husk as a silica source for NaA zeolite synthesis which by-product in rice manufacturing was obtained SUT farm
- Kaolin originating from Ranong province for α -Al₂O₃ support preparation was obtained from School of Ceramic Engineering, SUT. The composition of clay mixtures is given in Appendix A.
- 95 wt% ethanol was supplied by the Excise department of the Royal Thai Government.

6.3.2 Extraction of silica source from rice husk

Production of rice husk ash (RHA) started with the cleaning-up of the dusk and rice residual using tap water and then followed by stirring in boiling 1 M HCl for 3 hours. Afterward, the mixture was filtrated and cleaned with RO water 2 times for acid elimination. The cleaned rice husk was dried at 100°C overnight using a hot-air oven (Memmert,

Germany). Finally, dried rice husk was sintered at 350°C 30 min then 700°C for 4 hours (Carbolite RHF1600, UK.). The white amorphous solid was kept in a zip-lock plastic bag in order to exclude moisture.

6.3.3 The α -Al₂O₃ support preparation

The porous α -Al₂O₃ support was prepared by cleaning the kaolin 2 times using DI water and then filtered through No.1 filter paper. The wet kaolin was dried at 100°C overnight using hot-air oven (Memmert, Germany). The dried kaolin was milled and sieved at 80 – 100 mesh. Afterward, support was formed using 6 g of dried kaolin then pressed at 10,000 pounds using a hydraulic pressing machine. The diameter of support was 4 cm at 0.3 cm thickness. The formed support was sintered at 1200°C for 2 hours (ramp up and down at 4°C per min).

6.3.4 Preparation of the NaA seeds

The NaA seeds for the seeding method before the hydrothermal synthesis was prepared according to Li *et al.* (2006). The molar ratio of the resultant clear solution was 5SiO₂:Al₂O₃:50Na₂O:1000H₂O. The NaA solution was incubated in an autoclave heating module (Memmert, Germany). The synthesized NaA seeds were filtrated using No.1 filter paper and a suction pump. The synthesized NaA seeds were washed with DI water 2 times or until alkaline solution was washed-out (checked by pH paper). The cleaned NaA seeds were dried in a hot air oven (Memmert, Germany) at 80°C overnight. The properties of NaA seeds were detected via XRD and SEM. The average particle size of NaA seeds was determined using particle analyzer (HORIBA Particq LA-950V2, Japan).

6.3.5 The NaA zeolite formulation and synthesis

The NaA zeolite synthesis solution was prepared according to Li *et al.* (2006). The synthesis mixture was prepared by mixing an aluminate solution and a silicate solution. The aluminate solution was prepared by dissolving sodium hydroxide (12.5 g) in deionized water (51.2 g), then adding sodium aluminate (0.47 g) into the caustic solution. The silicate solution was prepared by mixing sodium hydroxide (0.2 g), sodium tri-silicate (1.54 g) and deionized water (10.0 g). The molar ratio of the resultant clear solution was $5\text{SiO}_2:\text{Al}_2\text{O}_3:50\text{Na}_2\text{O}:1000\text{H}_2\text{O}$. The calculation of molar to weight was completed (See Appendix B). The NaA zeolite solution was incubated at room temperature for 30 minutes before the hydrothermal synthesis step.

A porous $\alpha\text{-Al}_2\text{O}_3$ support was placed in the Teflon bucket and placed vertically in a stainless-steel housing, then the bucket was closed tightly. After that, the synthesis solution was added and the solution was hydrothermally incubated. Then, the crystallization was carried out in autoclave heating (Memmert, Germany). After the synthesis, the membrane was thoroughly washed with deionized water and dried at room temperature overnight.

In order to investigate the individual synthesis parameters on the characteristics and separation performances of synthesized membranes, membranes were also synthesized with different solution aging time, *in situ* aging temperature, *in-situ* aging time and different support pre-treatment.

6.3.6 Seeding procedures

The several seeding methods before hydrothermal synthesis were carried out as follow:

6.3.6.1 Dip-coating method

The 3 wt% of NaA seeds prepared from 6.3.5 was used as a seeding solution. The kaolin support was dipped in NaA solution for 5 seconds. The dipped support was dried at room temperature overnight.

6.3.6.2 Sonicate seeding method

The support was soaked in 3 wt% of NaA seeds solution. Then, sample was sonicated in sonicator (Crest Ultrasonic, USA.) at 30°C for 5 min. The support was dried at room temperature overnight.

6.3.6.3 Vacuum seeding method

The support was fixed in the vacuum flask and connected to the vacuum pump. Then, 5 mL of 3 wt% of NaA seeds solution was poured into support. The support was dried at room temperature overnight.

6.3.7 Membrane characterization

The finished membranes were characterized with respect to separation performance, crystallinity and morphology as follow:

6.3.7.1 Separation factor and flux

The separation and flux measurement were carried out using a self-made stainless-steel membrane housing module. The diagram of the membrane housing is shown in Figure 6.2. The detail of designed membrane housing as illustrated in Appendix C. The tested membrane was placed in a stainless steel-block with both side equipped by an

O-ring for tighten and prevent a leak during the experiment. In the bottom of the membrane housing, 50 g of 95 wt% ethanol was added and agitated by a magnetic stirrer. At the side of membrane housing, temperature and pressure probes and a safety valve were also installed. The top of the housing was covered by a heating tape with an electrical dimmer for membrane heating. The membrane housing was placed on a hot plate stirrer for heating up and vapor generation. The permeate side was connected with cold trap that contained liquid nitrogen and vacuum pump. The weight of the liquid in permeate side was measured as well as concentration of permeated water and ethanol were determined by Densitometer (L-Dens 313, Anton Paar, Germany).

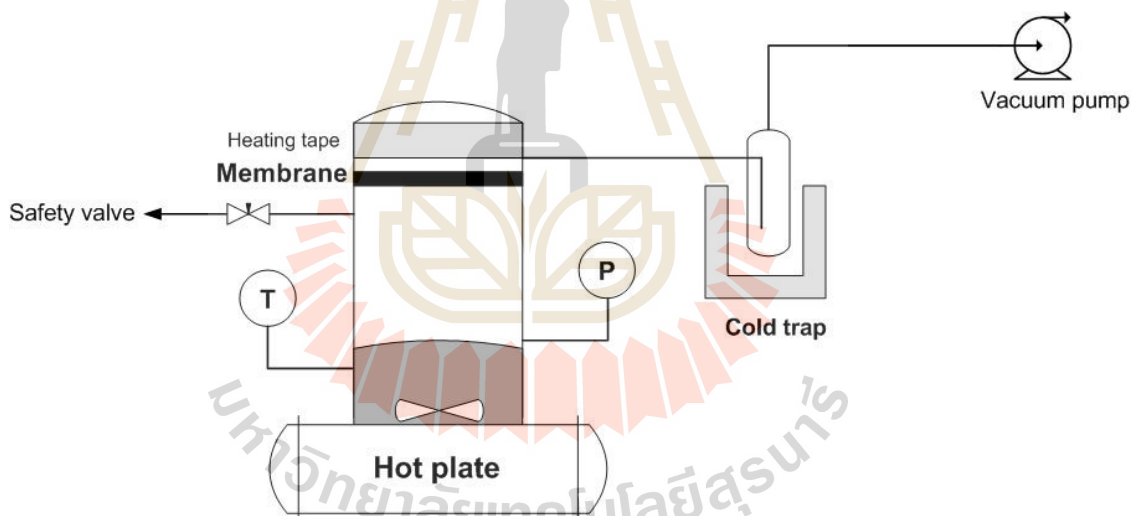


Figure 6.2 The diagram of self-made membrane testing module.

The permeate was collected in order to test the separation factor and mass flux, the separation factor or selectivity was calculated as follow:

$$\alpha = \frac{W_{Perm_EtOH} \cdot W_{Feed_H_2O}}{W_{Feed_EtOH} \cdot W_{Perm_H_2O}}$$

Where W_{Perm_EtOH} is mass fraction of ethanol in permeate side, W_{Perm_H2O} is mass fraction of water in permeate side, W_{Feed_EtOH} is mass fraction of ethanol in feed side and W_{Feed_H2O} is mass fraction of water in feed side. Mass flux was calculated as follow equation:

$$J = \frac{W}{A \cdot t}$$

Where J is the mass flux ($\text{kg}\cdot\text{hr}^{-1}\cdot\text{m}^{-2}$), W is the weight of permeate (kg), A is the membrane area (m^2) and t is the operation time (hr).

6.3.7.2 Crystallinity of NaA seeds using X-ray diffraction (XRD)

The crystallinity of NaA seeds and synthesized NaA in both membrane and powder as well as the non-synthesized support were determined using XRD (Bruker, D8 advance, Germany) The NaA seeds were slightly pressed into discs with 25.4 mm diameter and 3mm thickness in a powder sample holder. The coated NaA membranes were attached to the surface of a sample holder with a plasticine and Cu $K\alpha$ radiation operating at 40 kV and 50 mA of voltage and current, respectively. The coupled two theta/ theta was used as a scan type, the scanning time was 0.2 second and 2200 steps and total time was 468.8 seconds. The 2 theta was set at 5 to 50 and the theta was set at 2.5 to 25. The twin primary and secondary was set at 1 and 5.6, respectively.

6.3.7.3 Morphology of NaA seeds using SEM

The coated membrane surface and fractured cross-section were analyzed by SEM (JSM-6400 scanning microscope, Icospec WDX electron injector). The synthesized membrane samples were broken into a small pieces and then coated with gold as a conductive material using coating machine (Leica, EM ACE600, Germany). The morphology including arrangement of crystal and crystallinity as well as the thickness of

coated layer were observed on the top view and the cross sectional view of the membrane, respectively.

6.4 Results and discussions

6.4.1 Structural characterization of membrane support

After the α - Al_2O_3 supports were prepared, the morphology and crystallinity were investigated using SEM and XRD, respectively. Figure 6.3A and B illustrated the surface of the support from pure kaolin and support mixed with 3 wt% CaCO_3 .

The present of CaCO_3 in the mixture provided the more porous support surface when investigated with SEM. The average pore size of the support with pure kaolin was approximately 1-2 μm , while 4-8 μm of pore size was observed in the support mixed with CaCO_3 . The effect of CaCO_3 in the support preparation was described by Majhi *et al.* (2009). During the sintering step, the mixed CaCO_3 could be converted into CaO forms and the exiting CO_2 generates the pores on the surface of the clay support. The releasing of the gaseous products also changes the volume of clay support. The phase transformation of kaolin to metakaolin and mullite occurs in the studied sintering temperature which can be confirmed by XRD analysis (Khemakhem *et al.*, 2006). Nevertheless, the crystallinity of the support was unaffected when examined using XRD (Figure 6.3).

6.4.2 Synthesis of NaA seeds powder

The purpose of NaA seeds powder analysis was to determine the appropriate hydrothermal synthesis condition as well as the chemical formulation in order to obtain the pure NaA zeolite crystals. The NaA seeds powder was synthesized in difference silica sources including chemicals and silica from rice husk ash (RHA). The morphology of NaA seeds from difference silica sources is shown in Figure 6.5A and B. It includes the completed crystallinity of both chemical and RHA silica sources when observed with SEM. The average

NaA seed size was approximately 3-4 μm . The NaA seeds crystallinity was confirmed by XRD chromatograms (Figure 6.6A and B). The XRD results showed significant peaks 2θ at 7.0° , 10.0° , 12.3° , 16.0° , 21.6° , 24.0° , 27.0° , 30.0° and 34.0° , which further confirms the formation of the NaA zeolite structure from database (red line). The XRD patterns of NaA zeolite from RHA as a silica source was also according to the several authors (Bhavornthanayod and Rungrojchaipon, 2009; Tepamat *et al.*, 2013).

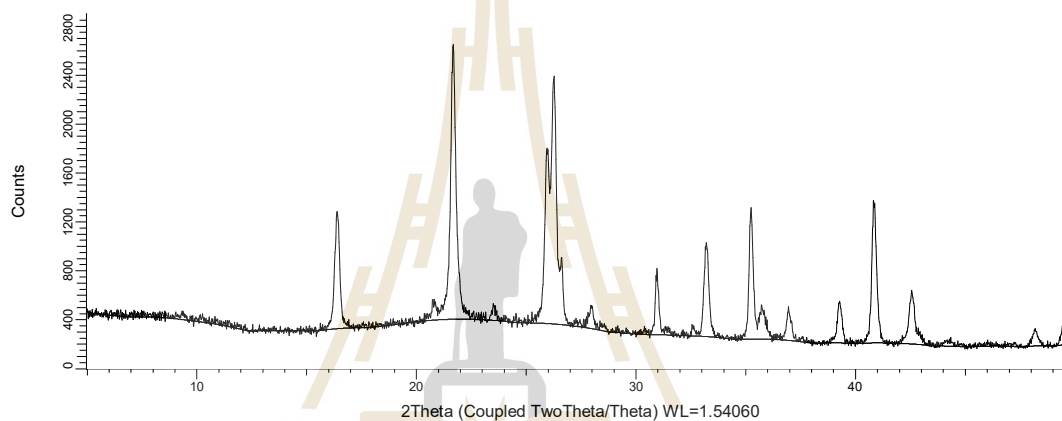


Figure 6.3 XRD chromatogram of the kaolin support.

6.4.3 Effect of seeding technique on the NaA membrane properties using chemical as a silica source

The seeding or secondary growth is a deposition of zeolite nano-sized seed crystals on the substrate (support) before the hydrothermal growth, which cause of the formation of a regularly arrangement of the NaA zeolite crystal. In other words, the preset of seed on the support surface provides a better control of the membrane formation process by forming a gel layer over the seed layer, causing of the crystal nucleation and growth (Tsokanis and Thompson, 1992; Huang *et al.*, 2009). In this study, the NaA seed was crystallized on the various supports including normal support, support with CaCO_3 and support that was dip-coated with 10 μm NaA seed. Effect on separation performance

including permeate ethanol concentration, flux and separation factor at various surface properties and seeding technique is shown in Table 6.1.

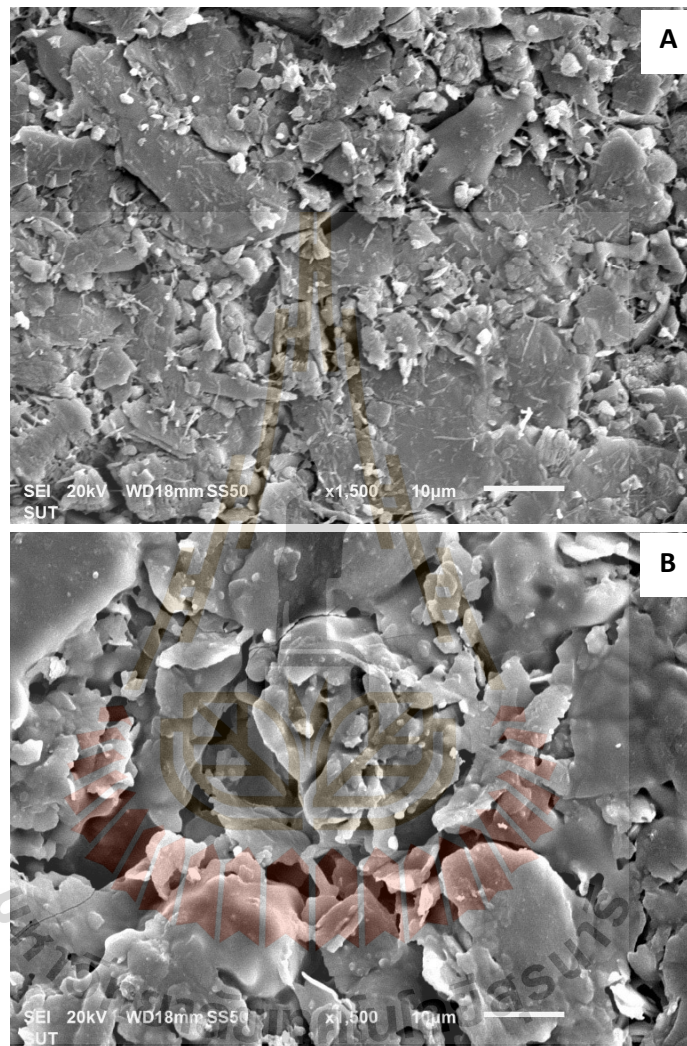


Figure 6.4 SEM images of the support from pure kaolin (A) and kaolin mixed with 3 wt% CaCO₃ (B).

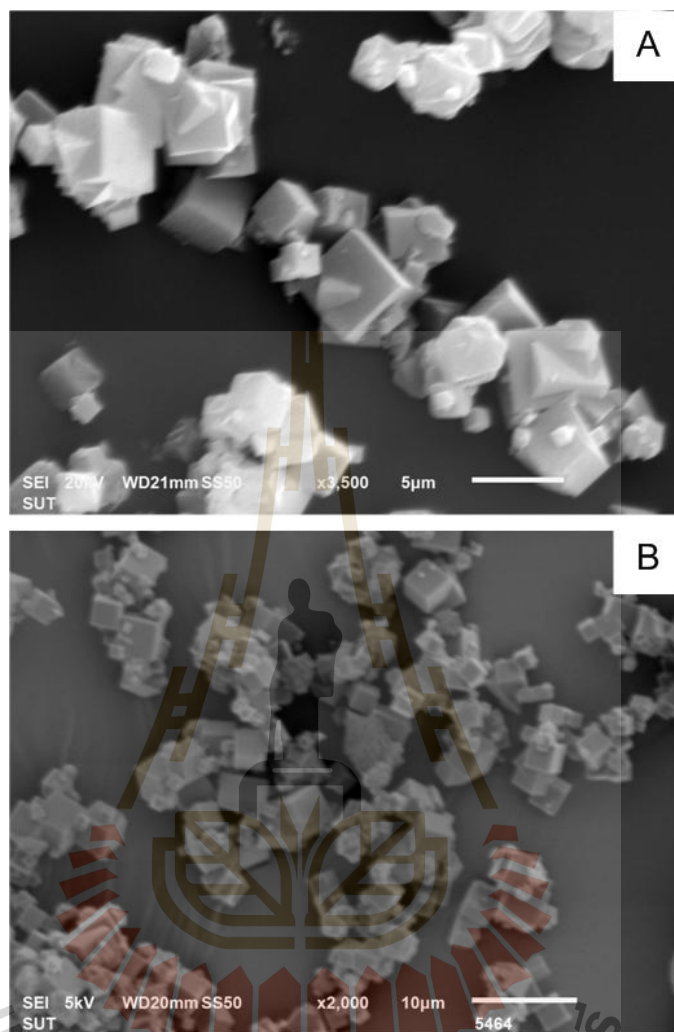


Figure 6.5 SEM images of the NaA seeds powder using chemical as a silica source (A) and RHA as a silica source (B).

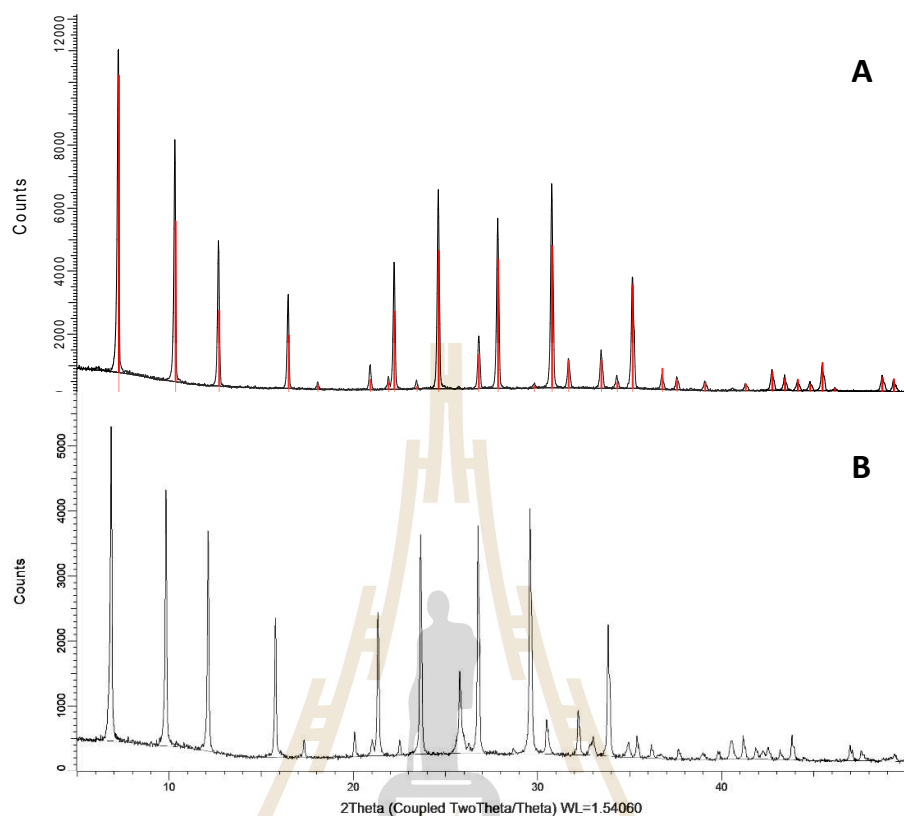


Figure 6.6 XRD chromatograms of the NaA seeds powder using chemical as a silica source (A) and RHA as a silica source (B) (red peak was a NaA chromatograms from database).

Table 6.1 Effect of permeate ethanol concentration, flux and separation factor at various surface properties and seeding technique.

Samples	Support properties & seeding methods	Incubation		Permeate water (wt%)	Flux (kg/m ² hr)	Separation factor (α)
		Temp (°C)	Time (hrs)			
048	Kaolin	85	5	89.01	0.11	153.84
044	Kaolin + 3% CaCO ₃	85	5	75.02	9.09	6.33
045	Kaolin with dip coating	85	5	91.98	0.6	217.95
043	Kaolin with dip coating (2 times)	85	5	72.39	10.98	7.25

The growth of NaA zeolite seed on substrate was presented when observed with XRD chromatograms (Figure 6.7A and B). Nevertheless, surface properties and porosity of kaolin significantly affected the separation efficiency. The synthesized membrane that was treated with CaCO_3 exhibited a lesser water separation performance than non-treated support. Approximately 89 wt% of water was extracted from 5 wt% at the feed side which contained $0.11 \text{ kg m}^{-2} \text{ hr}^{-1}$ flux and 153 separation factor, while 75 wt% permeate water with $9.09 \text{ kg m}^{-2} \text{ hr}^{-1}$ and 6.33 of flux and separation factor were observed from synthesized membranes that were treated with CaCO_3 , respectively. The SEM images of the synthesized membrane without seeding is shown in Figure 6.8A and B. The decreasing of the water separation performance due to the high porosity of the surface, the formation of NaA zeolite crystal could not be entirely develop or the incompletely crystalline formation that the reason of the ethanol passed through the coated substrate.

As a mention before, seeding or secondary growth on the substrate before crystallization resulted in a regular formation and nucleation of the NaA seed. The NaA seed was crystallized on the dip-coated substrate as presented in the XRD chromatograms (Figure 6.7C and D). Dip-coated membrane with $6 \mu\text{m}$ NaA seed showed higher separation factors and fluxes than membrane with non-treated substrate. The extracted water was 92 wt% at a flux and separation factor of $0.6 \text{ kg m}^{-2} \text{ hr}^{-1}$ and 218, respectively. Conversely, 2 times dip-coated technique illustrated a disadvantage on the separation performance. From the testing results, efficiency of water separation from synthesized membrane was relatively low when compared with commercial water separation membrane and previously several authors (Kita *et al.*, 2003; Sato and Nakane, 2007; Sato *et al.*, 2008; Kunnakorn *et al.*, 2011) that represented the separation factor more than 10,000.

A possible hypothesis for this phenomena is the size of the particle NaA seeds. For this study, $6 \mu\text{m}$ (average size) of seeds was applied in the dip-coated seeding technique

compared to less than 1 μm seed particle size used by many authors. The influence of seed size on the formation and structure of zeolite crystal have been reported (Zhang *et al.*, 2006). Zeolite seeds of approximately 100 nm, 600 nm, 1.5 μm , 3.0 μm and 7.5 μm were crystallized on porous α -alumina support and seeding using slip-casting technique. It has been found that, seed sizes have important effects on the formation of seed layers that determines the quality of regrown zeolite membranes. The seed layers and membranes prepared from smaller seeds have smoother surface and lesser defects. The smaller seed size resulted in a more uniform layer and continuity nucleation leading to a denser membrane. The larger seed provided a coarse surface with some voids on the membrane surface. In addition, the seed size over 7.5 μm leads to the formation of an inconinuous seed layer, which results in the formation of an inconinuous and uneven zeolite membrane. As a consequence, the synthesized membrane which was prepared from 10 μm NaA seed illustrated the incomplete seed crystal, coarse and voids on surface leading to the inefficient separation factor. The very thick of the seed layer (50 μm) when observed by SEM (Figure 6.8E) which were probably the main reason of the very low flux.

From that above, a small seed particle size is significant in order to obtain an appropriate and uniform membrane fabrication. Preparation of a small and event seed particles has been successful (Kuanchertchoo *et al.*, 2006). A nano-sized NaA zeolite seed was prepared using silatrane and alumatrane precursors via the sol-gel process and microwave techniques. The composition of SiO_2 : Al_2O_3 : $3\text{Na}_2\text{O}$: $410\text{H}_2\text{O}$ with 1–3 wt% of seed crystals using reaction temperatures ranging from 80 to 100 $^\circ\text{C}$ provided uniform and homogeneous distribution of 0.1–0.2 μm NaA zeolite crystals. The application of the small particle seed have been subsequently reported (Kuanchertchoo *et al.*, 2007). The NaA zeolite membranes prepared using a 0.5 μm NaA crystal seed concentration of 3 g/l via vacuum seeding, the optimum conditions were 90 $^\circ\text{C}$ and synthesis temperature for 15–20 min via

microwave heating. The approximately 10 μm thickness layer was detected using SEM image. The thin NaA layer leading to the higher flux and the separation factor were obtained at 1.6 $\text{kg}/\text{m}^2 \text{ h}$ and 1760.5, respectively. Likewise, results of the nano-size seed application was corresponding with (Kunnakorn *et al.*, 2011). The 0.5 μm NaA crystal seed concentration of 7 g/l was used for seeding and autoclave method was applied for hydrothermal synthesis. It was found that membrane thickness was observed at about 7-9 μm with 2.82 $\text{kg}/\text{m}^2 \text{ h}$ and separation factor of more than 10,000 was calculated.

6.4.4 Synthesis of NaA membrane using RHA as a silica source: effect of various seeding techniques and hydrothermal condition

The NaA zeolite using RHA as a silica source was successfully crystallized on the support surface. Effect of various seeding techniques on the separation performance including permeate water concentration, flux and separation factor are shown in Table 6.2. The leaked sample was found in the synthesized membrane that used the vacuum seeding technique. The inefficient resulting water separation was confirmed by SEM image (Figure 6.9A), the dense and incontinuous seed layer was observed on the surface of membrane. The results of vacuum seeding in the synthesis of NaA zeolite membrane was also disapprove by previous authors. The synthesis of NaA zeolite pervaporation membranes using the vacuum seeding method and applied to the dehydration of ethyl acetate/water mixture have been reported (Moheb Shahrestani *et al.*, 2013). They claimed that the vacuum condition could motivate the distribution of suspended seeds on the support surface. The synthesized membrane showed a very high separation factor value ($\alpha = 163,000$) and fairly permeation flux ($0.315 \text{ kg m}^{-2} \text{ h}^{-1}$), the seed layer was found to be approximately 45 μm thick.

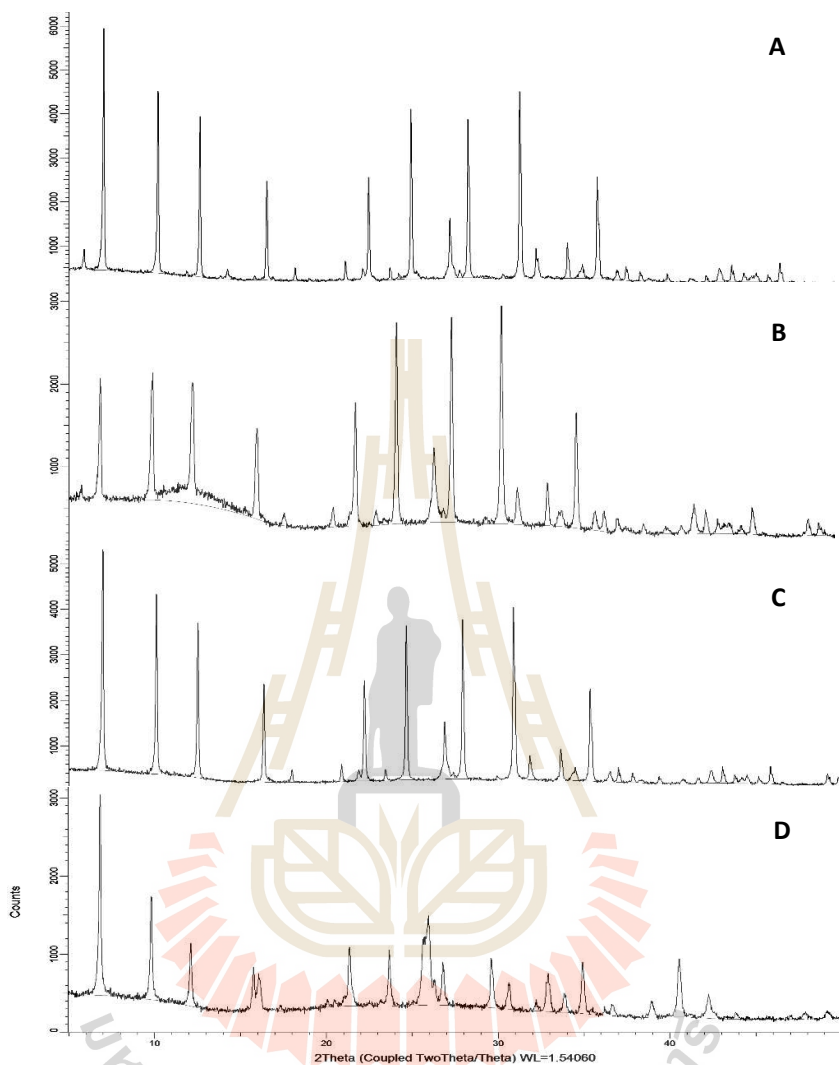


Figure 6.7 XRD chromatograms of the synthesized NaA zeolite membranes in various support properties including pure kaolin [048] (A), kaolin mixed with 3 wt% CaCO₃ [044] (B), various seeding techniques including dip coating 1 time [045] (C) and dip coating 2 times [043] (D).

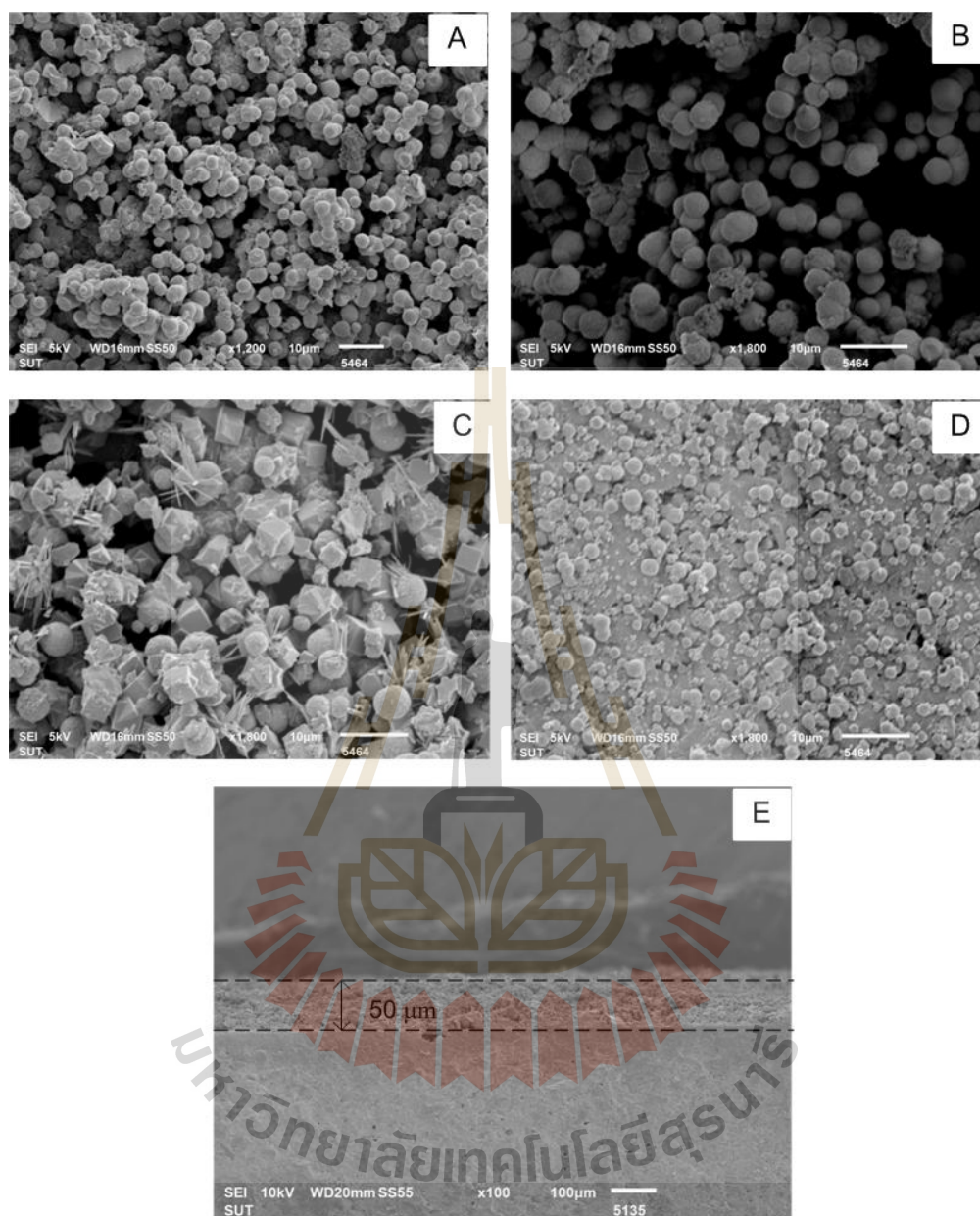


Figure 6.8 SEM images of NaA zeolite synthesized on the substrate in various support properties including pure kaolin [048] (A), kaolin mixed with 3 wt% CaCO_3 [044] (B), various seeding techniques including dip coating 1 time [045] (C), dip coating 2 times [043] (D) and cross-section of the sample [045] (E).

Table 6.2 Effect of permeate water concentration, flux and separation factor at various seeding technique on synthesized membrane using RHA as a silica source.

Samples	Seeding methods	Incubation		Permeate water (wt%)	Flux (kg/m ² hr)	Separation factor (α)
		Temp (°C)	Time (hrs)			
079	Vacuum seeding	85	7	Leak	-	-
075	Sonicate seeding	85	7	71.7	0.727	7.49
065	Dip-coating	100	3	76.7	1.382	5.77
068	Dip-coating (Double synthesis)	100	3	47.4	0.077	21.1

Apart from vacuum seeding, membrane synthesized with the sonication seeding were found to low fairly poor permeate water and flux at 71.7 wt% and 0.727 kg m⁻² h⁻¹, respectively. The synthesized membrane with the dip-coating as a secondary growth method gave the better results than the sonication seeding method at 76.7 wt% and 1.382 kg m⁻² h⁻¹ separation factor and flux, respectively. The improved crystallinity of dip-coated synthesized membrane was observed when compared with the sonication seeding by SEM images (Figure 6.9B and 6.9C). Remarkably, 2 times synthesis with dip-coating illustrated a poorer separation performance than a single synthesis. The 47.4 wt% permeated water was found with an extremely low flux (0.077 kg m⁻² h⁻¹). Dissolved and dense seeds were detected on the surface layer as a result of the non-crystalline NaA seeds. The XRD chromatograms confirmed the crystallinity of a single stage and double stages hydrothermal synthesis (Figure 6.10). It was concluded that, the longer synthesis time stimulates the dissolution of the NaA seeds leading to the inefficient separation performance.

In summary, the dip-coating method lead to membranes with good quality, but generally required very smooth and uniform supports surface. However, some pinholes and dents inevitably exist on the surface of supports for the industrial production, which could

significantly affect membrane quality. The drawback of vacuum suction method is that it needs supplementary equipment and is inconvenient to operate on large-scale production. For rub-coating, it is easy to coat seeds on support surface but it is difficult to achieve uniform coverage, which could result in low-quality membrane growth. The influence of seeding methods such as dip-coating, rubbing and combination coating have been studied by Liu and colleague (2011). They concluded that, combination of rubbing and dip-coating method provided a uniform and well-distributed seeds layer formed on the surface of support, which produced high performance NaA zeolite membranes with high reproducibility. The highest separation performance was represented in the synthesized membrane with a combined seeding pretreatment at $3.06 \text{ kg m}^{-2} \text{ h}^{-1}$ and 15,000 of flux and separation factor, respectively.

Subsequently, the effect of various hydrothermal incubation temperatures and times on permeate ethanol concentration, flux and separation factor were determined as shown in Table 6.3. When a lower aging temperature (60°C) was used, the formation of the NaA zeolite layer on the support surface was not favorable, which can be determined by SEM image and XRD pattern (Figure 6.11A and 6.12A). The amorphous peaks in the XRD chromatogram as well as the result was consistent with the SEM result. The possible reason is that germ nuclei formed during low temperature aging were not enough for the following crystal nucleation and growth during the hydrothermal synthesis.

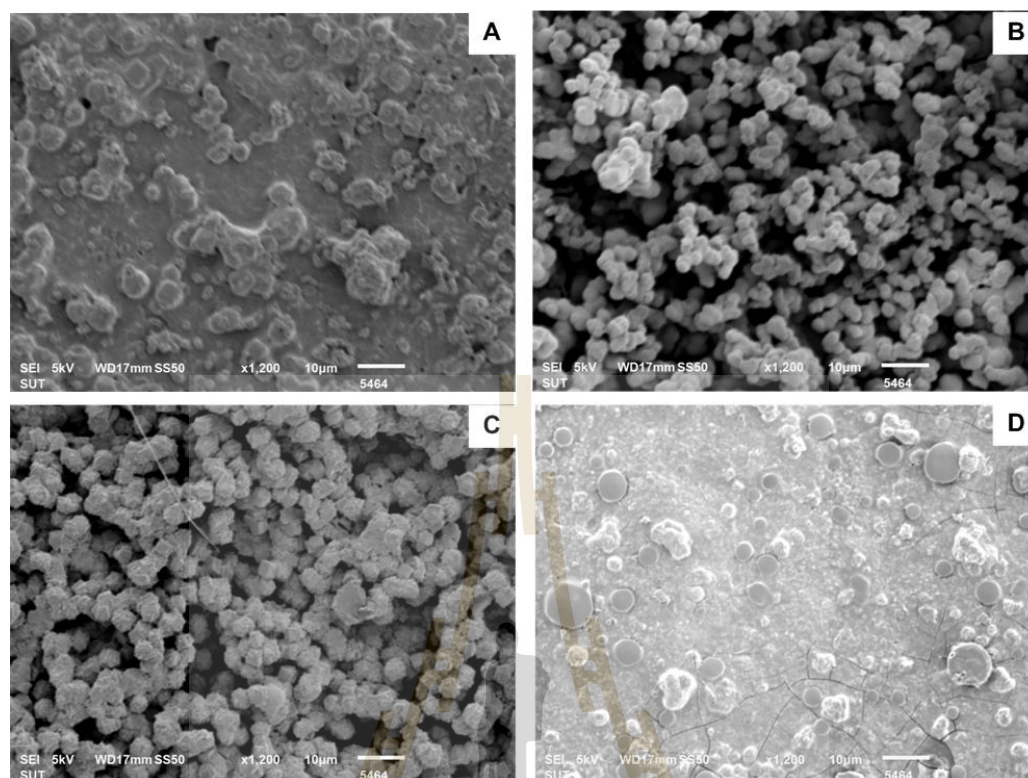


Figure 6.9 SEM images of NaA zeolite synthesized on the substrate using RHA as a silica source in various seeding techniques including vacuum seeding [079] (A), sonicate seeding [075] (B), dip-coating [065] (C) and 2 times dip-coating [068] (D).

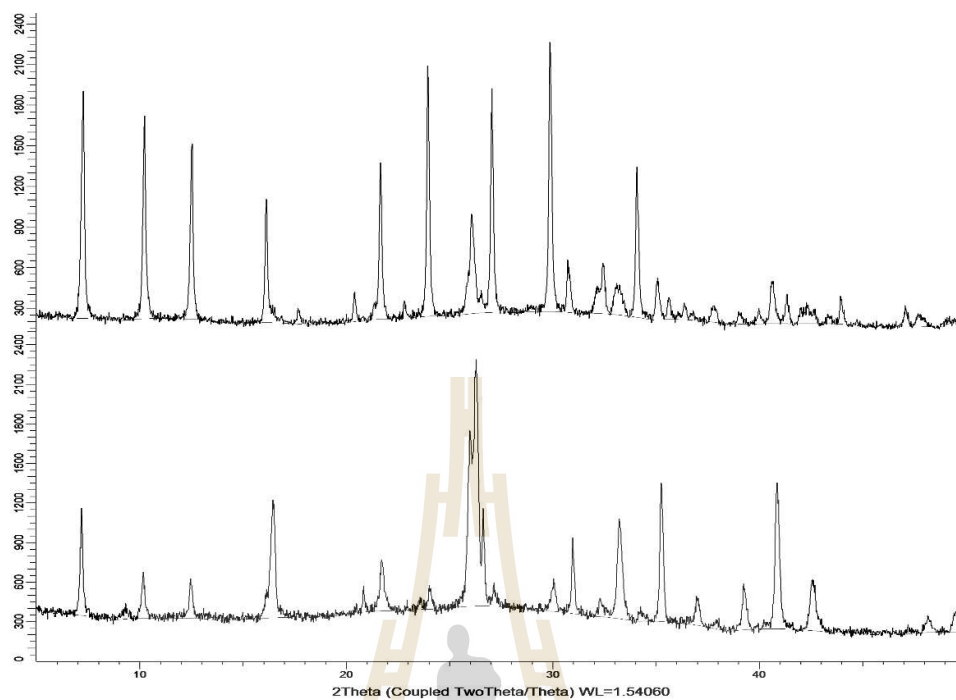


Figure 6.10 XRD chromatograms of NaA zeolite synthesized on the substrate using RHA as a silica source using dip-coating [065] (above) and 2 times dip-coating [068] (below) technique.

Table 6.3 Effect of permeate ethanol concentration, flux and separation factor at various hydrothermal incubate condition on synthesized membrane using RHA as a silica source.

Samples	Incubation		Permeate water (wt%)	Flux (kg/m ² hr)	Separation factor (α)
	Temp (°C)	Time (hrs)			
056	60	17	Leak	-	-
062	80	4	43.9	0.245	24.3
079	80	7	Leak	-	-
069	100	3	69.4	0.244	8.35
070	100	5	71.8	0.062	7.47

In contrast, a continuous NaA zeolite layer was formed on the support surface when a higher *in-situ* aging temperature (80 - 100°C) was applied. The promising NaA layer was confirmed by SEM images (6.9B, D and E) and XRD chromatogram (6.10B and C), whereas some impurities can also be seen in the XRD chromatogram. That is the main reason for the low separation performance (69.4 wt% permeate water). When *in-situ* aging was carried out at a higher temperature, the nucleation and growth of LTA zeolite had already taken place during the aging process. A non-effective separation factor indicating that the formed membrane was defective. There are two possible reasons: one is the negative affection of phase transformation (Xu *et al.*, 2001), the other is the systematic imperfections generated from the ever-occurring triangular-shaped gaps between the growing crystals on the support (McLeary and Jansen, 2004).

Beside *in-situ* aging temperature, *in-situ* aging time is another important factor. The *in-situ* aging time was varied from 3 – 17 hrs and the results determined using XRD and SEM images. It was concluded that, the morphologies were different at the various aging times, the longer aging times led to non-uniform and amorphous crystals (Figure 6.11A, C and Figure 6.12A). That results in the leaked membrane sample as shown in Table 6.4. This is probably because that the longer *in-situ* aging time resulted in the dissolution of NaA zeolite layer on the surface. Nevertheless, the short *in-situ* aging time also resulted in a relatively low crystal growth rate and uncompleted NaA layer forming on the surface. The results concluded that, 4 hrs is the suitable *in-situ* aging time for NaA zeolite hydrothermal synthesis.

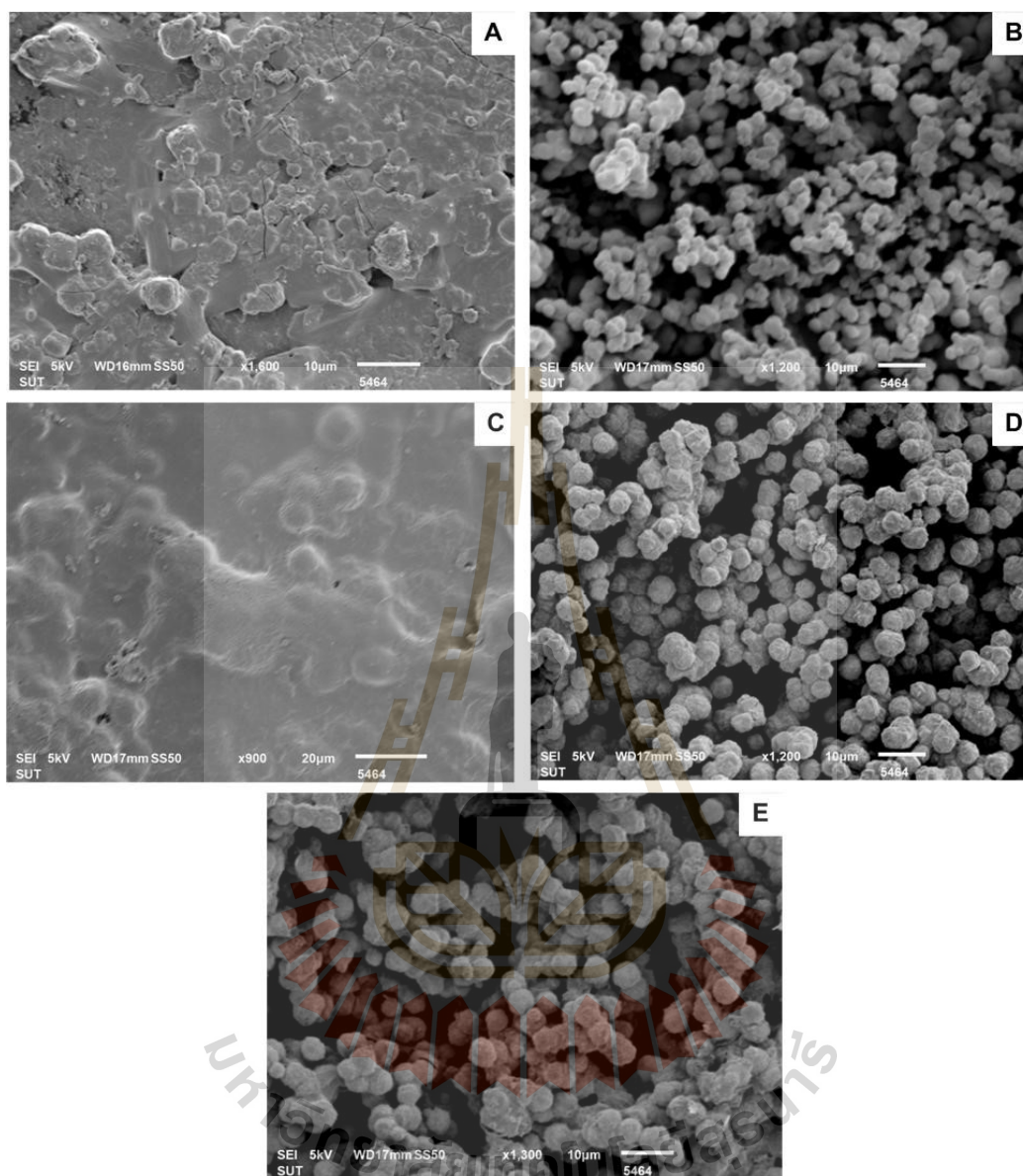


Figure 6.11 SEM images of NaA zeolite synthesized on the substrate using RHA as a silica source in various hydrothermal synthesis condition including 60°C 17 hrs [056] (A), 80°C 4 hrs [062] (B), 80°C 7 hrs [079], (C), 100°C 3 hrs [069] (D) and 100°C 5 hrs [070] (E).

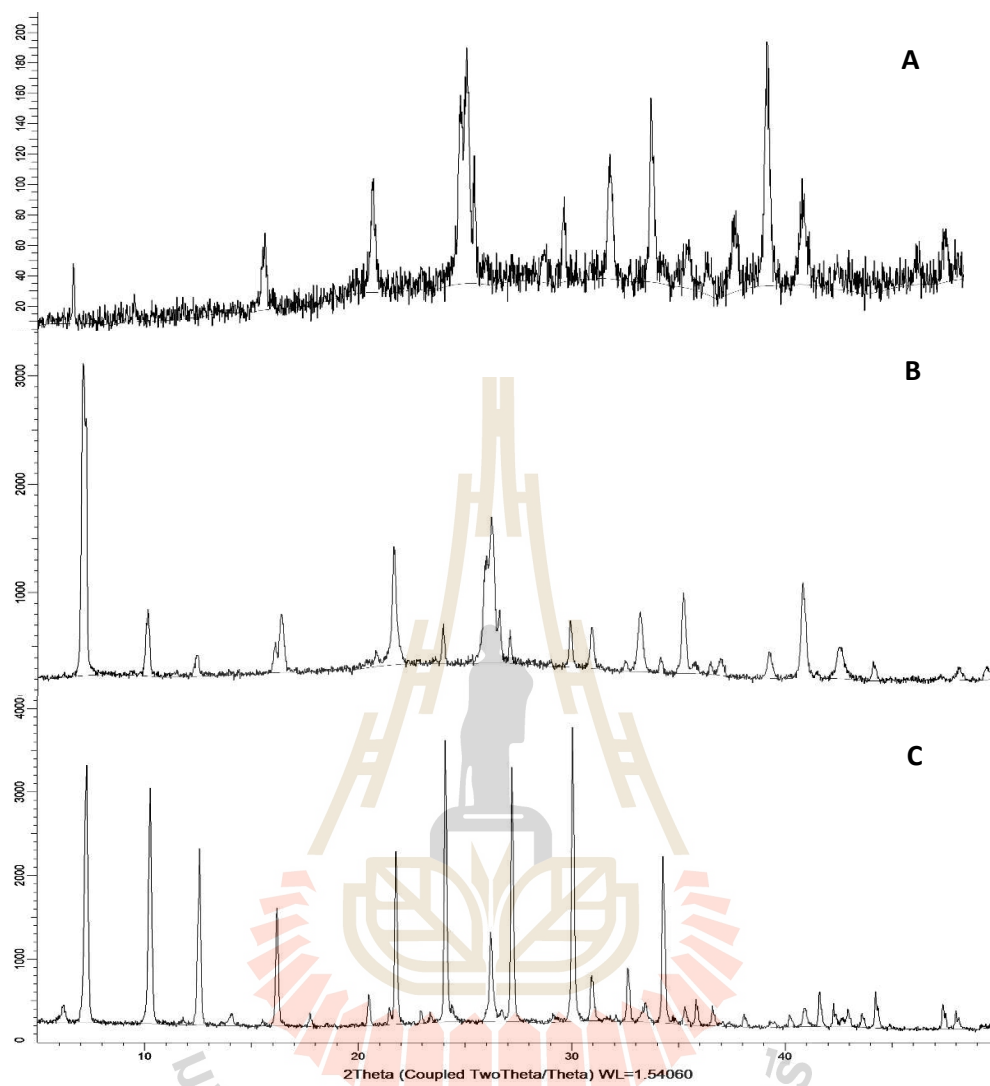


Figure 6.12 XRD chromatograms of NaA zeolite synthesized on the substrate using RHA as a silica source in various hydrothermal synthesis condition including 60°C 17 hrs [056] (A), 80°C 7 hrs [079], (B) and 100°C 3 hrs [069] (C).

6.5 Conclusion

The NaA zeolite membranes for water separation from ethanol were successfully fabricated from different silica sources including chemical and RHA. The average synthesized NaA seed size for seeding was approximately 3-4 μm . Dip-coated pretreatment with 6 μm NaA seed represented higher separation factor and flux than the non-treated substrate and various seeding technique. On the other hand, the separation performance on synthesized membrane was unfavorable when compared with previous authors and commercial hydrophilic membranes. The probable reason is the very large NaA seed size in the seeding technique. The literature has reported that the seed size lower than 1 μm was the most suitable for seeding. Whereas the approximately 6 μm was used in the experimental, that possibly resulted in lower separation factor and flux. Hence, the finest self-made membrane that made from chemical (sample number 045) was selected for mathematical study and simulation in order to scaling-up into the industrial scale in the future.

6.6 References

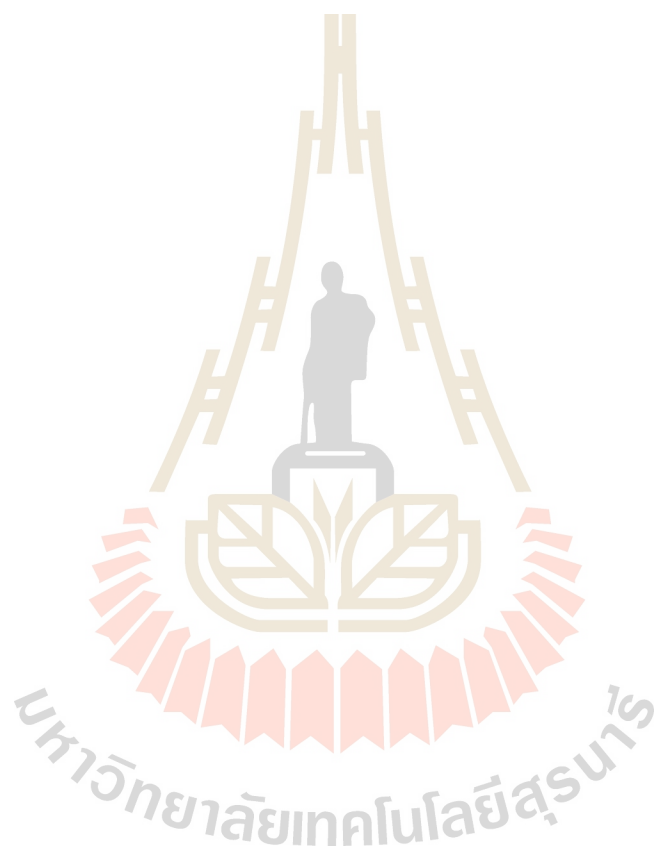
- Ali, I.O., Hassan, A.M., Shaaban, S.M. and Soliman, K.S. (2011). Synthesis and characterization of ZSM-5 zeolite from rice husk ash and their adsorption of Pb^{2+} onto unmodified and surfactant-modified zeolite. **Sep. Purif. Tech.** 83: 38-44.
- Artkla, S., Grisdanurak, N., Neramittagapong, S. and Wittayakun, J. (2008). Characterization and catalytic performance on transesterification of palm olein of potassium oxide supported on RH-MCM-41 from rice husk silica. **Suranaree J. Sci. Technol.** 15(2):133-138.
- Auerbach, S.M., Carrado, K.A. and Dutta, P.K. (2003) **Handbook of zeolite science and technology.** 1st ed. Marcel Dekker Inc. 1184 pp.

- Azizi, S.N. and Yousefpour, M. (2010). Synthesis of zeolites NaA and analcime using rice husk ash as silica source without using organic template. **J. Mat. Sci.** 45(20): 5692-5697.
- Bhavornthanayod, C and Rungrojchaipon, P. (2009). Synthesis of zeolite A membrane from rice husk ash. **J. Met. Mat. Min.** 19(2): 79-83.
- Chareonpanich, M., Namto, T., Kongkachuichay, P. and Limtrakul, J. (2004). Synthesis of ZSM-5 zeolite from lignite fly ash and rice husk ash. **Fuel Process. Techno.** 85(15): 1623-1634.
- Dalai, A.K., Rao, M.S. and Gokhale, K.V.G.K. (1985). Synthesis of NaX zeolite using silica from rice husk ash. **Ind. Eng. Chem. Prod. Res. Dev.** 24(3): 465–468.
- Dey, K.P., Ghosh, S. and Naskar, M.K. (2012). A facile synthesis of ZSM-11 zeolite particles using rice husk ash as silica source. **Mat. Lett.** 87: 87-89.
- Hagen, J. **Industrial catalysis: A practical approach.** (1999) 1st ed. Weinheim: Wiley-VCH. 525 pp.
- Huang, A., Lin, Y.S. and Yang, W. (2004). Synthesis and properties of A-type zeolite membranes by secondary growth method with vacuum seeding. **J. Membrane Sci.** 254(1-2): 41-51.
- Khemakhem, S. Larbot, A. and Ben Amar, R. (2006). Study of performances of ceramic microfiltration membrane from Tunisian clay applied to cuttlefish effluents treatment. **Desalination.** 200: 307
- Kita, H., Okamoto, K., Yamamura, T. and Abe, J. (2003). Zeolite membrane for fuel ethanol production. **Fuel. Chem. D. Preprints.** 48(1): 438.

- Kordatos, K., Gavela, S., Ntziouni, A., Pistiolas, K.N., Kyritsi, A and Kasselouri-Rigopoulou, V. (2008). Synthesis of highly siliceous ZSM-5 zeolite using silica from rice husk ash. **Micropor. Mesopor. Mat.** 115(1-2):189-196.
- Kordatos, K., Gavela, S., Ntziouni, A., Pistiolas, K.N., Kyritsi, A. and Kasselouri-Rigopoulou, V. (2008). Synthesis of highly siliceous ZSM-5 zeolite using silica from rice husk ash. **Micropor. Mesopor Mat.** 115(1-2): 189-196.
- Kuanchertchoo, N., Kulprathipanja, S., Aungkavattana, P., Atong, D., Hemra, K., Rirksomboon, T. and Wongkasemjit, S. (2006). Preparation of uniform and nano-sized NaA zeolite using silatrane and alumatrane precursors. **Appl. Organometal. Chem.** 20: 775–783.
- Kuanchertchoo, N., Suwanpreedee, R., Kulprathipanja, S., Aungkavattana, P., Atong, D., Hemra, K., Rirksomboon, T. and Wongkasemjit, S. (2007). Effects of synthesis parameters on zeolite membrane formation and performance by microwave technique. **Appl. Organometal. Chem.** 21: 841–848.
- Kunnakorn, D., Rirksomboon, T., Aungkavattana, P., Kuanchertchoo, N., Atong, D., Kulprathipanja, S. and Wongkasemjit, S. (2011). Performance of sodium A zeolite membranes synthesized via microwave and autoclave techniques for water–ethanol separation: recycle-continuous pervaporation process. **Desalination.** 269: 78–83.
- Kunnakorn, D., Rirksomboon, T., Aungkavattana, P., Kuanchertchoo, N., Atong, D., Hemra, K., Kulprathipanja, S. and Wongkasemjit, S. (2011). Optimization of synthesis time for high performance of NaA zeolite membranes synthesized via autoclave for water–ethanol separation. **Desalination.** 280: 259-265.
- Li, Y., Chen, H., Liu, J. and Yang, W. (2006). Microwave synthesis of LTA zeolite membranes without seeding. **J. Membrane Sci.** 277: 230–239.

- Liu, Y., Yang, Z., Yu, C., Gu, X. and Xu, N. (2011). Effect of seeding methods on growth of NaA zeolite membranes. **Micropor. Mesopor Mat.** 143: 348-356.
- Majhi, A., Monash, P. and Pugazhenti, G. (2009). Fabrication and characterization of γ - Al_2O_3 -clay composite ultrafiltration membrane for the separation of electrolytes from its aqueous solution. **J. Membrane Sci.** 340: 181-191.
- McLeary, E.E. and Jansen, J.C. (2004). Basic views on the preparation of porous ceramic membrane layers - a comparison between amorphous and crystalline layers, leading to a new method for the preparation of microporous continuous layers. **Topics Catal.** 29: 85.
- Mohamed, M.M., Zidan, F.I. and Thabet, M. (2008). Synthesis of ZSM-5 zeolite from rice husk ash: Characterization and implications for photocatalytic degradation catalysts. **Micropor. Mesopor Mat.** 108(1-3): 193-203.
- Moheb Shahrestani, M., Moheb, A. and Ghiaci, M. (2013). High performance dehydration of ethyl acetate/water mixture by pervaporation using NaA zeolite membrane synthesized by vacuum seeding method. **Vacuum.** 92: 70-76.
- Panpa, W. and Jinawath, S. (2009). Synthesis of ZSM-5 zeolite and silicalite from rice husk ash. **Appl. Catal. B. Envi.** 90(3-4): 389-394.
- Rawtani, A.V., Rao, M.S. and Gokhale, K.V.G.K. (1989). Synthesis of ZSM-5 zeolite using silica from rice-husk ash. **Ind. Eng. Chem. Res.** 28 (9): 1411-1414.
- Sato, K. and Nakane, T. (2007). A high reproducible fabrication method for industrial production of high flux NaA zeolite membrane. **J. Membrane Sci.** 301: 151-.

- Tan, W.C., Yap, S.Y., Matsumoto, A., Othman, R. and Yeoh, F.Y. (2011). Synthesis and characterization of zeolites NaA and NaY from rice husk ash. **Adsorption**. 17: 863-868.
- Tepamat, T, Mongkolkachit, C. and Wasanapiarnpong, T. (2013). Synthesis of zeolite NaA and activated carbon composite from rice husk. **Suranaree J. Sci. Technol.** 21(2):119-123.
- Tsokanis, E.A. and Thompson, R.W. (1992). Further investigations of nucleation by initial breeding in the Al-free NH₄-ZSM-5 system. **Zeolites**. 12(4): 369-373.
- Wang, H.P., Lin, K.S., Huang, Y.J., Li, M.C. and Tsaur, L.K. (1998). Synthesis of zeolite ZSM-48 from rice husk ash. **J. Hazard. Mater.** 58(1-3):147-152.
- Xu, X.C., Yang, W.S., Liu, J. and Lin, L.W. (2001). Synthesis of NaA zeolite membrane from clear solution. **Micropor. Mesopor. Mater.** 43: 299.
- Yusof, A.M., Keat, L.K., Ibrahim, Z., Majid, Z.A. and Nizam, N.A. (2010). Kinetic and equilibrium studies of the removal of ammonium ions from aqueous solution by rice husk ash-synthesized zeolite Y and powdered and granulated forms of mordenite. **J. Hazard. Mat.** 174(1-3): 380-385.
- Yusof, A.M., Nizam, N.A. and Rashid, N.A.A. (2009). Hydrothermal conversion of rice husk ash to faujasite-types and NaA-type of zeolites. **J. Porous Mat.** 17(1): 39-47.
- Zhang, X., Liu, H. and Yeung, K.L. (2006). Influence of seed size on the formation and microstructure of zeolite silicalite-1 membranes by seeded growth. **Mat. Chem. Phys.** 96: 42-50.



CHAPTER VII

A MATHEMETICAL MODEL OF BINARY MIXTURE

ETHANOL/WATER SEPARATION AND SIMULATION OF

ETHANOL DEHYDRATION PROCESS: A COMPARISON

BETWEEN SELF-MADE AND COMMERCIAL

MEMBRANES

7.1 Abstract

Three types of water separation membranes including a commercial ceramic and polymer membrane as well as a self-made synthesized membrane were tested and experimental data was used to calculate the diffusion coefficient (k -value). All type of membranes demonstrated the linearity of the total flux with operating pressure and water content in feed. The commercial ceramic membrane was selected for the determination of the k -value. It was found that, 2.5×10^{-9} and 4.52×10^{-6} mol.s⁻¹.m⁻².Pa⁻¹ of k_e and k_w value with 0.404 objective function (OF) value were successfully calculated from experimental and calculated dataset. The molar flux from experimental data and theoretical data was fitted with the calculated k -value. The simulation of ethanol dehydration was completely done using calculated k -value. The operating pressure including 400 kPa, 145°C, 25 kg/hr feed rate with 95 wt% of ethanol. The simulated data found that, 23.45 kg was produced from this membrane module with a 97.99 wt% ethanol concentration, while 16 membrane tubes were required for the absolute ethanol production (99.5 wt%).

Keywords: Ethanol dehydration process, Mathematical model, Diffusion coefficient (k -value), Process simulation, Sensitivity analysis

7.2 Introduction

Membrane technology has become an important separation technology over the past decade. The main advantage of membrane technology is the fact that it works without the addition of chemicals, with a relatively low energy use and allows simple and well-arranged process integration. Especially, ethanol/water separation is a main application of membrane technology as it accounts for a significant fraction of overall energy consumption in an ethanol plant.

The basic principle of membrane separation is the concentration gradient expressed in terms of partial vapor pressure. A number of different models have been developed to describe the vapor permeation process, the mass transfer across a vapor permeation membrane can be divided into three major steps including sorption of permeating components at the feed side into the membrane, transport of components across the membrane by diffusion according to Fick's law and desorption at the permeate side into vapor phase under vacuum. For the theory of gas permeability through membrane have been described by Fick's law for the macroscopic of transport process,

$$J = -D(c)\nabla c \quad (7.1)$$

Where J is the flux ($\text{mol m}^{-2} \text{s}^{-1}$), $D(c)$ is the concentration dependent diffusivity ($\text{m}^{-2} \text{s}^{-1}$), and c is the concentration (mol m^{-3})

Gas transport through micro porous or dense materials requires adsorption of molecules before the subsequent diffusion process. Numerous sorption models have been

reported in the literature based on different assumption about the state of the adsorbed gas (Ma 1996). In membrane applications for gas separation, adsorption is usually not multi-layer, and often well below a monolayer that has been described by the Langmuir adsorption model

$$\theta = \frac{q}{q_s} = \frac{bP}{1 + bP} \quad (7.2)$$

Where θ is the fractional occupancy of adsorption sites, q is the amount of adsorbed gas molecules per unit mass of adsorbent (mol g^{-1}), q_s is the saturation amount of adsorbed molecules, P is the pressure (Pa) and b is an equilibrium adsorption constant (Pa^{-1}). The dependency of the equilibrium adsorption constant on temperature is given by,

$$b = b_0 \exp\left(\frac{\Delta H_a}{RT}\right) \quad (7.3)$$

Where ΔH_a is the heat of adsorption. At low pressure and high temperature (small value of b), the Langmuir equation may be simplified to,

$$q = q_s bP = KP = K_0 \exp\left(\frac{\Delta H_a}{RT}\right) P \quad (7.4)$$

Where K is a Henry's constant ($\text{mol g}^{-1} \text{Pa}^{-1}$). In the Henry's law regime the amount of adsorbed molecules increases linearly with applied pressure.

Diffusion of molecules through a membrane can proceed in various ways depending on the nature of the interaction between the diffusion gas molecules and the membrane. Various gas diffusion processes were discussed by Burggraaf (1999) in terms of the associated energy potential well developed inside the pores of membrane. The shapes of these energy potential wells depend mainly on the distance between the pores walls and the

diffusing gas molecules. Therefore, the ratio of the molecular size of the diffusing gas and pore diameter plays a major role in determining which diffusion mechanism may apply.

Knudsen diffusion occurs when the mean free path of the diffusing gas molecules is much larger than pore size (Knudsen, 1909). In this regime the gas molecules pass through the pores undergoing random collisions with the pore walls, and the Knudsen diffusivity is obtained from the gas kinetic velocity and the geometric parameters associated with the membrane.

$$D = \frac{\varepsilon d_p}{3\tau} \left(\frac{8RT}{\pi M} \right)^{\frac{1}{2}} \quad (7.5)$$

Where ε is the porosity of the membrane, d_p is the pore diameter, τ is the tortuosity, R is the gas constant and M is molecular weight of the diffusing gas.

As the ratio of the pore size of the membrane versus the size of the diffusing gas molecule decreases, the energy potential in the pores will develop into a steep parabolic potential where the movement of gas molecules changes from a translational to a vibrational mode. A bound molecule in one sorption site will jump to other sorption sites with a vibrational frequency, ν_e , and a jump length, λ . In this regime the gas diffusion is similar to solid state diffusion, and the diffusivity is given by Burggraaf (1999):

$$D = g_d \lambda^2 \nu_e \exp\left(-\frac{\Delta E}{RT}\right) \quad (7.6)$$

Where g_d is a geometric constant and ΔE is the activation energy of diffusion. A model for solid state diffusion also can be obtained by a statistical approach. For gas diffusion in fused silica glass, a statistical model of monatomic gas diffusivity is given by Masaryk and Fulrath (1973):

$$D = \frac{1}{6} \left(\frac{kT}{h} \right) d^2 \frac{\left(e^{hv/2kT} - e^{-hv/2kT} \right)^3}{\left(e^{hv^*/2kT} - e^{-hv^*/2kT} \right)^2} e^{-\Delta E/RT} \quad (7.7)$$

Where k is Boltzmann's constant, h is Planck's constant, d is the distance between sorption sites in the structure, T is the absolute temperature, ν is the vibrational frequency of gas molecules on the sorption sites, ν^* is the vibrational frequency on the doorway sites, R is the gas constant, and ΔE is the activation energy of diffusion.

For the permeation of vapor, the flux ($\text{mol m}^{-2} \text{s}^{-1}$) of gas transport through the membranes is obtained using Fick's first law. In gas phase membrane applications permeance and permeability are usually used as measures of gas transport rate. The permeance, Q , ($\text{mol m}^{-2} \text{s}^{-1} \text{Pa}^{-1}$) is defined as the flux per unit pressure difference between the two sides of the membrane. If the thickness of the separation layer of the membranes is known, the permeability coefficient, P , ($\text{mol m}^{-1} \text{s}^{-1} \text{Pa}^{-1}$) is obtained by normalizing the permeance by the unit thickness of the separation layer.

Gas transport by Knudsen diffusion occurs in the gaseous state without involvement of adsorption. Therefore, the molar flux ($\text{mol m}^{-2} \text{s}^{-1}$) can be obtained using the Knudsen diffusivity and Fick's first law, where the concentration is obtained using the ideal gas law. The Knudsen permeance is then given by,

$$Q = \frac{\varepsilon d_p}{\tau L} \left(\frac{8}{9\pi MRT} \right)^{\frac{1}{2}} \quad (7.8)$$

Where L is the thickness of the membrane.

In many cases of gas permeation through microporous membranes, gas molecules adsorb on the membranes. This adsorption is followed by diffusion to the opposite side of the membranes where the molecules desorb to the gaseous state. In Henry's law regime the

amount of adsorption on the membrane is linearly proportional to the partial pressure (Eq. 7.4). Therefore, the permeance is obtained using the diffusivity and Henry's constant (K).

$$Q = \frac{\rho \varepsilon}{L} D_0(q) K_0 \exp\left(\frac{\Delta H_a}{RT}\right) \exp\left(\frac{-\Delta E_a}{RT}\right) = Q_0 \exp\left(\frac{\Delta H_a - \Delta E}{RT}\right) \quad (7.9)$$

Where ρ is the density of the membrane (g m^{-3}).

There also have been a few statistical studies describing adsorption and diffusion of gas molecules through vitreous silica glass (Studt *et al.*, 1970). The solubility ($\text{mol m}^{-3} \text{Pa}^{-1}$), S , of small gases in the silica glass is given by (Shackelford *et al.*, 1972):

$$S = \frac{n_s}{N_A P} = \left(\frac{h^2}{2\pi M k T}\right)^{\frac{3}{2}} (kT)^{-1} \frac{N_s}{N_A} \left(\frac{e^{-h\nu/2kT}}{1 - e^{-h\nu/2kT}}\right)^3 e^{E(0)/RT} \quad (7.10)$$

Where n_s is the number of gas molecules dissolved per m^3 of glass volume, P is the applied gas pressure, m is the mass of the molecule, h is Planck's constant, k is Boltzmann's constant, ν is the vibrational frequency of gas molecules on the sorption sites, T is temperature, N_s is the number of solubility sites available per m^3 of glass volume, N_A is Avogadro's number, R is the gas constant, and $E(0)$ is the binding energy of the physically dissolved gas molecule in an interstitial sorption site. The permeability, P , of a monatomic gas through silica glass is obtained by using the solubility equation (Eq. 6.10) and the diffusivity equation (Eq. 6.7), and the permeance is obtained by including the thickness of the separation layer, L , in the permeability equation Masaryk and Fulrath (1973).

$$Q = \frac{1}{6L} \left(\frac{d^2}{h}\right) \left(\frac{h^2}{2\pi m k T}\right)^{\frac{3}{2}} \frac{(N_s / N_A)}{\left(e^{h\nu^*/2kT} - e^{-h\nu^*/2kT}\right)^2} e^{-\Delta E_k/RT} \quad (7.11)$$

Where the ΔE_K is the activation energy for the permeation. In the case of polyatomic molecules rotational partition functions on the solubility site and sorption site are also considered in the model equation.

In this chapter, self-made NaA zeolite membrane was tested for water separation in ethanol dehydration process and compared with the commercial zeolite A membrane. The ethanol feed concentration and operating pressure were collected as experimental data. The mathematical model and mechanism of water transportation through membrane was studied and calculated using a mathematical program (MathCad). The k -value was calculated based on the regression model and objective function model. The obtained k -value was applied in the process simulation model of ethanol dehydration process using ASPEN PLUS.

7.3 Methodology

7.3.1 Commercial ceramic and polymer membrane

The NaA zeolite tubular membrane with the effective area of 325 cm² was purchased from Mitsui Engineering & Shipbuilding, Japan. The membrane surface was measured at 260 cm² based on the outer perimeter with a length of 75 cm. This composite membrane was made from hydrothermally synthesized NaA zeolite as the selective layer coated on kaolin as a porous supportive layer. The thickness of the selective layer was approximately 5 μ m as reported by the manufacturer. The flat sheet polymeric membrane is a polyvinyl alcohol as selective layer was purchased from Sulzer (Switzerland).

7.3.2 Mathematical analysis and process simulation

Mathematical transportation analysis of water and ethanol through the synthesized membrane was determined using MathCad 15 as a mathematical program. For the study of the component transportation through the membrane was calculated based on

the basis of the solution/diffusion model. The flux of component i across the membrane is proportional to its partial vapor pressure difference on both sides of the membrane as follows:

$$J_i = \frac{dq}{qA} = k_i (x_i P_F - y_i P_P) \quad (7.12)$$

Where J_i is the molar flux of the component i ($\text{mole}\cdot\text{s}^{-1}\cdot\text{m}^{-2}$), q is the molar transfer rate ($\text{mole}\cdot\text{s}^{-1}$), k_i is the diffusion coefficient of the component i ($\text{mole}\cdot\text{s}^{-1}\cdot\text{m}^{-2}\cdot\text{Pa}^{-1}$), A is the membrane area (m^2), x_i is the mole fraction in the feed side, P_F is the feed pressure (Pa), y_i is the mole fraction in the permeate, and P_P is the permeate pressure (Pa), respectively.

The synthesized membrane transportation mechanism was compared with the commercial hydrophilic membrane (ceramic and polymer). The diffusion coefficient (k -value) of both water and ethanol was calculated using MathCad, based on the experimental data using linear regression technique which adapted from Asthana *et al.* (2006). The calculated k -value was applied to the mathematical simulation in order to scale-up to the industrial scale further. The synthesized membrane was simulated and applied for the anhydrous ethanol production using ASPEN PLUS. The productivity and the cost of production were determined.

7.3.3 Simulation of ethanol dehydration process using ASPEN PLUS

The vapor permeation process in order to separate water was simulated in ASPEN PLUS. In this case, the separator was used as a membrane module and the separation was set according with the MathCad calculation including ethanol split fraction was 0.03 kg/hr and water split fraction was 0.747 kg/hr with 400 kPa feed flash and 100 kPa outlet flash. The permeate flow calculator was set as a discrepancy between feed and retentate flow. The units operation, models and operating condition in ethanol dehydration system applied in ASPEN PLUS were summarized in Table 7.1.

Table 7.1 The units operation, models and operating condition in ethanol dehydration system applied in ASPEN PLUS.

Unit operation	Aspen plus model	Operating detail
Heater	Heater	145°C, 1 bar
Membrane module	Separator	Outlet stream: Permeate EtOH split fraction: 0.03 kg/hr H ₂ O split fraction : 0.747 kg/hr Feed flash: 400 kPa Outlet flash: 100 kPa
Vacuum	Pump	Model: Turbine Discharge pressure: 4 kPa
Retentate condenser	Flash	25°C, 1 bar
Permeate condenser	Flash	-20°C, 1 bar
Permeate stream splitter	Calculator	Perm = Feed - Ret

7.4 Results and discussions

7.4.1 Influence of feed concentration and operating pressure on separation performance: comparison with commercial water separation membranes.

Three types of water separation membranes including commercial ceramic (Mitsui Engineering) and polymer (Sulzer) membrane as well as self-made synthesized membrane were tested for the separation performance. The obtained experimental data was used in order to calculate the diffusion coefficient (k -value) of both water and ethanol through the membranes. In this case, influence of ethanol feed concentration and operating pressure were varied, mass fraction of permeated ethanol and water, separation factor and flux were summarized in Table 7.2, 7.3, 7.4 and Figure 7.1, 7.2, 7.3, respectively.

All types of membrane demonstrated the linear dependency of the total flux on operating pressure as well as water content in feed, due to the selectivity and hydrophilic

properties. Interestingly, ceramic membrane are a more promising technique for dehydrated ethanol production than polymer membrane which was confirmed by the experimental data. The advantages of ceramic membranes for purification over polymer membrane have been reported. For instance, ceramic membrane have more efficiency in gas permeation than polymer membranes, longer life and reliability, higher temperature and mechanical stability under large pressure gradient, stability over large pH range and more ecological friendly and more favorable in separation technology (Sondhi *et al.*, 2003).

The diffusivity of vapor through the zeolite NaA has been studied. Gas permeation through the pore channels of NaA zeolite is controlled by molecular sieving or configurational diffusion mechanisms; gas permeation through the defects is controlled by Knudsen diffusion or capillary condensation or configurational diffusion mechanisms (Xu *et al.*, 2005). The permeance of water vapor will also be significantly higher than that of N₂ and O₂ because the small difference in the molecular kinetic diameter between water vapor (0.275 nm), O₂ (0.346 nm) and N₂ (0.364 nm) causes a significant difference in diffusion rate through the channels of NaA zeolite and the diffusion coefficient (Hedlund *et al.*, 2002).

Table 7.2 Mass fraction of permeated ethanol and water, separation factor and flux in difference feed concentration and pressure using commercial polymer (Sulzer) as a water separation membrane.

Feed EtOH conc (wt%)	Pressure (kPa)	x EtOH		x Water		Separation Factor (α)	Total flux ($\text{kg m}^{-2} \text{hr}^{-1}$)
		Feed	Permeate	Feed	Permeate		
85	100	0.850	0.031	0.150	0.969	176.08	0.352
	200	0.850	0.055	0.150	0.945	96.75	0.680
	300	0.850	0.077	0.150	0.923	68.06	0.925
	400	0.850	0.082	0.150	0.918	63.42	1.200
90	100	0.900	0.038	0.100	0.962	230.67	0.200
	200	0.900	0.065	0.100	0.935	129.48	0.400
	300	0.900	0.080	0.100	0.920	104.20	0.675
	400	0.900	0.087	0.100	0.913	94.37	0.833
95	100	0.950	0.054	0.050	0.946	335.28	0.157
	200	0.950	0.096	0.050	0.904	179.52	0.284
	300	0.950	0.100	0.050	0.900	170.53	0.456
	400	0.950	0.152	0.050	0.848	106.06	0.574
99	100	0.990	0.114	0.010	0.886	766.41	0.086
	200	0.990	0.134	0.010	0.866	641.11	0.140
	300	0.990	0.156	0.010	0.844	536.51	0.195
	400	0.990	0.163	0.010	0.837	507.27	0.244

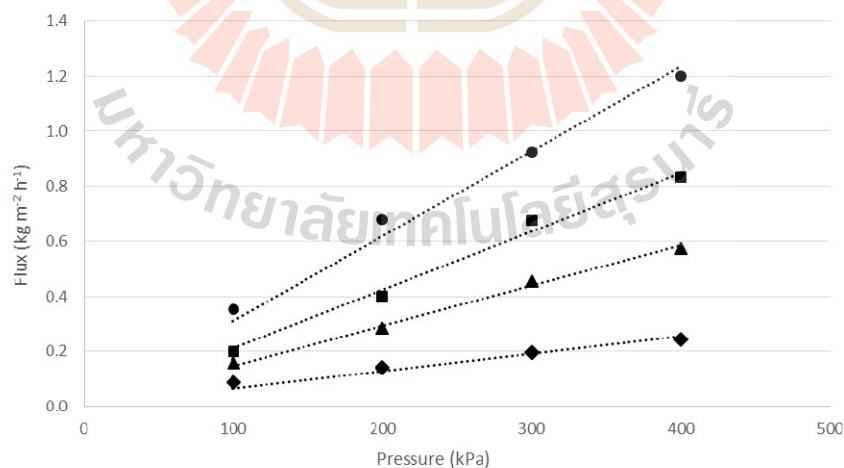


Figure 7.1 Total flux at various operating pressure using commercial polymer membrane (Sulzer) in various feed ethanol concentration: ● 85 wt%, ■ 90 wt%, ▲ 95 wt% and ◆ 99 wt%.

Table 7.3 Mass fraction of permeated ethanol and water, separation factor and flux in difference feed concentration and pressure using commercial ceramic (Mitsui Engineering) as a water separation membrane.

Feed EtOH conc (wt%)	Pressure (kPa)	x EtOH		x water		Separation Factor (α)	Total flux ($\text{kg m}^{-2} \text{hr}^{-1}$)
		Feed	Permeate	Feed	Permeate		
90.0	100	0.900	0.010	0.100	0.990	909.37	3.250
	200	0.900	0.008	0.100	0.992	1062.43	6.640
	300	0.900	0.012	0.100	0.988	766.86	8.830
	400	0.900	0.010	0.100	0.990	918.84	11.130
95.0	100	0.950	0.011	0.050	0.989	1773.45	2.340
	200	0.950	0.011	0.050	0.989	1724.12	4.260
	300	0.950	0.013	0.050	0.987	1453.87	5.750
	400	0.950	0.020	0.050	0.981	955.36	7.130
97.5	100	0.975	0.016	0.025	0.984	2445.08	1.650
	200	0.975	0.018	0.025	0.982	2176.91	2.860
	300	0.975	0.019	0.025	0.981	2035.47	3.650
	400	0.975	0.034	0.025	0.966	1121.71	4.780
99.0	100	0.990	0.022	0.010	0.978	4484.33	0.830
	200	0.990	0.024	0.010	0.976	4095.92	1.380
	300	0.990	0.027	0.010	0.973	3540.71	1.760
	400	0.990	0.040	0.010	0.960	2351.50	2.180

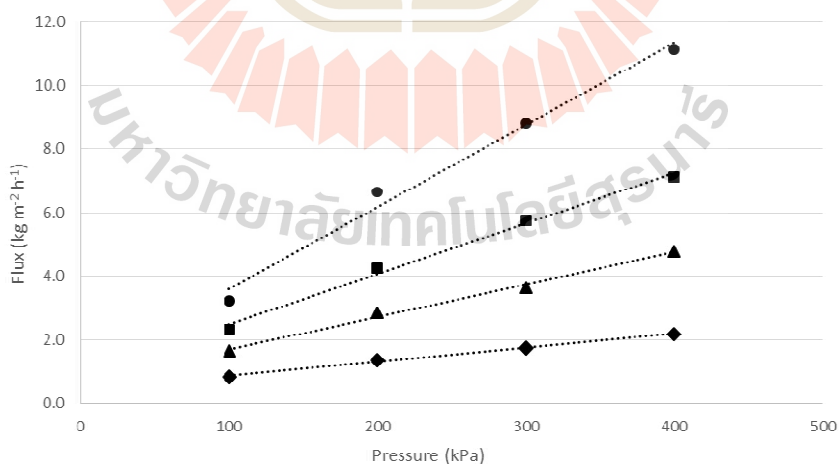


Figure 7.2 Total flux at various operating pressure using commercial ceramic membrane (Mitsui Engineering) in various feed ethanol concentration: ● 90 wt%, ■ 97.5 wt%, ▲ 95 wt% and ◆ 99 wt%.

Table 7.4 Mass fraction of permeated ethanol and water, separation factor and flux in difference feed concentration and pressure using self-made synthesized membrane (sample 045).

Feed EtOH conc (wt%)	Pressure (kPa)	x EtOH		x water		Separation Factor (α)	Total flux ($\text{kg m}^{-2} \text{hr}^{-1}$)
		Feed	Permeate	Feed	Permeate		
85	100	0.850	0.052	0.150	0.948	103.31	0.475
	200	0.850	0.060	0.150	0.940	88.78	0.758
	300	0.850	0.065	0.150	0.935	81.51	1.140
	400	0.850	0.078	0.150	0.922	66.98	1.600
90	100	0.900	0.069	0.100	0.931	121.43	0.346
	200	0.900	0.073	0.100	0.927	114.29	0.650
	300	0.900	0.080	0.100	0.920	103.50	0.886
	400	0.900	0.084	0.100	0.916	98.14	1.240
95	100	0.950	0.074	0.050	0.926	237.76	0.243
	200	0.950	0.080	0.050	0.920	217.91	0.600
	300	0.950	0.083	0.050	0.917	209.92	0.765
	400	0.950	0.086	0.050	0.914	201.93	0.956
99	100	0.990	0.093	0.010	0.907	965.52	0.120
	200	0.990	0.110	0.010	0.890	801.00	0.265
	300	0.990	0.126	0.010	0.874	686.71	0.326
	400	0.990	0.131	0.010	0.869	656.73	0.376

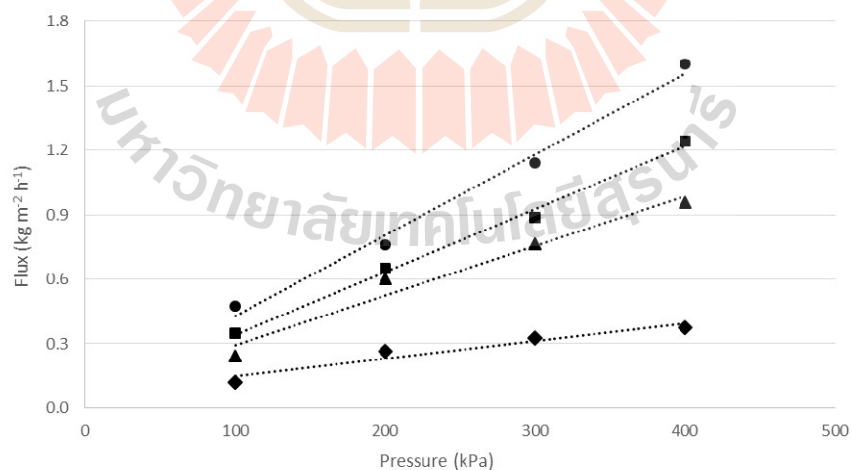


Figure 7.3 Total flux at various operating pressure using self-made synthesized membrane (sample 045) in various feed ethanol concentration: ● 85 wt%, ■ 90 wt%, ▲ 95 wt% and ◆ 99 wt%.

7.4.2 Consideration of the mathematical model equations

In order to calculate the diffusion coefficient (k -value) from the experimental data, the most important factor is the comparison between calculation data (or data from theory) and experimental data. Both of data must be statistically fitted using non-linear regression technique. For example, there are 2 data set for k -value calculation (x and y), the summation of square of variance between calculation and experimental data that called objective function (OF) value must be calculated as follow:

$$OF_i(x, y) = \left[\sum_{j=1}^{ndata} \sum_{i=1}^{ncomp} [x_{exp} - x_{calc}]^2 \right] + \left[\sum_{j=1}^{ndata} \sum_{i=1}^{ncomp} [y_{exp} - y_{calc}]^2 \right] \quad (7.13)$$

Where x_{exp} is the set of experimental data of x , x_{calc} is the set of calculation data set of x , y_{exp} is the set of experimental data of y , y_{calc} is the set of calculation data set of y , The minimum OF value referred to the most correctly value.

When consider the (6.12) equation of the binary component, the flux equation can be separated into water flux and ethanol flux as follow:

$$J_w = k_w(x_w P_F - y_w P_P) \quad (7.14) \quad y_w = \frac{J_w}{J_e + J_w} \quad (7.15)$$

$$J_e = k_e(x_e P_F - y_e P_P) \quad (7.16) \quad y_e = \frac{J_e}{J_e + J_w} \quad (7.17)$$

From that above, there are 4 equations and 4 unknown (J_w , J_e , y_w and y_e) the unknown data can be solved using MathCad as follow:

Substitute (7.15) to (7.14) and (7.17) to (7.16)

$$J_e = k_e \cdot \left[x_e \cdot PF - \frac{J_e}{(J_e + J_w)} \cdot PP \right] \quad (7.18)$$

$$A_e = k_e \cdot x_e \cdot PF \quad B_e = k_e \cdot PP$$

$$J_w = k_w \cdot \left[x_w \cdot PF - \frac{J_w}{(J_e + J_w)} \cdot PP \right] \quad (7.19)$$

$$A_w = k_w \cdot x_e \cdot PF \quad B_w = k_w \cdot PP$$

Substitute A_e and B_e in (7.18) and A_w and B_w in (7.19)

$$J_e = A_e - \frac{J_e}{J_e + J_w} \cdot B_e \quad (7.20) \quad J_w = A_w - \frac{J_w}{J_e + J_w} \cdot B_w \quad (7.21)$$

Substitute (7.20) to (7.21)

$$J_w = -J_e \cdot \frac{(-J_e + A_e - B_e)}{(-J_e + A_e)} = A_w + J_e \cdot \frac{(-J_e + A_e - B_e)}{(-J_e + A_e)} \cdot \left[J_e - J_e \cdot \frac{(-J_e + A_e - B_e)}{(-J_e + A_e)} \right] \cdot B_w \quad (7.22)$$

Equation (7.23) and (7.24) were used in order to calculate ethanol and water flux, respectively. Permeate component mass fraction (y_w and y_e) were calculated by substitution of calculated J_e and J_w to (7.15) and (7.17), respectively.

Solve J_e from (7.22)

$$J_e = \frac{1}{2 \cdot (-Be + Bw)} \cdot \left[Be^2 - Bw \cdot Be - Be \cdot Ae + 2 \cdot Bw \cdot Ae + Aw \cdot Be - \left(-2 \cdot Bw \cdot Be^2 \cdot Aw + 2 \cdot Be^2 \cdot Bw \cdot Ae + 2 \cdot Be^2 \cdot Ae \cdot Aw + Aw^2 \cdot Be^2 - \right) \cdot Be^3 \cdot Bw - 2 \cdot Be^3 \cdot Ae + 2 \cdot Be^3 \cdot Aw + Bw^2 \cdot Be^2 + Be^2 \cdot Ae^2 + Be^4 \right] \frac{1}{2}$$

Simplify J_e

$$J_e = \frac{1}{2} \cdot \left[\frac{Be^2 - Bw \cdot Be - Be \cdot Ae + 2 \cdot Bw \cdot Ae + Aw \cdot Be - \left[Be^2 \cdot \left(-2 \cdot Bw \cdot Aw + 2 \cdot Bw \cdot Ae + 2 \cdot Ae \cdot Aw + Aw^2 - 2 \cdot Bw \cdot Be - 2 \cdot Be \cdot \right) \right] \cdot Ae + 2 \cdot Aw \cdot Be + Bw^2 + Ae^2 + Be^2}{(-Be + Bw)} \right] \frac{1}{2} \quad (7.23)$$

Substitute (7.23) to (7.22)

$$J_w = - \frac{\left[\frac{-1}{2} \cdot \left[\frac{Be^2 - Bw \cdot Be - Be \cdot Ae + 2 \cdot Bw \cdot Ae + Aw \cdot Be - \left[Be^2 \cdot \left(-2 \cdot Bw \cdot Aw + 2 \cdot Bw \cdot Ae + 2 \cdot Ae \cdot Aw + Aw^2 - 2 \cdot Bw \cdot Be - 2 \cdot Be \cdot Ae + 2 \cdot Aw \cdot Be + Bw \right)^2 + Ae^2 + Be^2}{(-Be + Bw)} \right] \right] \frac{1}{2} \right] + Ae - Be}{\left[\frac{-1}{2} \cdot \left[\frac{Be^2 - Bw \cdot Be - Be \cdot Ae + 2 \cdot Bw \cdot Ae + Aw \cdot Be - \left[Be^2 \cdot \left(-2 \cdot Bw \cdot Aw + 2 \cdot Bw \cdot Ae + 2 \cdot Ae \cdot Aw + Aw^2 - 2 \cdot Bw \cdot Be - 2 \cdot Be \cdot Ae + 2 \cdot Aw \cdot Be + Bw \right)^2 + Ae^2 + Be^2}{(-Be + Bw)} \right] \right] \frac{1}{2} \right] + Ae} \quad (7.24)$$

7.4.3 Calculation of diffusion coefficient (k -value)

As mention above, the calculated diffusion coefficient (k -value) can be performed based on linear regression and objective function (OF) value. From experimental data set of water separation membranes. Propose that, operating temperature was 418 K, P_{out} was 2 kPa J_{mass} was the mass flux from experimental data, J_{calc} was the mass flux from theory, x_F was feed component mass fraction (ethanol and water), y_P was permeate component mass fraction and molar unit base was applied in this calculation. The data set and parameters were clarified in matrix model. The k -value of the commercial ceramic membrane was calculated as follows:

Variables:

$T_w :=$	$\begin{pmatrix} 418 \\ 418 \end{pmatrix}$	K	$P_{in} :=$	$\begin{pmatrix} 100 \\ 200 \\ 300 \\ 400 \\ 100 \\ 200 \\ 300 \\ 400 \\ 100 \\ 200 \\ 300 \\ 400 \\ 100 \\ 200 \\ 300 \\ 400 \end{pmatrix}$	kPa	$P_{out} :=$	$\begin{pmatrix} 2 \\ 2 \end{pmatrix}$	kPa	$x_F :=$	$\begin{pmatrix} 0.99 & 0.01 \\ 0.99 & 0.01 \\ 0.99 & 0.01 \\ 0.99 & 0.01 \\ 0.975 & 0.025 \\ 0.975 & 0.025 \\ 0.975 & 0.025 \\ 0.975 & 0.025 \\ 0.95 & 0.05 \\ 0.95 & 0.05 \\ 0.95 & 0.05 \\ 0.95 & 0.05 \\ 0.95 & 0.05 \\ 0.95 & 0.05 \\ 0.9 & 0.1 \\ 0.9 & 0.1 \\ 0.9 & 0.1 \\ 0.9 & 0.1 \\ 0.9 & 0.1 \end{pmatrix}$
----------	---	---	-------------	--	-----	--------------	---	-----	----------	---

Results:

$J_{\text{mass}} :=$	$\left(\begin{array}{c} 0.83 \\ 1.38 \\ 1.76 \\ 2.18 \\ 1.65 \\ 2.86 \\ 3.65 \\ 4.78 \\ 2.34 \\ 4.26 \\ 5.75 \\ 7.13 \\ 3.25 \\ 6.64 \\ 8.83 \\ 11.13 \end{array} \right)$	$\frac{\text{kg}}{\text{hr} \cdot \text{m}^2}$	$Y_P :=$	$\left(\begin{array}{cc} 0.0216 & 0.9784 \\ 0.0236 & 0.9764 \\ 0.0272 & 0.9728 \\ 0.0404 & 0.9596 \\ 0.0157 & 0.9843 \\ 0.0176 & 0.9824 \\ 0.0188 & 0.9812 \\ 0.0336 & 0.9664 \\ 0.0106 & 0.9894 \\ 0.0109 & 0.9891 \\ 0.0129 & 0.9871 \\ 0.0195 & 0.9805 \\ 0.0098 & 0.9902 \\ 0.0084 & 0.9916 \\ 0.0116 & 0.9884 \\ 0.0097 & 0.9903 \end{array} \right)$
----------------------	---	--	----------	---

Conversion of mass base to molar base when J_{emol} was ethanol flux in molar unit and $J_{\text{w mol}}$ was water flux in molar unit:

$$mw := \left(\begin{array}{c} 46 \\ 18 \end{array} \right) \frac{\text{kg}}{\text{kmol}} \quad J_{\text{mol}_j} := \frac{J_{\text{mass}_j} \cdot Y_{P_{j,1}}}{mw_1} + \frac{J_{\text{mass}_j} \cdot Y_{P_{j,2}}}{mw_2}$$

Calculate molar flux:

$$J_{\text{emol}_j} := J_{\text{mol}_j} \cdot Y_{P_{j,1}}$$

$$J_{\text{w mol}_j} := J_{\text{mol}_j} - J_{\text{emol}_j}$$

	1		1		1
$J_{mol} =$	1 0.013	$m^{-2} \cdot s^{-1} \cdot mol$	1 $2.73 \cdot 10^{-4}$	$J_{emol} =$	1 0.012
	2 0.021		2 $4.954 \cdot 10^{-4}$		2 0.02
	3 0.027		3 $7.265 \cdot 10^{-4}$		3 0.026
	4 0.033		4 $1.326 \cdot 10^{-3}$		4 0.031
	5 0.025		5 $3.959 \cdot 10^{-4}$		5 0.025
	6 0.044		6 $7.685 \cdot 10^{-4}$		6 0.043
	7 0.056		7 $1.047 \cdot 10^{-3}$		7 0.055
	8 0.072		8 $2.428 \cdot 10^{-3}$	$J_{wmol} =$	8 0.07 $m^{-2} \cdot s^{-1} \cdot mol$
	9 0.036		9 $3.803 \cdot 10^{-4}$		9 0.035
	10 0.065		10 $7.118 \cdot 10^{-4}$		10 0.065
	11 0.088		11 $1.136 \cdot 10^{-3}$		11 0.087
	12 0.109		12 $2.12 \cdot 10^{-3}$		12 0.107
	13 0.05		13 $4.886 \cdot 10^{-4}$		13 0.049
	14 0.102		14 $8.563 \cdot 10^{-4}$		14 0.101
	15 0.135		15 $1.57 \cdot 10^{-3}$		15 0.134
	16 0.171		16 $1.656 \cdot 10^{-3}$		16 0.169

The flux from experimental data (J_{mol}) was successfully carried out. Thereafter, calculation of J_{calc} in the function of feed mass fraction, operating pressure, pressure out, k_e and k_w . The calculated J of each component and mass fraction (y_{calc}) in the function of feed concentration, P_{in} , P_{out} , k_e and k_w were performed according to (7.23) and (7.24) as follow:

$$\begin{aligned}
 J_{\text{calc}}(x_F, P_{\text{in}}, P_{\text{out}}, ke, kw) &:= \begin{cases} Ae \leftarrow ke \cdot x_F \cdot P_{\text{in}} \\ Be \leftarrow ke \cdot P_{\text{out}} \\ Aw \leftarrow kw \cdot [(1 - x_F) \cdot P_{\text{in}}] \\ Bw \leftarrow kw \cdot P_{\text{out}} \\ J_{\text{emol}} \leftarrow \frac{1}{2} \cdot \frac{\left[Be^2 - Bw \cdot Be - Ae \cdot Be + 2 \cdot Bw \cdot Ae + Aw \cdot Be - \left[Be^2 \cdot (-2 \cdot Ae \cdot Be + Ae^2 + Be^2 - 2 \cdot Bw \cdot Aw + 2 \cdot Bw \cdot Ae + Bw^2 - 2 \cdot Bw \cdot Be + 2 \cdot Aw \cdot Be + 2) \cdot Aw \cdot Ae + Aw^2 \right]^{\frac{1}{2}} \right]}{(-Be + Bw)} \\ J_{\text{wmol}} \leftarrow -J_{\text{emol}} \cdot \frac{\left[\frac{-1}{2} \cdot \frac{\left[Be^2 - Bw \cdot Be - Be \cdot Ae + 2 \cdot Bw \cdot Ae + Aw \cdot Be - \left[Be^2 \cdot (-2 \cdot Bw \cdot Aw + 2 \cdot Bw \cdot Ae + 2 \cdot Ae \cdot Aw + Aw^2 - 2 \cdot Bw \cdot Be - 2 \cdot Be \cdot Ae + 2 \cdot Aw \cdot Be + Bw)^2 + Ae^2 + Be^2 \right]^{\frac{1}{2}} \right]}{(-Be + Bw)} + Ae - Be \right]}{\left[\frac{-1}{2} \cdot \frac{\left[Be^2 - Bw \cdot Be - Be \cdot Ae + 2 \cdot Bw \cdot Ae + Aw \cdot Be - \left[Be^2 \cdot (-2 \cdot Bw \cdot Aw + 2 \cdot Bw \cdot Ae + 2 \cdot Ae \cdot Aw + Aw^2 - 2 \cdot Bw \cdot Be - 2 \cdot Be \cdot Ae + 2 \cdot Aw \cdot Be + Bw)^2 + Ae^2 + Be^2 \right]^{\frac{1}{2}} \right]}{(-Be + Bw)} + Ae \right]} \end{cases} \\
 \begin{pmatrix} J_{\text{emol}} \\ J_{\text{wmol}} \end{pmatrix}
 \end{aligned}$$

$$J_{\text{calc_total}}(x_F, P_{\text{in}}, P_{\text{out}}, ke, kw) := \begin{cases} J1 \leftarrow J_{\text{calc}}(x_F)_1, P_{\text{in}}, P_{\text{out}}, ke, kw \\ (J1_1 + J1_2) \end{cases} \quad y_{\text{calc}}(x_F, P_{\text{in}}, P_{\text{out}}, ke, kw) := \begin{cases} J1 \leftarrow J_{\text{calc}}(x_F), P_{\text{in}}, P_{\text{out}}, ke, kw \\ J_{\text{total}} \leftarrow (J1_1 + J1_2) \\ \frac{J1}{J_{\text{total}}} \end{cases}$$

Suppose that k_e and k_w were 5×10^{-5} and 1×10^{-4} mol.s⁻¹.m⁻².Pa⁻¹, respectively.

$$k_e := 0.00005 \frac{\text{mol}}{\text{s} \cdot \text{m}^2 \cdot \text{Pa}} \quad k_w := 0.0001 \frac{\text{mol}}{\text{s} \cdot \text{m}^2 \cdot \text{Pa}} \quad j := 1..16$$

Flux of each components and mole fraction were calculated according to the following equations (referred as 1 was water and 2 was ethanol):

$$J_{\text{calc}} \left[\left[\left(x_F^T \right)^{\langle j \rangle} \right]_1, P_{\text{in},j}, P_{\text{out},j}, k_e, k_w \right]_1 \quad J_{\text{calc}} \left[\left[\left(x_F^T \right)^{\langle j \rangle} \right]_1, P_{\text{in},j}, P_{\text{out},j}, k_e, k_w \right]_2$$

$$y_{\text{calc}} \left[\left[\left(x_F^T \right)^{\langle j \rangle} \right]_1, P_{\text{in},j}, P_{\text{out},j}, k_e, k_w \right]_1 \quad y_{\text{calc}} \left[\left[\left(x_F^T \right)^{\langle j \rangle} \right]_1, P_{\text{in},j}, P_{\text{out},j}, k_e, k_w \right]_2$$

Suppose that k_e and k_w were 5×10^{-5} and 1×10^{-4} mol.s⁻¹.m⁻².Pa⁻¹, respectively.

$$k_e := 0.00005 \frac{\text{mol}}{\text{s} \cdot \text{m}^2 \cdot \text{Pa}} \quad k_w := 0.0001 \frac{\text{mol}}{\text{s} \cdot \text{m}^2 \cdot \text{Pa}} \quad j := 1..16$$

Flux of each components and mole fraction were calculated according to the following equations (referred as 1 was water and 2 was ethanol):

$$J_{\text{calc}} \left[\left[\left(x_F^T \right)^{\langle j \rangle} \right]_1, P_{\text{in},j}, P_{\text{out},j}, k_e, k_w \right]_1 \quad J_{\text{calc}} \left[\left[\left(x_F^T \right)^{\langle j \rangle} \right]_1, P_{\text{in},j}, P_{\text{out},j}, k_e, k_w \right]_2$$

$$y_{\text{calc}} \left[\left[\left(x_F^T \right)^{\langle j \rangle} \right]_1, P_{\text{in},j}, P_{\text{out},j}, k_e, k_w \right]_1 \quad y_{\text{calc}} \left[\left[\left(x_F^T \right)^{\langle j \rangle} \right]_1, P_{\text{in},j}, P_{\text{out},j}, k_e, k_w \right]_2$$

The calculated flux and mole fraction were summarized in Table 7.5.

Table 7.5 Calculated flux and mole fraction of water and ethanol at various operating pressure and feed concentration.

Data set	J_{calc_w}	J_{calc_e}	y_{calc_w}	y_{calc_e}
1	4.944	0.1	0.98	0.02
2	9.894	0.2	0.98	0.02
3	14.844	0.3	0.98	0.02
4	19.794	0.4	0.98	0.02
5	4.869	0.249	0.951	0.049
6	9.744	0.499	0.951	0.049
7	14.619	0.749	0.951	0.049
8	19.494	0.999	0.951	0.049
9	4.745	0.499	0.905	0.095
10	9.495	0.999	0.905	0.095
11	14.245	1.499	0.905	0.095
12	18.995	1.999	0.905	0.095
13	4.495	0.998	0.818	0.182
14	8.995	1.998	0.818	0.182
15	13.495	2.998	0.818	0.182
16	17.995	3.998	0.818	0.182

According to Table 7.4, flux and mole fraction of water and ethanol at various operating pressure and feed concentration were successfully calculated. The OF value referred as a variation between sum square of experimental and calculated data was calculated according to equation (7.13), $weight_j$ denoted that significant level between molar flux and mole fraction dataset:

$$\begin{aligned}
 OF(ke, kw) := & \left[\sum_{j=1}^{ndata} \left[\sum_{i=1}^2 \left[\left[(y_P^T)^{<j>} \right]_i - y_{calc} \left[\left[(x_F^T)^{<j>} \right]_1, P_{in_j}, P_{out_j}, ke, kw \right] \right]_i \right]^2 \right] \\
 & + \left[weight_J \cdot \sum_{j=1}^{ndata} \left[J_{mol_j} - J_{calc_total} \left[\left[(x_F^T)^{<j>} \right]_1, P_{in_j}, P_{out_j}, ke, kw \right] \right]^2 \right] \quad (7.25)
 \end{aligned}$$

As described above, the most fitted value referred as the OF value that nearly zero. Hence, k_e and k_w that make minimum OF value was calculated as follow:

$$\text{OF}(k_e, k_w) = 0 \quad \text{result} := \text{Minerr}(k_e, k_w)$$

$$\text{result} = \begin{pmatrix} 2.5 \times 10^{-9} \\ 4.52586 \times 10^{-6} \end{pmatrix}$$

$$\text{OF}(k_e, k_w) = 0.404$$

It was found that, 2.5×10^{-9} and $4.52 \times 10^{-6} \text{ mol.s}^{-1}.\text{m}^{-2}.\text{Pa}^{-1}$ of k_e and k_w value with 0.404 OF value were successfully calculated from experimental and calculated dataset. The comparison between experimental data and calculated data (after k -value adjustment) of both flux and mole fraction as summarized in Figure 7.4.

According to Figure 7.4, the molar flux experimental data and theoretical data was fitted with the calculated k -value, especially the lower ethanol feed concentration and operating pressure ($j = 8 - 16$). Additionally, exponentially increased of molar flux in the function of operating pressure and slightly decreased when feed ethanol concentration increased were represented as demonstrated in Figure 7.5. Nevertheless, permeate mole fraction showed the significantly different among experimental and theoretical data. The permeate mole fraction affected with the feed concentration, likewise operating pressure was unaffected.

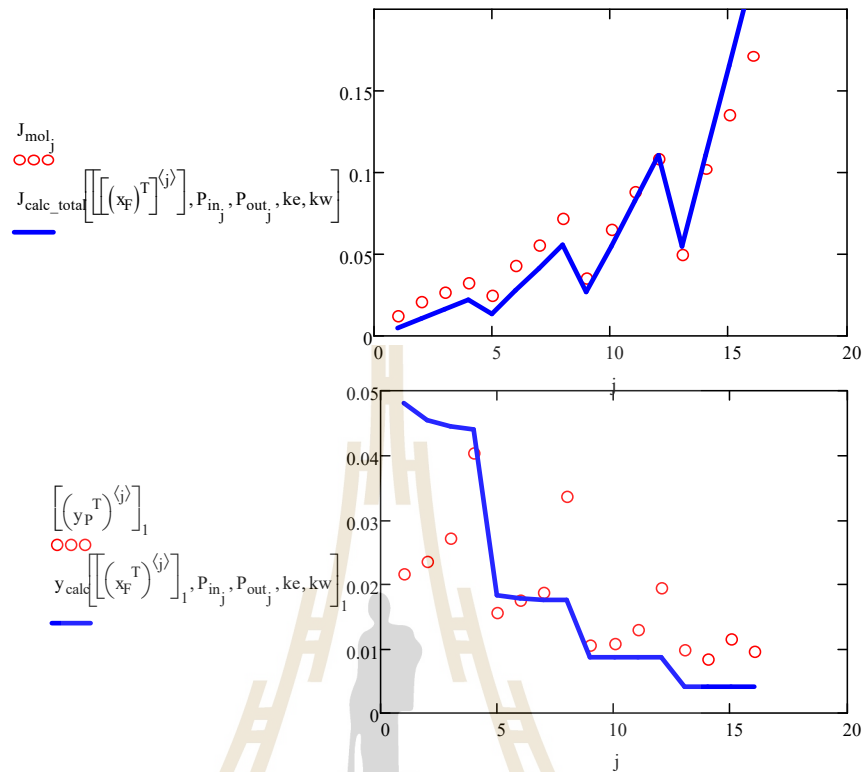


Figure 7.4 The comparison between experimental data (○) and calculated data (after k -value adjustment) (-) of molar flux (above) and mole fraction (below).

One of the interesting parameter was the k_w/k_e ratio which indicated that variation between k_e and k_w value in other word, the water separation performance in membrane. Higher k_w/k_e ratio value illustrated the high separation factor. This value can be also calculated using regression and OF value. The lowest OF value referred that it was fitted with the experimental dataset. In case of commercial ceramic membrane, approximately 7,500 of k_w/k_e ratio was calculated as represented in Figure 7.6.

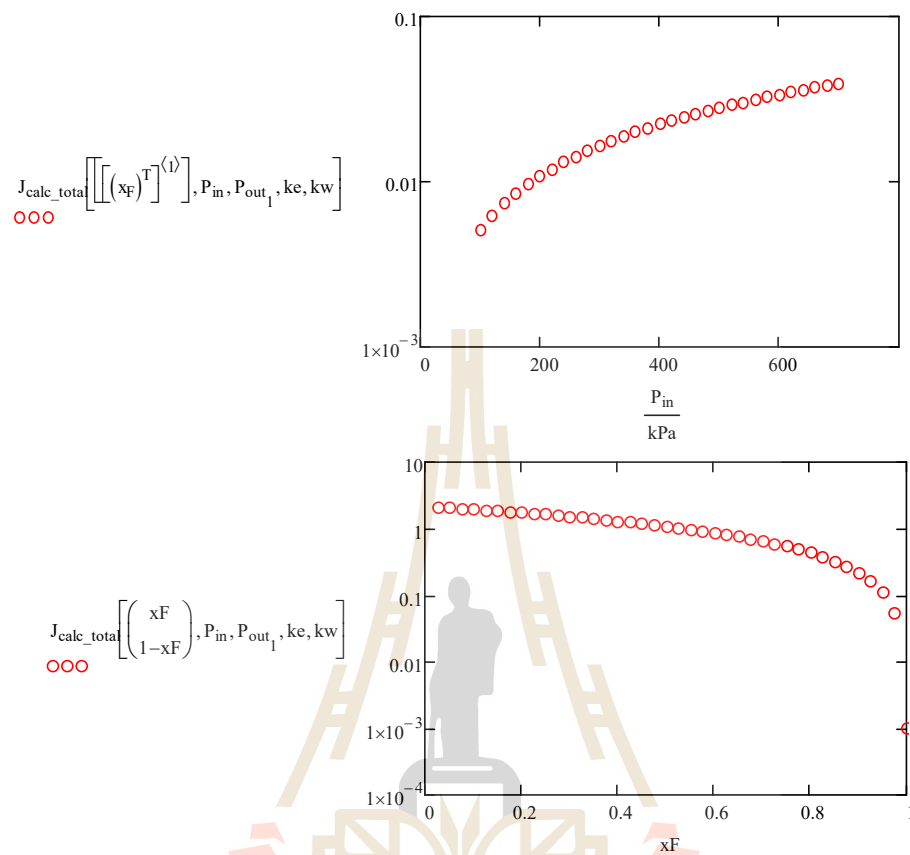


Figure 7.5 Theoretical molar flux in various operating pressure (above) and ethanol feed concentration (below).

At the same time, k -value, OF value and k_w/k_e ratio in another 2 types of water separation membranes were completely calculated which summarized in Table 7.5. The calculation of k -values of polymer and self-made membrane is illustrated in Appendix D. Another 2 membranes including polymer and self-made membrane were less efficiency in water separation than the commercial ceramic membrane that found the k_w at 3.25×10^{-7} and $4.87 \times 10^{-7} \text{ mol.s}^{-1}.\text{m}^{-2}.\text{Pa}^{-1}$, respectively. The resulting membranes were also confirmed via k_w/k_e ratio, approximately 3.5 times of polymer and self-made membrane which lower than the commercial ceramic membrane.

Table 7.6 Comparison of calculated k -value, OF value and k_w/k_e ratio in three types water separation membranes.

Membrane types	k -value ($\text{mol}\cdot\text{s}^{-1}\cdot\text{m}^{-2}\cdot\text{Pa}^{-1}$)		OF-value	k_w/k_e ratio
	k_e	k_w		
Ceramic	2.50×10^{-9}	4.53×10^{-6}	0.404	7,500
Polymer	6.35×10^{-10}	3.25×10^{-7}	0.102	1,800
Sample 045	6.25×10^{-10}	4.87×10^{-7}	0.104	2,200

On the whole, the k -value regression which indicated the separation capability of various types of membrane were performed. The application of k -value in the realistic situation was represented in the next topic.

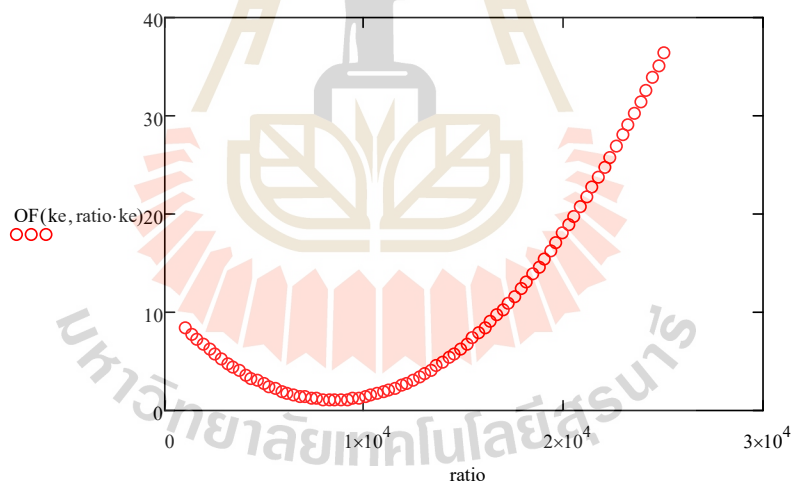


Figure 7.6 The calculated minimum value of k_w/k_e ratio

7.4.4 Simulation of ethanol dehydration process using calculated k -value and real parameters

The obtained k -values were applied in the ethanol dehydration process. In this case, the commercial ceramic membrane was simulated using an actual parameters. The separation efficiency including flux and permeate mass fraction was calculated in accordance

with previous topic. The details of pre-pilot plant dehydration process that existed in the laboratory were represented as follow:

- Contain 10 tubes in the membrane module.
- Membrane tube have 1.25×10^{-2} m diameter and 0.75 m length.
- Operating pressure was 400 kPa, 145°C.
- 25 kg/hr feed rate with 95 wt% of ethanol.

Suppose that, k_e was 1.2×10^{-10} $\text{kg} \cdot \text{m}^{-2} \cdot \text{s}^{-1} \cdot \text{Pa}^{-1}$, k_w was 8.15×10^{-8} $\text{kg} \cdot \text{m}^{-2} \cdot \text{s}^{-1} \cdot \text{Pa}^{-1}$, F_{in} was feed rate and X_F was feed ethanol mass fraction. Calculation of component feed rate was performed as follow:

$$\begin{aligned} \text{fin} &:= 25 \frac{\text{kg}}{\text{hr}} & x_F &:= 0.95 \\ \text{efin} &\leftarrow \text{fin} \cdot x_F & \text{fin} &= \begin{pmatrix} 23.75 \\ 1.25 \end{pmatrix} \text{kg} \cdot \text{hr}^{-1} \\ \text{wfin} &\leftarrow \text{fin} - \text{efin} \\ \begin{pmatrix} \text{efin} \\ \text{wfin} \end{pmatrix} & \end{aligned}$$

Calculation of components and total mass flux (J_{calc_total}) and mass fraction (y_{perm_calc}) according to Eq. (7.23), (7.2), (7.15) and (7.17), respectively.

$$J_{calc}(x_F, P_{in}, P_{out}, T, k_e, k_w) = \begin{pmatrix} 2.848 \times 10^{-5} \\ 7.054 \times 10^{-4} \end{pmatrix} \text{s}^{-1} \cdot \text{m}^{-2} \cdot \text{kg}$$

$$J_{calc_total}(x_F, P_{in}, P_{out}, T, k_e, k_w) = 2.642 \text{m}^{-2} \cdot \text{kg} \cdot \text{hr}^{-1}$$

$$y_{perm_calc}(x_F, P_{in}, P_{out}, T, k_e, k_w) := \begin{array}{l} J1 \leftarrow J_{calc}(x_F, P_{in}, P_{out}, T, k_e, k_w) \\ J_{total} \leftarrow (J1_1 + J1_2) \\ \hline \frac{J1}{J_{total}} \end{array}$$

$$y_{perm_calc}(x_F, P_{in}, P_{out}, T, k_e, k_w) = \begin{pmatrix} 0.039 \\ 0.961 \end{pmatrix}$$

Then, the actual value of the separation membrane module ($J_{realpar}$) was calculated by multiply with total membrane area (0.294 m²).

$$J_{realpar} := J_{calc}(x_F, P_{in}, P_{out}, T, k_e, k_w) \cdot \text{totarea}$$

$$J_{realpar} = \begin{pmatrix} 0.03 \\ 0.748 \end{pmatrix} \text{kg} \cdot \text{hr}^{-1}$$

$$J_{realpar_total} := J_{realpar_1} + J_{realpar_2}$$

$$J_{realpar_total} = 0.778 \text{kg} \cdot \text{hr}^{-1}$$

It is clear that, the total flux was 0.778 kg/hr from permeate side with 3.9 wt% ethanol and 96.1 wt% water. Then, calculation of mass flow (*ret total*) and component mass fraction (y_{ret_calc}) were completed in the retentate side (product) as follow.

$$\text{ret} := \text{fin} - J_{realpar_total}$$

$$\text{ret} = \begin{pmatrix} 22.972 \\ 0.472 \end{pmatrix} \text{kg} \cdot \text{hr}^{-1} \quad \text{ret_total} = 23.445 \text{kg} \cdot \text{hr}^{-1}$$

$$y_{ret_calc} := \begin{pmatrix} y_{ret_calc_1} \\ y_{ret_calc_2} \end{pmatrix} \leftarrow \begin{pmatrix} \frac{\text{ret}_1}{\text{ret_total}} \\ \frac{\text{ret}_2}{\text{ret_total}} \end{pmatrix}$$

$$\begin{pmatrix} y_{ret_calc_1} \\ y_{ret_calc_2} \end{pmatrix}$$

$$y_{ret_calc} = \begin{pmatrix} 0.9799 \\ 0.0201 \end{pmatrix}$$

It was concluded that, 23.45 kg was produce from this membrane module with a 97.99 wt% ethanol concentration using 25 kg/hr feed rate with 95 wt% ethanol. However, dehydrated ethanol product was lower than the absolute ethanol standard (99.5 wt%). There

are 2 techniques in order to improve the product quality including reduction of feed rate and increase the membrane surface (number of tubes) in the membrane module.

Along with the commercial ceramic membrane, another 2 types of membrane (polymer and self-made membrane) were accordingly simulated using the same condition. The application of dehydration process from another 2 types of membrane were demonstrated in Appendix D. The total mass flux and mass fraction from both permeate and retentate side as well as number of tubular membrane to obtained 99.5 wt% ethanol were summarized in Table 7.7.

According to Table 7.7, ethanol was increased from 95.0 wt% feed to only 95.23 and 95.32 wt% which obtained from polymer and self-made membrane, respectively. Whereas, retentate flow rate improved at 24.874 and 24.821 kg/hr as a result of higher water content in solution. The number of tubular tubes to obtained 99.5 wt% ethanol is an appropriate factor in order to evaluate the separation efficiency of the membrane. It was concluded that, 16 tubes of membrane can produce the absolute ethanol from 95 wt% using commercial ceramic membrane. Meanwhile, the extremely high amount of tubular membranes were applied for the production of absolute ethanol (182 and 128 tubes) via polymer and self-made membrane which unreasonable in the actual situation. As a consequence, flat sheet polymer membrane is widely applied in the pervaporation process than the vapor permeation due to the lower pressure tolerant.

Table 7.7 Comparison of various membrane types on total flow and mass fraction of permeate and retentate side as well as number of tubular membrane to obtained 99.5 wt% ethanol.

Types of membrane	Total flow (kg/hr)		EtOH fraction		H ₂ O fraction		No. tube to 99.5 wt%
	Perm	Ret	Perm	Ret	Perm	Ret	
Ceramic	0.78	23.44	0.04	0.98	0.96	0.020	16
Polymer	0.063	24.87	0.12	0.95	0.88	0.048	182
Sample 045	0.089	24.82	0.081	0.95	0.92	0.047	128

7.4.5 Sensitivity analysis of simulated ethanol dehydration process

The purpose of sensitivity analysis of simulated ethanol dehydration process is determine the most appropriate and worthiness condition of the process. In addition, optimized the process in a scaling-up model. In this topic, sensitivity analysis of several categories such as suitable number of membrane tubes of a various feed capacity, different ethanol feed concentration or ethanol product concentration in various feed rate. In this simulation, the operating conditions were used including pressure was 400 kPa, temperature 145°C and commercial ceramic membrane was applied.

The analysis of membrane tube quantities have a benefit in economical factor and worthiness of dehydration process design in order to predict the appropriate number of membranes that fitted with feeding-in or product flow requirement. The quantities of tubular membranes for absolute ethanol production in various feed rate represented in Figure 7.8. Higher level of feed rate required a numerous of membrane tubes in a consequence of higher water input. In particular, feed rate at 10 kg/hr required 6 membrane tubes to absolute ethanol production, exponentially more than 60 tubes were used in order to obtain absolute ethanol when feed rate was set at 100 kg/hr. The results was in accordance with Figure 7.9. Higher

level of feed rate affected on the product concentration. The permeate mass fraction decreased sharply at the start of feed leveling until 50 kg/hr, then slightly decreased up to nearly 95 wt% as same as feed concentration.

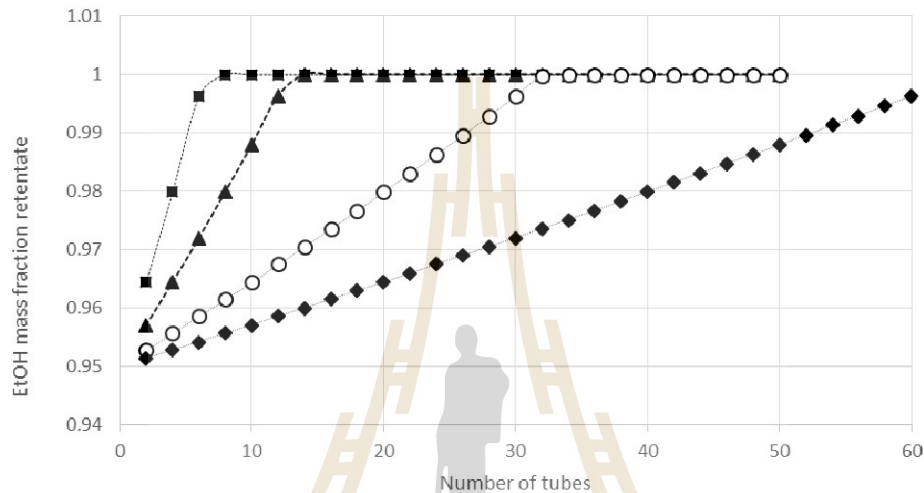


Figure 7.7 Amount of tubular membranes in order to obtain absolute ethanol (retentate side) in various feed rate including 10 kg/hr (■), 20 kg/hr (▲), 50 kg/hr (○) and 100 kg/hr (◆) using 95 wt% feed.

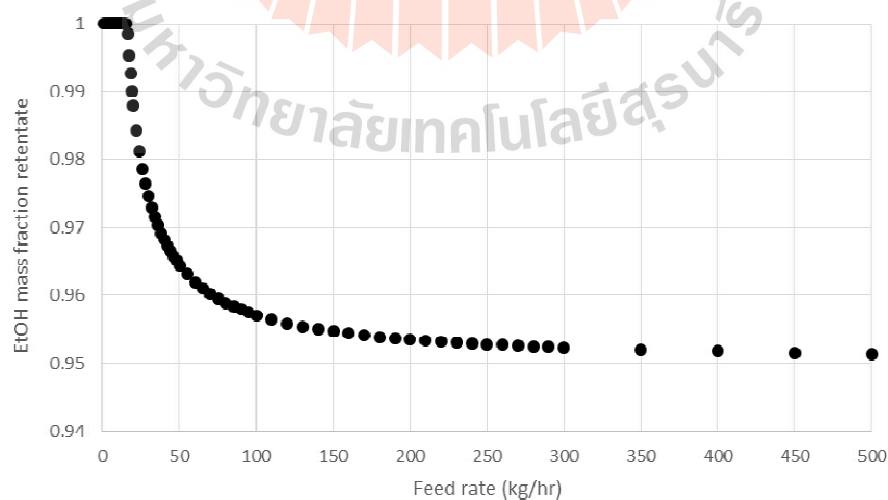


Figure 7.8 Ethanol product mass fraction in various feed rate when 10 membrane tubes with 95 wt% feed rate were used.

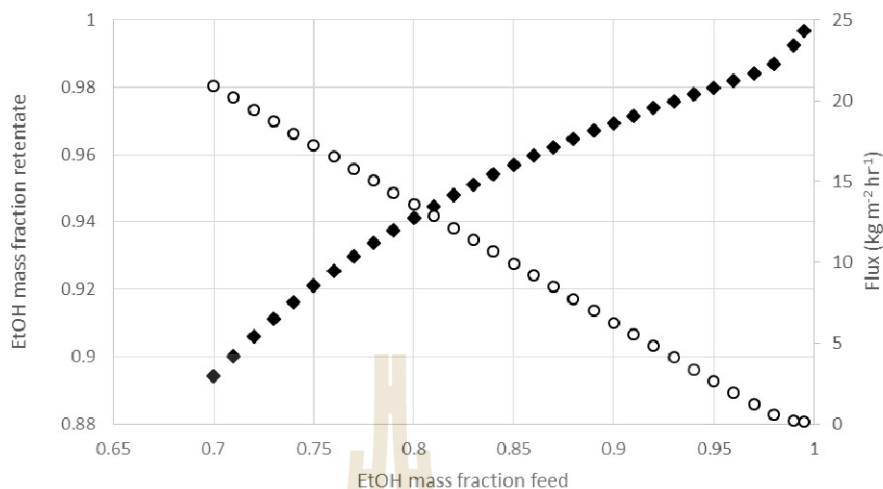


Figure 7.9 Ethanol product mass fraction (◆) and mass flux (○) in various feed concentration when 10 membrane tubes with 25 kg/hr feed rate were used.

The effect of feed concentration on flux and product concentration is shown in Figure 7.9 when 10 membrane tubes with 25 kg/hr feed rate were used. The ethanol product concentration directly varied with the feed concentration. The ethanol mass fraction increased continuously with higher ethanol feed. Whereas, slight reduction of mass flux was observed.

Number of membrane tubes for absolute ethanol production in various feed concentration, product flow rate and ethanol in permeate side was simulated and summarized in Table 7.7. Surprisingly, 95 wt% ethanol feed required the membrane tubes more than 70 wt% feed. In other words, the requirement of membrane tubes of lower ethanol feed concentration was less than the higher feed concentration. Furthermore, more ethanol concentration was detected in permeate side. As a result, lower concentration of water requires more separation materials than a higher water level, this phenomena is described via the electronegativity and hydrogen bonding. The hydrogen bonding from lower water concentration is more strength than higher water concentration.

Table 7.8 Product flow rate, ethanol in permeate side and number of tubes to obtain 99.5 wt% ethanol in various feed concentration.

Feed conc. (wt%)	No. tube to 99.5 wt%	Product flow (kg/hr)	Permeate EtOH (wt%)
70	13	8.995	0.4
75	13	11.797	0.4
80	13	14.598	0.5
85	13	17.399	0.9
90	14	19.826	1.5
95	16	22.511	3.9

7.4.6 Simulation of ethanol dehydration process: economical evaluation

After successfully simulating the transport mechanism in MathCad, the process simulation of dehydration was subsequently performed in ASPEN PLUS software using data from previous study and the production cost evaluation was performed. The dehydration process was designed as shown in Figure 7.10.

Table 7.9 demonstrated the ethanol and water mass flows and mass fraction of the dehydration process after completely simulating via ASPEN PLUS. The resulting simulated data from this software was in accordance with the results from the mathematical program and realistic. It was found that the product flow from the experiment was 23.9 kg/hr with 97.6 wt% ethanol (data not shown), which was slightly different from the simulated data at 97.9 wt% and 24.223 kg/hr flow.

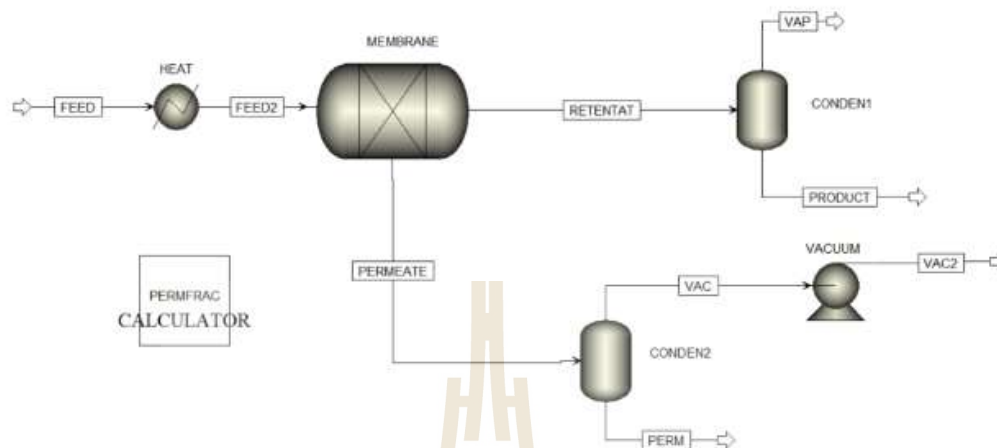


Figure 7.10 Dehydration process designed in ASPEN PLUS.

Table 7.9 Composition mass flow and mass fraction of the dehydration process.

	FEED	PERM	PRODUCT
Mass flow (kg/hr)			
EtOH	23.75	0.03	23.72
H ₂ O	1.25	0.747	0.503
Mass fraction			
EtOH	0.95	0.03861	0.979235
H ₂ O	0.05	0.96139	0.020765
Total flow (kg/hr)	25	0.777	24.223
Temperature (°C)	25	-20	15
Pressure (bar)	1	1	1

The economic analysis including utility usage and utility cost of the dehydration process was carried out and illustrated in Table 7.10. The major utility costs were found especially in the heating and cooling unit (heater and permeate condenser) at 13.95 and 12.89 Baht per hour which was the 49.6% and 45.8% of the overall production cost, respectively. The excessive cost of the permeate condenser originated from the extremely low temperature

(-20°C) that was chosen in order to condense the permeate solution at low pressure (4 kPa). The application of Venturi for this vacuum system is a remarkably technique for energy and production cost reduction.

Table 7.10 Utility usage and utility cost of dehydration process.

Unit operation	Heater	Vacuum	Retentate condenser	Permeate condenser
Usage (kW)	8.31	0.0055	0.602	7.67
Cost (Baht/hr)	13.95	0.23	1.03	12.89

7.5 Conclusion

The simulation of the ethanol dehydration process was accomplished in order to determine the most appropriate and efficient condition, especially for the scaling-up model. From experimental data, the ceramic membrane is a promising option for dehydrated ethanol production compared to polymer membrane due to its higher efficiency in gas permeation, longer life as well as higher permeation temperature and mechanical stability. The diffusion coefficient (k - value) was successfully calculated based on experimental data using a non-linear regression technique. The obtained k -values were applied in the ethanol dehydration process using actual parameters. The simulation and dehydration process design especially with respect to number of membrane tubes quantities analysis have a benefit in economical and worthiness in order to predict the appropriate number of membranes that match feed and product flow requirement. Additionally, the process design and utility cost analysis was established by ASPEN PLUS.

7.6 References

- Asthana, N.S., Kolah, A.K., Vu, D.T., Lira, C.T. and Miller, D.J. (2006). A kinetic model for the esterification of lactic acid and its oligomers. **Ind. Eng. Chem. Res.** 45: 5251 – 5257.
- Burggraaf, A.J. (1999). Single gas permeation of thin zeolite (MFI) membranes: theory and analysis of experimental observations. **J. Membrane Sci.** 155: 45-65.
- Hedlund, J., Sterte, J., Anthonis, M., Bons, A.J., Carstensen, B., Corcoran, N., Cox, D., Deckman, H., de Gijst, W., de Moor, P.P., Lai, F., McHenry, J., Mortier, W., Reinoso, J. and Peters, J. (2002). High-flux MFI membranes. **Micropor. Mesopor. Mater.** 52: 179–189.
- Knudsen, M. (1909). Eine Revision der Gleichgewichtsbedingung der Gase. Thermische Molekularströmung. **Ann. Phys.** 336(1): 205-229.
- Masaryk, J.S. and Fulrath, R.M. (1973). Diffusivity of helium in fused silica. **J. Chem. Phys.** 59(3): 1198.
- Shackelford, J.F., Studt, P.L. and Fulrath, R.M. (1972). Solubility of gases in glass II. He, Ne and H₂ in fused silica. **J. Appl. Phys.** 43: 1619.
- Sondhi, R., Bhave, R. and Jung, G. (2003). Applications and benefits of ceramic membranes. **Membrane Tech.** November: 5-8.
- Studt, P.L., Shackelford, J.F. and Fulrath, R.M. (1970). Solubility of gases in glass – a monatomic model. **J. Appl. Phys.** 41: 2777.
- Xu, X., Bao, Y., Song, C., Yang, W., Liu, J. and Lin, L. (2005). Synthesis, characterization and single gas permeation properties of NaA zeolite membrane. **J. Membrane Sci.** 249: 51–64.



CHAPTER VIII

KINETIC ANALYSIS OF DIETHYL SUCCINATE (DES) PRODUCTION VIA VAPOR PERMEATION-ASSISTED ESTERIFICATION TECHNIQUE: MATHEMATICAL MODEL AND PROCESS SIMULATION

8.1 Abstract

The kinetic study of succinic acid/ethanol esterification intended for diethyl succinate (DES) production is required for scaling-up and process simulation. The integrated membrane process including vapor permeation process was employed. The kinetic parameters such as reaction rate constant (k -value), activity coefficient (γ), activation energy (E_a) and equilibrium constant (k_{EQ}) were determined based on pseudo-homogeneous mixture and NRTL model. It was found that, the activity coefficient of SA, EtOH, MES, DES and H₂O were 0.288, 1.049, 0.854, 8.957 and 1.74, respectively. Additionally, the calculated net rate of SA to MES (r_1) and MES to DES (r_2) were 1.659×10^{-4} and $0 \text{ mol.s}^{-1}.\text{m}^{-3}$, respectively at the start of reaction. The succinic acid/ethanol esterification from experiment was compared with the predicted mole fraction profile. It can be seen that, there was good agreement between calculated and experimental data. It also confirmed that, calculated OF value referred to the variation between two datasets were 1.7×10^{-2} and 5.548×10^{-4} . The kinetic parameters were applied

to the simulation software and VP-assist esterification of succinic acid/ethanol was simulated. The simulated DES resulted in 0.27 kmol/hr productivity and 93.23% conversion yield from succinic acid. Three types of membrane including commercial ceramic, polymer and self-made membrane were applied and simulated in VP-assisted esterification. The commercial ceramic membrane showed the highest DES productivity due to the high performance in water separation compared to the other tested membrane. While the conversion yield from self-made membrane and polymer membrane were 82.7 and 79.3%, respectively.

Keywords: Succinic acid/ Esterification/ Vapor permeation/ Kinetic analysis/ Process simulation

8.2 Introduction

Succinic acid (SA) is an important chemical that can be used in food, pharmaceutical, and chemical industries. Recently, it has been recognized as a renewable building platform for many chemical derivatives of industrial interest such as 1,4-butanediol, tetrahydrofuran, N-methyl pyrrolidinone, and especially polybutylene-succinate (PBS) (Hermann and Patel, 2007; Cukalovic and Stevens, 2008; Delhomme *et al.*, 2009). Nowadays, the most utilization of bioplastic production is polylactic acid or polylactide (PLA) and the estimated potential market for PBS is expected at 270,000 tons per year (McKinlay *et al.*, 2007). In term of SA purification, cost for recovery of SA from fermentation broths constitute a high portion of approximately 50–70% of the total production cost (Kurzrock and Weuster-Botz, 2010; Cheng *et al.*, 2012). Because of the complex reaction catabolism, the major challenges

to reduce recovery cost include low titer of the SA, the requirement for pH control that leads to the formation of succinate salts, presence of other organic acids as by-products, and loss of selectivity via by-product formation.

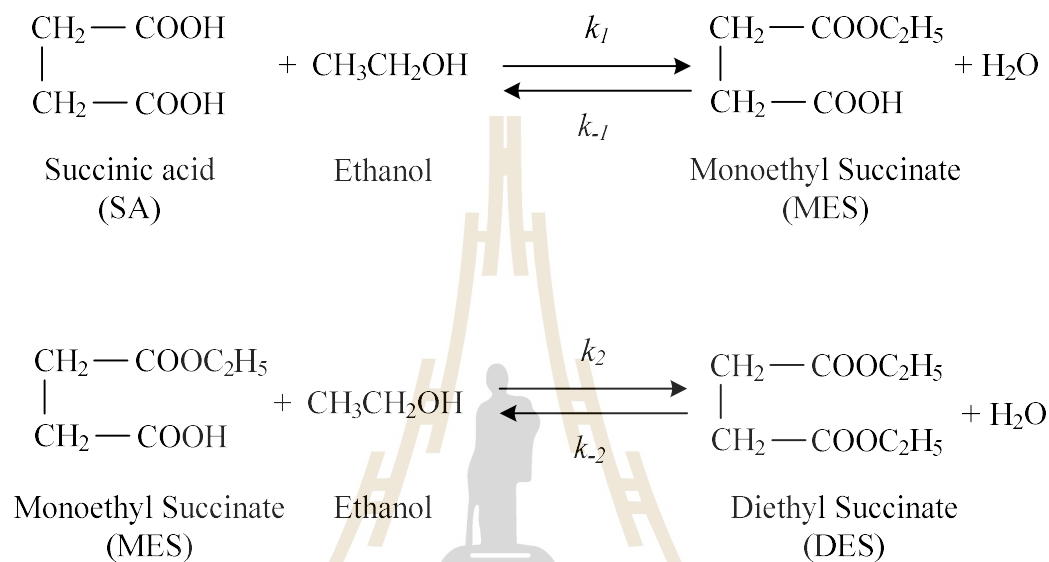


Figure 8.1 Schematic diagram for esterification of succinic acid with ethanol.

Among the several purification techniques, esterification is an effective downstream process that can remove contaminating organic acids by altering the boiling points of their respective ester compounds. According to recent studies, recovery of succinic acid from these mixtures can be accomplished by esterification with ethanol (EtOH) through a series reaction scheme in the presence of an acid catalyst, with monoethyl succinate (MES) as intermediate and diethyl succinate (DES) as final product. In addition, 2 mol of water are produced as shown in Figure 8.1. Because of chemical equilibrium limitations in the esterification step and the low solubility of SA in ethanol solution, excess EtOH is required in the reaction. Additionally, achieving

high rates and driving the reaction to accomplishment requires continuous water (H_2O) removal.

Recently, vapor permeation-assisted esterification technique coupled with nanofiltration in SA purification has been reported from our lab (Lubsungneon *et al.*, 2014). An integrated membrane process that consists of nanofiltration (NF) and vapor permeation (VP) was successfully employed for the separation and purification of fermentation-derived succinic acid. The diagram of experimental setup of NF and VP-assisted esterification is shown in Figure 8.2. The results for VP-assisted esterification revealed an enhanced yield and productivity of DES. Experimental results showed that most succinic acid was converted into DES at the end of the VP-assisted esterification reaction.

In this chapter, the kinetic of DES production via succinic acid/ethanol esterification was studied. The vapor permeation technique was applied in order to remove the by-product water. The kinetic parameters such as reaction rate constant (k -value), activity coefficient (γ_i), activation energy (E_a) and equilibrium constant (k_{EQ}) were determined based on pseudo-homogeneous and NRTL model. The obtained parameters were applied in process simulation program (ASPEN PLUS). Hence, productivity and cost of production were calculated.

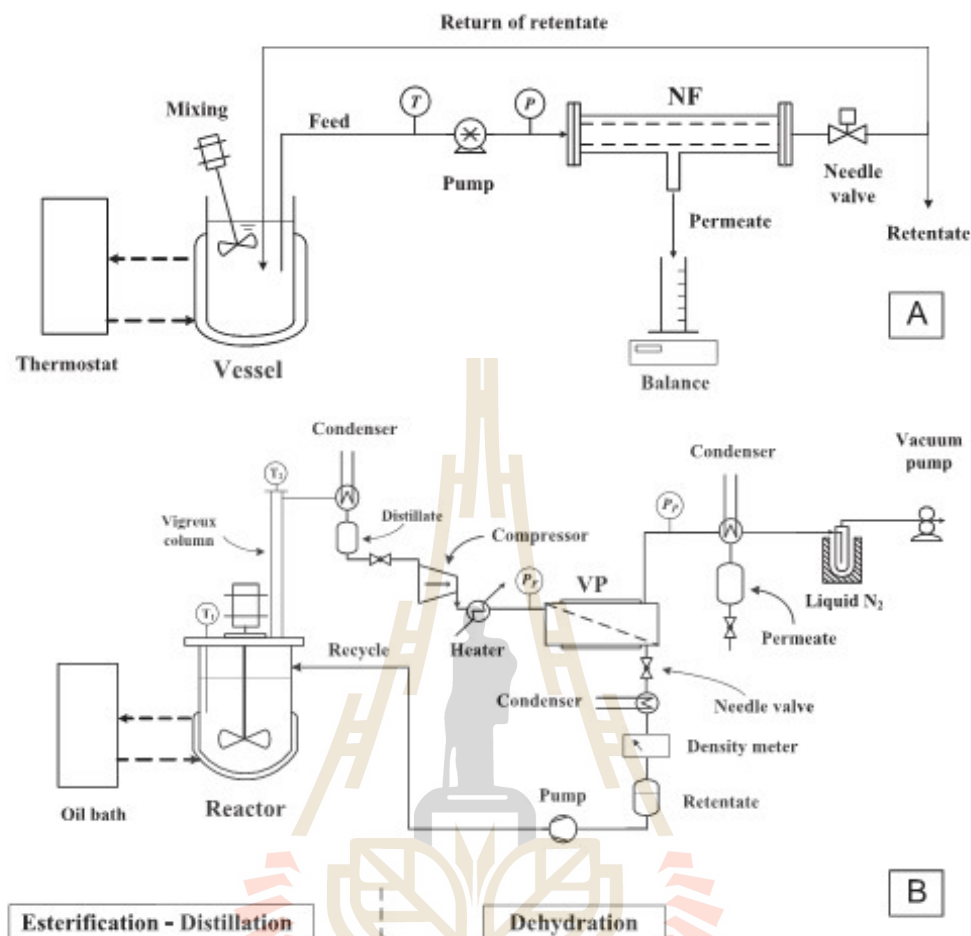


Figure 8.2 Schematic diagrams for the experimental setup of NF (A), and VP-assisted esterification reaction between SA and ethanol (B).

8.3 Methodology

8.3.1 Chemicals

Succinic acid crystal was purchased from Sigma (Singapore). Amberlyst-15 E as a catalyst, MES, and DES were supplied by Fluka (United Kingdom). Ethanol 95 wt% was purchased from the liquor distillery organization, Excise department (Thailand).

8.3.2 Esterification of succinic acid

The esterification of succinic acid was accomplished in a 2 liter glass reactor equipped with a 40 cm long Vigreux column. The initial concentration ratio of succinic acid/ethanol/water was 3.5/5.5/1.0. The temperature of the reaction mixture was controlled at 90°C using a heating circulator (Julabo, Germany). Esterification reaction commenced by addition of conc. H₂SO₄ until the pH reached 2.5, then 50 grams of Amberlyst-15 E was added to the reactor. During the reaction, succinic acid, ethanol, MES, DES and water concentration were analyzed.

8.3.3 Analysis

8.3.3.1 Succinic acid concentration

Organic acids were analyzed by HPLC (Agilent 1200, Agilent Technology Inc., U.S.A.), and quantification by UV detection was made at the wavelength of 210 nm. Samples were analyzed using a mobile phase of 1% acetonitrile +99% 20 mM Na₂HPO₄ (pH 2) at a flow rate of 1 mL/min. The column was ZORBAX SB-Aq (4.6 mm ×150 mm).

8.3.3.2 Volatile compounds and ethanol concentration

Ester forms of succinic acid and ethanol concentrations were analyzed using a gas chromatograph (GC) equipped with a FID detector (SRI Instrument, USA). Helium, 99.99% pure, was used as carrier gas. The GC column (Carbowaxs, Restek, USA) was a 30 m×0.32 mm bonded phase fused silica capillary column. The injector and detectors were set at 250 and 300 °C. The oven was operated

at programmed increasing temperature, from 50 to 250 °C, at the rate of 15 °C /min. The injection volume of liquid samples was 0.5 µL.

8.3.3.3 Water content analysis

Water content of the esterification reaction was determined using a Karl–Fischer automatic titrator (TitroLine alphas, Schott, Germany).

8.3.4 Kinetic model consideration

The kinetic model of succinic acid/ethanol esterification has been described by Orjuela (2010). In a batch reactor, the change in number of moles N_i of component i participating in m reactions can be expressed as

$$\frac{dN_i}{dt} = N_T \frac{dx_i}{dt} = \left(\sum_{m=1}^m \theta_{i,m} r_m \right) V \quad (8.1)$$

Here N_T is the total number of moles in the reactor, V is the reaction volume, r_m is the rate of reaction m per unit volume and x_i is the mole fraction of component i in the liquid mixture. The parameter $\theta_{i,m}$ is the ratio of stoichiometric coefficients of component i with respect to the reference component in reaction m . Equation 8.1 can be expressed in terms of total molar concentration in the liquid phase C_T ($V/N_T = 1/C_T$) calculated from average molecular weight (MW_{Avg}) and the density of the solution.

$$\frac{dx_i}{dt} = \frac{1}{C_T} \left(\sum_{m=1}^m \theta_{i,m} r_m \right) = \frac{MW_{Avg}}{\rho_{Sol}} \left(\sum_{m=1}^m \theta_{i,m} r_m \right) \quad (8.2)$$

Using a pseudo-homogeneous model for the reversible esterification reactions (Figure 8.1), the rate of reaction of succinic acid with ethanol can be expressed as:

$$r_1 = w_{CAT} \rho_{Sol} k_0^1 \exp\left(\frac{-E_a^1}{RT}\right) \left[(x_{SA} \gamma_{SA})(x_{EtOH} \gamma_{EtOH}) - \frac{(x_{MES} \gamma_{MES})(x_{H_2O} \gamma_{H_2O})}{K_{EQ}^1} \right] \quad (8.3)$$

Simultaneously, the same approach for the second step of SA esterification, the rate of formation of DES is described by:

$$r_2 = w_{CAT} \rho_{Sol} k_0^2 \exp\left(\frac{-E_a^2}{RT}\right) \left[(x_{MES} \gamma_{MES})(x_{EtOH} \gamma_{EtOH}) - \frac{(x_{DES} \gamma_{DES})(x_{H_2O} \gamma_{H_2O})}{K_{EQ}^2} \right] \quad (8.4)$$

Where r is the reaction rate, w_{CAT} is the weight of catalyst, ρ_{Sol} is the solution density, x_i and γ_i are mole fraction and activity coefficient of component i , respectively, k_0^m and E_a^m represented the pre-exponential factor and the energy of activation of the forward reaction m , respectively. The equilibrium constant of reaction K_{EQ}^m referred to the ratio of forward and reverse rate constants.

In order to calculate the rate of reaction, the activity coefficient (γ_i) is the important parameter to determine. An activity coefficient is a factor used in thermodynamics to account for deviations from ideal behavior in a mixture of chemical substances. The non-random two-liquid (NRTL) model is an activity coefficient model the correlates the activity coefficient of a compound i with its mole fraction (x_i) in the liquid phase concerned. The general equation for γ_i for species i in a mixture of n component as follow:

$$\ln(\gamma_i) = \frac{\sum_{j=1}^n x_j \tau_{ji} G_{ji}}{\sum_{k=1}^n x_k G_{ki}} + \sum_{j=1}^n \frac{x_j G_{ij}}{\sum_{k=1}^n x_k G_{kj}} \left(\tau_{ij} - \frac{\sum_{m=1}^n x_m \tau_{mj} G_{mj}}{\sum_{k=1}^n x_k G_{kj}} \right) \quad (8.5)$$

$$G_{ij} = \exp(-\alpha_{ij}\tau_{ij}) \quad (8.6)$$

$$\tau_{ij} = a_{ij} + \frac{b_{ij}}{T} \quad (8.7)$$

The values of binary parameter which applied in Eq. (8.6) and (8.7) for succinic acid purification have been summarized in Table 8.1

8.3.5 Simulation of DES production using VP-assisted esterification technique via ASPEN PLUS

The simulation of succinic acid/ethanol esterification and DES production using VP-assisted esterification technique was achieved. The RBatch was used as a reactor and kinetic parameters were set according to Figure 8.1 and Table 8.2. The catalyst loading was set at 0.08 kg with the reaction temperature at 90°C. The stop criteria was fixed when the concentration of succinic acid was zero. The VP system which coupled in the esterification process was applied according to the topic 7.4.6 in Chapter 7.

Table 8.1 Binary parameters of the related components for NRTL model (Orjuela, 2010).

<i>i</i>	<i>j</i>	<i>a_{ij}</i>	<i>a_{ji}</i>	<i>b_{ij}</i>	<i>b_{ji}</i>	<i>α_{ij}</i>
H ₂ O	EtOH	0.54285	0.806535	444.8857	-266.533	0.4
H ₂ O	SA	0	0	296.7226	-328.506	0.3
H ₂ O	DES	4.384591	-1.58	184.7326	1136.555	0.36842
H ₂ O	MES	0	0	880.7603	-200.977	0.3
EtOH	SA	0	0	-605.634	113.4481	0.3
EtOH	DES	0	0	653.8819	-158.856	0.3
EtOH	MES	0	0	-292.308	400.6306	0.3
SA	DES	0	0	1946.876	218.2243	0.3
SA	MES	0	0	-368.762	1039.777	0.3
DES	MES	0	0	-44.2052	137.2218	0.3

8.4 Results and discussions

8.4.1 Esterification of succinic acid

Time-dependence of product and reactant concentrations during the esterification reaction of succinic acid and ethanol are shown in Figure 8.3. It can be seen that, DES, MES and water increased gradually at the start of reaction until 50 min which consistent with the decreasing of succinic acid and ethanol. After that, compositions reached the plateau after 60 min until the end of reaction. The calculated molar productivity of diethyl succinate was obtained at 0.094 M hr⁻¹ for the first 60 min. The conversion yield at equilibrium was obtained at around 90% which according to the previous study (Lubsungneon *et al.*, 2014). They reported that, effect of operating temperature plays important role on both volumetric productivity and conversion yield. The volumetric productivity was observed at 2.59, 11.12 and 11.13 g.L⁻¹.hr⁻¹ and

conversion yield at 90.18, 90.32 and 90.81% in the operating pressure at 65, 80 and 90°C, respectively.

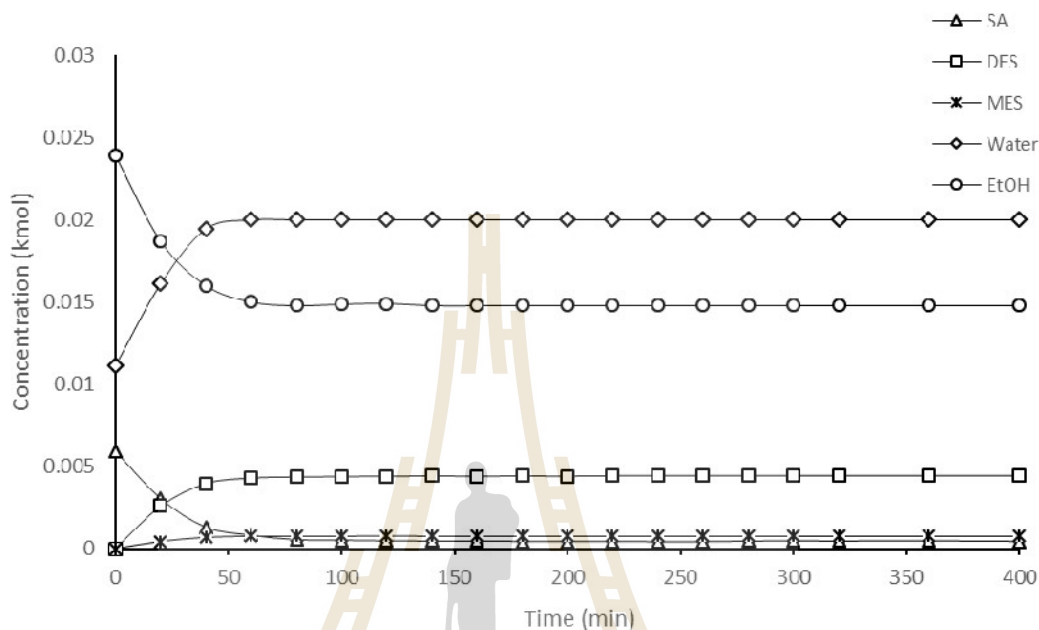


Figure 8.3 Concentration profile of succinic acid (\triangle), diethyl succinate (\square), monoethyl succinate (\times), water (\diamond) and ethanol (\circ) during esterification reaction of SA and ethanol.

8.4.2 Reaction kinetics of succinic acid/ethanol esterification: comparison between predicted and experimental data

The kinetics of succinic acid/ethanol esterification was studied and the molar concentration during the reaction was predicted. According to Eq. (8.3) and (8.4), the activity coefficient for each component was successfully calculated based on NRTL model in accordance with Gmehling *et al.* (2012). The obtained predicted data was compared with the realistic experimental data in order to evaluate the reaction kinetic

constants. The parameters for pseudo-homogeneous reaction based on activity kinetic model are summarized in Table 8.2.

Table 8.2 Kinetic parameters for pseudo-homogeneous model (Orjuela, 2010).

Reactions	Parameters	Value
SA to MES	k^1 (kmol/kg _{CAT} /s)	10,400
	E_a^1 (kJ/kmol)	46,200
	k^{-1} (kmol/kg _{CAT} /s)	212.68
	E_a^{-1} (kJ/kmol)	46,200
	K_{EQ}^1	48.9
MES to DES	k^2 (kmol/kg _{CAT} /s)	2,110
	E_a^2 (kJ/kmol)	46,600
	k^{-2} (kmol/kg _{CAT} /s)	208.09
	E_a^{-1} (kJ/kmol)	46,600
	K_{EQ}^1	10.1

Table 8.2 shows the kinetic parameters of both SA to MES and MES to DES on forward and backward reactions. It was noticed that, the activation energy from forward and reverse reactions (E_a^1 and E_a^{-1}) has the same value. As a consequence of the enthalpy of formation (ΔH) from succinic acid to MES and MES to DES is zero, whereas the reaction rate forward and backward (k^1 and k^{-1}) are difference. It was concluded that, the energy or enthalpy in order to exchange between components was equal but the reaction rates are totally different.

On the assumption that, R_{gas} is 8.314 J/mol K, temperature was 90°C, weight of catalyst was 0.05 kg and solution density was 20 kmol/m³. Mole fraction of the succinic esterification at t = 0 was set as follow:

$$x := \begin{pmatrix} 0.1447 \\ 0.5839 \\ 0 \\ 0 \\ 0.2713 \end{pmatrix}$$

Where 1 was succinic acid, 2 was ethanol, 3 was MES, 4 was DES and 5 was water. In order to calculate the activity coefficient, The G_{ij} and τ_{ij} for each component was calculated according to Eq. (8.6) and (8.7) using the binary parameters for NRTL model (Table 8.1) which expressed as a matrix as follow:

$$a_{NRTL} := \begin{pmatrix} 0 & 0 & 0 & 0 & 0 \\ 0 & 0 & 0 & 0 & 0.806535 \\ 0 & 0 & 0 & 0 & 0 \\ 0 & 0 & 0 & 0 & -1.58 \\ 0 & 0.514285 & 0 & 4.384591 & 0 \end{pmatrix}$$

$$b_{NRTL} := \begin{pmatrix} 0 & 113.4481 & -368.762 & 1946.876 & -328.506 \\ -605.634 & 0 & 400.6306 & 653.8819 & -266.533 \\ 1039.777 & -292.308 & 0 & 137.2218 & -200.977 \\ 218.2243 & -158.856 & -44.2052 & 0 & 1136.555 \\ 296.7226 & 444.8857 & 880.7603 & 184.7326 & 0 \end{pmatrix} K$$

$$\alpha := \begin{pmatrix} 0 & 0.3 & 0.3 & 0.3 & 0.3 \\ 0.3 & 0 & 0.3 & 0.3 & 0.4 \\ 0.3 & 0.3 & 0 & 0.3 & 0.3 \\ 0.3 & 0.3 & 0.3 & 0 & 0.36842 \\ 0.3 & 0.4 & 0.3 & 0.36842 & 0 \end{pmatrix}$$

According to the a_{NRTL} , b_{NRTL} and α value, the G_{ij} and τ_{ij} for the various were calculated. For example, G_{ij} and τ_{ij} of SA and EtOH (1,2) was calculated as follow:

$$\tau(T, i, j) := a_{\text{NRTL}_{i,j}} + \frac{b_{\text{NRTL}_{i,j}}}{T} \quad \tau(T, 1, 2) = 0.313$$

$$G(T, i, j) := e^{(-\alpha_{i,j} \cdot \tau(T, i, j))} \quad G(T, 1, 2) = 0.911$$

The G_{ij} and τ_{ij} value was used as a parameters in activity coefficient calculation. The overall interaction of each component related with the succinic acid/ethanol esterification must be considered and determined. The calculated G_{ij} and τ_{ij} value of all components are shown in Table 8.3. Additionally, the activity coefficient of each component was calculated using MathCad in accordance with Eq. (8.5) as follow:

The activity coefficient (γ_i) each component in the function of temperature and mole fraction was completely computed.

$$\gamma(T, x) = \begin{pmatrix} 0.288 \\ 1.049 \\ 0.854 \\ 8.957 \\ 1.74 \end{pmatrix}$$

Consistent with the results, the activity coefficient of SA, EtOH, MES, DES and H₂O were 0.288, 1.049, 0.854, 8.957 and 1.74 at the start of reaction, correspondingly. In contrast, the variation of activity coefficient values vary due to change in mixture composition.

Table 8.3 The calculated G_{ij} and τ_{ij} value of each component related with the succinic acid/ethanol esterification

i	j	G_{ij}	G_{ji}	τ_{ij}	τ_{ji}
SA	EtOH	0.911	1.65	0.313	-1.668
SA	MES	1.356	0.423	-1.016	2.864
SA	DES	0.2	0.835	5.363	0.601
SA	H ₂ O	1.312	0.783	-0.905	0.817
EtOH	MES	0.718	1.273	1.104	-0.805
EtOH	DES	0.583	1.14	1.801	-0.438
EtOH	H ₂ O	0.972	0.499	0.072	1.74
MES	DES	0.893	1.037	0.378	-0.122
MES	H ₂ O	1.181	0.483	-0.554	2.426
DES	H ₂ O	0.565	0.165	1.551	4.893

Subsequently the activity coefficient were estimated, the rate of succinic acid to monoethyl succinate (r_1) monoethyl succinate to diethyl succinate (r_2) were calculated according to Eq. (8.3), (8.4) and used kinetic parameters following to Table 8.2.

$$r_1(T, x) := \begin{cases} \gamma_1 \leftarrow \gamma(T, x) \\ \text{for } i \in 1..n_{\text{comp}} \\ a_i \leftarrow x_i \cdot \gamma_i \\ w_{\text{cat}} \cdot \rho \cdot k_{101} \cdot \exp\left(\frac{-E_{1a1}}{R_{\text{gas}} \cdot T}\right) \cdot \left(a_{\text{SA}} \cdot a_{\text{EtOH}} - \frac{a_{\text{MES}} \cdot a_{\text{H}_2\text{O}}}{K_{1\text{eq1}}}\right) \end{cases}$$

$$r_2(T, x) := \begin{cases} \gamma_1 \leftarrow \gamma(T, x) \\ \text{for } i \in 1..n_{\text{comp}} \\ a_i \leftarrow x_i \cdot \gamma_i \\ w_{\text{cat}} \cdot \rho \cdot k_{201} \cdot \exp\left(\frac{-E_{2a1}}{R_{\text{gas}} \cdot T}\right) \cdot \left(a_{\text{MES}} \cdot a_{\text{EtOH}} - \frac{a_{\text{DES}} \cdot a_{\text{H}_2\text{O}}}{K_{2\text{eq1}}}\right) \end{cases}$$

$$r_1(T, x) = 1.659 \times 10^{-4} \text{ mol} \cdot \text{s}^{-1} \cdot \text{m}^{-3}$$

$$r_2(T, x) = 0 \text{ mol} \cdot \text{s}^{-1} \cdot \text{m}^{-3}$$

Therefore, the calculated net rate of succinic acid to monoethyl succinate (r_1) monoethyl succinate to diethyl succinate (r_2) were 1.659×10^{-4} and $0 \text{ mol} \cdot \text{s}^{-1} \cdot \text{m}^{-3}$, respectively. The reaction rate of r_2 was zero due to the absent of the reactant (MES) at the start of reaction. Consequently, the reactions were performed in the function of time. The reaction rate during esterification for each component were described in term of molar concentration over a certain period of time as present:

$$\frac{d n_{SA}}{dt} = -r_1 \qquad \frac{d n_{DES}}{dt} = +r_2$$

$$\frac{d n_{EtOH}}{dt} = -r_1 - r_2 \qquad \frac{d n_{H_2O}}{dt} = +r_1 + r_2$$

$$\frac{d n_{MES}}{dt} = +r_1 - r_2$$

$$r_{vec}(t, x) := \begin{pmatrix} -r_1(T, x) \\ -r_1(T, x) - r_2(T, x) \\ r_1(T, x) - r_2(T, x) \\ r_2(T, x) \\ r_1(T, x) + r_2(T, x) \end{pmatrix}$$

Providing that, the reaction time (t_{end}) was 400 min. The time-dependent of succinic acid esterification (n_{calc}) was predicted according to the 4th order Runge-Kutta method with adaptive step-size in the function of mole fraction from experimental (x_{exp}), reaction time (t_{end}), and reaction rate (r_{vec}) as follow:

$$n_{calc} := \text{Rkadapt} \left[\left(x_{exp}^T \right)^{\langle 1 \rangle}, 0, \frac{t_{end}}{s}, 20, r_{vec} \right]$$

The comparison of the experimental and predicted mole fraction data during the succinic acid esterification with ethanol is presented in Figure 8.4. It can be seen that, the experimental mole fraction profile was be in particularly agreement with the predicted profile when the kinetic constant in Table 8.2 were applied. On the other hand, the mole fraction profile of MES from experimental and predicted data was moderately different. It was concluded that, the kinetic constant fitted with the experimental performed. The results presented in Figure 8.3 agree well with those reported for similar catalyst in the literature (Kolah *et al.*, 2008). The model fitting between the experimental and predicted profile was confirmed using non-linear regression and OF value. The OF value referred to the variation between two dataset were calculated at 1.7×10^{-2} and 5.548×10^{-4} , respectively.

$$\begin{array}{l}
 \text{OF} := \left\{ \begin{array}{l}
 \text{OF} \leftarrow 0 \\
 \text{for } i \in 2..n_{\text{data}} \\
 \quad \text{mat} \leftarrow \text{rkfixed} \left[\left(x_{\text{exp}}^T \right)^{\langle i-1 \rangle}, t_{\text{exp}_{i-1}}, t_{\text{exp}_i}, 1, r_{\text{vec}} \right] \\
 \quad \text{for } j \in 1..n_{\text{comp}} \\
 \quad \quad \text{OF} \leftarrow \text{OF} + \left[\left[\left(x_{\text{exp}}^T \right)^{\langle i \rangle} \right]_j - \left[\left(\text{mat}^T \right)^{\langle 2 \rangle} \right]_{j+1} \right]^2 \\
 \text{OF} \leftarrow \frac{\text{OF}}{n_{\text{data}} \cdot n_{\text{comp}}} \quad \text{OF} = 0.017
 \end{array} \right.
 \end{array}$$

$$\begin{array}{l}
 \text{OF} := \left\{ \begin{array}{l}
 \text{OF} \leftarrow 0 \\
 \text{for } i \in 2..n_{\text{data}} \\
 \quad \text{mat} \leftarrow \text{rkfixed} \left[\left(x_{\text{exp}}^T \right)^{\langle 1 \rangle}, 0, t_{\text{exp}_i}, 10, r_{\text{vec}} \right] \\
 \quad \text{for } j \in 1..n_{\text{comp}} \\
 \quad \quad \text{OF} \leftarrow \text{OF} + \left[\left[\left(x_{\text{exp}}^T \right)^{\langle i \rangle} \right]_j - \left[\left(\text{mat}^T \right)^{\langle 11 \rangle} \right]_{j+1} \right]^2 \\
 \text{OF} \leftarrow \frac{\text{OF}}{n_{\text{data}} \cdot n_{\text{comp}}} \quad \text{OF} = 5.548 \times 10^{-4}
 \end{array} \right.
 \end{array}$$

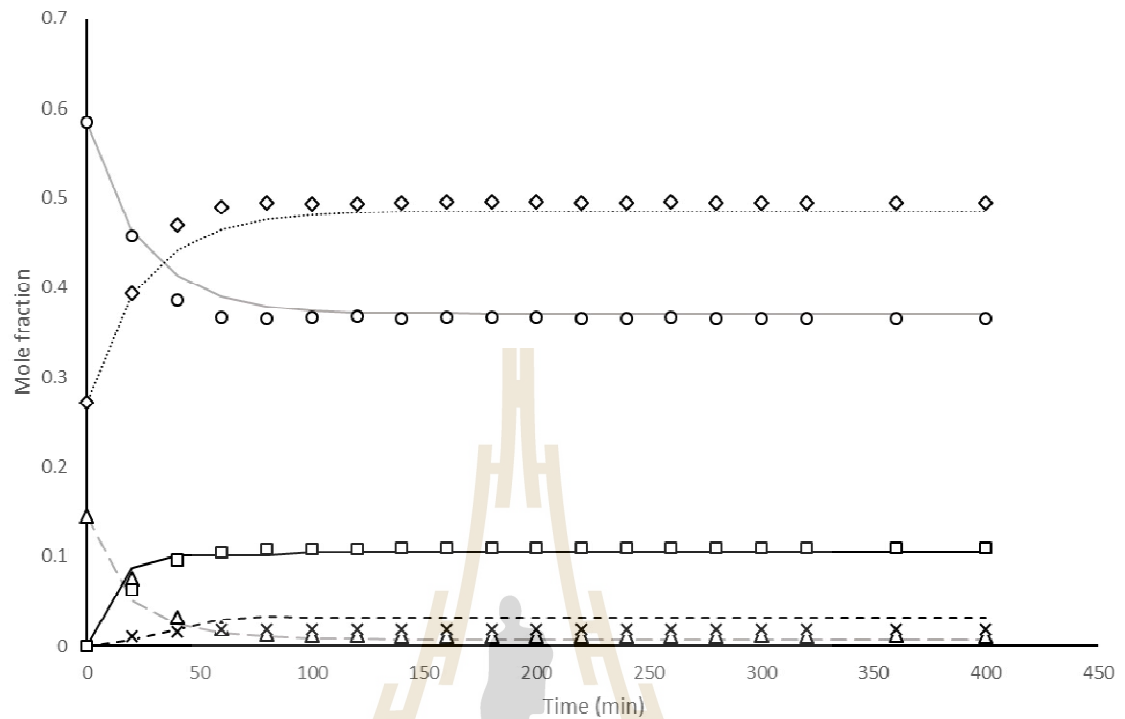


Figure 8.4 Comparison between experimental mole fraction profile of succinic acid (Δ), diethyl succinate (\square), monoethyl succinate (\times), water (\diamond) and ethanol (\circ) and predicted mole fraction profile of succinic acid ($- -$), diethyl succinate ($-$), monoethyl succinate ($- -$), water (\cdots) and ethanol ($-$).

8.4.3 Process simulation of DES production using VP-assisted esterification

In this section, the esterification coupled with VP for water separation was simulated using ASPEN PLUS. The various membrane types were applied in simulated VP. The VP module was completed in accordance with the topic 7.4.6 in Chapter 7. The designed model is shown in Figure 8.5.

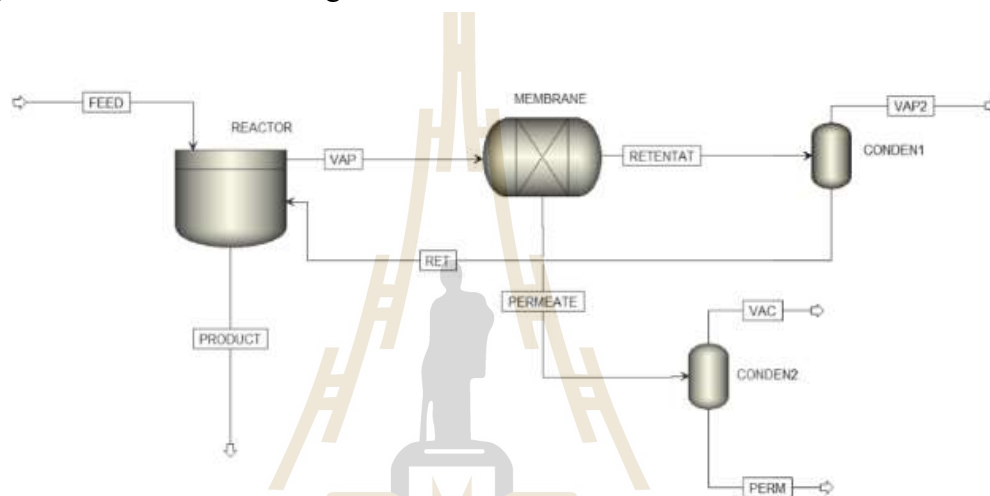


Figure 8.5 The VP-assisted esterification of succinic acid/ethanol designed model.

Simulated component mole flow, total mole and volume flow during succinic acid/ethanol esterification via VP assisted esterification are shown in Table 8.4. The returning dehydrated ethanol stream was observed at approximately 98.5 wt% with 1.75 L/min flow rate, while water elimination from permeate stream was 94 wt% at 0.32 L/min. The product stream contains approximately 0.24 kmol/hr of DES and calculated conversion from succinic acid was obtained at 93.23% which fairly agrees with another study. Orjuela and colleague (2012) studied the synthesis of diethyl succinate using reactive distillation. The esterification process has been simulated using the Radfrac ASPEN module and found the succinic acid conversion approaching 100% and DES yield up to 98%.

Table 8.4 Components mole flow, total mole and volume flow of simulated VP assisted esterification when simulated using ASPEN PLUS.

Components	Feed	Product	Perm	Ret
Mole flow (kmol/hr)				
SA	0.29	0	0	1.93×10^{-6}
EtOH	1.17	0.53	0.073	1.80
H ₂ O	0.54	0.039	1.08	0.036
DES	0	0.27	0	0.0022
MES	0	0	0	1.75×10^{-6}
Total	2	0.84	1.16	1.84
Total volume flow (L/min)				
	1.71	1.29	0.32	1.75

The comparison of esterification performance between various types of membrane compared with non-VP module (control) are given in Table 8.5. The commercial ceramic membrane illustrated the highest DES production as a consequence of the high performance in water separation than other tested membrane. The conversion yield of SA/DES from self-made membrane and pervaporative polymer membrane were 82.7 and 79.3%, respectively. The lower DES conversion due to the high level of remaining water in the system. Contrarily, the DES conversion yield from non-VP system was found at 16% owing to the high level of water and intermediate substance (MES). The results confirmed that, the coupled VP particularly improved the esterification efficiency in succinic acid/ethanol system, especially the high flux and water separation membrane.

Table 8.5 Simulated data of product stream mole flow and volume flow of various types of membrane in VP assisted esterification.

Components	Control	VP-coupled SA esterification		
		Ceramic	Self-made	Polymer
Mole flow (kmol/hr)				
SA	0	0	0	0
EtOH	0.13	0.53	0.49	0.46
H ₂ O	0.22	0.040	0.18	0.30
DES	0.047	0.27	0.24	0.23
MES	0.012	0	0	0
Total	0.41	0.84	0.93	1.23
Total volume flow (L/min)				
	0.38	1.29	1.38	1.49

8.5 Conclusions

The kinetic of DES production via succinic acid/ethanol esterification was studied. The kinetic parameters of the reaction such as rate constant (k -value), activity coefficient (γ_i), activation energy (E_a) and equilibrium constant (k_{EQ}) from literature were used and compared with the experimental dataset. There was good agreement between calculated and experimental data for both datasets. It can be seen that, calculated OF value referred to the variation between two dataset were 1.7×10^{-2} and 5.548×10^{-4} , respectively. In was summarized that, the kinetic parameters could be applied to the simulation software. The simulated succinic acid/ethanol esterification which coupled VP module found the DES production at 0.24 kmol/hr. The commercial

ceramic membrane illustrated a valuable option for water separation during esterification approach.

8.6 References

- Cheng, K.K., Zhao, X.B., Zeng, J., Wu, R.C., Xu, Y.Z., Liu, D.H. and Zhang, J.A. (2012). Downstream processing of biotechnological produced succinic acid. **Appl. Microbiol. Biotechnol.** 95: 841–850.
- Cukalovic, A. and Stevens, C.V. (2008). Feasibility of production methods for succinic acid derivatives: a marriage of renewable resources and chemical technology. **Biofuels, Bioprod. Biorefin.** 2 (6): 505-529.
- Delhomme, C., Weuster-Botz, D. and Kühn, F.E. (2009). Succinic acid from renewable resources as a C₄ building-block chemical—a review of the catalytic possibilities in aqueous media. **Green Chem.** 11: 13-26.
- Gmehling, J., Kolbe, B., Kleiber, M. and Rarey, J. (2012). **Chemical Thermodynamics for Process Simulation.** 1st ed. Wiley-VCH Verlag GmbH & Co. KGaA.
- Hermann, B. and Patel, M. (2007). Today's and tomorrow's bio-based bulk chemicals from white biotechnology: a techno-economic analysis. **Appl. Biochem. Biotechnol.** 136: 361 – 388.

- Kolah, A.K., Asthana, N.S., Vu, D.T., Lira, C.T. and Miller, D.J. (2008). Reaction kinetics for the heterogeneously catalyzed esterification of succinic acid with ethanol. **Ind. Eng. Chem. Res.** 47(15): 5313–5317.
- Kurzrock, T. and Weuster-Botz, D. (2010). Recovery of succinic acid from fermentation broth. **Biotechnol. Lett.** 32: 331–339.
- Orjuela, A. (2010). **Separation of succinic acid from fermentation broth and esterification by a reactive distillation method**, [Ph.D thesis]. Chemical engineering, Michigan State University, U.S.A., 300p.
- Lubsungneon, J., Srisuno, S., Rodtong, S. and Boontawan, A. (2014). Nanofiltration coupled with vapor permeation-assisted esterification as an effective purification step for fermentation-derived succinic acid. **J. Membr. Sci.** 459: 132-142.
- McKinlay, J. B., Vieille, C., Zeikus, J. G. (2007). Prospect for a bio-based succinate industry. **Appl. Microbiol. Biotechnol.** 76: 727-740.
- Orjuela, A., Kolah, A., a, Hong, X., Lira, C.T. and Miller, D.J. (2012). Diethyl succinate synthesis by reactive distillation. **Sep. Purif. Tech.** 88: 151–162.

CHAPTER IX

OVERALL CONCLUSION

Product and substrate inhibition is a major problem in ethanol production. The ethanol productivity decreases sharply when the product concentration (P'_m) was approximately 100 g/L. The productivity decreased gradually when ethanol in fermented broth increased. The extractive fermentation showed the reducing of product inhibition effect by continuously removing the ethanol from the fermented broth. It can be seen that, approximately 60% of yeast survive occurred in the extractive fermentation system, moreover 80 wt% of ethanol was continuously removed from the fermentation broth. Subsequently, the activated cells in the fermentation broth were used in the repeated-batch mode. There were 8 cycles of fermentation using only 1 time inoculation. The ethanol was continuously fractionated from the system at the average rate of 10.2 g/h with the concentration of approximately 80 wt%. Unfortunately, productivity and relative viability for each fermentation cycle continuously decrease due to the accumulation of toxic substances from molasses. The continuous extractive fermentation could avoid this problem. The simulation of a 200 liter extractive fermentation system was successfully performed using ASPEN PLUS software. The simulated system can be divided into 3 parts including fermentation, fractionation and Venturi system. A Venturi system supplied vacuum and product harvesting simultaneously. Actually, 18.5 liter which contains 82 wt% ethanol solution was produced from 200 liters extractive fermentation per day with a production cost of 27.50 Baht per liter. The economic development was carried out including recovery of waste

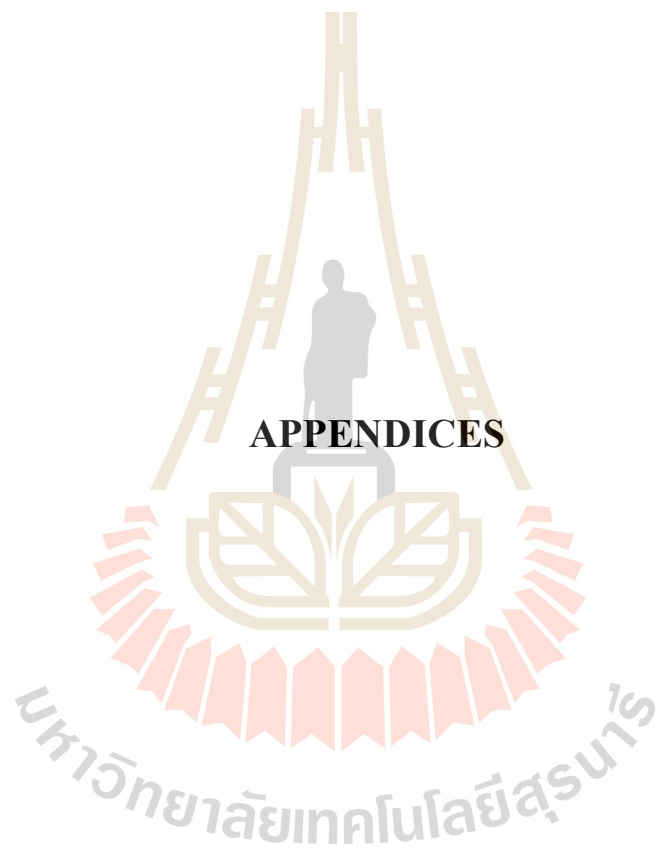
stream and changing the boundary condition. Roughly 30% of production cost decreased after process improvement.

A self-made laboratory high-performance distillation system was established which is appropriate for a small fuel-ethanol factory or local distillation business. The distillation system showed high efficiency in ethanol rectification. The maximum concentration of 93 wt% ethanol solution was extracted from any ethanol content in fermentation broth. Though, the deficiency of stripping performance was represented in this system. The small-scale distillatory was simulated using ASPEN PLUS. The adjustment of heating unit leading to the reduction of utilities cost by approximately 43.8%. The optimization of heating duty including flash and reboiler is a necessary step in order to specify the worthiness of production and installation cost. Likewise, this also holds for the heat exchanger and its surface area.

The zeolite NaA membranes for water separation from ethanol was fabricated in different silica sources including chemical and RHA and various seeding technique. Dip-coated pretreatment with 6 μm NaA seed represented higher separation factor and flux than the non-treated substrate and various seeding technique. The extracted water was 92 wt% with flux and separation factor at 0.6 $\text{kg m}^{-2} \text{hr}^{-1}$ and 218, respectively. On the other hand, the separation performance on synthesized membrane was unfavorable when compared with previous authors and commercial hydrophilic membranes. The very large NaA seed was used throughout seeding technique. The formation of an incontinuous and uneven zeolite membrane led to a low separation factor when the large seeding size was used. The mathematical kinetics to describe the mobility of substances through different kinds of membrane including commercial ceramic, polymer and self-

made membrane was derived. The diffusion coefficient (k - value) was successfully calculated based on experimental data using non-linear regression technique. The calculated k - value at 2.5×10^{-9} and 4.52×10^{-6} mol.s⁻¹.m⁻².Pa⁻¹ of k_e and k_w value of commercial ceramic membrane were successfully determined from experimental and calculated dataset. Thereafter, the obtained k - value was applied in order to simulate the ethanol dehydration process design and especially membrane tubes quantity analysis.

The kinetics of DES production via succinic acid/ethanol esterification was studied. The vapor permeation technique was employed in this process which is in accordance with the calculated flux and separation performance in previous chapter. The kinetic parameters reaction rate constant (k -value), activity coefficient (γ_i), activation energy (E_a) and equilibrium constant (k_{EQ}) from literature were used and compared with the experimental dataset. The results illustrated good agreement between calculated and experimental data when proved by OF value. It was concluded that, the obtained kinetic parameters fitted in the simulation software. The simulated succinic acid/ethanol esterification which coupled VP module found the DES production at 0.24 kmol/hr. The commercial ceramic membrane illustrated a promising material for water separation during esterification approach.



APPENDICES

มหาวิทยาลัยเทคโนโลยีสุรนารี

APPENDIX A

COMPOSITION OF KAOLIN

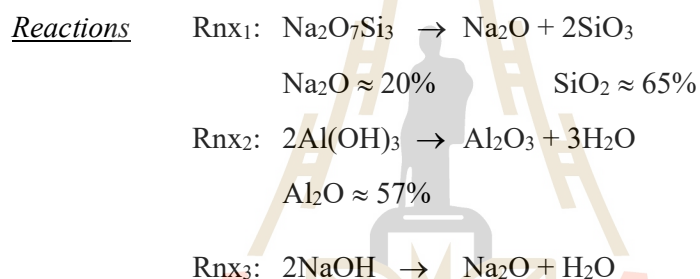
Table 1A Composition of experimental kaolin

Compositions	%w/w
SiO ₂	44.85%
Al ₂ O ₃	37.98%
Fe ₂ O ₃	0.97%
CaO	0.06%
MgO	0.12%
Na ₂ O	0.04%
K ₂ O	1.23%
TiO ₂	0.07%
H ₂ O	0.65%
Loss on ignition	13.94%

APPENDIX B

ZEOLITE A FORMULAR CALCULATION

<u>Composition of mixture</u>	NaOH	MW = 40 g/mol
	Al(OH) ₃	MW = 78 g/mol
	Na ₂ O ₇ Si ₃	MW = 242.23 g/mol
	H ₂ O	MW = 18 g/mol



Zeolite NaA formula

$$50 \text{ Na}_2\text{O} : \text{Al}_2\text{O}_3 : 5 \text{ SiO}_2 : 1000 \text{ H}_2\text{O} \text{ (mol ratio basis)} \quad (1)$$

Divided (1) by 5

$$\therefore 10 \text{ Na}_2\text{O} : 0.2 \text{ Al}_2\text{O}_3 : \text{SiO}_2 : 200 \text{ H}_2\text{O} \quad (2)$$

$$1 \text{ g of SiO}_2 = \frac{1 \text{ g}}{60 \text{ g mol}^{-1}} = 0.017 \text{ mol}$$

Multiply (2) by 0.017

$$0.17 \text{ Na}_2\text{O} : 0.034 \text{ Al}_2\text{O}_3 : 0.017 \text{ SiO}_2 : 3.4 \text{ H}_2\text{O}$$

SiO₂ solution calculation

From Rxn₁: 65 g of SiO₂ come from 100 g of Na₂O₇Si₃

$$\text{Thus, 1 g of SiO}_2 \text{ used } \frac{1 \text{ g} \times 100 \text{ g}}{65 \text{ g}} = 1.54 \text{ g of Na}_2\text{O}_7\text{Si}_3$$

SiO₂ solution 10 mL contained 10 mL of 1M of NaOH (0.01 mol) and 1.54 g of Na₂O₇Si₃

Thus, Na_2O from SiO_2 solution = $0.01 \text{ mol} \times 40 \text{ g/mol} = 0.2 \text{ g}$

Na_2O from Na_2O from $\text{Na}_2\text{O}_7\text{Si}_3 = 1.54 \times 0.2 = 0.31 \text{ g}$

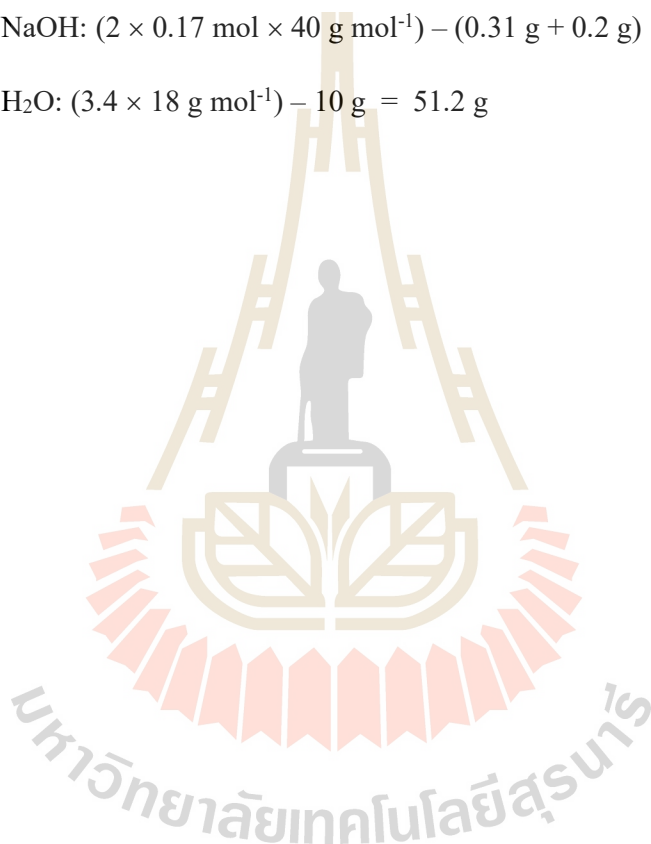
Chemicals weight calculation

SiO_2 solution: 10 mL

$\text{Al}(\text{OH})_3$: $0.034 \text{ mol} \times 78 \text{ g mol}^{-1} \times 100 \text{ g}/57 \text{ g} = 0.47 \text{ g}$

NaOH : $(2 \times 0.17 \text{ mol} \times 40 \text{ g mol}^{-1}) - (0.31 \text{ g} + 0.2 \text{ g}) = 12.5 \text{ g}$

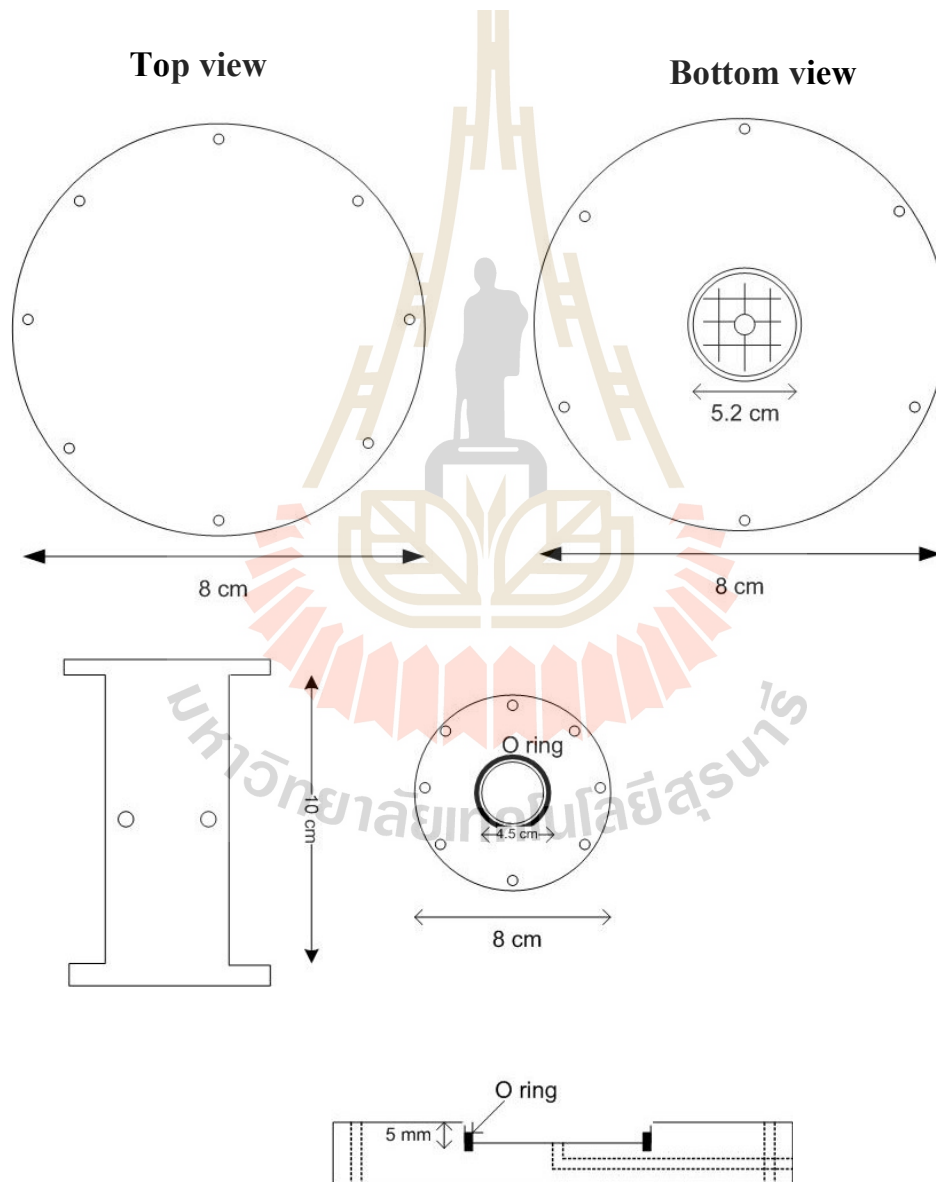
H_2O : $(3.4 \times 18 \text{ g mol}^{-1}) - 10 \text{ g} = 51.2 \text{ g}$



APPENDIX C

GEOMETRICALLY DESIGN OF SELF-MADE MEMBRANE

HOUSING



APPENDIX D

CALCULATION OF DIFFUSION COEFFICIENT

***k*-value of polymer membrane**

Table 1D Calculated flux and mole fraction of water and ethanol at various operating pressure and feed concentration of polymer membrane.

Data set	J_{calc_w}	J_{calc_e}	y_{calc_w}	y_{calc_e}
1	4.944	0.1	0.98	0.02
2	9.894	0.2	0.98	0.02
3	14.844	0.3	0.98	0.02
4	19.794	0.4	0.98	0.02
5	4.745	0.499	0.905	0.095
6	9.495	0.999	0.905	0.095
7	14.245	1.499	0.905	0.095
8	18.995	1.999	0.905	0.095
9	4.495	0.998	0.818	0.182
10	8.995	1.998	0.818	0.182
11	13.495	2.998	0.818	0.182
12	17.995	3.998	0.818	0.182
13	4.246	1.497	0.739	0.261
14	8.496	2.997	0.739	0.261
15	12.746	4.497	0.739	0.261
16	16.996	5.997	0.739	0.261

$$\text{result} = \begin{pmatrix} 6.25 \times 10^{-10} \\ 3.25177 \times 10^{-7} \end{pmatrix} \text{mol} \cdot \text{s} \cdot \text{m}^{-1} \cdot \text{kg}^{-1}$$

$$\text{OF}(k_e, k_w) = 0.102$$

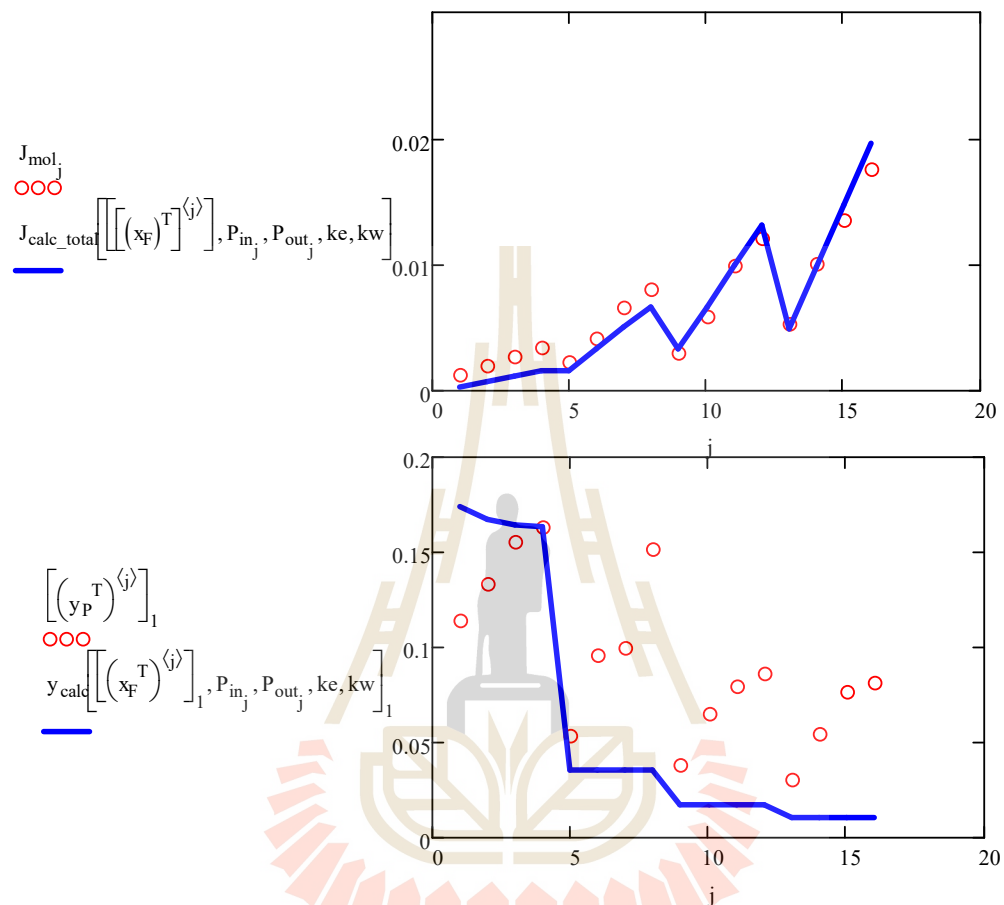


Figure 1D The comparison between experimental data (○) and calculated data (after k -value adjustment) (-) of molar flux (above) and mole fraction (below) of polymer membrane.

k*-value of self-made membrane (sample 045)*Table 2D** Calculated flux and mole fraction of water and ethanol at various operating pressure and feed concentration of self-made membrane (sample 045).

Data set	J_{calc_w}	J_{calc_e}	y_{calc_w}	y_{calc_e}
1	4.944	0.1	0.98	0.02
2	9.894	0.2	0.98	0.02
3	14.844	0.3	0.98	0.02
4	19.794	0.4	0.98	0.02
5	4.745	0.499	0.905	0.095
6	9.495	0.999	0.905	0.095
7	14.245	1.499	0.905	0.095
8	18.995	1.999	0.905	0.095
9	4.495	0.998	0.818	0.182
10	8.995	1.998	0.818	0.182
11	13.495	2.998	0.818	0.182
12	17.995	3.998	0.818	0.182
13	4.246	1.497	0.739	0.261
14	8.496	2.997	0.739	0.261
15	12.746	4.497	0.739	0.261
16	16.996	5.997	0.739	0.261

$$\text{result} = \begin{pmatrix} 6.25 \times 10^{-10} \\ 4.86863 \times 10^{-7} \end{pmatrix} \text{mol} \cdot \text{s} \cdot \text{m}^{-1} \cdot \text{kg}^{-1}$$

$$\text{OF}(k_e, k_w) = 0.104$$

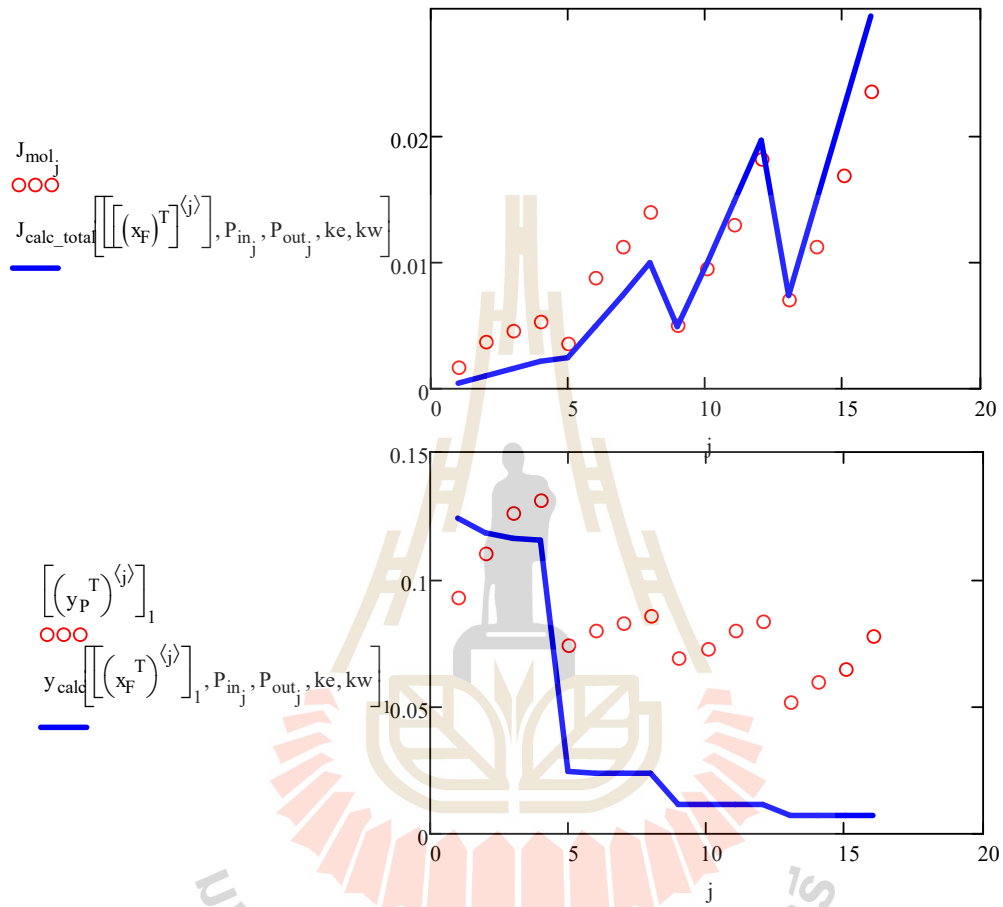


Figure 2D The comparison between experimental data (○) and calculated data (after k -value adjustment) (-) of molar flux (above) and mole fraction (below) of self-made membrane (sample 045).

BIOGRAPHY

Mr. Artit Kongkaew was born on April 23rd, 1984 in Nakhon Ratchasima, Thailand. In 2002, he studied in Food Technology, Suranaree University of Technology, Nakhon Ratchasima. He received his Bachelor's degree of science (Food Technology) in 2005. In 2007, he decided to further study master's degree in the field of Biotechnology. During study, he received financial support from Suranaree University of Technology. He graduated the Master's of Science in Biotechnology in 2009. His master thesis topic was "Optimization of Beer Production from Rice Malt Based using Response Surface Methodology". His topic "Optimization of wort production from rice malt using enzymes and barley malt" was accepted to be published in African Journal of Biotechnology, volume 11. He continued his Ph.D. studied in 2013 in Biotechnology program and received financial support from Suranaree University of Technology. His dissertation title was "Process Development and Simulation of Anhydrous Ethanol Production and Application in Vapor Permeation-Assist Esterification of Succinic acid". During this time, he had studied in "Chemical process development" course at Technische Chemie, Carl von Ossietzky Universität Oldenburg, Germany.